NASA CR-165337

Internal Coating of Air-Cooled Gas Turbine Blades

Final Report

by

L. Hsu and A.R. Stetson

SOLAR TURBINES INTERNATIONAL
An Operating Group of International Harvester

December 1980

CONTRACT NAS3-21841

Prepared for

NATIONAL AERONAUTICS AND SPACE ADMINISTRATION

Lewis Research Center
21000 Brookpark Road
Cleveland, Ohio 44135

1. Report No.	2. Government Accession No.	3. Recipient's Catalog No.
NASA CR-165337		

4. Title and Subtitle	5. Report Date
INTERNAL COATING OF AIR-COOLED GAS TURBINE BLADES	December, 1980
	6. Performing Organization Code

7. Author(s)	8. Performing Organization Report No.
L. L. Hsu and A. R. Stetson	SR81-R-4828-16
	10. Work Unit No.

9. Performing Organization Name and Address	11. Contract or Grant No.
Solar Turbines International 2200 Pacific Highway, P.O. Box 80966 San Diego, California 92138	NAS3-28142
	13. Type of Report and Period Covered Final May 1979-November 1980

12. Sponsoring Agency Name and Address	14. Sponsoring Agency Code
National Aeronautics & Space Administration Washington, DC	

15. Supplementary Notes
Project Manager: John P. Merutka, NASA-Lewis Research Center
21000 Brookpark Road, Cleveland, Ohio 44135

16. Abstract

Four modified aluminide coatings were developed for IN-792 + Hf alloy using a powder pack method applicable to internal surfaces of air-cooled blades. The coating compositions are Ni-19Al-1Cb, Ni-19Al-3Cb, Ni-17Al-20Cr, and Ni-12Al-20Cr. Cyclic burner rig hot corrosion (900°C) and oxidation (1050°C) tests indicated that Ni-Al-Cb coatings provided better overall resistance than Ni-Al-Cr coatings. Tensile properties of Ni-19Al-1Cb and Ni-12Al-20Cr coated test bars were fully retained at room temperature and 649°C. Stress-rupture results exhibited wide scatter around uncoated IN-792 baseline, especially at high stress levels. High-cycle fatigue lives of Ni-19Al-1Cb and Ni-12Al-20Cr coated bars (as well as RT-22B coated IN-792) suffered approximately 30 percent decrease at 649°C. Since all test bars were fully heat treated after coating, the effects of coating/processing on IN-792 alloy were not recoverable.

Internally coated Ni-19Al-1Cb, Ni-19Al-3Cb, and Ni-12Al-20Cr blades were included in 500-hour endurance engine test and the results were similar to those obtained in burner rig oxidation testing.

17. Key Words (Suggested by Author(s))	18. Distribution Statement
Internal Coating Air-Cooled Blades Alloy Coating Oxidation Resistant Coatings Engine Test Hot Corrosion Pack Process	Unclassified - Unlimited

19. Security Classif. (of this report)	20. Security Classif. (of this page)	21. No. of Pages	22. Price*
Unclassified	Unclassified	160	

* For sale by the National Technical Information Service, Springfield, Virginia 22161

TABLE OF CONTENTS

TABLE OF CONTENTS (CONT)

LIST OF FIGURES

LIST OF FIGURES (CONT)

LIST OF FIGURES (CONT)

LIST OF FIGURES (CONT)

LIST OF FIGURES (CONT)

LIST OF FIGURES (CONT)

LIST OF TABLES

LIST OF TABLES (CONT)

EXECUTIVE SUMMARY

The objective of this program was to develop and evaluate four modified aluminide coating compositions from a preceeding program (NAS3-21039) that can be applied to the internal surfaces of air-cooled turbine blades using the powder pack method in two stages. The coatings are Ni-19Al-1Cb, Ni-19Al-3Cb, Ni-17Al-20Cr and Ni-12Al-20Cr and compositions were confirmed by SEM/EDX techniques. The program alloy was IN-792. The coating systems were initially applied to the external surfaces of test specimens and the processes were subsequently modified for internal application to air-cooled blades.

Metallurgical and SEM/EDX analyses of the coatings revealed multiple zone microstructures generally associated with medium pack activities. The columbium coatings were characterized by a brittle columbium intermetallic at the coating surface. Chromium, in the Ni-Al-Cr coatings, was found to be finely dispersed throughout the coating. Coating thicknesses as measured on external surfaces were generally 60 to 120 microns. However, upon application to internal surfaces of Mars stage 1 blades, it was found that coating thickness was decreased by 30 percent as a result of the limited packing volume available. This decrease in coating thickness was most pronounced at the trailing edge exit holes, where the pack was totally depleted to form the coating.

All four compositions were externally applied to test pins for evaluation in burner rig 900°C hot corrosion and 1050°C oxidation tests. Results obtained, as determined by metallographic techniques, indicated that the Ni-19Al-3Cb coating exhibited the best resistance with Ni-19Al-1Cb a close second. However, the Ni-19Al-3Cb coating was found to be significantly less diffusionally stable than Ni-19Al-1Cb. During test exposure, the columbium-rich zone remained at the coating surface and columbium was detected in the oxide scale formed. It is believed that the presence of columbium near the oxide/coating interface accounted for the excellent resistance by formation of a thin, adherent oxide scale in contrast to the thick, porous oxide layer developed in Ni-Al-Cr coatings. In both hot corrosion and oxidation testing, Ni-Al-Cr coatings were found to have undergone degradation at the surface and also internally near the coating/alloy interface.

In addition to rig testing, coated test specimens were also exposed to 1029 hours of furnace oxidation. Results confirmed that dynamic burner rig test environments produced accelerated degradation in 170 hours, significantly exceeding static oxidation attack in a furnace after over 1000 hours of exposure. Acicular phase formation in IN-792 alloy adjacent to the coating/substrate interface was observed in all specimens after the prolonged furnace test. The columbium-rich zone was also markedly absent in the Ni-Al-Cb coatings in furnace oxidation. Ranking of coatings after environmental resistance testing is as follows: Ni-19Al-3Cb > Ni-19Al-1Cb, Ni-12Al-20Cr > Ni-17Al-20Cr.

Mechanical property testing (tensile, stress rupture, high cycle fatigue and strain tolerance) of selected coating systems were performed. Tensile properties of Ni-19Al-1Cb and Ni-12Al-20Cr coated test bars were fully retained at room temperature and 649°C. Stress-rupture results exhibited wide scatter around uncoated IN-792 baseline data, especially at high stress levels. High cycle fatigue lives of Ni-19Al-1Cb and Ni-12Al-20Cr coated bars (as well as RT-22B* coated IN-792) suffered approximately a 30 percent decrease at 649°C. Since all test bars were fully heat treated after coating, it was assumed that the effects of coating/processing on IN-792 were not readily recoverable.

Internally coated Ni-19Al-1Cb, Ni-19Al-3Cb and Ni-12Al-20Cr blades were included in a 500-hour endurance engine test operating alternately on natural gas and Diesel No. 2. Each blade was sectioned at 50 percent span and metallographically analyzed. Findings were similar to those obtained in burner rig testing. Both Ni-19Al-1Cb and Ni-19Al-3Cb coatings performed better than Ni-12Al-20Cr, which was severely attacked at the internal trailing edge. Oxidation attack in the Ni-Al-Cb coatings was limited to <15 percent of the coating. The coatings at the trailing edge were found to be 30 to 50 percent thinner than that at the internal leading edge, due to pack depletion in a confined volume. The Ni-19Al-3Cb was also applied to the external surface of one of the blades and localized pitting attack accompanied by thermal fatigue cracks were detected.

The engine test demonstrated that Ni-19Al-1Cb coatings can be successfully used to protect the internal surfaces of air-cooled blading. Such protection is derived from both the aluminum content of the coating and the desirable characteristics of the columbium-containing oxide layer. However, a significant factor remains to be resolved, that of degradation of stress rupture and high cycle fatigue properties. Deviation from baseline data was not limited to program coatings. Further investigations are required to determine the source of the degradation and hence, methods of recovering substrate properties.

---

* RT-22B is a Pt-Rh containing aluminide coating applied by the Chromalloy American Corporation.

1

INTRODUCTION

1.1 BACKGROUND

The life-limiting components of aircraft gas turbine engines are typically the hot section airfoils that are exposed to high-temperature combustion gases. In striving to achieve maximum efficiency and power output, both materials and designs have aggravated the hot section problem. For example:

- Development of high-temperature alloys (including gamma/gamma prime precipitation strengthened superalloys, oxide dispersion strengthened superalloys, and directionally solidified eutectics) with improved strength and less environmental resistance.

- Extensive utilization of complex air cooling passages, especially in stage 1 blades and vanes, to minimize metal operating temperatures.

- Increase in thrust-to-weight ratio by reducing airfoil wall thickness.

The combination of the above factors have led to improved engine performance, generally at the expense of alloy resistance to the environment by decreasing chromium and aluminum levels and increasing the levels of strengthening element, e.g., tungsten, tantalum, columbium, etc. Therefore, oxidation and corrosion resistant coatings are often essential to the use of certain alloys. In addition, there has been increasing evidence of oxidation/corrosion attack occurring at internal surfaces of air-cooled blading. The combined degradation of internal and external surfaces can seriously compound the problem of achieving adequate service life, especially in thin walled components (0.5 mm [0.020 in.] or less).

A commonly found example is provided in Figure 1 which shows a cross section of an uncoated B1900 1st-stage blade (Fig. 2) from a JT-8D engine. Internal attack has consumed ten percent of the structural cross section. While this degree of attack would not necessarily be life-limiting in this engine component, it could seriously jeopardize the structural strength of an advanced blade design with wall thickness in the 0.5 mm range.

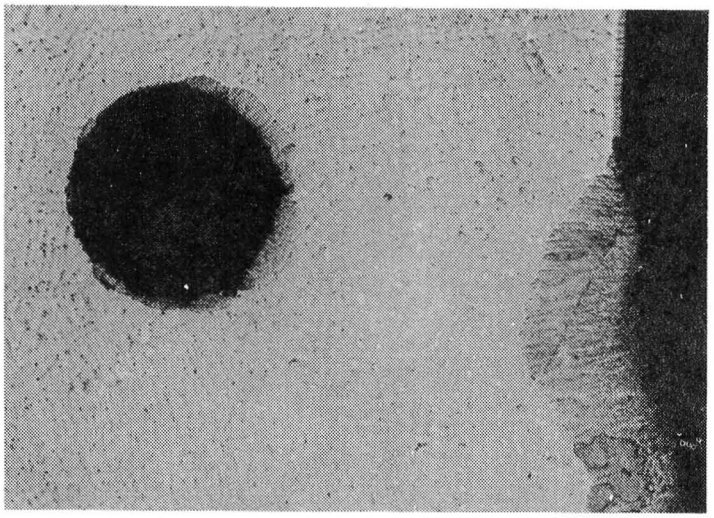

Magnification: 20X

Mount No. 7037

Figure 1. JT-8D First-Stage Blade (B-1900) Showing Internal Attack

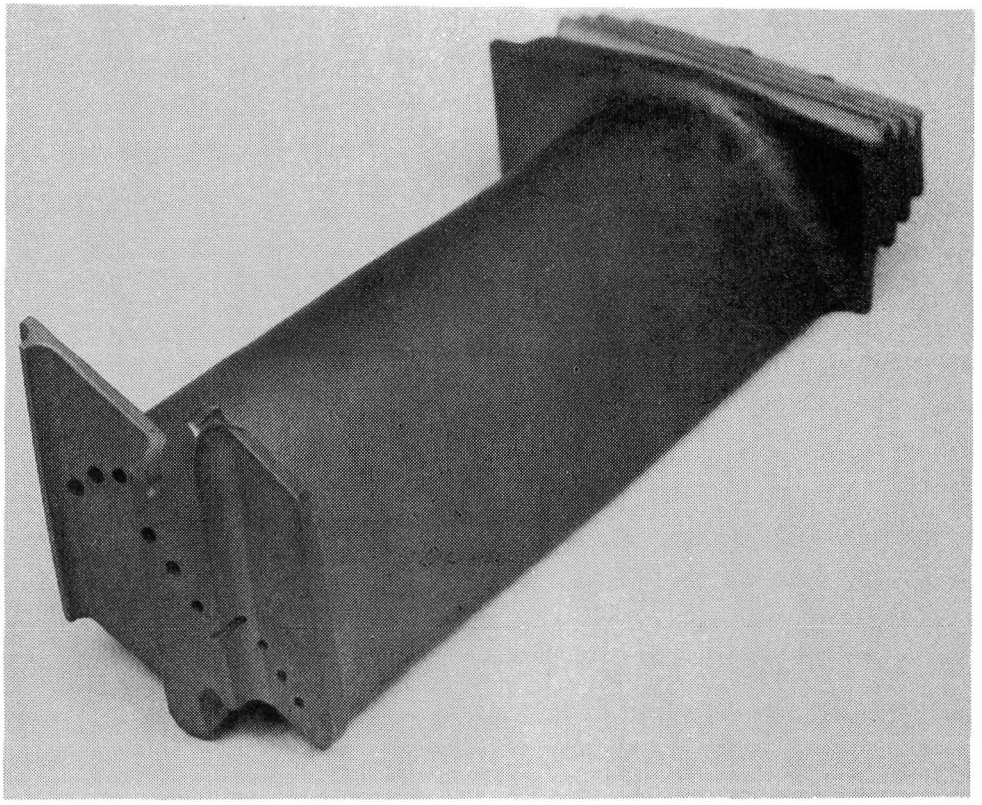

Figure 2. First-Stage Blade of JT-8D Engine - B-1900 Alloy

Protective coatings for external surfaces range from simple diffusion aluminides to multi-element overlay coatings and more recently, refractory oxide coatings. However, the application processes are generally not suitable for coating of complex internal surfaces or high aspect ratio cavities. A number of investigators (Refs. 1, 2, 3) have studied modifications of conventional processes, e.g., powder packs, slurry packs, chemical vapor deposition, fused salt electrolysis and electroless nickel plating. Most of these coatings depend on the availability of aluminum in the form of beta NiAl to form the refractory Al_2O_3 scale for oxidation resistance. The main difficulty encountered in all of these techniques is the control of the deposition process in the inaccessible areas in the serpentine passages such as in the cutaway view of the Mars stage 1 blade in Figure 3.

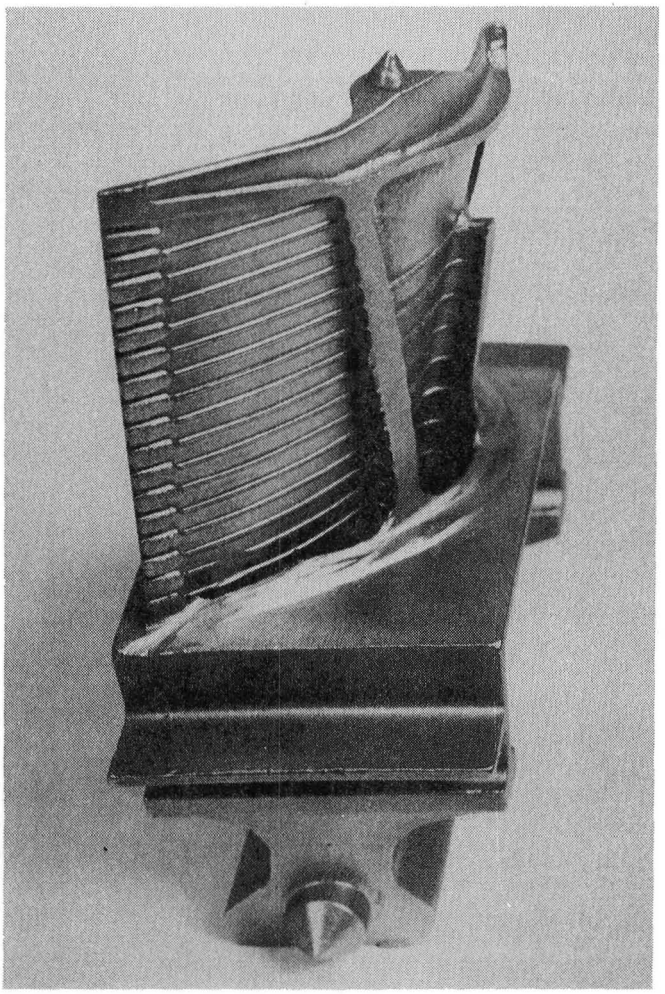

Figure 3.

Cut-Away View of Mars First-Stage Air-Cooled Blade

In a previous program (Ref. 4) both powder and slurry packs were investigated in the development of various diffusion aluminide coatings suitable for application to internal surfaces of air-cooled (DS) MAR-M200 + Hf blading. These coatings included Ni-Al, Ni-Al-Cb, Ni-Al-Cr, Ni-Al-Si, Ni-Al-Cr-Cb, and

Ni-Al-Cr-Si systems. Two significant conclusions from hot corrosion/oxidation burner rig testing and strain tolerance evaluation were: (1) Ni-Al-Cb and Ni-Al-Cr systems exhibited the most promising potential as ductile, resistant coatings; and (2) powder packs are easier to handle from the standpoint of pack removal than slurry packs since wet slurry compaction inside the blade promotes interparticle sintering. Based on the above conclusions, this investigation was performed to optimize the Ni-Al-Cb and Ni-Al-Cr systems for application to engine hardware. In addition, the earlier results indicated the unusual effect that approximately one weight percent columbium in the NiAl coating matrix, manifested significant enhancement of ductility relative to a similar columbium-free Ni-Al coating.

In this program, special emphasis was placed on columbium in the developmental coatings and an attempt was made to elucidate the role of columbium and its interaction with the coating matrix. While there is extensive utilization of columbium in various steels as a carbide strengthener and in gamma/gamma prime superalloys in solid solution strengthening and in formation of coherent stable intermetallic compounds such as $Ni_3(Cb,Al,Ti)$ (Ref. 5), little else is known about the effect of small quantities of columbium in an aluminide coating matrix. Another study (Ref. 6) reported an improvement in alloy hot corrosion resistance upon the addition of columbium and tantalum, within limits.

1.2 PROGRAM OBJECTIVES

The objectives of the program were to develop and optimize the Ni-Al-Cb and Ni-Al-Cr coating/processing systems for application to internal surfaces of air-cooled turbine blades. The developmental coatings were evaluated for hot corrosion/oxidation resistance in burner rig tests and selected coatings were evaluated in thermomechanical property tests. Finally, engine testing was performed to demonstrate the potential of the coating system as a solution to the internal oxidation/corrosion problems encountered with advanced blades.

1.3 PROGRAM PLAN

The following coating compositions were investigated:

- Variation A - Ni-19Al-1Cb
- Variation B - Ni-19Al-3Cb
- Variation C - Ni-17Al-20Cr
- Variation D - Ni-12Al-20Cr

These coatings were developed on hot isostatically pressed (HIPed) IN-792 superalloy test specimens and blades. The blade configuration selected for

this program was the stage 1 IN-792 + Hf blade of Solar's 10,000 hP Mars engine, see Figure 3.

The program was divided into three main tasks, as follows:

- Task I - Coating/Process System Development
- Task II - Coating/Process System Characterization
- Task III - Engine Test

This Page Intentionally Left Blank

2

EXPERIMENTAL

This section covers materials and provides details of test procedures and diagnostic techniques used in the program.

2.1 MATERIALS

Materials used in formulating powder packs are listed in Table 1.

Table 1

Program Materials For Powder Pack Processing

Material	Supplier	Analysis	Comments
Aluminum powder	Alcoa	-	201
Aluminum oxide	Norton	-	220 grit fused Al_2O_3
Chromium powder	Alcan	0.23 Fe, 0.04Ni, 0.03 Al, 0.035-0.01 C, 0.01 Si, 0.006 P	MD101 approximately 150 microns
Columbium powder	Teledyne Wah Chang	650 ppm O_2, 5 ppm H_2, 39 ppm N_2, 63 ppm Al, 63 ppm Fe, <50 ppm Si, 746 ppm Ta, <50 ppm C, balance Cb	-100 +325 mesh
Nickel powder	Glidden	0.005 C, 99.59 Ni	-325 mesh 96.3% <44 microns
Nickel oxide	Harshaw Chemical	-	-
Polyvinylchloride (PVC)	B.F. Goodrich	-	-

Tensile bars, rig pins and hourglass specimens per Solar Specification ES9-266 were obtained from Howmet. The specified composition of IN-792 Mod 5A alloy is given in Table 2 together with vendor's certified analysis of the program heat, No. PE001, used in casting test specimens. Solar's specification for this alloy includes hot isostatic pressing (HIP). HIP parameters are 1204°C (2200°F) at 103.4 MPa (15 ksi) for 4 hours. All castings were fully heat treated according to the following procedure:

- 1204°C (2200°F)/2 hours/rapid cool
- 1121°C (2050°F)/2 hours/rapid cool
- 843°C (1550°F)/24 hours/air cool.

Table 2

Composition of IN-792 Castings

Element	IN-792 Specification % Min	IN-792 Specification % Max	Analysis of Master Heat PE001 Test Specimens	IN-792 + Hf Specification % Min	IN-792 + Hf Specification % Max	Analysis of Heat CE024 Blades
Chromium	12.0	13.0	12.35	11.60	12.70	12.20
Cobalt	8.50	9.50	9.00	8.50	9.50	8.80
Titanium	3.75	4.20	3.99	3.90	4.25	4.18
Aluminum	3.15	3.60	3.40	3.30	3.70	3.30
Titanium + Aluminum	7.20	7.70	7.39	-	7.70	7.48
Tantalum	3.85	4.50	3.95	3.60	4.20	3.82
Molybdenum	1.65	2.15	1.95	1.65	2.15	1.85
Tungsten	3.85	4.50	3.95	3.50	4.10	3.62
Columbium	-	0.50	<0.10	-	-	-
Hafnium	-	-	-	0.40	0.60	0.55
Zirconium	0.01	0.05	0.02	0.03	0.07	0.10
Carbon	0.06	0.10	0.08	0.10	0.14	0.10
Boron	0.01	0.02	0.015	0.01	0.02	0.14
Silicon	-	0.20	0.02	-	0.20	<0.10
Manganese	-	0.15	0.01	-	0.15	<0.10
Sulfur	-	0.015	0.0014	-	0.015	0.0009
Phosphorus	-	0.015	0.001	-	0.015	0.001
Iron	-	0.50	0.12	-	0.50	0.08
Copper	-	-	-	-	0.10	<0.10
Lead	-	5.0 ppm	1.0 ppm	-	10 ppm	1 ppm
Bismuth	-	0.5 ppm	<0.3 ppm	-	0.5 ppm	<0.3 ppm
Silver	-	5.0 ppm	<5.0 ppm	-	5.0 ppm	-
Nickel	Bal	Bal	Bal	Bal	Bal	Bal

Test specimens received are shown in Figure 4. Inspection of radiographs furnished with the castings indicated no discontinuities or internal defects. Subsequent to this program, stage 1 blades were poured and a persistent hot tear problem near the blade platform was identified. This problem was resolved by going to a hafnium-containing IN-792 composition. Consequently, engine hardware, processed in the latter stages of the program, had approximately 0.5 weight percent hafnium in the alloy. Solar's specification for IN-792 + Hf differs only minimally from that of hafnium-free IN-792, as can be seen in Table 2. Because of the lower incipient melting point of the hafnium alloy, HIP parameters were modified to accommodate this.

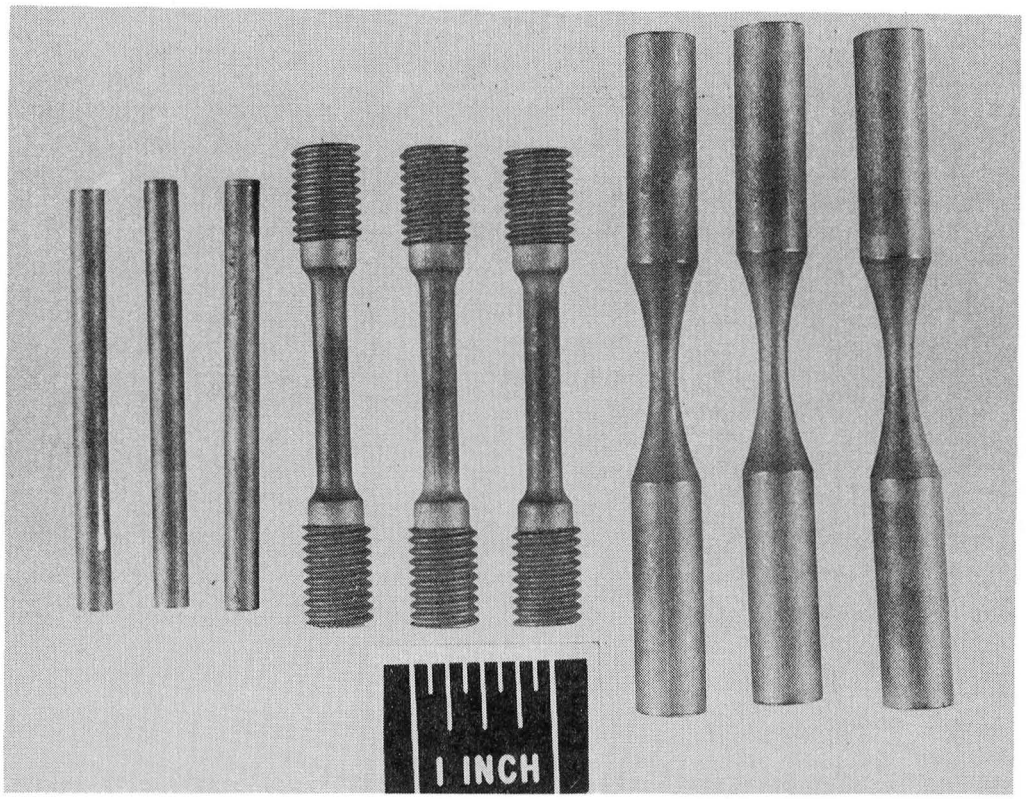

Figure 4. Cast and HIPed IN-792 Test Specimens

2.2 COATING APPLICATION PROCESS

The coating application process utilized in this program was the dry powder pack method. This method produces a diffusion aluminide coating with composition and phase distribution governed by pack activity and firing cycle as well as substrate alloy chemistry. Extensive studies (Refs. 7, 8, 9) have been conducted on formation of different types of aluminide coatings. The low activity alminide coatings studied in this work are formed by nickel diffusion outward in contrast to high activity packs where aluminum diffusion inward is the predominant mode.

2.3 EVALUATION TECHNIQUES

2.3.1 Hot Corrosion Burner Rig Testing

Complete details of Solar's environmental simulator burner rig test facilities have been given elsewhere (Refs. 4, 10) and are summarized here. Figure 5 shows a schematic of the burner rig system. An overall view of the burner rig and specimen are shown in Figure 6. An aviation fuel, JP-4, was used in all burner rig tests which had a sulfur content of 0.05 weight percent which met specified requirements.

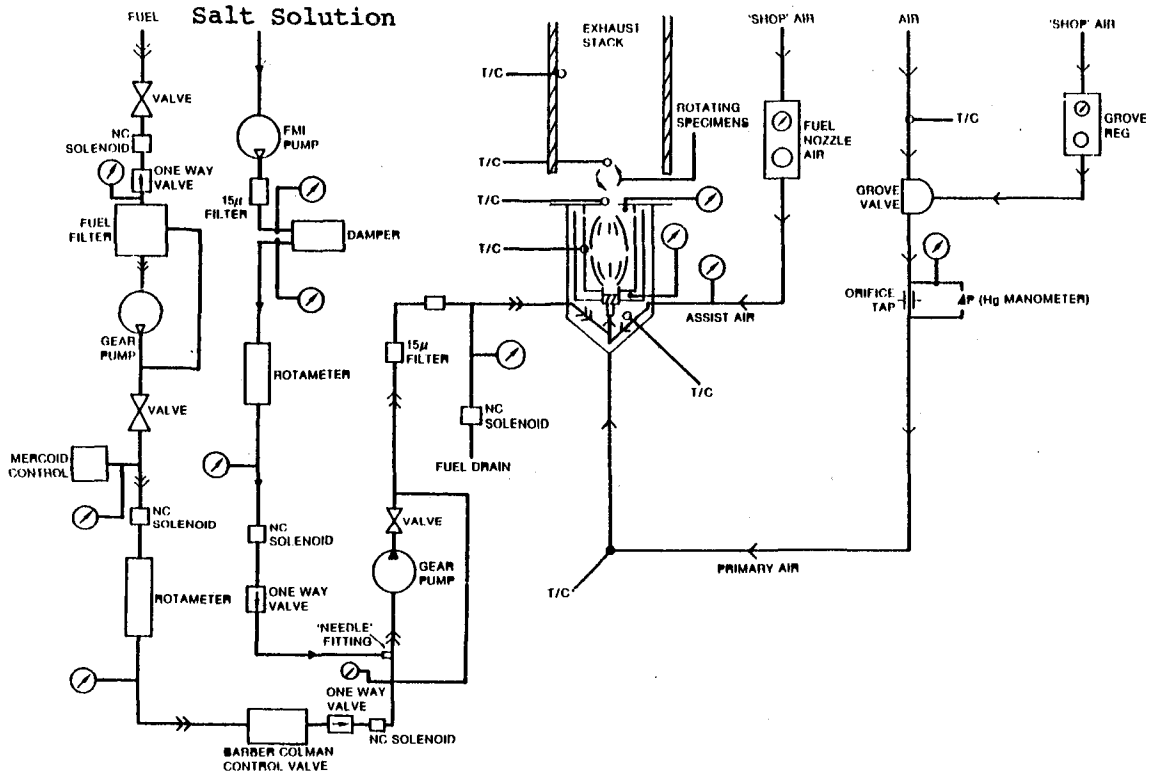

Figure 5. Schematic of Environmental Burner Rig

Synthetic sea salt solution was introduced into the fuel by means of a mixing gear pump which essentially breaks up the smaller volume of salt solution to form an emulsion. The salt composition was prepared according to Federal Test Method Std. 151, Method 812. Table 3 gives the weight percent of the various ions present in solution. The dispersion of salt in the fuel is shown in Figure 7, which is a fuel sample collected on a metal plate downstream of the mixing pump. Maximum diameter of the salt crystals is approximately 75 microns.

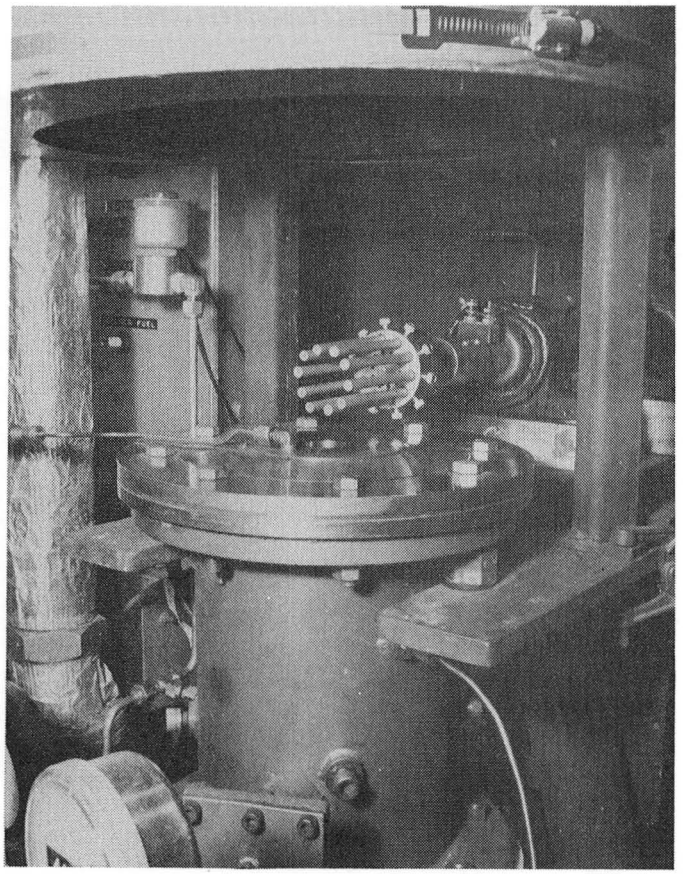

Figure 6.

Specimen Holder and Combustor of Environmental Simulator Burner Rig

Table 3

Synthetic Sea Salt

Ions	Wt %
Na^+	30
K^+	1
Mg^{2+}	4
Ca^{2+}	1
Cl^-	55
Br	2
SO_4^{2-}	7

The salt containing combustion gases are discharged to ambient pressure through a 25.4 mm diameter nozzle opening. The coated specimens are rotating approximately 25.4 mm above the plane of the nozzle, as shown in Figure 6 and 8. A sheathed (IN600) chromel-alumel 3 mm diameter thermocouple was inserted in a hollow control specimen which was fabricated from Hastelloy X and subsequently aluminized. The actual position of the thermocouple junction was determined on a trial and error basis in order to locate, as closely

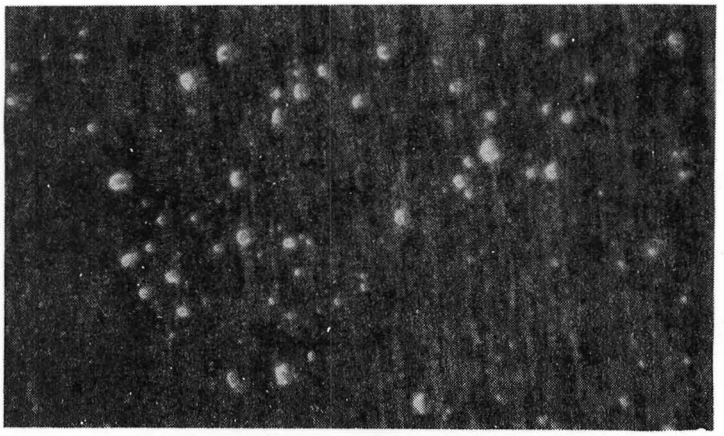

Magnification: 44X

Figure 7. Fuel Sample Collected on Metal Plate Showing Dispersion of Salt Solution in the Fuel

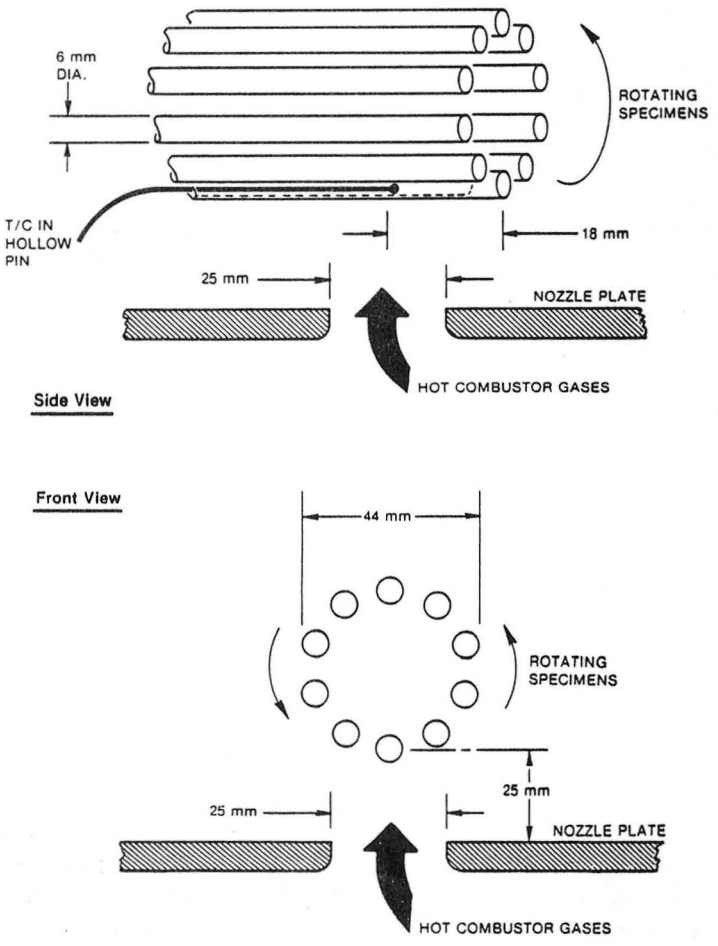

Figure 8. Sketch of Placement of Specimens Relative to Combustor Nozzle Plate

as possible, the hottest areas on the specimen. This thermocouple provided the triggering signal through a feedback loop to an electro-pneumatic fuel controller, thus regulating combustion and specimen temperature as desired. The outer surfaces of the test specimen circumscribes a circle of 44 mm diameter which exceeds the nozzle diameter of 25 mm. Since rotation is at 1725 rpm, it can be assumed that transients in and out of the hot gas zone are minimized, especially since expansion and perturbation of the gas stream by the specimens produces noticeable widening of the flow of combustion gases. For the purposes of this test, temperature readings obtained with a calibrated optical pyrometer are reported as the specimen test temperature. In-house studies have indicated that the hot test area of these rotating specimens lies on the inside face where radiation and convection heat losses are kept to a minimum by the semicontinuous ring of specimens. However, due to ready assessibility by optical pyrometry, the outside face temperature is monitored and reported.

Temperature values based on radiation phenomena have been corrected, assuming an emissivity of 0.9 (see Ref. 11 for values given for oxidized 80Ni-20Cr alloy) for an effective radiation wavelength of 0.653 micron. Table 4 lists the operating parameters of hot corrosion testing.

Table 4

Burner Rig Test Parameters For Hot Corrosion Tests

Specimen temperature(1)	899 ±28°C (1650 ±50°F)
Gas temperature (2)	1088 ±28°C (1990 ±50°F)
Ambient air temprature(3)	10-27°C (50-80°F)
Air flow	4.49 kg/min
Fuel flow (JP-4)	0.128 kg/min
Air-to-fuel ratio	38
Mach number	0.9
Gas velocity	600 m/sec
Salt level in air	4 ppm
Cycle	1-hour to 100°C

(1) Temperature as measured with an optical pyrometer corrected for emissivity.
(2) Maximum calculated value at vena contracta.
(3) Wide range due to extremes in daily temperature.

2.3.2 Dynamic Oxidation Burner Rig Testing

The experimental setup for oxidation rig test was basically identical to the hot corrosion test with one exception. No salt solution was added to the JP-4 fuel. Control system and operating procedures were also similar and test parameters are summarized in Table 5.

Table 5

Burner Rig Test Parameters for Oxidation Testing

Specimen temperature(1)	1050 ±28°C (1920 ±50°F)
Gas temperature (2)	1418 ±28°C (2580 ±50°F)
Amient air temprature(3)	15-32°C (60-90°F)
Air flow	4.6 kg/min
Fuel flow (JP-4)	0.170 kg/min
Air-to-fuel ratio	28
Mach number	0.9
Air velocity	670 m/sec
Salt level in air	None
Cycle	1-hour to 100°C

(1) Temperature as measured with an optical pyrometer corrected for emissivity.
(2) Maximum calculated value at vena contracta.
(3) Wide range due to extremes in daily temperature.

Specimen configuration was modified from the standard solid 6 mm diameter by 76 mm bar to that shown in Figure 9. The entire external surfaces of the specimen was coated as well as the internal surfaces of the 25 mm deep bore. It was believed at the time that this configuration had the advantage of allowing both externally and internally processed coatings to be evaluated. The externally processed coating was exposed directly to the high-velocity hot gas stream while the internally processed coating was expected to be the same temperature, although in a quasi-static environment. Even though this is a simple approximation of the internal surfaces of air-cooled blades, oxidation phenomenon was expected to differ, reflecting the differences between aerodynamics and composition of the two gaseous environments.

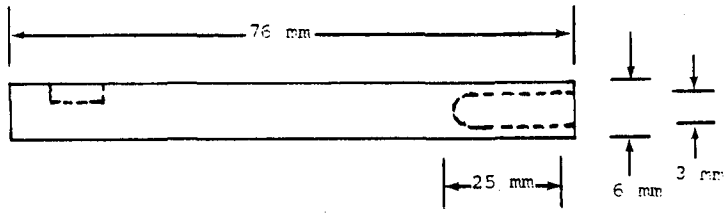

Figure 9. Sketch of Modified Burner Rig Specimen For Oxidation Testing

2.3.3 Mechanical Property Tests

Three mechanical property tests were performed on coated and heat treated specimens. These were tensile, stress rupture, and high cycle fatigue. The stress rupture tests were performed with standard procedures. The details of the tensile and fatigue tests are noted below.

- Tensile testing - Strain rate 0.127 mm/mm/min. (0.005 in./in./min.) to 0.2 percent offset strain and 1.27 mm/mm/min. (0.050 in./in./min.) to failure. Strain curves were recorded on each specimen.

- Fatigue testing - Fatigue testing was performed with an axial fatigue machine. The machine was of the combination mechanical/hydraulic type. Figure 10 shows the machine with specimen and furnace installed. Fatigue loads were measured dynamically during test and temperature of the specimen was controlled to $\pm$6°C. An A ratio of 1 was used, and cycle frequency was 30 Hz.

2.3.4 Strain Tolerance Testing

The ductility of the coatings were evaluated in a strain-to-cracking test which is basically an interrupted tensile test. The specimens were loaded onto the testing machine and brought to temperature. A series of temperatures were selected between ambient and 649°C (1200°F), and at each temperature the specimen was incrementally strained until coating cracks appeared. The strain rate was kept at 0.86 mm/mm/min (0.034 in./in./min) and the strain increments were varied according to the strain tolerance of each coating. After each increment, the test specimens were cooled, unloaded, and dye penetrant examined for cracks. The process was continued until cracking was initiated.

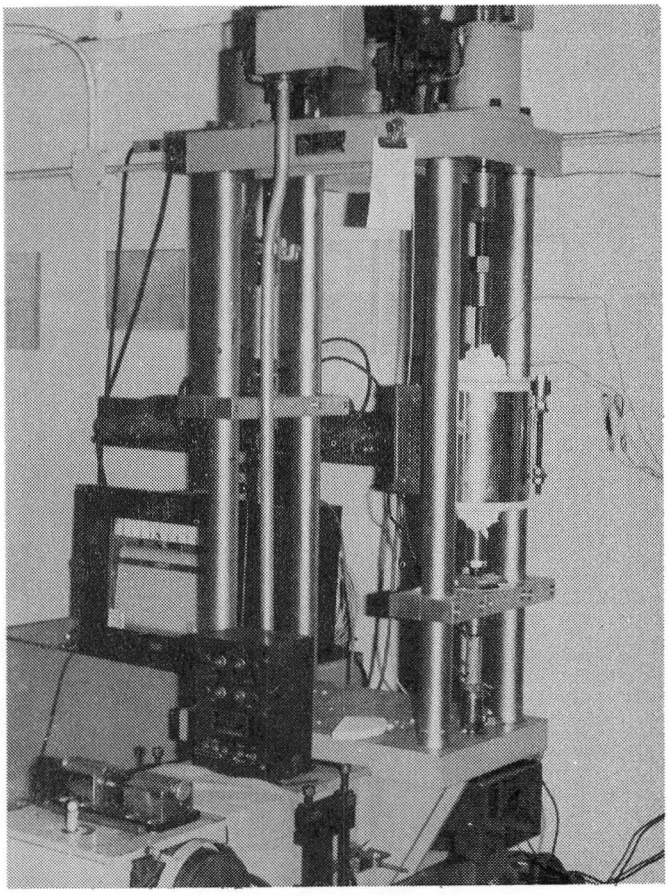

Figure 10.

Axial Fatigue Machine With Furnace and Pull Rods Installed

3

TASK I - COATING/PROCESS SYSTEM DEVELOPMENT

The four candidate coatings can be grouped into two coating systems, Ni-Al-Cb and Ni-Al-Cr. Discussion of process development will be presented under these two subsections and will be followed by aspects of process development common to both coating systems such as pack removal, mass flow, masking and process reproducibility.

- Ni-Al-Cb coating systems
- Ni-Al-Cr coating systems
- Processing considerations
  - Masking
  - Reproducibility
  - Pack removal and particle sintering
- Application to engine hardware.

The coating development work was conducted on solid test specimens, such as shown in Figure 11. Even though these coatings were developed for internal application, coupon specimens were used which were actually coated in an external manner. A distinction should be made here regarding external and internal pack application besides the obvious physical implication of external and internal confinement of the activated pack powder. In the case of the former, gas phase diffusion can be treated as occurring between a constant surface activity and an infinitely extended medium, or pack. In contrast to this, the internal pack process is basically limited by the volume of pack in the internal cavity and aluminum transport to the surface is restricted accordingly.

3.1 Ni-Al-Cb COATING SYSTEMS

The powder pack method was used in development of the two columbium-containing coatings, Ni-19Al-1Cb (Variation A) and Ni-19Al-3Cb (Variation B). The desired compositions were obtained in two steps, initial deposition of columbium to the specimen surface followed by a second pack aluminization cycle. The advantage of this duplex process is the added versatility for varying the amount of coating elements deposited through control of pack composition.

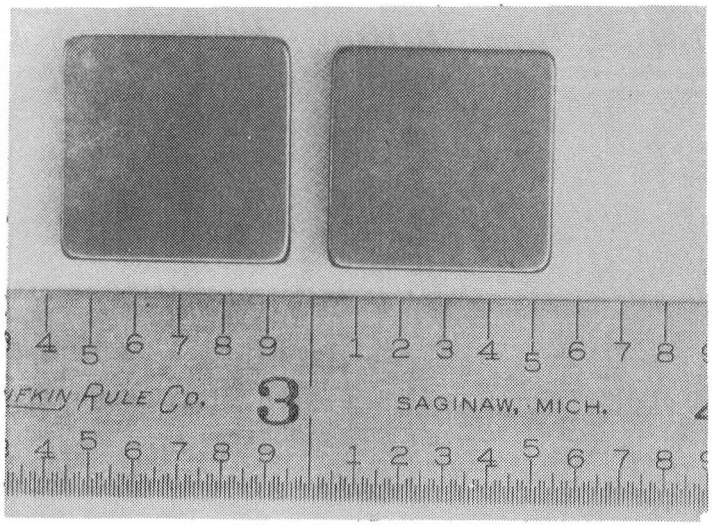

Figure 11.

IN-792 Test Specimens

Initial coating development work with formation of columbium diffusion coatings on IN-792 specimens used two pack formulations; 75Cb-25Al_2O_3 and 50Cb-50Al_2O_3. Each pack was activated with 0.5 percent polyvinyl chloride (PVC) and the specimens were completely surrounded by the pack powder. The sealed retorts were argon purged and fired at 1121°C (2050°F) for six hours. However, repeated runs were not reproducible in both weight gain and surface appearance. Figure 12 shows both sides of a specimen fired in the 75Cb-24Al_2O_3 pack which resulted in a weight gain of 0.8 mg/cm^2. Previous work (Ref. 4) showed that this pack composition and process parameters produced approximately 0.5 mg/cm^2 of columbium on MAR-M200 + Hf alloy. However, since that alloy contains about 0.8 to 0.9 percent columbium, while IN-792 Mod 5A is specified to contain <0.5 percent, it is expected that the latter would provide a greater driving force for the diffusion of columbium from the pack vapors. Another attempt at columbium diffusion under similar conditions resulted in edge spallation, as shown in Figure 13. In this case, though, it was suspected that the furnace control system malfunctioned during the test and overheating can result in chemical reduction of columbium halides at a considerable distance from the substrate surface (Ref. 12). This would produce non-adherent deposits which will spall upon cooldown. X-ray fluorescent analysis (using Cb-752 alloy as standard) of specimens in Figure 13 revealed that the columbium count was high in both spalled and unspalled areas, >20 percent.

Besides the non-adherent deposits, another phenomenon was also observed, particle sintering. Similar observations were noted by Gadd, et al (Ref. 13) regarding the sintering of fine refractory metal particles to the substrate surface and it was noted that this problem can be minimized by reducing pack diffusion temperature. In doing so, heavier deposits would be difficult to attain. However, since the nominal compositions for the columbium coating are 1 and 3 weight percent, this was not expected to be limiting.

Subsequently, a series of specimens were processed in columbium powder packs fired at lower temperatures, as noted in Table 6. The weight gain values range between 4.4 and 5.0 mg/cm^2 and surface appearances were uniformly matte

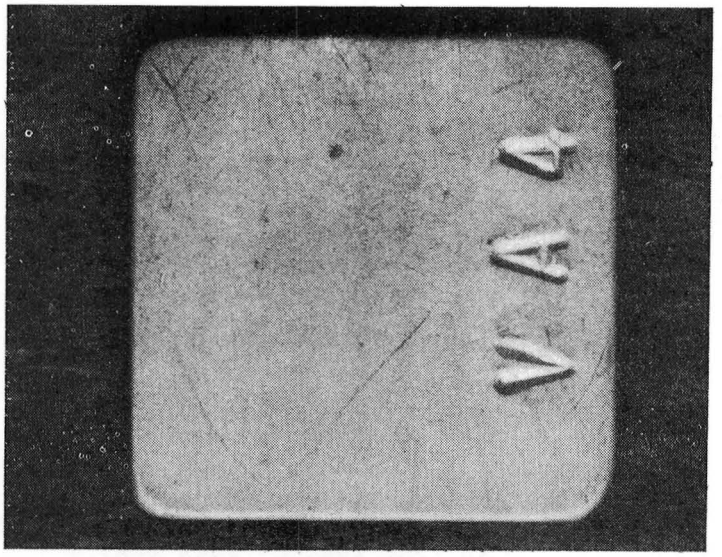

Front

Magnification: 5X

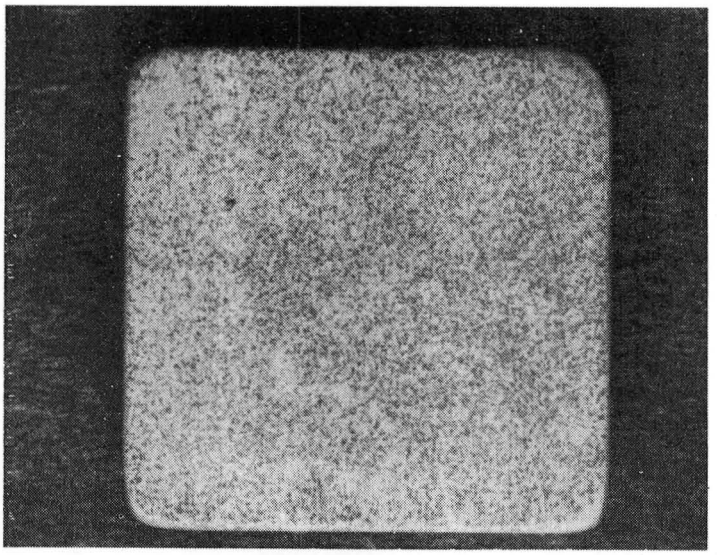

Back

Magnification: 5X

Figure 12. Columbium Coated IN-792 Specimen Processed in 75Cb-25Al_2O_3 Pack (No. VA3). Note Inconsistent Surface Appearance

grey. The packs contained varying amounts of columbium, from 20 to 75 percent, but since pack activity was kept at unity, the coating process was independent of the amount of elemental columbium. In addition, all four packs were prepared in the same bulk batch and processed identically, thus eliminating further variations due to handling procedures. The microstructure of a typical coated specimen, shown in Figure 14, is observed to be uniform and 18 microns thick.

In past work (Ref. 4) a pack of composition 60Al_2O_3-24Ni-16Al-0.5PVC (Al/Ni ratio is 0.67) was used to form Ni-20Al on MAR-M200 alloy. IN-792 and MAR-M200 contain 3.30 and 4.95 percent aluminum, respectively. The lower

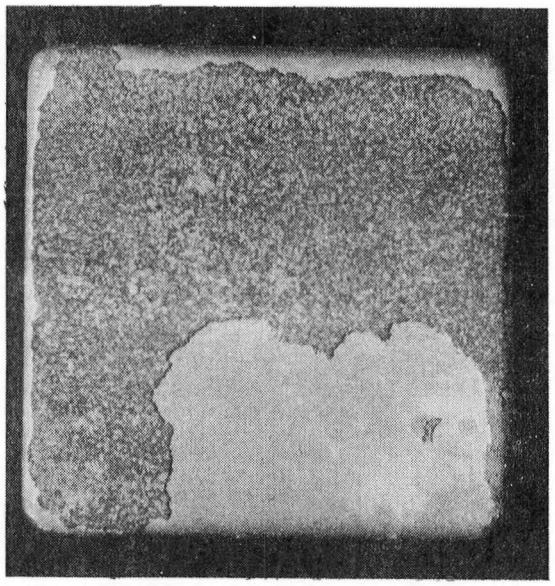

Figure 13.

Spalled Specimen Processed in 75Cb-25Al_2O_3 Pack (VA5)

Table 6

Pack Diffusion of Columbium on IN-792, Mod 5A (HIPed) Test Specimens

Specimen Number	Pack Composition (weight percent)	Furnace Cycle (°C/Hrs)	Weight Gain (mg/cm^2)
VA9	20Cb-80Al_2O_3-0.5PVC*	990/6	4.6
VA10	50Cb-50Al_2O_3-0.5PVC	990/6	5.0
VA11	75Cb-25Al_2O_3-0.5PVC	990/6	4.4
VA12	75Cb-25Al_2O_3-0.5PVC	990/6	4.8

* PVC = polyvinyl chloride

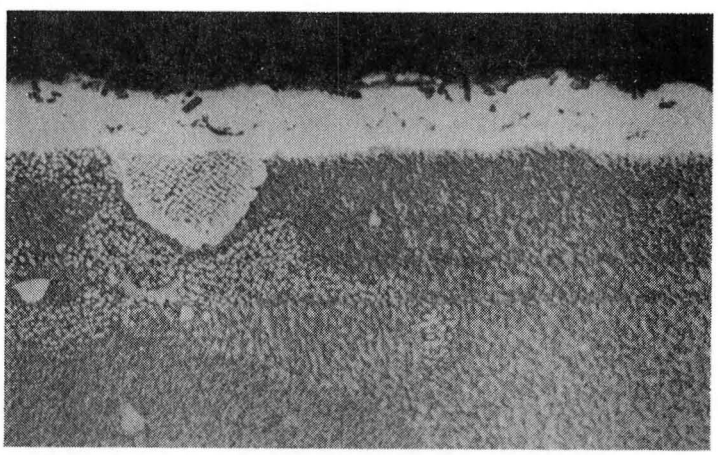

2% Chromic Etch

Magnification: 500X

Mount No. 9131

Figure 14. Typical Microstructure of Columbium Coated IN-792 Specimen (VA9)

aluminum level in the former alloy would conceivably produce a greater aluminum concentration gradient and hence increased potential for diffusion. The two specimens, VA10 and VA11, were aluminized in the above-mentioned controlled activity pack for 16 hours at 1050°C and their respective weight gains were 5.7 and 6.0 mg/cm^2. Once again, the two values were in close agreement. A typical microstructure of columbium and aluminum coated IN-792 is shown in Figure 15.

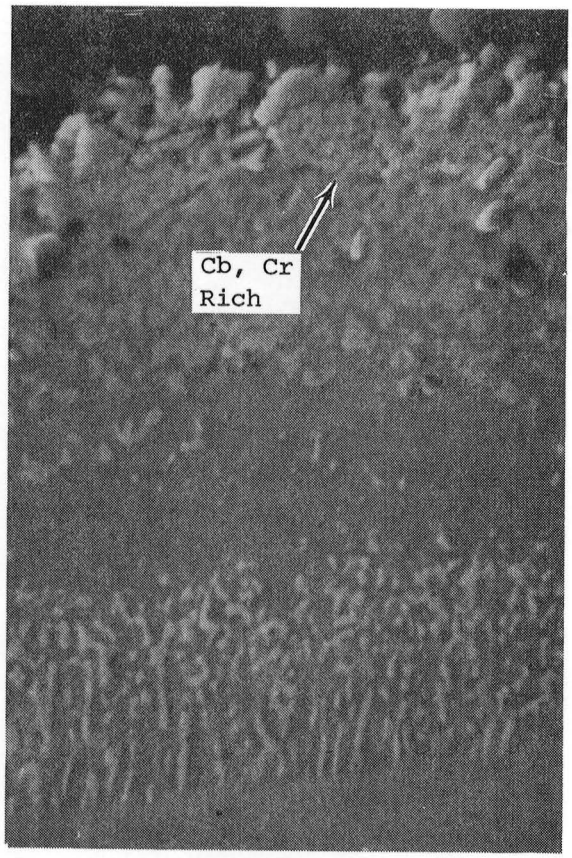

Magnification: 1600X

Mount No. 9180

Figure 15. SEM Photomicrograph of Columbium and Aluminum Coated IN-792 Test Specimen (VA10)

The coating appears to be layered structurally with some porosity near the outer portions and a single-phase zone in the center. The matrix is comprised of a grey phase with a concentration of light grey secondary phases in two zones, one near the outside and the other near the interface. SEM/EDX analysis indicated that the light grey phase near the outside was rich in columbium and chromium.

With the aid of the SEM and EDX analysis, using the substrate alloy as standard, an approximate composition was determined for this particular coating; Ni-15 to 19Al-3 to 5 Cb. This agrees well with the desired program composition, Ni19Al-3Cb.

To achieve the other coating variation, Ni-19Al-1Cb, the firing temperature was reduced to 930°C and the furnace time was held to 4 hours. Specimen VA15, processed under these conditions, was found to have a negative weight gain. However, Xray fluorescent analysis (with IN-738 and Cb752 as standards) revealed the presence of 1.2 weight percent columbium. It can be deduced that simultaneous depletion of the alloy had also occurred during the process, possibly by chromium loss, to react with the columbium in the pack. In the work by Gadd, et al (Ref. 13), it was pointed out that a reversal in vapor phase transfer could occur in refractory metal packs. Since the thermodynamic stability of the halides is similar to or greater than the refractory metal halide, the initial transfer of refractory metal decreases as the metal is lost from the substrate onto the high surface area of the pack particles. Consequently, progressive poisoning of the refractory pack material could occur over an extended time period due to the reversed transfer. Eventually, the effective refractory metal surface area and hence concentration becomes sufficiently low and columbium deposition tapers off.

Therefore, it was not unusual to note varying amounts of specimen weight gain/loss in the 1Cb pack process. Subsequent work indicated that even with negative weight gain values, the specimen surface exhibited a noticeable increase in columbium content, thus providing support to the reversed deposition argument.

A summary of the processes utilized in application of Ni-19Al-1Cb (Variation A) and Ni-19Al-3Cb (Variation B) coatings is given in Table 7. A detailed process specification is included as Appendix A for these columbium coatings as well as the chromium coatings reported in Section 3.2. Using these process specifications, 16 test specimens were processed in two lots with each of the Ni-Al-Cb coatings. The objective was to establish characteristic microstructures and demonstrate process reproducibility.

Table 8 shows the weight change data of the test specimens after columbium and aluminum deposition. Again, it was noted that specimens VA22, VA23, VA26 to VA28 exhibited weight loss after the 1Cb pack cycle. X-ray fluorescent analysis (using IN-738 and Cb752 standards) confirmed that columbium was present at the substrate surface in concentrations ranging between 0.9 and 1.3 weight percent. Aluminum weight gain for all test specimens were in the range of 9 to 10 mg/cm^2 except for VB35 to VB38 which had lower values.

Typical microstructures of Variation A, Ni-19Al-1CB, are shown in Figures 16 and 17. In the as-coated condition, specimens VA22 and VA26 were coated to 76 and 72 microns, respectively. The coating is a two layered structure. The outer zone is characterized by small, light colored dispersed phases while the inner zone etched a lighter grey comparable to the gamma/gamma prime in the substrate. After heat treating, diffusion caused the coating to grow in thickness by 18 to 19 percent from 76 to 90 microns and 72 to 86 microns. Most of the growth appeared to have occurred in the darker grey outer zone while the inner zone remained constant. At the same time, partial breakdown of the once homogeneous grey zone can be observed (especially in Fig. 17, No. VA27) as nickel and aluminum interdiffusion continued and the amount of beta is decreased. Similar interdiffusional effects can also be seen in the inner zones and a distinct light interfacial zone appeared.

Table 7

Summary of Process Parameters for Application of Ni-Al-Cb Internal Coatings

Coating Variation	Nominal Composition	Pack Composition (Wt. %)	Furnace Cycle (°C/Hrs)
A	Ni-19Al-1Cb	50Cb-50Al_2O_3-0.5PVC (P100) 60Al_2O_3-24Ni-16Al-0.5PVC (P200)	930/4 1050/16
B	Ni-19Al-3Cb	50Cb-50Al_2O_3-0.5PVC (P100) 60Al_2O_3-24Ni-16Al-0.5PVC (P200)	990/6 1050/16

Table 8

Batch Processing of Ni-Al-Cb Coatings

Specimen Number	Weight (mg/cm^2)		Total Weight Gain (mg/cm^2)
	Columbium Deposition	Aluminum Deposition	
Variation A (Ni-19Al-1Cb)			
VA21	0.04	9.27	9.31
VA22	-0.08	10.08	10.00
VA23	-0.02	9.64	9.62
VA24	0.04	9.54	9.58
Avg.	-	9.63	9.63
VA25	0.29	-	-
VA26	-0.08	9.37	9.29
VA27	-0.04	9.29	9.25
VA28	-0.06	9.45	9.39
Avg.	-	9.37	9.31
Variation B (Ni-19Al-3Cb)			
VB31	2.77	-	-
VB32	3.77	8.99	12.76
VB33	3.64	9.67	13.31
VB34	3.29	10.92	13.88
Avg.	3.29	9.86	13.32
VB35	3.56	-	-
VB36	3.86	6.66	10.52
VB37	3.73	7.06	10.79
VB38	3.82	6.99	10.81
Avg.	3.74	6.90	10.71

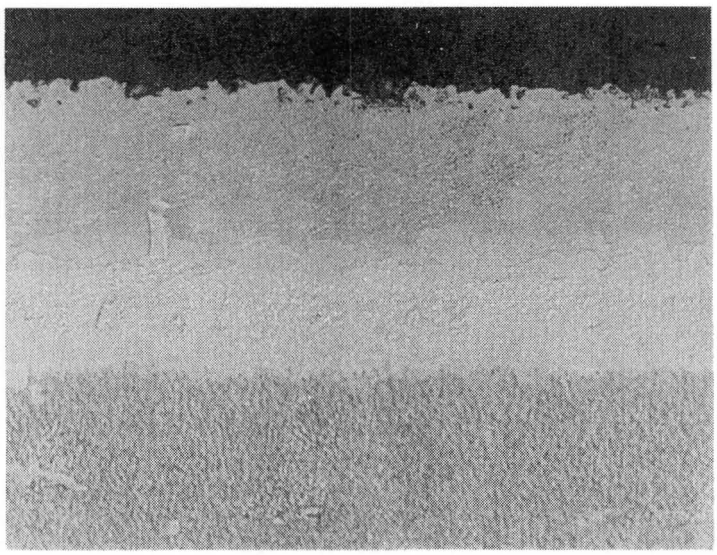

Specimen VA22

Ni-19Al-1Cb Coated

10% Electrolytic Oxalic Etch

Magnification: 500X

Mount No. 9507

Specimen VA23

Ni-19Al-1Cb Heat Treated

Magnification: 500X

10% Electrolytic Oxalic Etch

Mount No. 9507

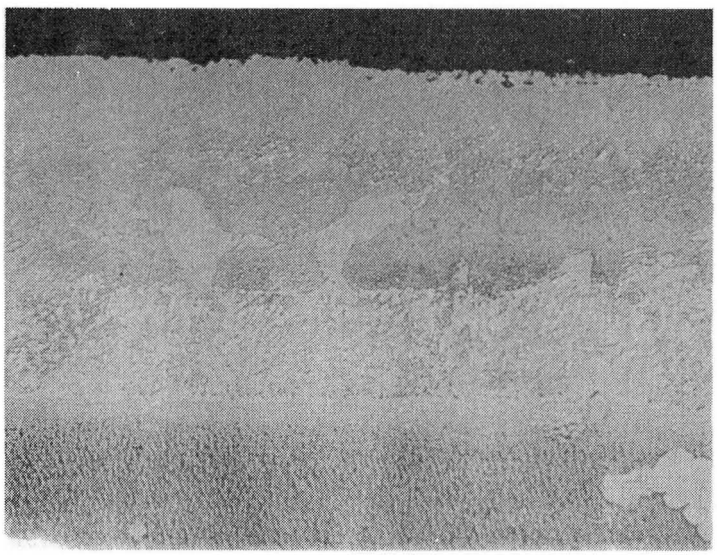

Figure 16. First Batch of Ni-19Al-1Cb (Variation A) Coated IN-792 Specimens.

The next set of photomicrographs, Figures 18 and 19, are of Variation B, Ni-19Al-3Cb. Deposition of columbium was found to have penetrated 12 and 14 microns, respectively. A line of small voids is in evidence at the mid-point of the coating which may or may not be of the Kirkendall type. There is also very fine (clearly visible only at 4000X) voids in the outer coating region. The large included material in this coating is due to inclusion of angular alumina particles from the pack. As can be seen, Figures 18 and 19, in subsequent aluminization of this layer the voids in the columbium-rich layer are not retained. The aluminized layer of the Ni-19Al-3Cb coating is of the typical low activity type with an outer beta NiAl layer with inclusions, a diffusionally clean denuded zone of essentially pure beta NiAl and/or mixed beta NiAl-gamma Ni_3Al plus other secondary phases. After heat treatment a

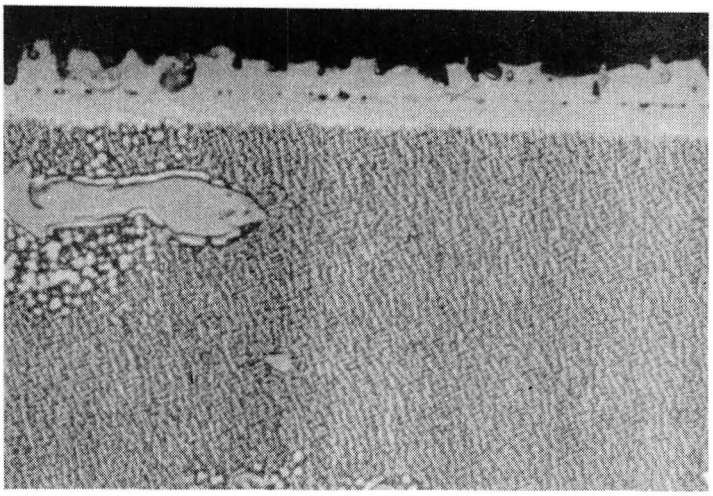

Specimen VA25

Columbium Deposit Only

Magnification: 1000X

10% Electrolytic Oxalic Etch

Mount No. 9508

Specimen VA26

Ni-19Al-1Cb Coated

Magnification: 500X

10% Electrolytic Oxalic Etch

Mount No. 9508

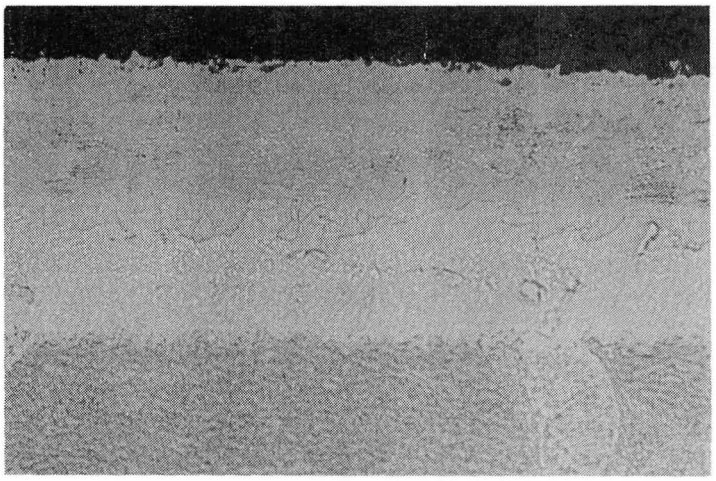

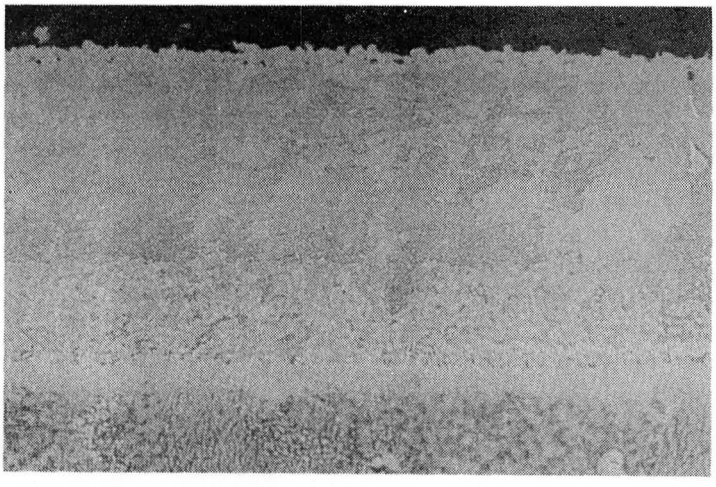

Specimen VA27

Ni-19Al-1Cb Heat Treated

Magnification: 500X

10% Electrolytic Oxalic Etch

Mount No. 9508

Figure 17. Second Batch of Ni-19Al-1Cb (Variation A) Coated IN-792 Specimens

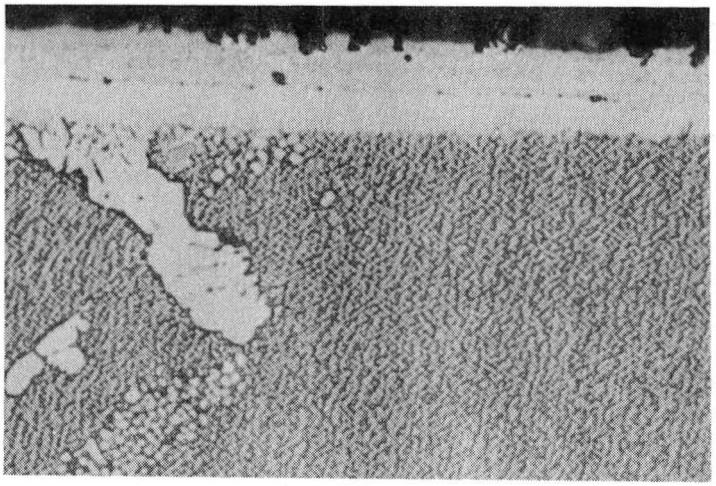

Specimen VB31

Columbium Deposit Only

Magnification: 1000X

10% Electrolytic Oxalic Etch

Mount No. 9509

Specimen VB32

Ni-19Al-3Cb Coated

Magnification: 500X

10% Electrolytic Oxalic Etch

Mount No. 9509

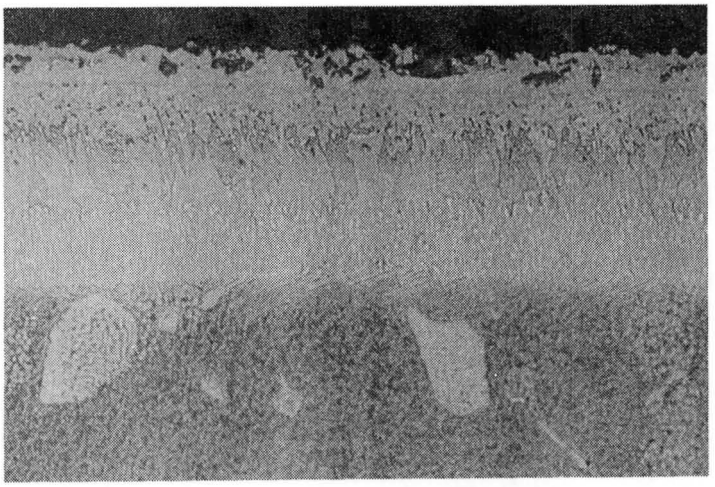

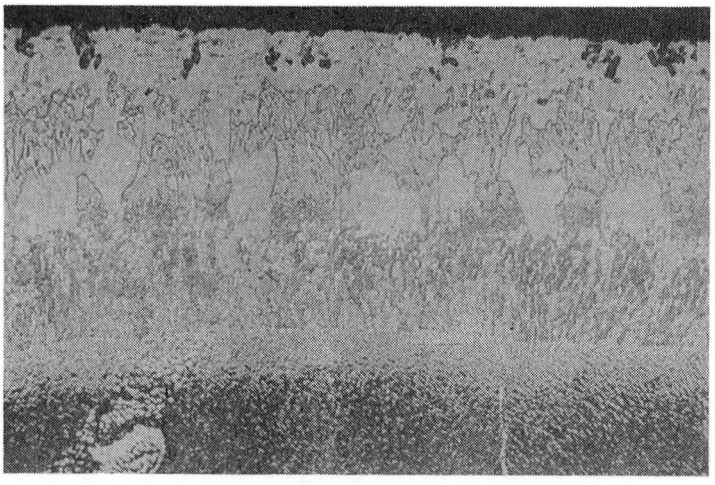

Specimen VB33

Ni-19Al-3Cb Heat Treated

Magnification: 500X

10% Electrolytic Oxalic Etch

Mount No. 9509

Figure 18. First Batch of Ni-19Al-3Cb (Variation B) Coated IN-792 Specimens

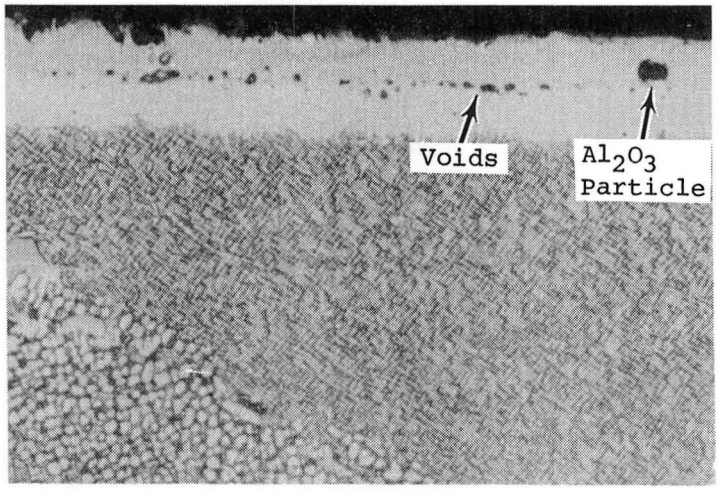

Specimen VB35

Columbium Deposit Only

Magnification: 1000X

10% Electrolytic Oxalic Etch

Mount No. 9510

Specimen VB36

Ni-19Al-3Cb Coated

Magnification: 500X

10% Electrolytic Oxalic Etch

Mount No. 9510

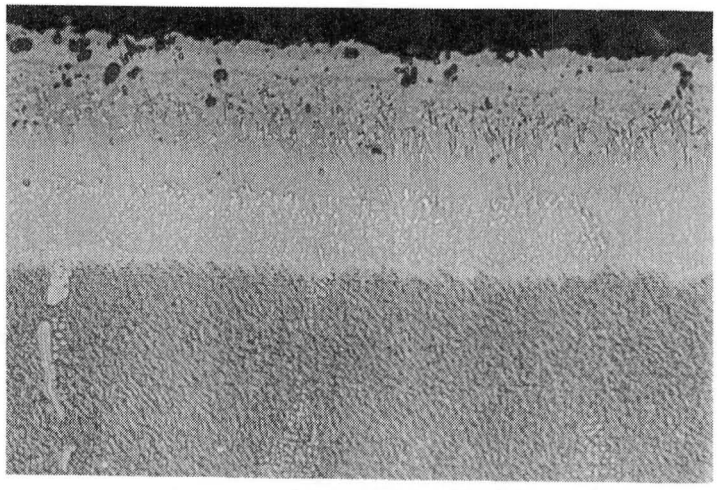

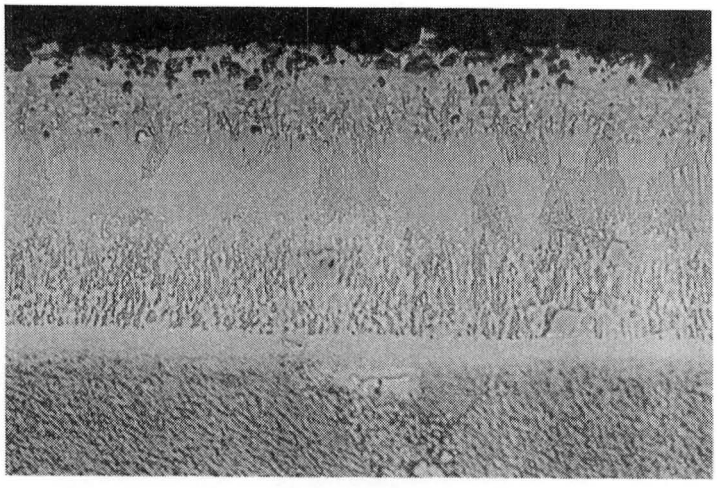

Specimen VB37

Ni-19Al-3Cb Heat Treated

Magnification: 500X

10% Electrolytic Oxalic Etch

Mount No. 9510

Figure 19. Second Batch of Ni-19Al-3Cb (Variation B) Coated IN-792 Specimens

continuous layer is formed at the substrate/coating interface. Except for the complexity of the outer layer, this coating is similar to the Ni-19Al-1Cb coating.

The Ni-Al-Cb coating specification is presented in Appendix A.

3.2 Ni-Al-Cr COATING SYSTEMS

The nominal composition of the two chromium-containing coatings are Ni-17Al-20Cr (Variation C) and Ni-12Al-20Cr (Variation D). The higher aluminum coating, which should provide better environmental resistance, was expected to be more brittle than the 12 percent aluminum coating, which closely simulates the NiCrAlY class of coatings but minus the <0.5 percent yttrium.

IN-792 specimens were found to be successfully chromized using $80Al_2O_3$-20Cr-0.5NaCl packs fired at 1060°C for 4 hours, Table 9. The resultant microstructure is shown in Figure 20. The coating, approximately 20 microns thick, has a wide interface region consisting of a light grey phase separated by a slightly darker boundary phase. Specimens VC5 and VC6 were aluminized at 1050°C for 16 hours in $60Al_2O_3$-24Ni-16Al-0.5PVC (Al/ Ni = 0.67). A photomicrograph of the coating is shown in Figure 21. Coating thickness is about 70 microns. A light grey phase(s) can be found near the interface and lightly dispersed in the other regions of the coating. A SEM micrograph of the same specimen is shown in Figure 22; the light grey phase near the interface was found to be tungsten- and tantalum-rich in a gamma prime matrix extending into the substrate. The light areas near the surface of the coating are high in chromium. The overall composition of the coating, as compared to the substrate, was determined to be Ni-14Al-24Cr. This lies within the $\pm$20 percent tolerance limit of the Ni-12Al-20Cr composition.

The fourth program composition was Ni-20Cr-17Al. In order to increase aluminum deposition under the same process parameters, the activity of the pack was increased to $60Al_2O_3$-22Ni-18Al-0.5PVC (Al/Ni = 0.82). After 16 hours at 1050°C, the weight gain was found to be 15.8 mg/cm^2. The coating formed was higher in aluminum than desired and is mostly beta phase. It was estimated that the desired pack would have an intermediate activity of $60Al_2O_3$-17Al-23Ni-0.5PVC (Al/Ni = 0.74). EDX analysis of specimens processed in this pack indicated that the aluminum concentration was within 20 percent of the nominal composition.

A series of specimens were coated with each of the packs in two batches and coating data are reported in Table 10. The chrome pack deposited on the average 2.49 mg/cm^2 with a standard deviation of 0.38 mg/cm^2. Except for batch VD51 to VD54, the other three batches of chrome coated specimens show good agreement in weight gain. The aluminization of these chromized specimens fell in two areas, the 17Al coating gained an average of 15.48 mg/cm^2 while the 12Al coating gained 9.55 mg/cm^2.

Table 9

Chromized IN-792 Specimens
(Pack: $80Al_2O_3$-20Cr-0.5PVC, 1060°C/4 Hours)

Specimen Number	Area (cm^2)	Weight Gain (mg/cm^2)
VC5	5.2	4.5
VC6	5.3	4.5
VD5	5.2	4.3
VD6	5.2	4.6
VD7	5.3	4.5
VD8	5.1	4.4

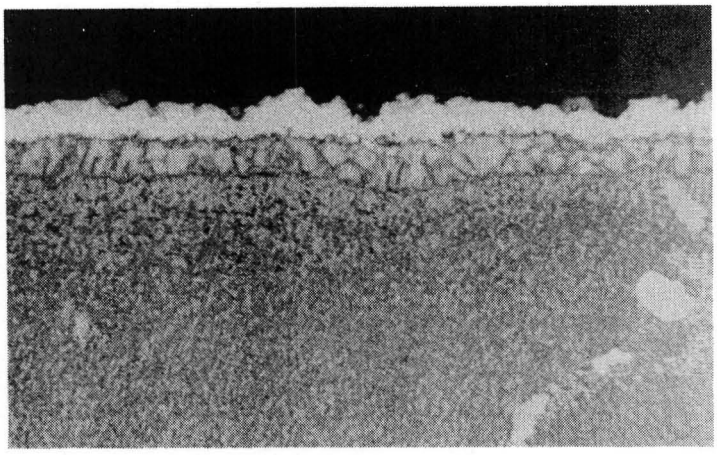

Magnification: 500X

2% Chromic Etch

Mount No. 9135

Figure 20.

Microstructure of Chromized IN-792 Specimen VC1

Magnification: 1000X

Mount No. 9180

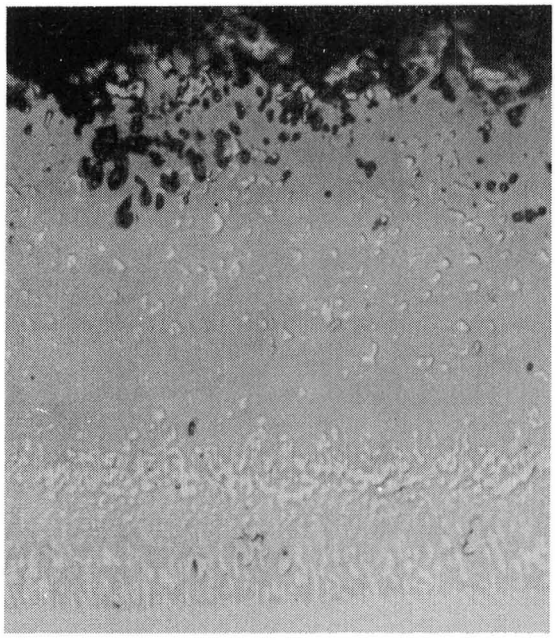

Figure 21.

Microstructure of Aluminum Coated IN-702 Specimen VC5

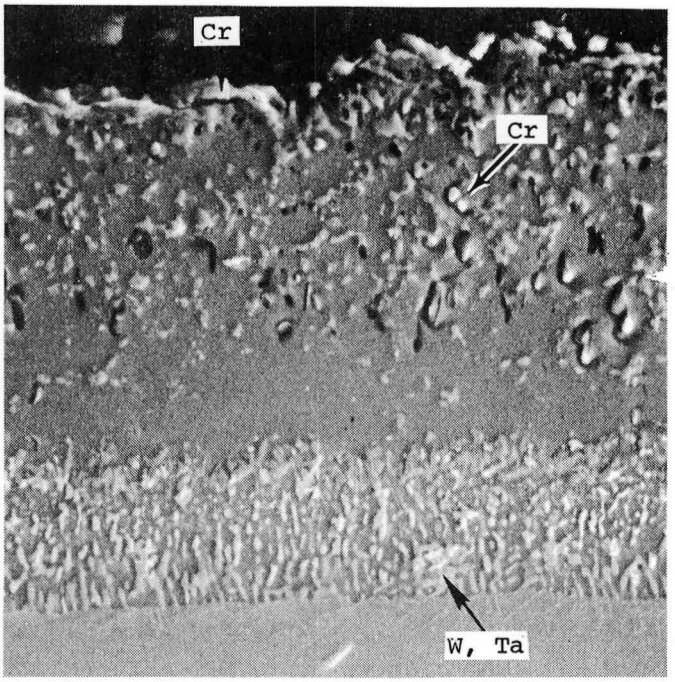

Cerium Oxide Polish

Magnification: 1100X

Figure 22.

SEM Photomicrograph of Cr-Al Coated IN-792 Specimen VC5

Table 10

Batch Processing of Ni-Al-Cr Coatings

Specimen Number	Chromium Deposition (mg/cm^2)	Aluminum Deposition (mg/cm^2)	Total Weight Gain (mg/cm^2)
Variation C (Ni-17Al-20Cr)			
VC41	2.75	-	-
VC42	2.82	14.50	17.32
VC43	2.78	14.02	16.80
VC44	2.75	13.88	16.63
Avg.	2.78	14.13	16.92
VC45	1.93	-	-
VC46	2.15	16.34	18.49
VC47	2.17	15.77	17.94
VC48	2.19	18.35	20.54
Avg.	2.11	16.82	18.99
Variation D (Ni-12Al-20Cr)			
VD51	3.09	-	-
VD52	2.18	9.25	11.43
VD53	2.10	9.12	11.22
VD54	1.91	9.28	11.19
Avg.	2.32	9.22	11.28
VD12	2.68	-	-
VD13	2.69	9.55	12.24
VD14	2.79	10.40	13.19
VD15	2.28	9.76	12.52
Avg.	2.75	9.90	12.65

Figures 23 and 24 show typical microstructures of two coating batches of Variation C, Ni-17Al-20Cr, which consists of approximately 8 microns of chromium surface enrichment and 100 to 105 microns of the final coating. The chromium layer appears to be mostly alpha solid solution.

Diffusion of aluminum into the alloy surface resulted in precipitation of a finely dispersed chromium-rich phase. The coating near the interface exhibits a typical two-phase microstructure resembling the gamma/gamma prime structures in the alloy. A 5 to 20 percent growth was observed after heat treat, although the microstructure was little changed except for the formation of a single-phase zone. The alloy substrate near the interface is affected by interdiffusion, as seen by the appearance of a homogeneous light grey zone, probably the result of nickel diffusion outwards.

The Ni-12Al-20Cr coatings are shown in Figures 25 and 26. Heavy aluminide inclusions were obtained in specimen VD51 in Figure 25. As noted in Table 10, this particular specimen had an unusually large weight gain of 3.09 mg/cm^2 while the other specimens in the same batch picked up approximately 2.10 mg/cm^2. Since the chromium cycle is essentially identical to that in the Ni-17Al-20Cr (Variation C) coating, the microstructure of specimen VD12, and specimens VC41 and VC45, would be expected. The aluminization of this coating was at a lower activity than that used in Variation C. Therefore, the microstructural features are nearly exact replicas of the other coatings exhibiting the three-zone structure with a denuded zone in the center and finely divided chromium-rich secondary phases in the outer regions. However, the thickness of Variation D coating is slightly less than Variation C.

3.3 PROCESSING

Several of the process steps of internal blade coatings are of sufficient significance to warrant fuller discussion. These are:

- Masking
- Coating reproducibility
- Pack removal and particle sintering
- Heat treatment.

3.3.1 Masking

An integral part of the coating process is the formulation of a masking process to protect the blade firtree during coating in order to retain alloy high-temperature cycle fatigue and creep properties. It was planned that application of external and internal coatings, as well as the maskant, will be integrated into the process flow sequence of the Mars first-stage blade.

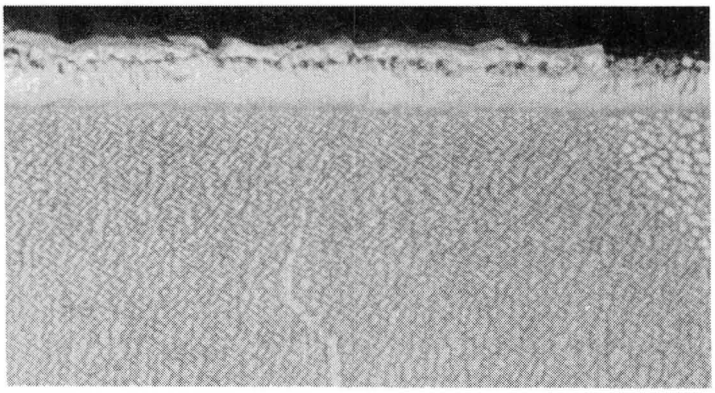

Specimen VC41

Chromium Deposit Only

Magnification: 1000X

10% Electrolytic Oxalic Etch

Mount No. 9506

Specimen VC42

Ni-17Al-20Cr Coated

Magnification: 500X

10% Electrolytic Oxalic Etch

Mount No. 9506

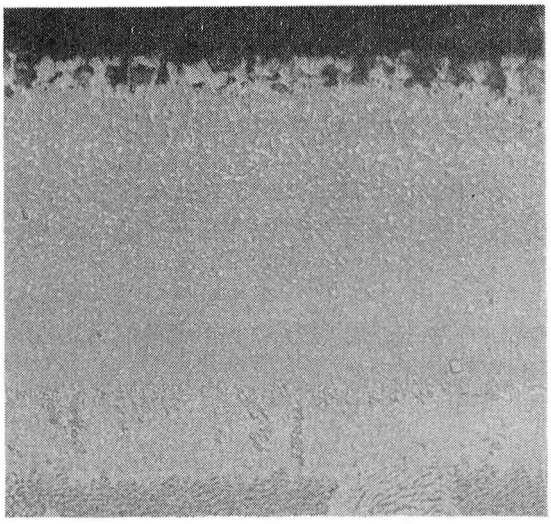

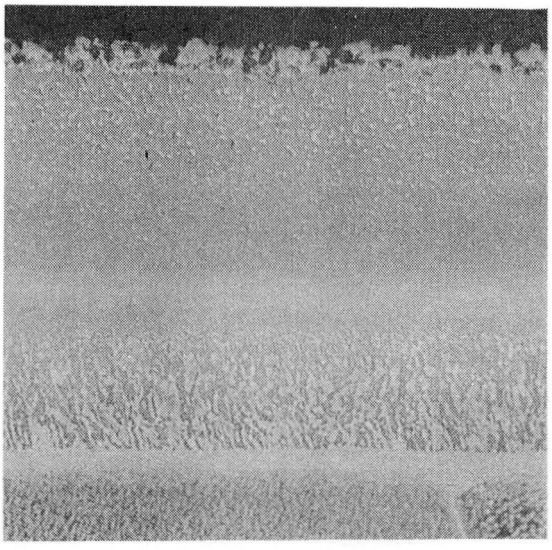

Specimen VC43

Ni-17Al-20Cr Heat Treated

Magnification: 500X

10% Electrolytic Oxalic Etch

Mount No. 9506

Figure 23. First Batch of Ni-17Al-20Cr (Variation C) Coated IN-792 Specimens

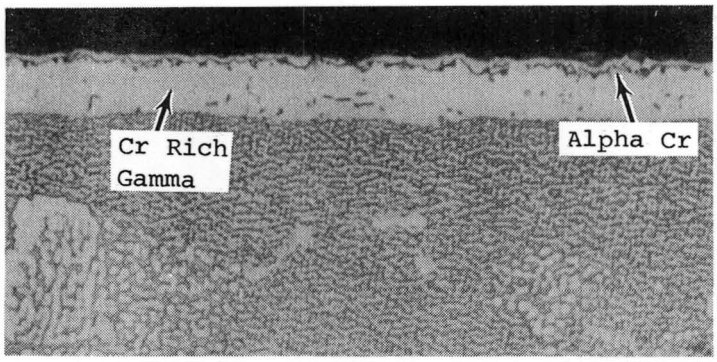

Specimen VC45

Chromium Deposit Only

Magnification: 1000X

10% Electrolytic Oxalic Etch

Mount No. 9509

Specimen VC46

Ni-17Al-20Cr Coated

Magnification: 500X

10% Electrolytic Oxalic Etch

Mount No. 9509

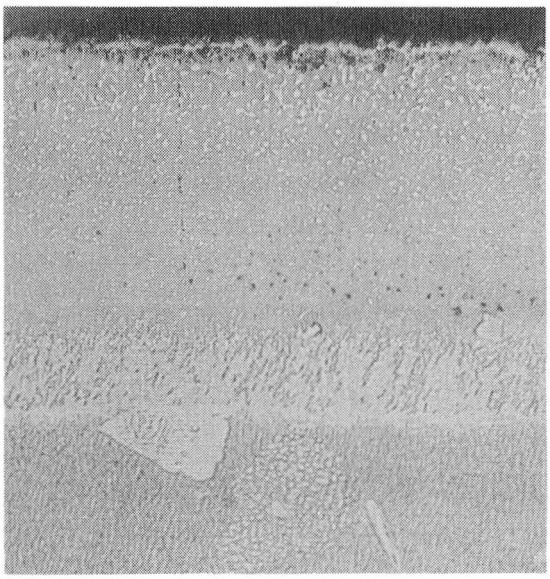

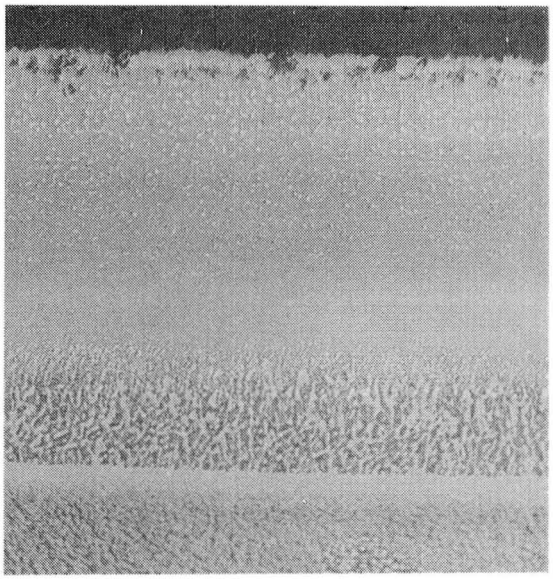

Specimen VC47

Ni-17Al-20Cr Heat Treated

Magnification: 500X

10% Electrolytic Oxalic Etch

Mount No. 9509

Figure 24. Second Batch of Ni-17Al-20Cr (Variation C) Coated IN-792 Specimens

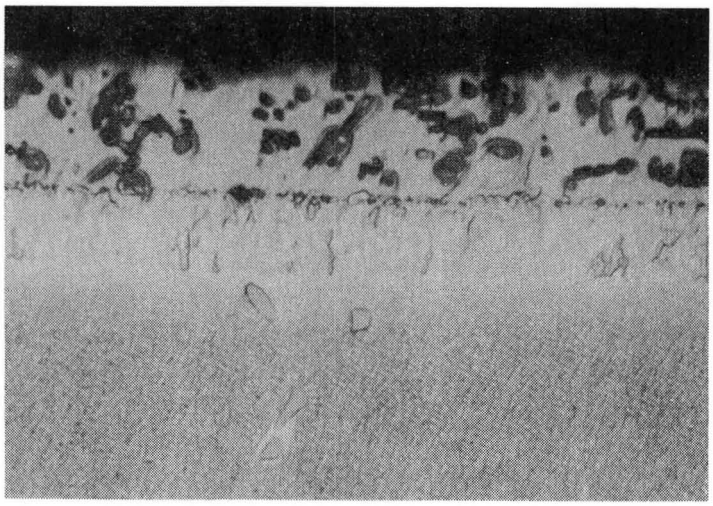

Specimen VD51

Chromium Deposit Only

Magnification: 1000X

10% Electrolytic Oxalic Etch

Mount No. 9504

Specimen VD52

Ni-12Al-20Cr Coated

Magnification: 500X

10% Electrolytic Oxalic Etch

Mount No. 9504

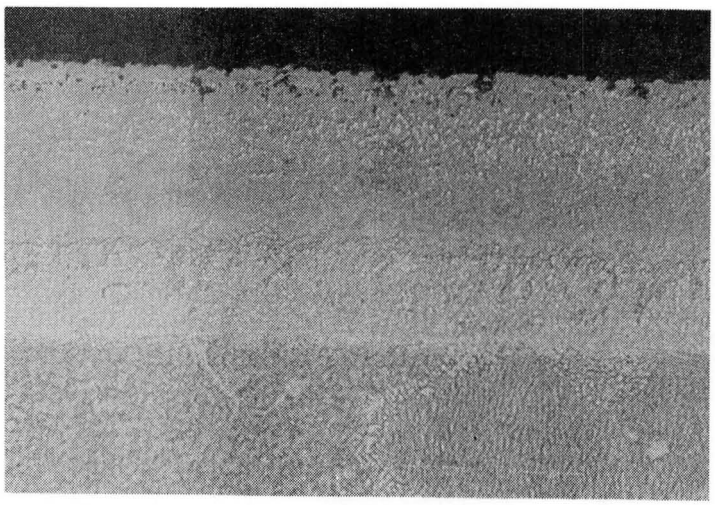

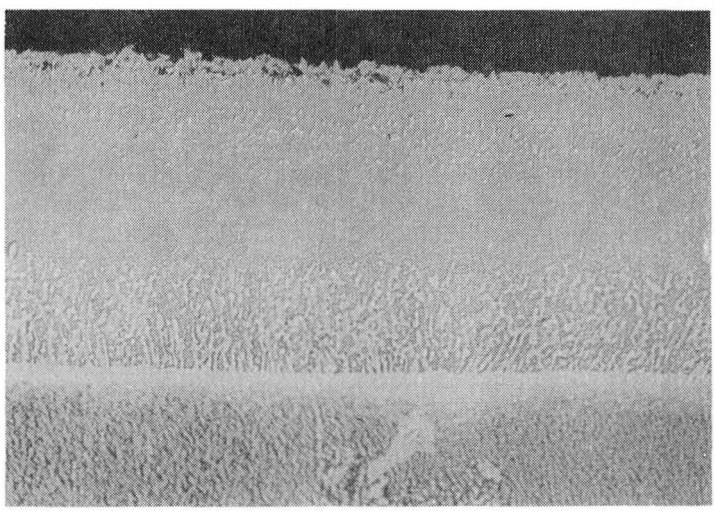

Specimen VD53

Ni-12Al-20Cr Heat Treated

Magnification: 500X

10% Electrolytic Oxalic Etch

Mount No. 9504

Figure 25. First Batch of Ni-12Al-20Cr (Variation D) Coated IN-792 Specimens

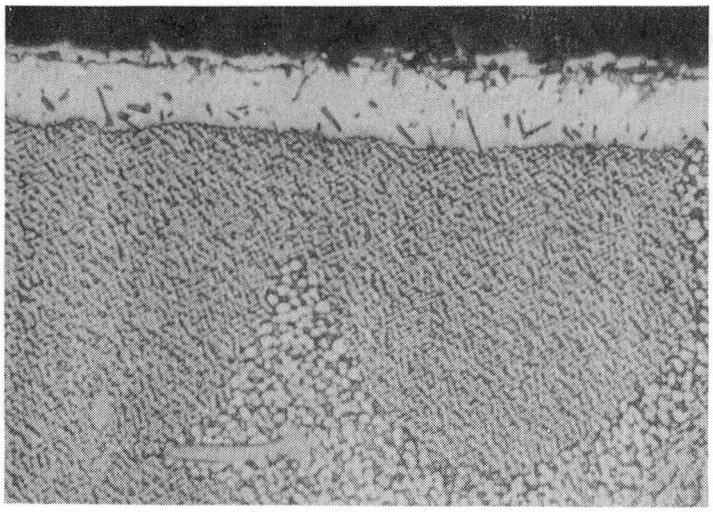

Specimen VD12

Chromium Deposit Only

Magnification: 1000X

10% Electrolytic Oxalic Etch

Mount No. 9503

Specimen VD13

Ni-12Al-20Cr Coated

Magnification: 500X

10% Electrolytic Oxalic Etch

Mount No. 9503

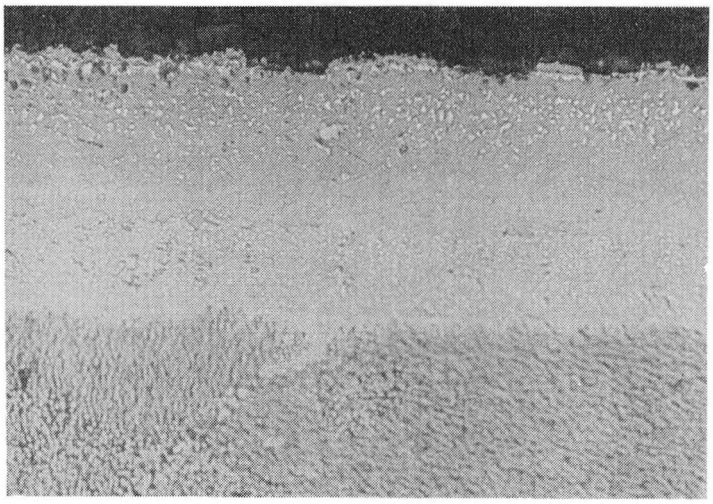

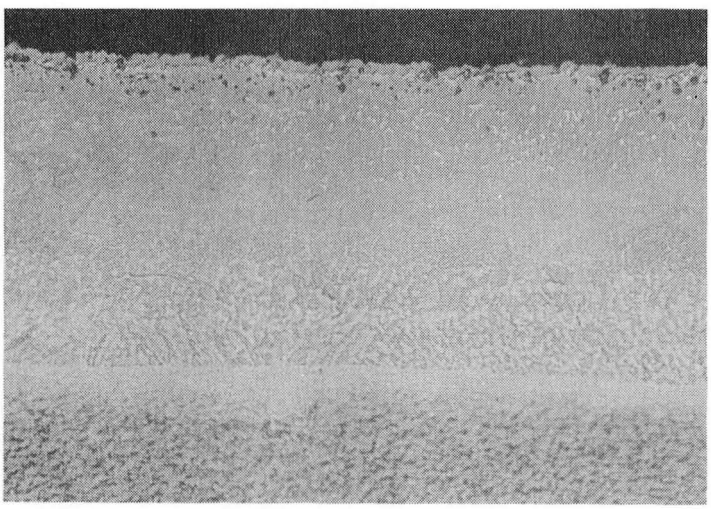

Specimen VD14

Ni-12Al-20Cr Heat Treated

Magnification: 500X

10% Electrolytic Oxalic Etch

Mount No. 9503

Figure 26. Second Batch of Ni-12Al-20Cr (Variation D) Coated IN-792 Specimens

In formulating maskant compositions, the aluminum pack was selected for optimization as it had the most reactive environment from the standpoints of time, temperature and thermodynamic driving potential. The approach taken was a two-layer mask on the surfaces to be protected. The first coat acts as an inert base to effect a physical separation between the alloy surface and the reactive material in the top coat. The top coat typically contains a reactive component that will "getter" or react with the incoming flux of active metal vapors.

Initially, commercial braze stopoff and boron nitride were used in the base coat with a NiO top coat, as noted in Table 11. After air drying, the specimens were pack aluminized. The specimens were then cleaned and grit blasted prior to inspection. The base coat without a top coat was found to be ineffective in preventing aluminization of the substrate. The $50NiO\text{-}50Al_2O_3$ top coat was the most effective. However, neither Nicrobraz nor boron nitride were entirely satisfactory as an inert barrier and Al_2O_3 was substituted next in the form of a commercially available stopoff.

Table 11

Masking Composition

Specimen Number	Base Coat	Top Coat
100	Nicrobraz (stop-off green)	None
101	Nicrobraz (" ")	NiO
102	Nicrobraz (" ")	50 v/o NiO-50 v/o Al_2O_3
200	Boron nitride	None
201	Boron nitride	NiO
202	Boron nitride	50 v/o NiO-50 v/o Al_2O_3

Five test specimens of a nickel-base superalloy (MAR-M421) were used in a masking study using five different top coat compositions, listed in Table 12. Each specimen was first coated with Wal Colmonoy white (water-base) stopoff which was allowed to dry thoroughly before the top coat was applied. Each of the five maskant top coats was applied in layers until the buildup was approximately 0.2 to 0.3 cm thick. The specimens were then packed in an aluminization pack and fired at 1050°C for 16 hours. After cleanup the specimens were grit blasted and prepared for metallographic examination. The microstructures of the five specimens are shown in Figure 27. The surfaces of M3 and M4 were totally unaffected. The alloy structure and composition appeared to be successfully retained without a trace of aluminum. Specimen M1 exhibited alloy depletion along grain boundaries. A similar but much less severe effect was also noted on specimens M2 and M5.

Some semi-quantitative work was performed with SEM/EDX analysis in an attempt to define the unusual appearance of the three structures, M1, M2, and M5. A SEM photomicrograph of a typical denuded grain boundary of specimen M5 is shown in Figure 28. The areas labeled 1, 2, and 3 were analyzed using EDXA

Table 12

Composition of Maskant Top Coats

Specimen Number	Maskant Composition (Wt %)
M1	50NiO-50Al_2O_3(-325 grit)
M2	50NiO-30Al_2O_3(-325)-20Al_2O_3(220 grit)
M3	25NiO-75Al_2O_3(-325 grit)
M4	50NiO-35Al_2O_3(-325)-15Al_2O_3(220 grit)
M5	50NiO-50Al_2O_3(220 grit)

and the energy spectra are plotted in Figure 29 from 0.4 KeV to 9 KeV. Chromium appears to have been selectively lost from the grain boundaries (area 2) and columbium and titanium are also lower than in areas 1 and 3. The aluminum signals are too low in intensity to make comparisons; however, one can expect some aluminum depletion to occur in conjunction with loss of chromium.

Parallel analysis of specimens masked with Al_2O_3 base coat provided similar findings. Therefore, it was concluded that the following maskant composition would be utilized in blade processing:

- Base coat: Al_2O_3 (A14) or Wall Colmonoy white stopoff
- Top coat: 50NiO-35Al_2O_3(-325)-15Al_2O_3(220 grit)

3.3.2 Coating Reproducibility

An effort was made to demonstrate the reliability of the coating process (without entering into a statistically significant iterative test) by control of the process parameters such as temperature tolerance limits, retort volumes, pack handling, pack porosity, etc. Most of these controls need to be adjusted to the requirements of the coating.

From the values reported in Tables 8 and 9, the following can be calculated for the test specimens processed in the same pack but in different batches:

	Weight Gain Average	Standard Deviation
-1Cb process	0.01 mg/cm^2	0.12
-3Cb process	3.56 mg/cm^2	0.37
-20Cr process	2.33 mg/cm^2	0.78
-19Al process	9.02 mg/cm^2	1.24
-17Al process	15.51 mg/cm^2	1.78
-12Al process	9.56 mg/cm^2	0.47

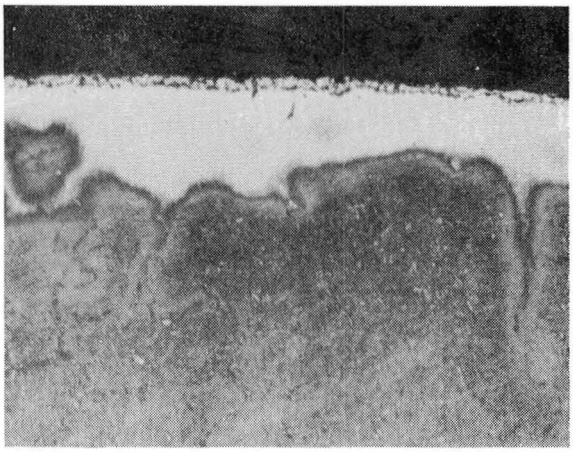

Specimen M1

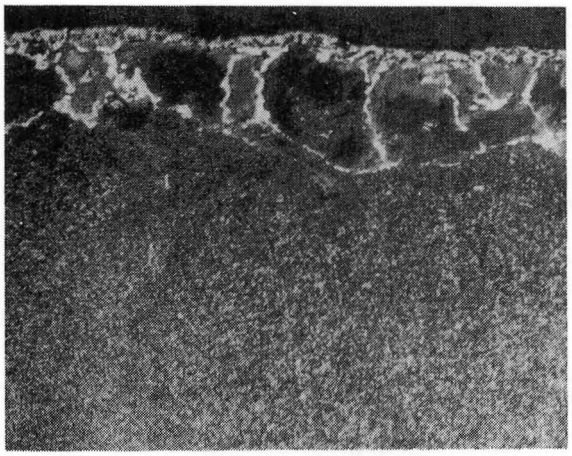

Specimen M2

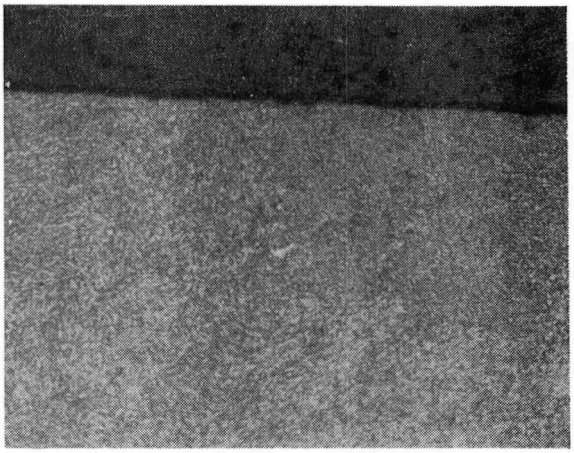

Specimen M3

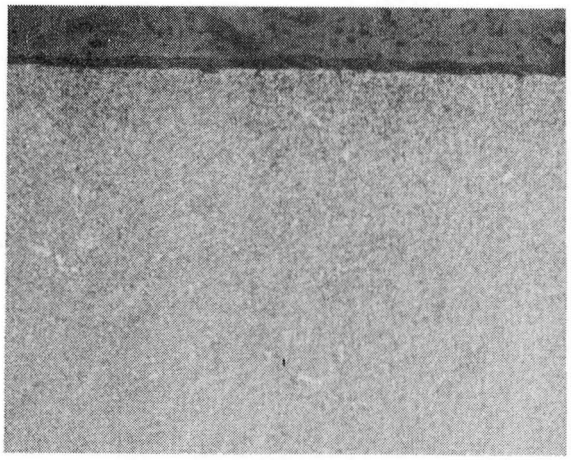

Specimen M4

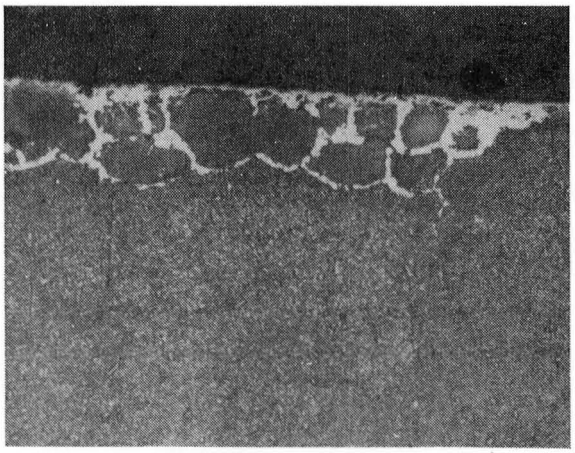

Specimen M5

Magnification: 250X

2% Electrolytic Chromic Etch

Mount No. 9540

Figure 27. Microstructures of Masked MAR-M421 Specimens After Aluminization Cycle

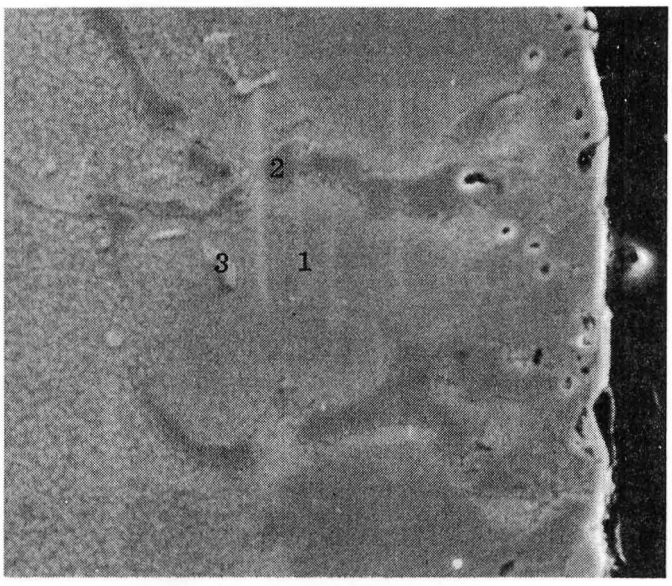

Magnification: 900X

Mount No. 9540

Figure 28. SEM Photomicrograph of Masked MAR-M421 Specimen M5

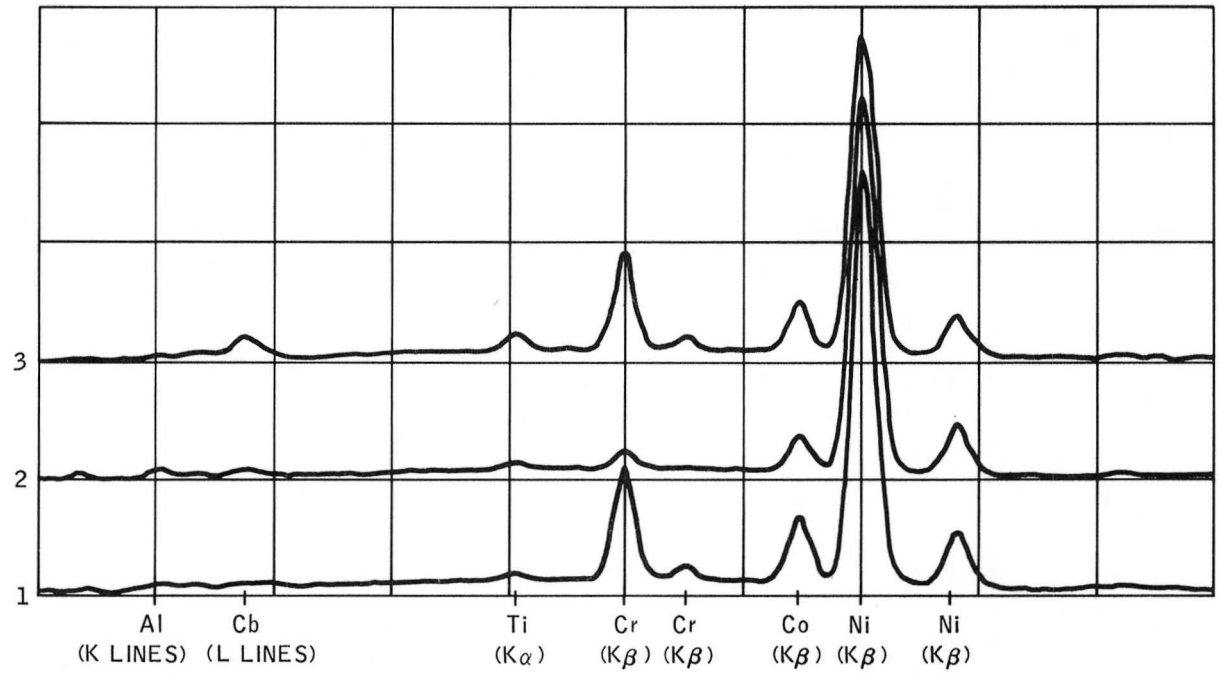

Figure 29. Energy Spectra of Three Areas on Masked MAR-M421 Specimen M5 (See Fig. 28)

Except for the -1Cb process, all standard deviations lie within 20 percent of the mean value. However, notwithstanding the good agreement found in this test with coupon specimens, it was later found that specimen shape/configuration is an additional factor that can influence weight gain.

3.3.3 Pack Removal and Particle Sintering

One of the major problems encountered in using the pack method for internal coating application is that of pack removal. Even though the active elements in these powder packs are typically diluted with inert Al_2O_3 particles, vapor phase transport to the component surface followed by condensation and reaction, according to the Levine and Caves model (Ref. 7), could result in transistory low melting species that will enhance particle sintering. Other factors that can contribute to particle sintering are solid state diffusion and the fluxing action of halide which tends to clean the surface and promote sintering (Ref. 13). In general, the fines or finely divided particles in the <12 micron range were found to be the most susceptible to particle sintering.

Several methods were undertaken to ease pack removal, the most successful of which was to condition or pre-alloy the pack. In other words, the virgin pack was processed under identical coating conditions to allow surface reaction to occur in the absence of specimens. Pre-conditioned packs exhibited minimum interparticulate and substrate sintering, especially in low-activity aluminum packs in which the rate of aluminum transport to the surface is low.

Another method of aiding pack removal, which had been effectively demonstrated (Ref. 14), was to employ low-temperature firing cycles. Since deposition is a function of temperature, there is a practical minimum below which reaction kinetics would limit coating formation.

Increasing volume of inert diluent was demonstrated to reduce sintering to some extent by reducing the amount of active metal particles in the pack and increasing interparticle spacing. Again, this eventually affected the rate at which metal deposition occurred once a minimum was established for that particular pack.

The selection of activator is known to play a significant role in aluminide coating formation (Ref. 7). In this work, an empirical approach was taken in determining the appropriate activator to be used in each pack, NaCl in the chromium pack and polyvinyl chloride in the columbium and aluminum packs.

3.3.4 Heat Treatment

The Solar specified heat treatment cycles for IN-792 alloy are as follows:

- 1204°C (2200°F)/2 hours/rapid cool

- 1121°C (2050°F)/2 hours/rapid cool
- 843°C (1550°F)/24 hours/air cool

Although all castings were received in the fully heat treated condition, the coating cycles disrupted the critically balanced gamma/gamma prime microstructure. The slow cooldown rate in a pack is known to be especially detrimental to the substrate alloy structure. Hence, all coated specimens were given the 1121°C and 843°C heat treatment prior to testing.

The effect of the heat treatment cycles on coating thickness is shown in Table 13. In the as-coated condition, Ni-17Al-20Cr was found to have the thickest coating, with the Ni-19Al-3Cb measuring only approximately 60 microns and the other two coatings intermediate. This can be readily explained by the fact that the Ni-17Al-20Cr was fired in the highest activity aluminum pack while the other three coatings used a lower activity pack. Because of the thermodynamic potential driving the reaction during pack aluminizing, all coatings are generally in a highly non-stable condition, governed partly by aluminizing parameters and cooldown rate. In the subsequent heat treatment, the phases tend to move toward equilibrium through solid state diffusion, both within the coating itself and across the interface. Evidence of the diffusional changes can be seen in the coating thickness increases noted in the last two columns in Table 13. A reversed trend was observed where the thickest coatings had the smallest increase. The significance of this trend is not readily understood.

Table 13

Coating Thickness Measurements

Nominal Coating Composition	Batch Number	Coating Thickness (μm) Typical Areas		
		As-Coated	After Heat Treat	Percent Increase
Ni-19Al-1Cb	1	76	90	18
	2	72	96	19
Ni-19Al-3Cb	1	62	82	32
	2	60	76	27
Ni-17Al-20Cr	1	105	110	5
	2	100	110	10
Ni-12Al-20Cr	1	74	82	11
	2	70	80	14

3.4 APPLICATION TO ENGINE HARDWARE

In any coating process, surface preparation prior to application is considered an integral and critical part of the entire process. This is especially true in internal coating application where the surface finish and conditions cannot be readily viewed, as exemplified by the Mars stage 1 blade shown in Figure 3. Several methods of surface preparation were investigated for cleanup of internal as-cast surface, a typical example of which is shown in Figure 30.

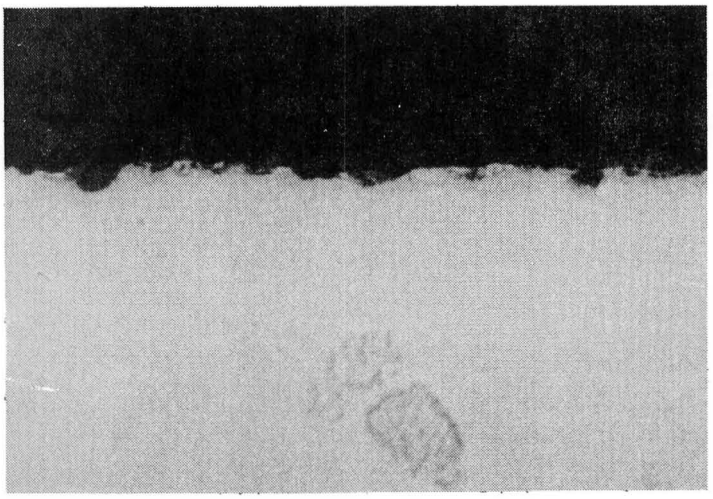

Magnification: 500X

2% Chromic Etch

Figure 30. Internal Surface of As-Received IN-792 Mod 5A (Plus HIPed) Blade Section

Methods employed included hot alkali leaching, muriatic acid, liquid honing and hydrochloric acid etch. The objective of the cleanup was two-fold, to prepare surfaces and to remove physical obstructions (remnants of core and other foreign materials) from the internal passages. The HCl cleanup was judged the most successful as demonstrated by airflow values reported in Table 14. (The flow function is given as a more useful indication of mass flow as it combines the air mass flow rate, plenum pressure and temperature condition.) Note that for essentially all of the blades, the flow function increased (significantly in blades such as N14) after HCl cleanup, indicating the removal of internal debris which had reduced the total flow of air.

It should be pointed out that for this particular blade, the controlling orifice in the cooling air passage is determined, not by the trailing edge exit holds, but instead by an orifice plate which is brazed onto the bottom of the firtree. Furthermore, this blade was originally designed such that a significant variation about the designed mean can be tolerated through subsequent sizing of the orifice plate. Therefore, barring major internal obstructions, all coated blades with approximately 10 percent reduction in air flow can be adjusted for in selection of orifice diameter.

Table 14

Flow Values of Mars Blades Used in Process Development

Blade Number	Before Cleanup		After Acid Cleanup	
	Airflow (Kg/sec)	Flow Function ($\sqrt{K}$ m/sec)	Airflow (Kg/sec)	Flow Function ($\sqrt{K}$ m/sec)
N2	1.036	0.1271	0.121	0.1372
N3	1.147	0.1407	1.203	0.1473
N4	0.323	0.0397	0.372	0.0456
N5	0.948	0.1163	1.117	0.1367
N6	0.653	0.0801	0.763	0.0934
N7	1.111	0.1363	1.103	0.1350
N8	0.691	0.0848	0.754	0.0922
N9	1.202	0.1475	1.185	0.1450
N10	0.928	0.1139	0.935	0.1145
N11	1.092	0.1340	1.108	0.1356
N13	0.739	0.0934	0.840	0.1078
N14	Very low flow		1.294	0.1584
N15	0.711	0.0873	0.713	0.0872
N16	1.150	0.1412	1.167	0.1428

Four IN-792 plus HIPed blades were processed with each of the four candidate coating compositions per the coating specifications in Appendix A.

The results of coating processing of four blades with the program compositions are reported in Table 15. Note that the Mars blade is capable of containing about 7 grams of columbium pack and 5 to 6 grams of chromium or aluminum pack. Pack removal was performed manually, first imparting sufficient mechanical action to the part to dislodge most of the pack material, followed by a pressure washing process. The latter operation appeared to be quite effective in removing the last remnants of the pack. The weight gain column shows that for coatings A and B, the second aluminizing process deposited between 280 and 310 mg of aluminum to the internal surfaces of the blade. Some discrepancy is noted in the columbium weight gain values for blades N9 and N16. The large gain reported for blade N9 is suspect, and could be the result of improper cleanup and pack removal. The C and D coating variations registered weight gains of 67.5 and 66.9 mg for blades N5 and N11, respectively, showing good agreement for the deposition of chrome. The subsequent aluminizing step resulted in gains of 381 and 258 mg, representing 17 and 12 percent aluminum deposition.

Each blade was cold flowed before and after coating and the values obtained are also reported in Table 15. The unusual increase in flow measured for N5 and N11 could be attributed to the removal of some internal obstruction as a result of the processing operation. Typically, the other two blades registered <10 percent flow reduction which would be quite acceptable by quality control standards.

Table 15

Data From Processing of Air-Cooled Blading

Blade Number	Pack	Weight of Cleaned Blade (g)	Weight of Pack (g)	Weight of Blade After Pack Removal (g)	Weight of Blade After Pressure Washing (g)	Weight Gain (mg)	Flow Before K msec	Flow After K msec	Flow Reduction (%)
Variation A (Ni-19Al-1Cb)									
N9	Cb	107.5841	7.1668	108.2837	107.6968	112.7*			
	Al	107.6915	5.7488	-	107.9733	281.8			
				Total Weight Gain = 394.5 mg			0.145	0.138	4.8
Variation B (Ni-19Al-3Cb)									
N16	Cb	107.3806	6.9831	107.6098	107.4271	46.5			
	Al	107.4257	5,8473	-	107.7352	309.5			
				Total Weight Gain = 356.0 mg			0.143	0.131	8.4
Variation C (Ni-17Al-20Cr)									
N5	Cr	107.0670	5.1172	107.1909	107.1345	67.5			
	Al	107.1345	5.4150	-	107.5151	380.6			
				Total Weight Gain = 448.1 mg			0.137	0.188	(+37.2)**
Variation D (Ni-12Al-20Cr)									
N11	Cr	107.7080	5.1375	107.8149	107.7749	66.9			
	Al	107.7749	5,4403	-	108.1328	257.9			
				Total Weight Gain = 324.8 mg			0.136	0.157	(+15.4)**

* Possible error due to incomplete pack removal.

** Flow was increased as a result of coating processing which could be indicative of removal of some internal obstruction in a self-cleaning manner during processing.

In internal coating processing, the amount of pack available for coating formation is limited to the total internal volume of the blade configuration. Also, the highly irregular and circuitous passageways can cause varying quantities of active pack materials to be available to the internal surfaces. Based on weight gain values and measured pack densities of 1.5 to 2.0 mg/cm^2, the amount of pack depletion can be estimated. The powder packs typically contain 15-20 weight percent active metal. The extent of pack depletion as a result of vapor transfer to the substrate surface is calculated to be approximately 0.44 mm. Therefore, the amount of pack material in the central cavities of the blade (approximately 5 mm diameter) would be more than sufficient for standard coating formation. However, in the vicinity of the small exit holes in the trailing edge where dimensions are 0.51 by 0.91 mm, the pack should be fully depleted.

Each of the above processed blades was sectioned and metallographically prepared, as shown in Figure 31. Two horizontal cuts were made, 6 mm from the blade tip and 6 mm above the black platform. Representative microstructures are shown in Figures 32 through 39.

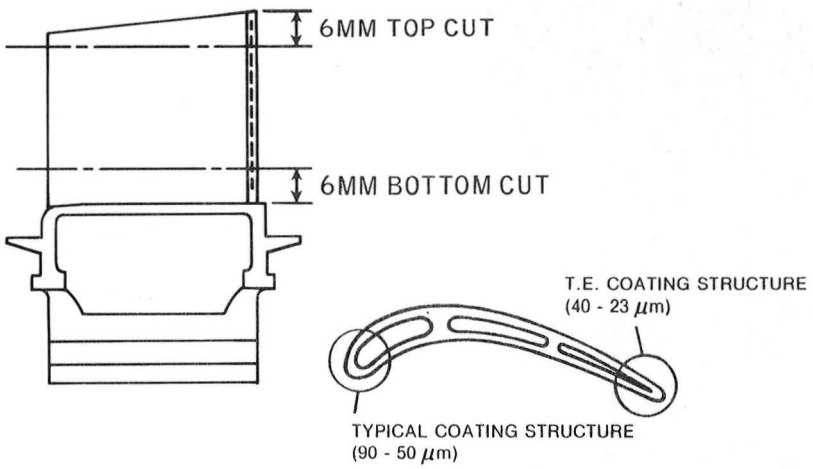

Figure 31. View of Blade Showing Metallographic Sectioning

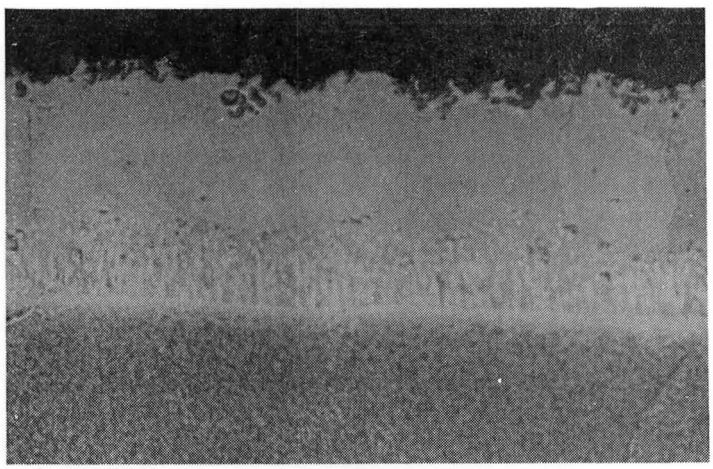

Blade N9

Typical Microstructure

Magnification: 500X

Oxalic Etch

Mount No. 9579

Blade N9

Near Trailing Edge

Magnification: 500X

Oxalic Etch

Mount No. 9579

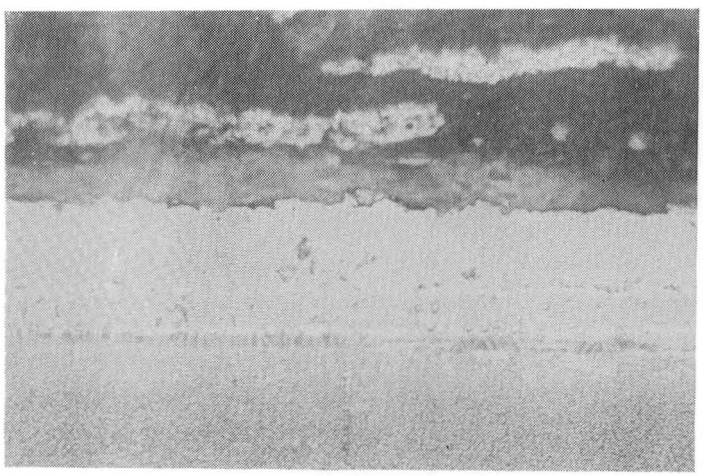

Figure 32. Coating Microstructure of Ni-19Al-1Cb (Variation A) as Viewed From 6 mm From the Blade Tip (Top Cu)

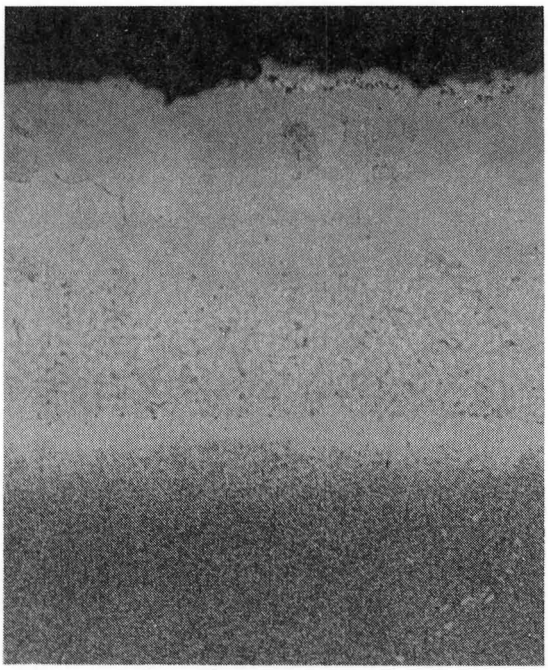

Blade N9

Typical Microstructure

Magnification: 500X

Oxalic Etch

Mount No. 9580

Blade N9

Near Trailing Edge

Magnification: 500X

Oxalic Etch

Mount No. 9580

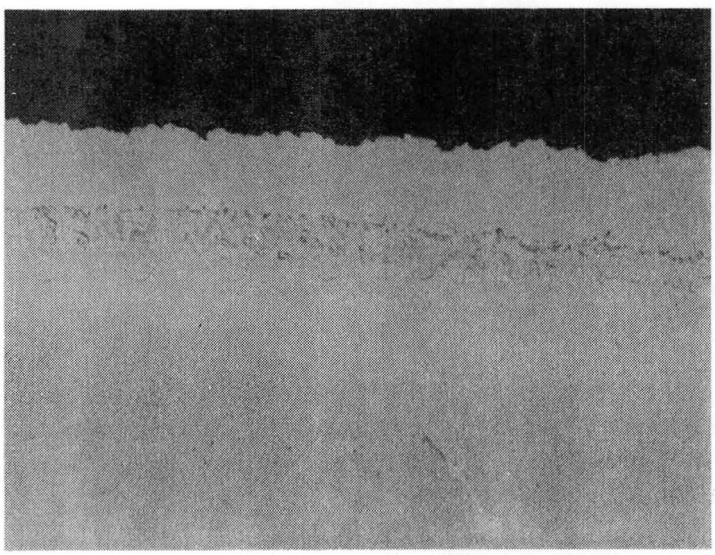

Figure 33. Coating Microstructure of Ni-19Al-1Cb (Variation A) Coating as Viewed 6 mm From Blade Platform (Bottom Cut)

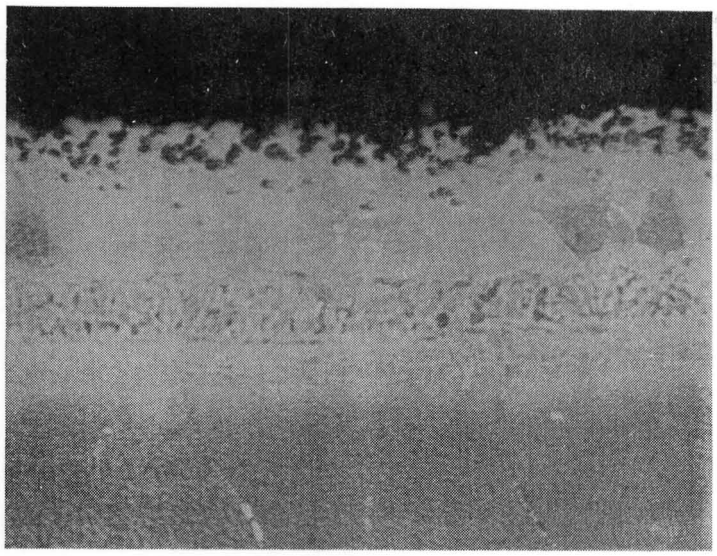

Blade N16

Typical Microstructure

Magnification: 500X

Oxalic Etch

Mount No. 9583

Blade N16

Near Trailing Edge

Magnification: 500X

Oxalic Etch

Mount No. 9583

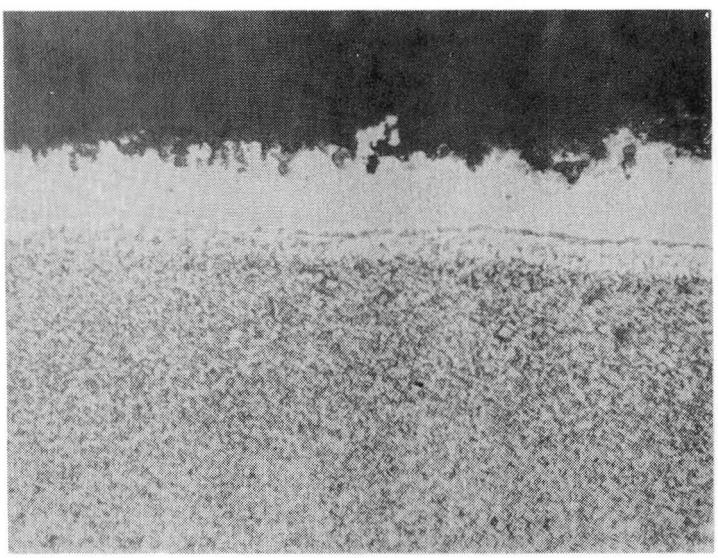

Figure 34. Coating Microstructure of Ni-19Al-3Cb (Variation B) as Viewed 6 mm From Blade Tip (Top Cut)

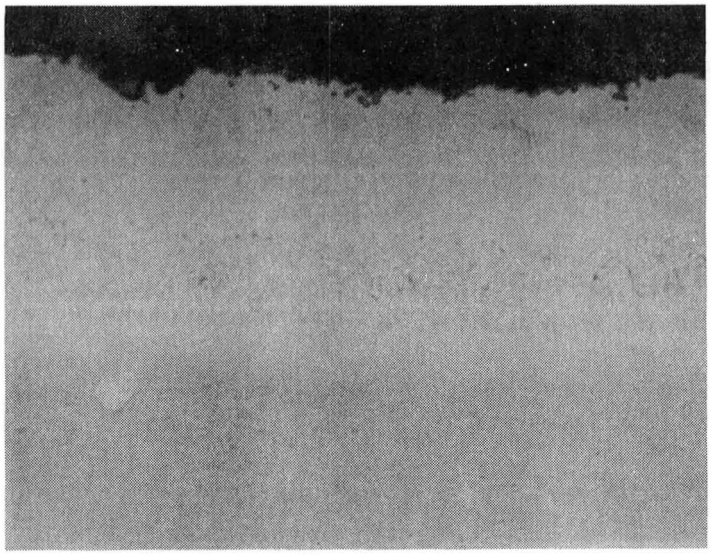

Blade N16

Typical Microstructure

Magnification: 500X

Oxalic Etch

Mount No. 9584

Blade N16

Near Trailing Edge

Magnification: 500X

Oxalic Etch

Mount No. 9584

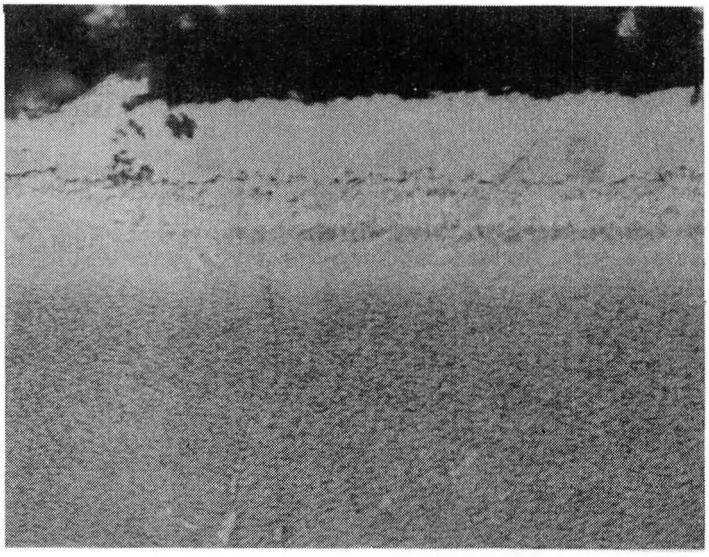

Figure 35. Coating Microstructure of Ni-19Al-3Cb (Variation B) as Viewed 6 mm From Blade Platform (Bottom Cut)

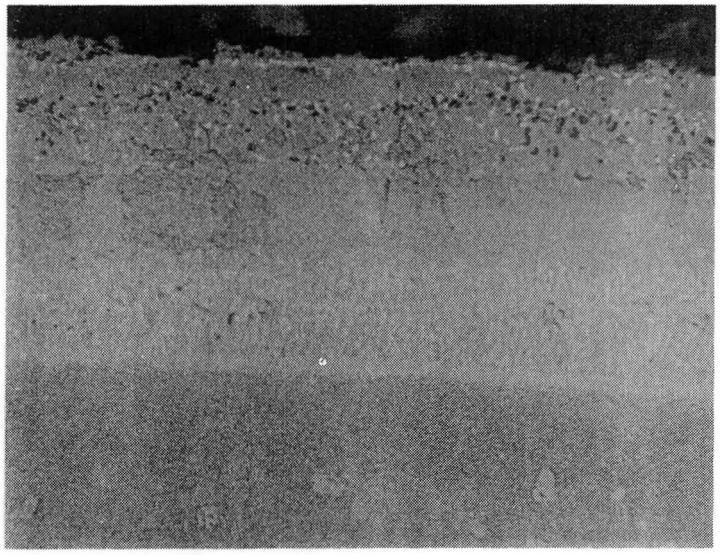

Blade N5

Typical Microstructure

Magnification: 500X

Oxalic Etch

Mount No. 9577

Blade N5

Near Trailing Edge

Magnification: 500X

Oxalic Etch

Mount No. 9577

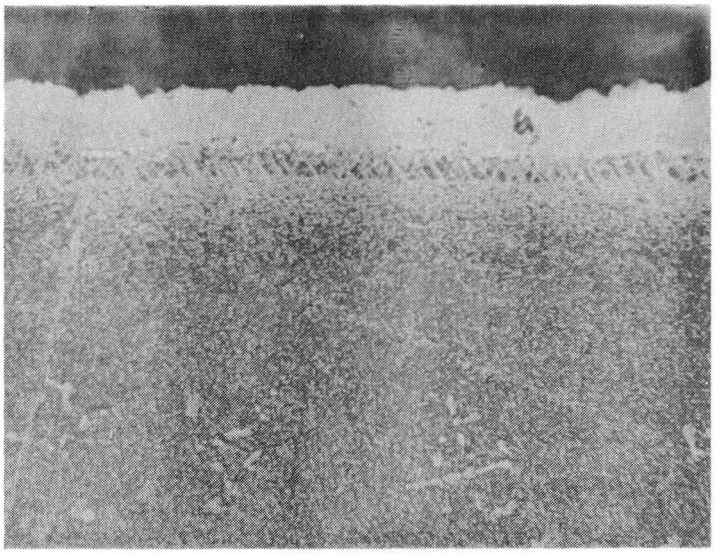

Figure 36. Coating Microstructure of Ni-17Al-20Cr (Variation C) as Viewed 6 mm From Blade Tip (Top Cut)

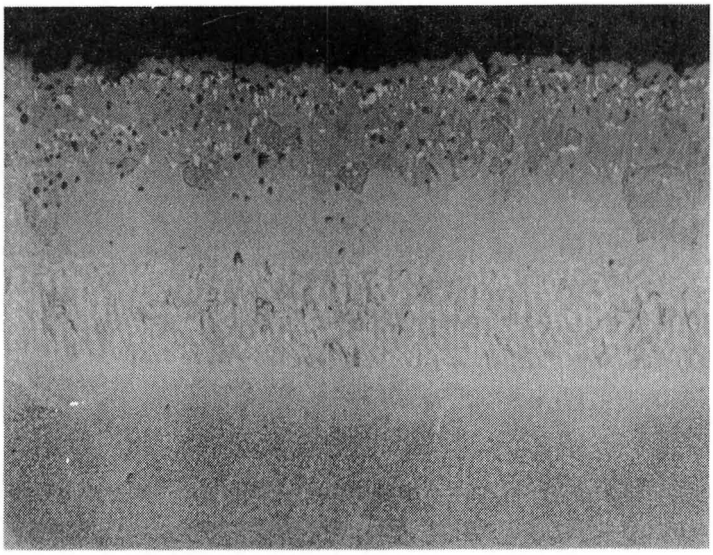

Blade N5

Typical Microstructure

Magnification: 500X

Oxalic Etch

Mount No. 9578

Blade N5

Near Trailing Edge

Magnification: 500X

Oxalic Etch

Mount No. 9578

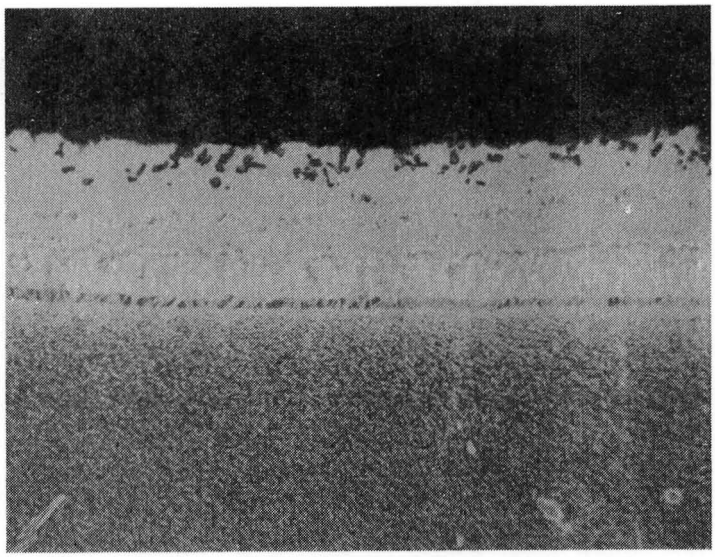

Figure 37. Coating Microstructure of Ni-17Al-20Cr (Variation C) as Viewed 6 mm From Blade Platform (Bottom Cut)

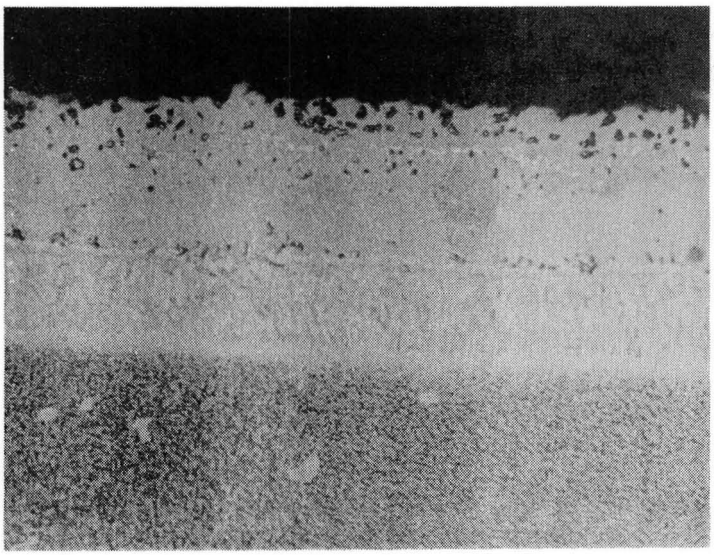

Blade N11

Typical Microstructure

Magnification: 500X

Oxalic Etch

Mount No. 9581

Blade N11

Near Trailing Edge

Magnification: 500X

Oxalic Etch

Mount No. 9581

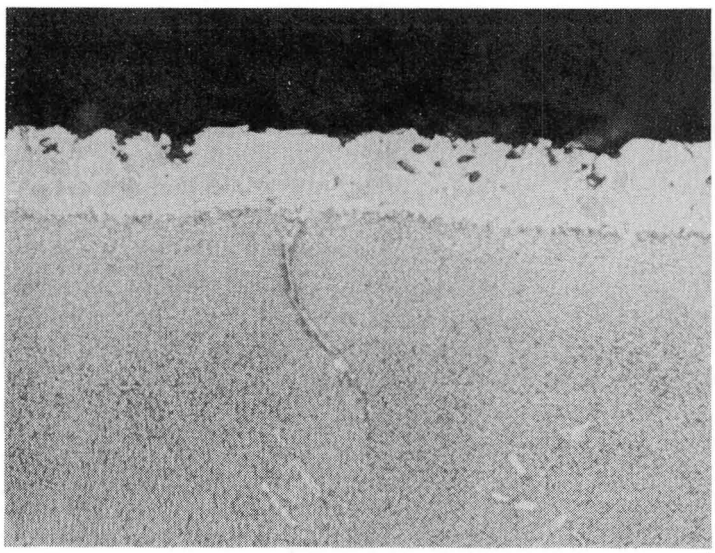

Figure 38. Coating Microstructure of Ni-12Al-20Cr (Variation D) as Viewed 6 mm From Blade Tip (Top Cut)

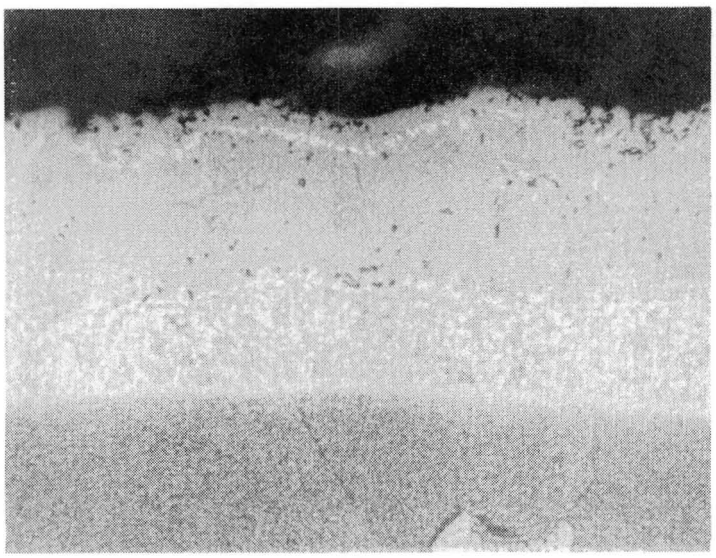

Blade N11

Typical Microstructure

Magnification: 500X

Oxalic Etch

Mount No. 9582

Blade N11

Near Trailing Edge

Magnification: 500X

Oxalic Etch

Mount No. 9582

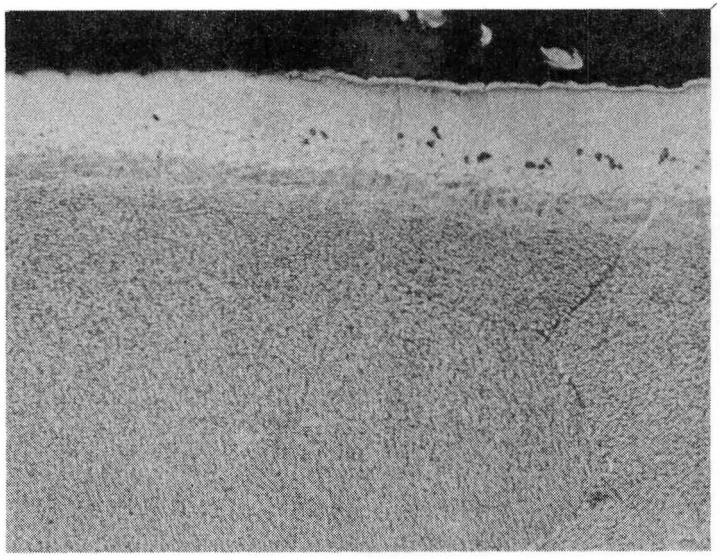

Figure 39. Coating Microstructure of Ni-12Al-10Cr (Variation D) as Viewed 6 mm From Blade Platform (Bottom Cut)

Coating Variation A, Ni-19Al-1Cb, applied to Blade N9 is shown in Figures 32 and 33. The coating thickness varied from 61 to 90 microns inside most of the blade and tapered to 40 to 36 microns near the trailing edge. The coating was dense and well bonded.

In Figures 34 and 35, Variation B, Ni-19Al-3Cb is shown. Once again, the coating is thickest in the central cavities (51 and 66 microns) and thins out near the trailing edges to 30 and 40 microns. Blade N16, Figure 34, also exhibits some inclusions in the coating surface although the bulk of the coating remains dense and well bonded to the substrate. A demarcation line can be observed in the thin coating near the leading edge.

Variation C, Ni-17Al-20Cr, was applied to blade N5 and representative photomicrographs are shown in Figures 36 and 37. A similar decrease in coating thickness was also observed here near the trailing edge in both top and bottom sections; coating ranged from 81 to 25 microns. Some inclusions were noted in the outer coated zone, interspersed with the light grey secondary phase.

The fourth variation, Ni-12Al-20Cr (Figs. 38 and 39) on blade N11 is also characterized by the coating thickness differences, ranging from 81 to 23 microns. Note that in Figure 39, instead of a random distribution of the light grey phase near the coating surface, a semi-continuous band can be observed. As a result of the much thinner coating, the microstructures near the trailing edge are losing their multi-zone structure.

Coating thicknesses are measured and listed in Table 16 and they indicated that a significant decrease in coating thickness can be expected at the trailing edge, as well as smaller decreases near the blade tip. Keeping in mind that the blades were loaded and fired with the tip down, the thickness reduction could be caused by either pack segregation or smaller volume in the tip. The central core of this blade is essentially separated by two wall structures into three connecting compartments forming the cooling air passages. The leading edge compartment and the center compartment are larger in volume and nearly elliptical. The filled trailing edge cooling holes are limited in volume and are not necessarily capable of providing all the required active metals. Kinetics, governed primarily by the short mean free path (approx. 7×10^{-6} microns) in the vapor and the firing time preclude significant utilization of active metals in the body of the blade where a large excess of active metal exists. Of the four packs used in this study, the columbium and chromium packs are unit activity systems with 50 and 20 weight percent of metal, respectively. Taking the case of the smallest radius in the exit hole, 0.25 mm, it can be calculated that the unit volume of that radius is 1.96×10^{-3} cm^3. With pack densities ranging from 1.5 to 2.0 g/cm^3, the amount of pack material contained in this volume is 2.95 to 3.92 mg. To deposit 4 mg/cm^2 of columbium onto the substrate in the cooling hole, 0.64 mg of active metal is required and since the columbium pack is 50 percent columbium metal, the amount of columbium available in this unit volume is approximately 1.5 to 2.0 mg, which far exceeds the necessary 0.64 mg. Similarly, it can be calculated that in order to deposit 3 mg/cm^2 (see Table 10) of chromium, 0.48 mg is required, which is available in the volume of pack powder confined in this unit volume, active metal content being 0.69 mg. However, the situation is different in the case of

Table 16

Coating Thickness Measurements

Location (See Fig. 33)	Coating Thickness (μm)			
	A	B	C	D
Top cut, typical	62	54	88	70
Top cut, near trailing edge	38	22	38	24
Bottom cut, typical	96	60	88	80
Bottom cut, near trailing edge	24	22	42	24

the two low-activity aluminum packs where aluminum is present to only 16 and 17 weight percent. Applying the same method of calculation to the aluminum packs, it was found that in the immediate vicinity of the 0.25 mm radius the pack was 100 percent depleted, resulting in the formation of only 30 to 50 percent of the full coating thickness. In addition, the microstructure of the thin coatings are losing their multi-zone structure.

The Ni-19Al-1Cb coated blade, N9, was further sectioned and examined, as shown in Figure 40. Besides the decrease in thickness noted in the trailing edge holes, a small gradient in coating thickness was also observed in the blade tip to firtree direction. Coating thickness appeared to be considerably greater in area A, 200-240 microns (see Fig. 40) compared to 140 microns in areas marked B, C, and D. Little change was observed in the coating along the vertical axis as the bore diameter remained constant. Again, this confirms that since coating thickness is governed by the internal capacity of the blade.

(A)

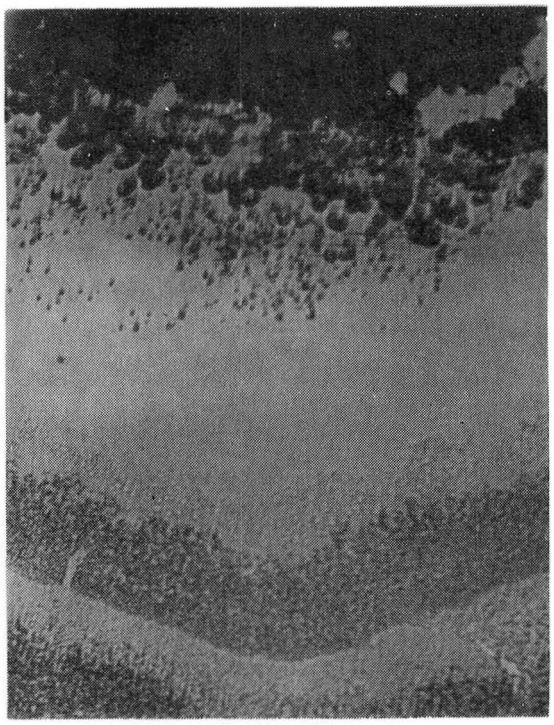

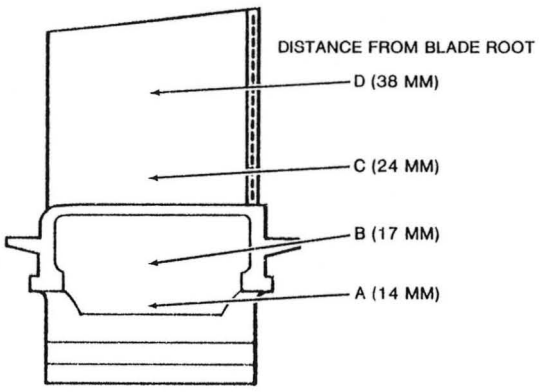

Blade No. N9

Ni-19Al-1Cb Coating

Electrolytic Chromic Etch

Magnification: 250X

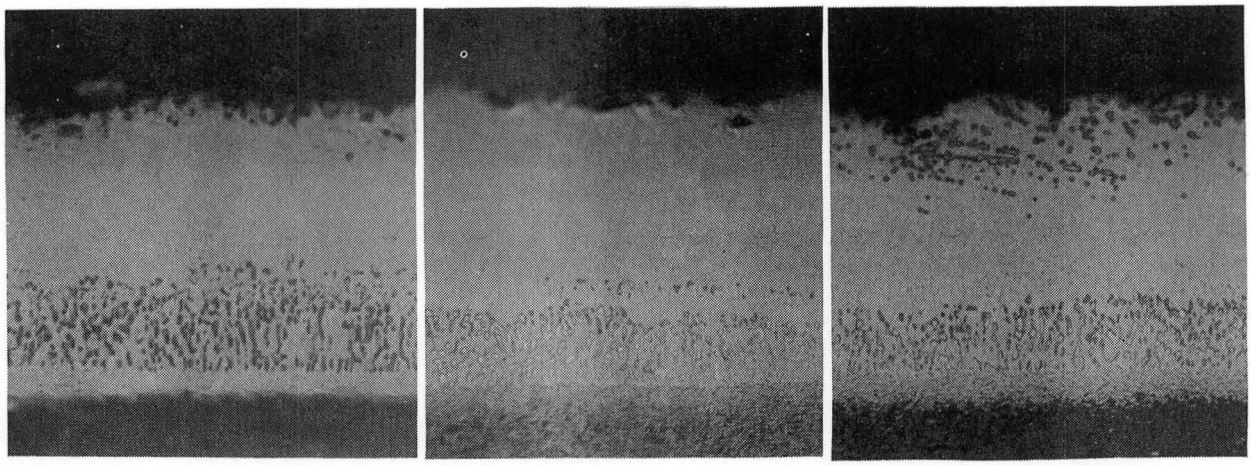

(B) (C) (D)

Figure 40. Comparison of Coating Thickness Along Blade Axis

This Page Intentionally Left Blank

4

TASK II - COATING/PROCESS CHARACTERIZATION

Since the coating systems developed in Task I were motivated by environmental protection of the substrate alloy, burner rig tests were conducted to evaluate and compare their resistance to hot corrosion and oxidation attack. Based on the results, mechanical properties of coated test bars were selectively evaluated to assess the influence of the coating and/or process on thermomechanical behavior of IN-792 alloy.

4.1 HOT CORROSION BURNER RIG TESTING

A total of 20 solid 6.4 mm bars were processed with the four candidate coatings for 899°C (1650°F) hot corrosion testing. The 76 mm long solid rods were coated up to 64 mm, leaving 12 mm uncoated. Each specimen was carefully packed in the activated pack such that 12 mm of the rod was exposed above the pack level. The weight gain values of the 20 test specimens, together with the control specimens, are reported in Table 17. Generally, weight gain values for the control specimens are lower than the burner rig specimens. This is partly due to the fact that the 12 mm portion of each rod that was kept above the pack reacted, although to a lesser degree with the metal vapors, thus increasing the total weight gain. Another more significant observation is the variation from batch to batch. The entire coating process was carefully reviewed to locate the source of the variation. It was found that all operations were controlled and well documented with one possible discrepancy. The gas fired furnace used in processing is routinely calibrated to $\pm$14°C. However, in some of the batch runs, a large retort was used and the volume of this retort appeared to have extended outside of the homogeneous heat zone of the furnace, resulting in differences in firing temperature. To illustrate the criticality of temperature and weight gain in aluminization, Figure 41 is shown using the averaged weight gain values from Tasks I and II. The slope of each line can be taken as an indication of the sensitivity of aluminum pickup to temperature fluctuation. Aluminide formation in coating Variation C appears to be the most affected by temperature inconsistencies. Therefore, temperature control in the order of $\pm$14°C could conceivably produce almost 7 mg/cm^2 differences in aluminum gain in this coating process. The other aluminization specimens, albiet less critical, would also need to be critically controlled to reduce compositional differences.

In order to accommodate all test specimens, two 300-hour rig tests were conducted. The total exposure times are summarized in Table 18. In each group of coatings, specimens were exposed to approximately 100, 200 and 300 hours. At approximately 200 hours, one specimen of each composition was removed and replaced by a fresh coated specimen.

Table 17

Weight Gain Data of Coated Specimens

	Specimen Number	Columbium Wt. Gain (mg/cm^2)	Aluminum Wt. Gain (mg/cm^2)
Variation A			
Batch 1	R1	2.61	11.07
	R2	3.00	13.56
	C1*	2.43	8.24
Batch 2	R3	3.28	10.90
	R4	3.37	10.58
	C2*	2.84	7.74
Batch 3	R69	1.05	13.10
	R70	1.17	13.83
	C9*	2.33	11.19
Variation B			
Batch 1	R5	8.40	11.01
	R6	7.80	9.24
	C3*	9.19	6.65
Batch 2	R7	7.32	9.10
	R8	8.13	8.48
	C4*	5.44	6.41
Batch 3	R71	7.34	11.16
	R72	6.87	11.33
	C10*	6.13	8.10
Variation C		Cr Wt. Gain	
Batch 1	R9	6.05	21.52
	R10	6.41	22.80
	C5*	5.26	20.41
Batch 2	R11	4.85	19.47
	R12	4.82	21.31
	C6*	4.18	20.26
Variation D			
Batch 1	R13	6.01	14.03
	R14	6.02	14.15
	C7*	4.73	11.05
Batch 2	R15	4.89	12.51
	R16	4.85	12.65
	C8*	3.68	10.33

* Control coupons fully surrounded by pack materials

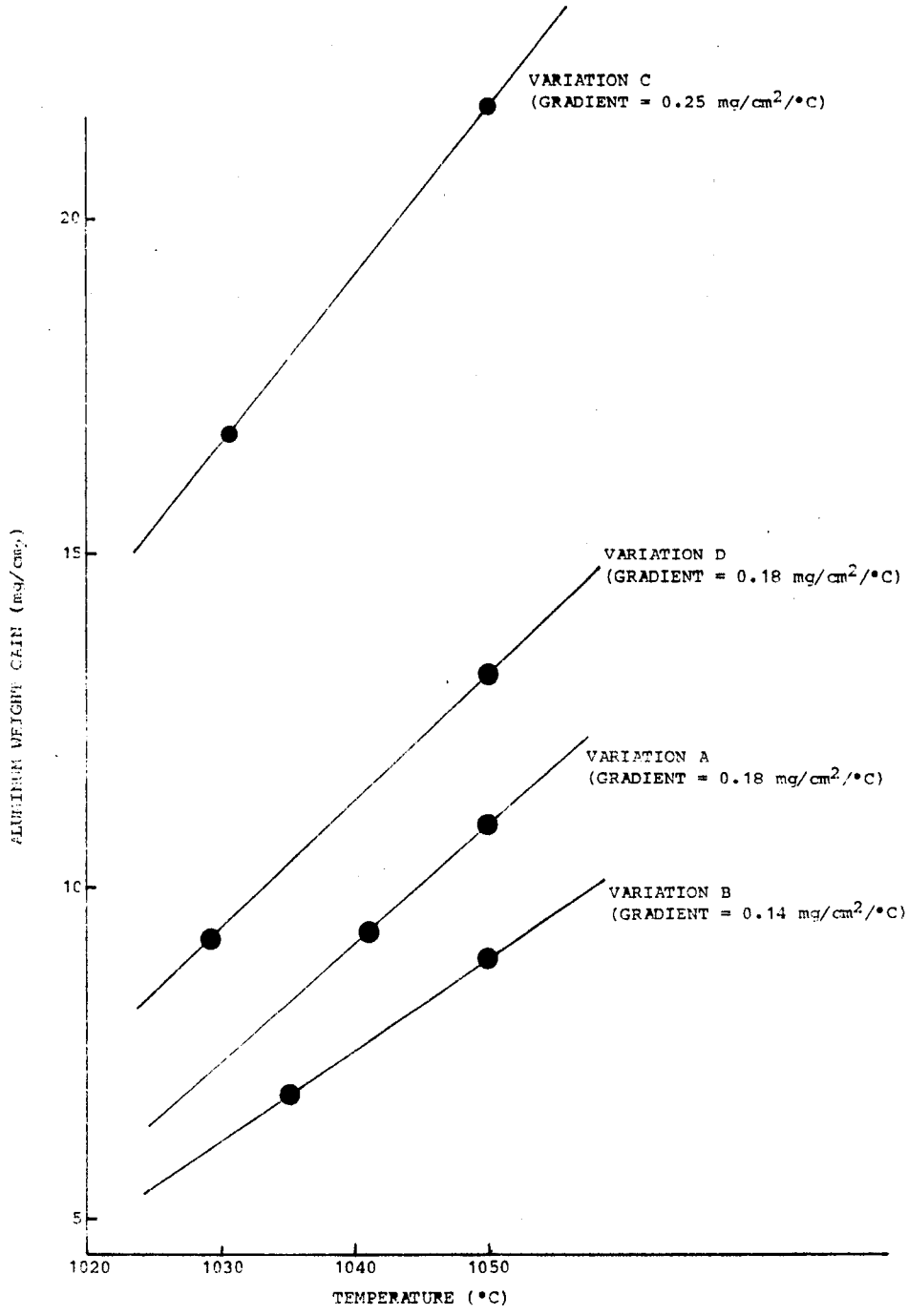

Figure 41. Effect of Temperature on Deposition of Aluminum in Pack Processing

Table 18

Summary of Hot Corrosion Test Specimens

Spec. #	Batch	Coating System	Test Time (Hrs)
Test 1 (#3-010)			
R1	1	A	314
R2	1		314
R3	2		212
R4	2		314
R69	3		102
R5	1	B	314
R6	1		314
R7	2		314
R8	2		212
R71	3		102
Test 2 (#3-011)			
R9	1	C	318
R10	1		318
R11	2		318
R12	2		214
R40	3		104
R13	1	D	318
R14	1		318
R15	2		318
R16	2		214
R41	3		104

Note: A = Ni-19Al-1Cb
B = Ni-19Al-3Cb
C = Ni-17Al-20Cr
D = Ni-12Al-20Cr

The surface appearance of all specimens, regardless of the number of cycles, were very similar and typical specimens are shown in Figure 42. The entire specimen length was covered with varying deposits, salt with localized spallation of the encrusted deposit. The salt deposits varied in color from a fluffy white through hues of grey with some yellow at the cooler areas. Since the salts used to prepare synthetic sea water were all white in color, white deposits are expected on these specimens. Careful scraping of the loose top layer of deposits (both white and yellow) uncovered a continuous, uniform greyish yellow adherent scale on all surfaces. Scrapings were taken from these specimens and submitted for chemical analysis for identification of the compounds. The washings from the specimens, containing water

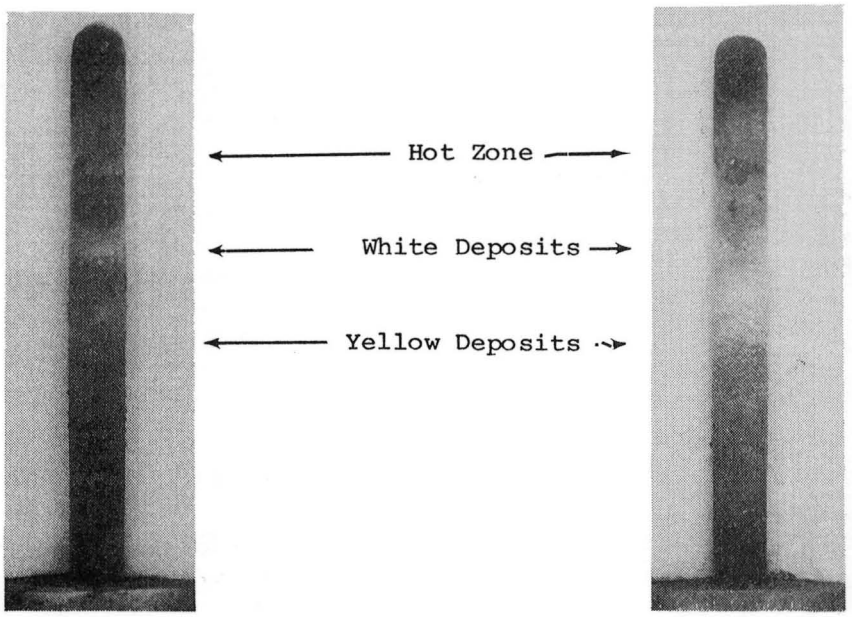

Figure 42. Surface Appearance of Rig Specimens After 212 Cycles (Hours) at 900°C (1650°F) in Corrosion Rig Test

soluble salts, were also submitted for analysis. After water washing, the fine deposits were completely removed and the underlying substrate appeared to be discolored, as seen in Figure 43. However, close examination showed no visible pitting or spallation other than roughening of the alloy, especially in the hot zone.

Even at the end of 300 hours of exposure, no significant coating degradation was observed and there were no visible differences in all specimens except for degree of deposit buildup. The sections of the specimen in the hot zone of the combustion gas streams generally are exposed to the maximum gas velocity and temperature. Consequently, little deposition or condensation of the salt particles occur. However, in the cooler flame regions and further along the specimen length, the entrained salts can readily condense, forming a thick crust which spalled in some instances. Again, little surface attack was observed, as can be seen in Figure 44. Physical appearance of all unwashed test specimens are shown in Appendix B.

Deposits from three areas on a Ni-19Al-1Cb coated (R3) specimen were analyzed by X-ray fluorescence and diffraction and results are reported in Table 19. Using powder diffraction standards PDF 5-0631, 4-0835 and 10-699, crystalline compounds Na_2SO_4, NiO and $FeSO_4 \cdot 4H_2O$, respectively, were detected in all three samples. The synthetic sea salt composition used is predominant in NaCl. However, upon ingestion into the hot gas stream, it is generally

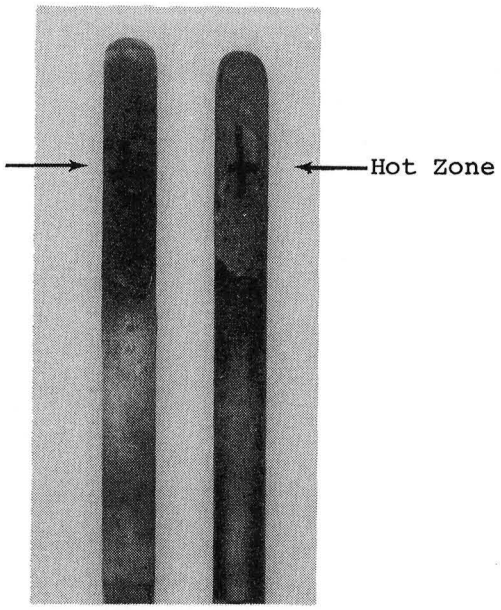

Figure 43.

900°C (1650°F) Hot Corrosion Rig Specimens After Washing and Removal of Surface Deposits, Revealing Substrate Discoloration

accepted (Refs. 15, 16) that conversion to Na_2SO_4 occurs and this is substantiated by the presence of Na_2SO_4 identified in the surface deposits. The iron sulfate species must have been introduced as contamination (rust) from the lines bearing air and fuel to the combustor.

Chemical compositions of the deposits, as reported in Table 19, indicate that sulfur (presumably in the form of sulfate) is the major constituent of the yellow deposit while nickel predominates in the grey deposits B and C. Deposits obtained from the Ni-Al-Cr systems after hot corrosion exposure were also analyzed. Two deposits were taken from two areas on the trailing edge of the specimens; sample E was an adherent grey deposit in the center of the hot gas path while sample D was a loose brown deposit found in the cooler regions on the trailing edge. X-ray diffraction analysis identified the presence of Na_2SO_4 and nickel oxides in both samples, with sample D containing more Na_2SO_4 and less NiO than sample E. Since Na_2SO_4 has fairly low vapor pressures at temperatures less than 899°C, condensation is expected to occur at the cooler specimen areas.

The test specimens were sectioned in a transverse manner at the center of the hot zone which was located approximately 12 to 18 mm from the tip. Photomicrographs of typical areas of each coating batch are included in Appendix C of this report.

In general, limited attack was noted on some of the specimens, with intergranular oxidation in the case of Ni-19Al-1Cb coated R69, Figure C-3. However, no catastrophic coating degradation was found and all evidence of oxide formation and attendant voiding due to loss of aluminum to the surface environment was confined to less than the top 30 percent of the coating. An interesting but

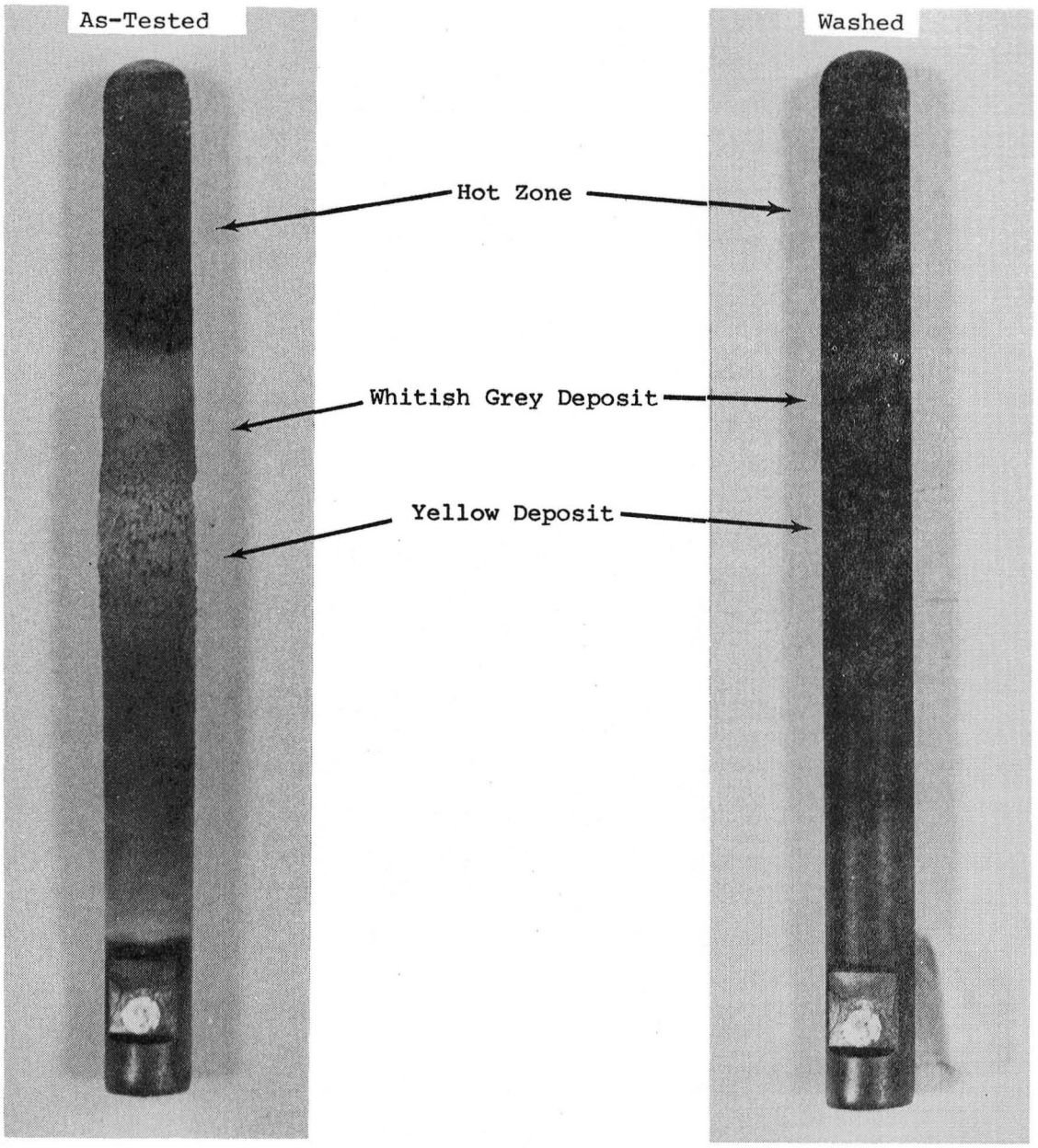

Figure 44. Surface Appearance of Rig Specimen (Ni-12Al-20Cr, R15) After 318 Hours of Exposure. Magnification 2X

Table 19

X-Ray Analysis of Deposits on Surface of Corrosion Specimen R3 (Coated With Ni-19Al-1Cb) After 212 Hours of Testing

Element	Weight Percent		
	A *	B *	C *
Aluminum	0.0014	0.0025	0.0023
Calcium	1.04	0.18	0.51
Chlorine	0.09	0.16	0.36
Chromium	0.09	0.014	0.012
Iron	4.32	4.67	5.40
Nickel	2.33	45.02	43.56
Niobium	0.01	0.003	0.006
Potassium	1.04	0.27	0.36
Sulfur	53.17	28.98	28.46
(See Fig. 42)			

* A = Yellow deposits
B = Whitish grey deposits
C = Deposits on other side of specimen away from flame

inexplicable fact is the lack of correlation between the degree of penetration and exposure time. A possible hypothesis is that the oxidation/corrosion rates experienced here were within the 'incubation' or threshold of time dependent corrosion phenomenon.

In all exposed specimens, a continuous oxide layer was found at the surface, even those that were washed prior to metallographic mounting. This oxide scale appeared to be thinner and more adherent when developed on Ni-Al-Cb systems (A and B), Figures C-1 through C-6, relative to the Ni-Al-Cr coatings (C and D), Figures C-7 through C-12. Furthermore, even after sectioning and polishing, the thin oxide scale did not separate or pull away from the base metal, unlike the thicker oxides formed on Ni-Al-Cr coatings.

Depth of penetration measurements were taken and are shown in Table 20. Penetration values in each coating show some scatter but a trend towards greater attack can be noted in Variation C (Ni-17Al-20Cr) and also in Variation D (Ni-12Al-20Cr). The columbium containing coatings generally exhibit dark areas near the surface, which were found to be oxides and/or voids. On the other hand, the chromium-rich coatings were susceptible to intergranular oxidation resulting in dark etching grain boundaries. Close examination also revealed breakdown of the coating structure to dark grey and light grey phases which are gamma/gamma prime.

Returning to Table 20, a list of coating thickness values are reported, both for coated control (unexposed) specimens and also for coated test pieces. In all instances, except for Coating D, Batch 3, the coatings increased in thickness during testing. This increase is probably a result of solid state diffusion between the two meta-stable systems, coating and superalloy. Since

Table 20

Hot Corrosion Test Results

Specimen #	Coating	Batch	Test Time (Hrs)	Coating Thickness (μm)	Penetration (μm)
C1	A	1	0	95	--
R1			314	102	25
R2			314	89	32
C2	A	2	0	89	--
R3			212	95	0
R4			314	102	22
C9	A	3	0	95	--
R69			102	114	29
C3	B	1	0	79	--
R5			314	95	13
R6			314	102	19
C4	B	2	0	84	--
R7			314	98	< 19
R8			212	95	19
C10	B	3	0	71	--
R71			102	83	25
C5	C	1	0	135	--
R9			318	152	32
R10			318	152	32
C6	C	2	0	135	--
R11			318	146	50
R12			214	159	50
C10	C	3	0	111	--
R40			104	127	32
C7	D	1	0	102	--
R13			318	105	32
R14			318	111	32
C8	D	2	0	95	--
R15			318	102	25
R16			214	95	19
C11	D	3	0	105	--
R41			104	102	32
R37	None		100	-	300 to 400

diffusional stability is a critical concern in coating evaluation, comparison is made for the four coatings after approximately 300 hours. The averaged values are reported in the bar chart in Figure 45. Interestingly, the two coatings exhibiting the best stability are Variations A and D, which contain 19 and 12 percent aluminum, respectively. Assuming the major driving potential for interdiffusion is the movement towards aluminum equilibrium, one would expect a correlation between aluminum in the coating and diffusional growth. Instead, the data would suggest that phase formations and interactions with the columbium or chromium additive to the matrix may be diffusion controlling by acting as selective diffusion barriers or chemical potential modifiers.

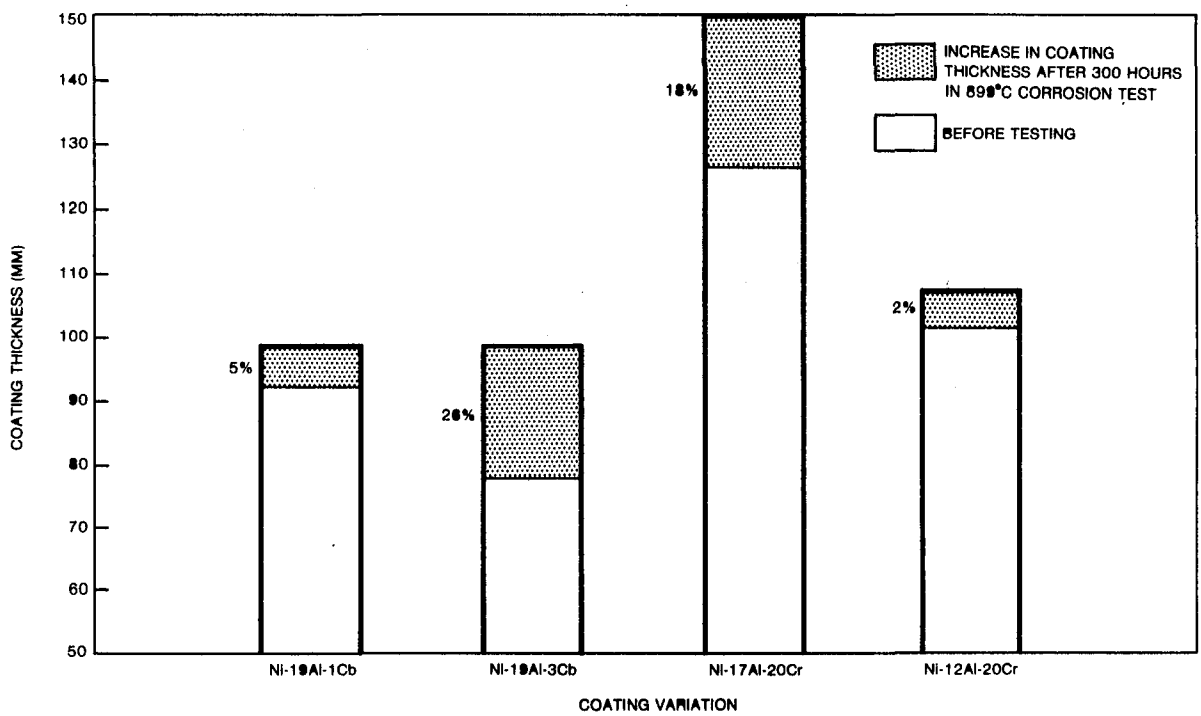

Figure 45. Coating Thickness Growth During Testing

A note is made here of a single hairline crack observed in specimen R8, Ni-19Al-3Cb coated with 212 hours test time. The crack penetrated the entire coating (Fig. 46) and extended into the substrate. The crack could have originated (1) during thermal cycling in the burner rig, or (2) while the specimen was being prepared for metallography. The second explanation is favored since no other cracks were observed and the crack does not appear to follow grain boundaries and, even more significantly, no evidence of any external oxidation attack is found along the crack.

In an effort to further increase understanding of the performance of these coatings in 900°C (1650°F) hot corrosion rig tests, SEM/EDX analyses were conducted and results are discussed here.

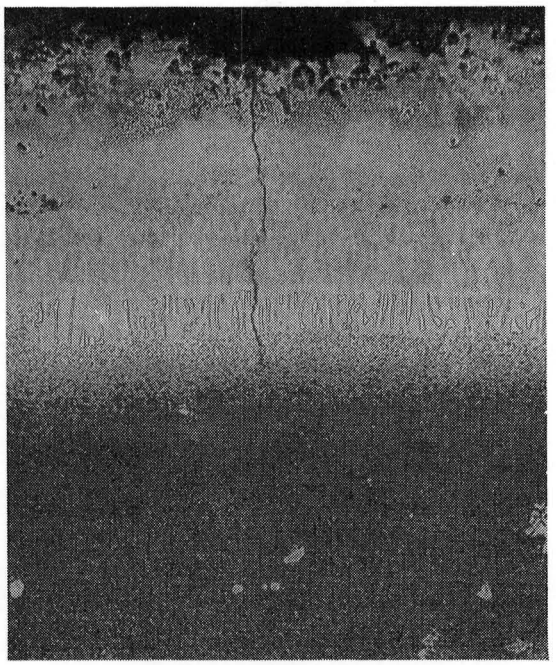

10% Electrolytic Oxalic Etch

Magnification: 400X

Mount No. 133

Figure 46. Single Hairline Crack Observed on Ni-19Al-3Cb (Variation B) Coated IN-792 Specimen After 900°C Corrosion Rig Test

Ni-19Al-1Cb Coating

The SEM photomicrographs of the as-coated (plus heat treated) C1 specimen in Figure 47 clearly show a narrow zone near the coating surface (A) followed by a light grey dispersed phase in the coating matrix (B). Near the interface, an elongated substructure, rich in the elements: titanium, tungsten, tantalum and molybdenum, precipitated from the substrate alloy.

The distribution of aluminum and columbium in the as-coated and as-tested conditions are shown in the electron dot maps in Figures 47 and 48. Prior to testing, aluminum is concentrated in the denuded zone near the surface. Columbium is concentrated near the coating surface in a continuous narrow band (see Fig. 47). After 314 hours of cyclic exposure at 900°C (1650°F), a little diffusion of columbium is noted, see Figure 48. The immobility of columbium is marked by the high density band near the coating/ oxide scale interface. Another point to note is that instead of the relatively uniform distribution of aluminum in the as-heat treated (unexposed) condition, aluminum diffusion outwards occurred during thermal exposure.

The zones marked A and B in Figure 47 were scanned for aluminum, columbium and nickel and semi-quantitative results are reported in Table 21 normalized to aluminum. The columbium/aluminum ratio is higher in A than in B, indicating higher relative amounts of columbium in the outer zone A. Figure 49 shows a high magnification photomicrograph of the same area. The spots labeled C, D and E were scanned to compare columbium, aluminum and nickel levels.

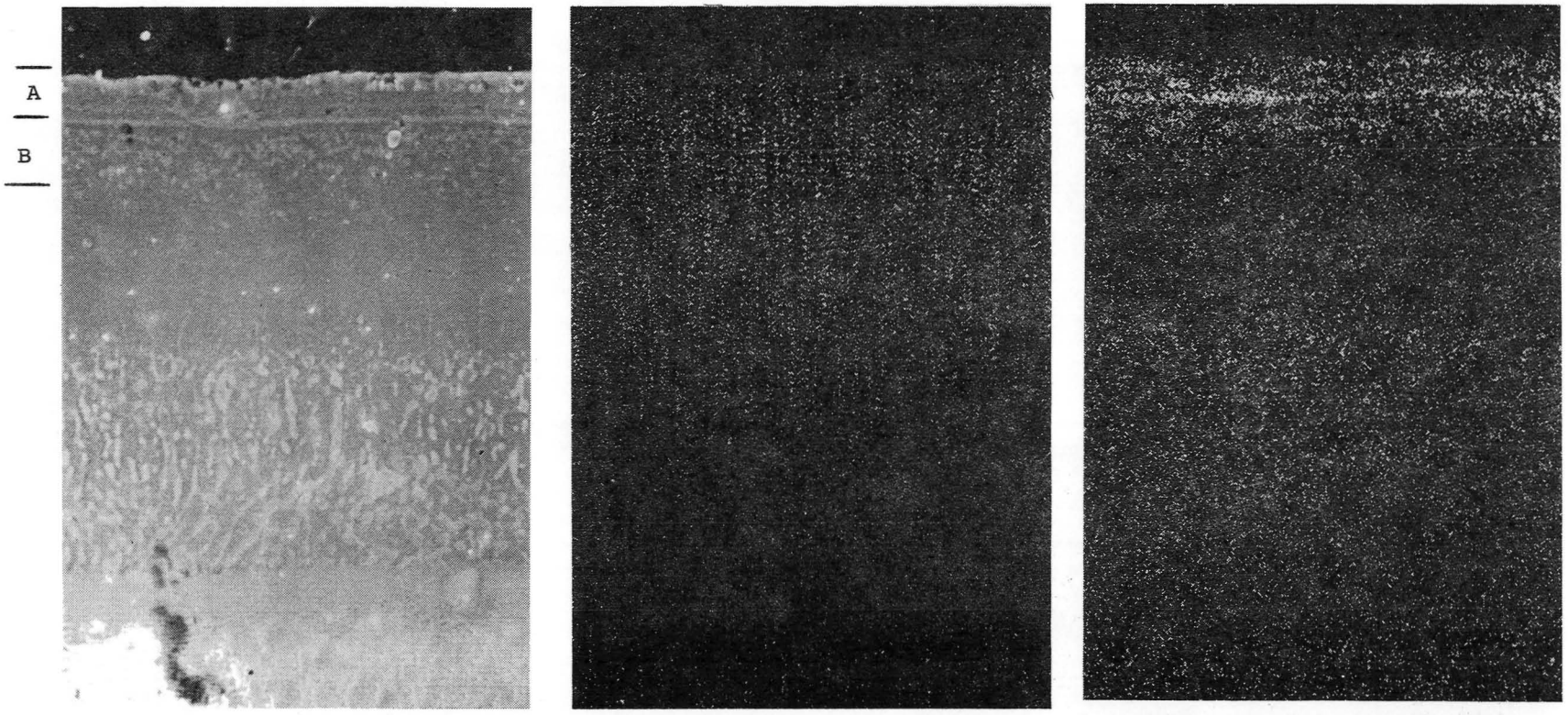

Specimen No. C1 | Aluminum Dot Map | Columbium Dot Map

Magnification: 1000X

Figure 47. SEM Micrograph and Dot Maps of Ni-19Al-1Cb Coating on IN-792 Alloy After Heat Treatment (1121°C/2 hrs, 843°C/24 hrs)

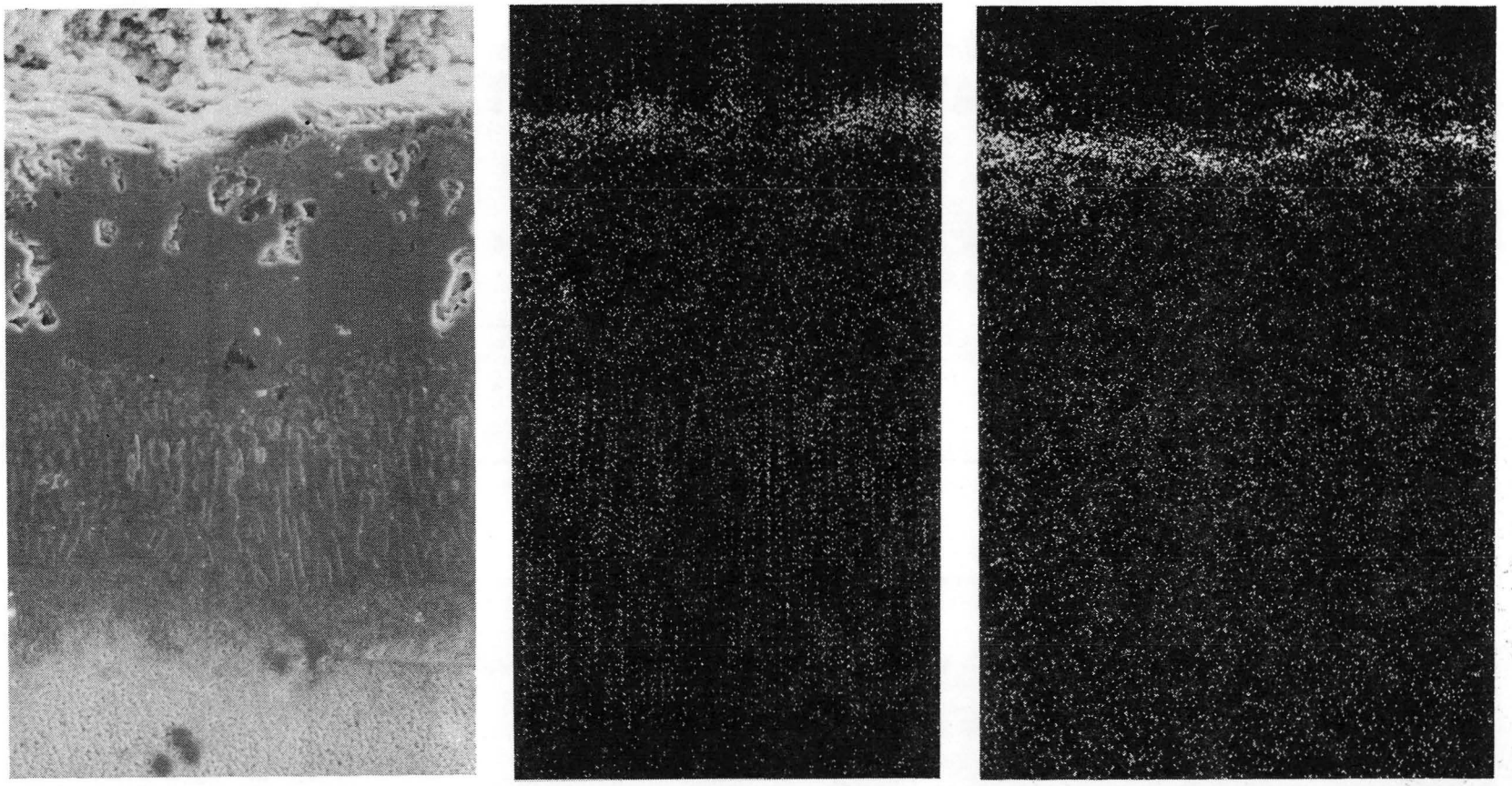

Specimen No. R1 | Aluminum Dot Map | Columbium Dot Map

Magnification: 1000X

Figure 48. SEM Micrograph and Dot Maps of Ni-19Al-1Cb Coating on IN-792 Alloy After 314 Hours of 900°C Hot Corrosion Rig Test

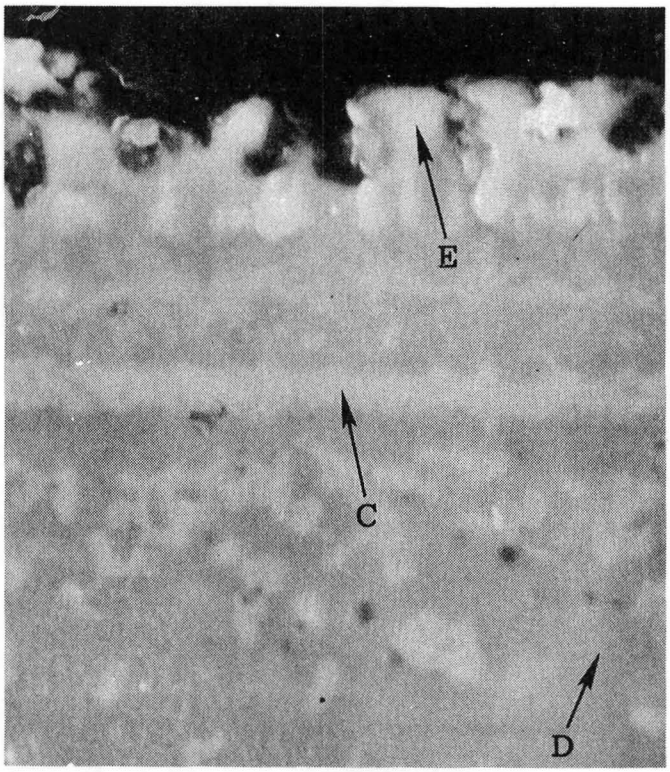

Specimen C1

Magnification: 7600X

Figure 49.

Photomicrograph of Columbium-Rich Zone of Ni-19Al-1Cb Coating, Heat Treated

Table 21

Relative Concentration of Aluminum, Columbium and Nickel in Columbium-Rich Zones in Ni-19Al-1Cb Coating

Ratio to Aluminum	A	B	C	D	E
Aluminum	1	1	1	1	1
Columbium	1.11	0.35	4.80	2.35	2.15
Nickel	4.49	2.72	4.91	4.15	2.90
	(See Fig. 47)		(See Fig. 49)		

Even though ratio values cannot be regarded as absolute figures, they are representative of the relative concentrations of the elements. The continuous band marked C is definitely rich in columbium and nickel. The matrix labeled D is probably nickel aluminide while E marks the aluminum-rich phase near the surface. After exposure, the narrow C band is expanded into a wide columbium-rich zone adjacent to (or at) the oxide scale. The significance of these columbium containing phases in hot corrosion resistance could be their stability under oxidizing conditions and their well-placed location near the coating surface.

Ni-19Al-3Cb Coating

The next set of photomicrographs, Figures 50 and 51, shows Ni-19Al-3Cb in the coated and as-tested conditions. A notable difference between this coating coating and the lower columbium coating, Ni-19Al-1Cb, is the absence of a continuous columbium-rich band near the surface in the as-coated condition. However, a similar light grey discrete columbium-rich phase is observed extending about 50 percent into the coating. Random probe of this columbium-rich phase revealed that the columbium-aluminum ratio ranged from 7 to 9.

After 314 hours of rig testing, Figure 51 shows that columbium is concentrated immediately beneath the oxide/coating interface. In the aluminum and columbium dot maps, it can be seen that next to the aluminum-rich darker etching phase, a partially depleted zone is formed as noted in Figure 51. The coating structure near the coating/substrate interface is basically unchanged.

Comparison of coating Variation A and B (Figs. 47 and 50), leads to the conclusion that the major difference resulting from the two columbium deposition processes is the distribution of the columbium in the heat treated condition. The lower columbium process produced a high concentration of columbium in a narrow band near the surface and is essentially non-diffusing even under thermal exposure. The 3Cb coating, on the other hand, exhibits some columbium diffusion to the coating surface. Since diffusional movement in any direction must be accompanied by diffusion in the counter direction, the Ni-19Al-3Cb can be expected to undergo greater diffusional changes during testing. This is supported by thickness growth measurements reported earlier where Ni-19Al-1Cb was found to be more stable than Ni-19Al-3Cb. Another point of comparison is the composition of the oxide formed on each coating. The oxides developed on Ni-19Al-3Cb contain considerably more columbium than does the Ni-19Al-1Cb oxide scale, again pointing to greater diffusion to replenish the columbium lost in oxide formation.

Ni-17Al-20Cr Coating

The nickel-chrome-aluminide system is shown in Figures 52 and 53. Prior to testing, the coating is composed of fine dispersions of a light grey phase with a finger-like substructure near the coating/alloy interface. The outer two-thirds of the coating, rich in aluminum and chromium, appears to be also concentrated near the surface. Energy dispersive X-ray analysis revealed that the small light grey spots do indeed correspond to high chromium (and tungsten) levels, see Figure 54. After 318 hours of exposure, stratification of chromium can be observed, Figure 53. Chromium and also aluminum have undergone diffusion to the oxidation front, leaving a denuded zone.

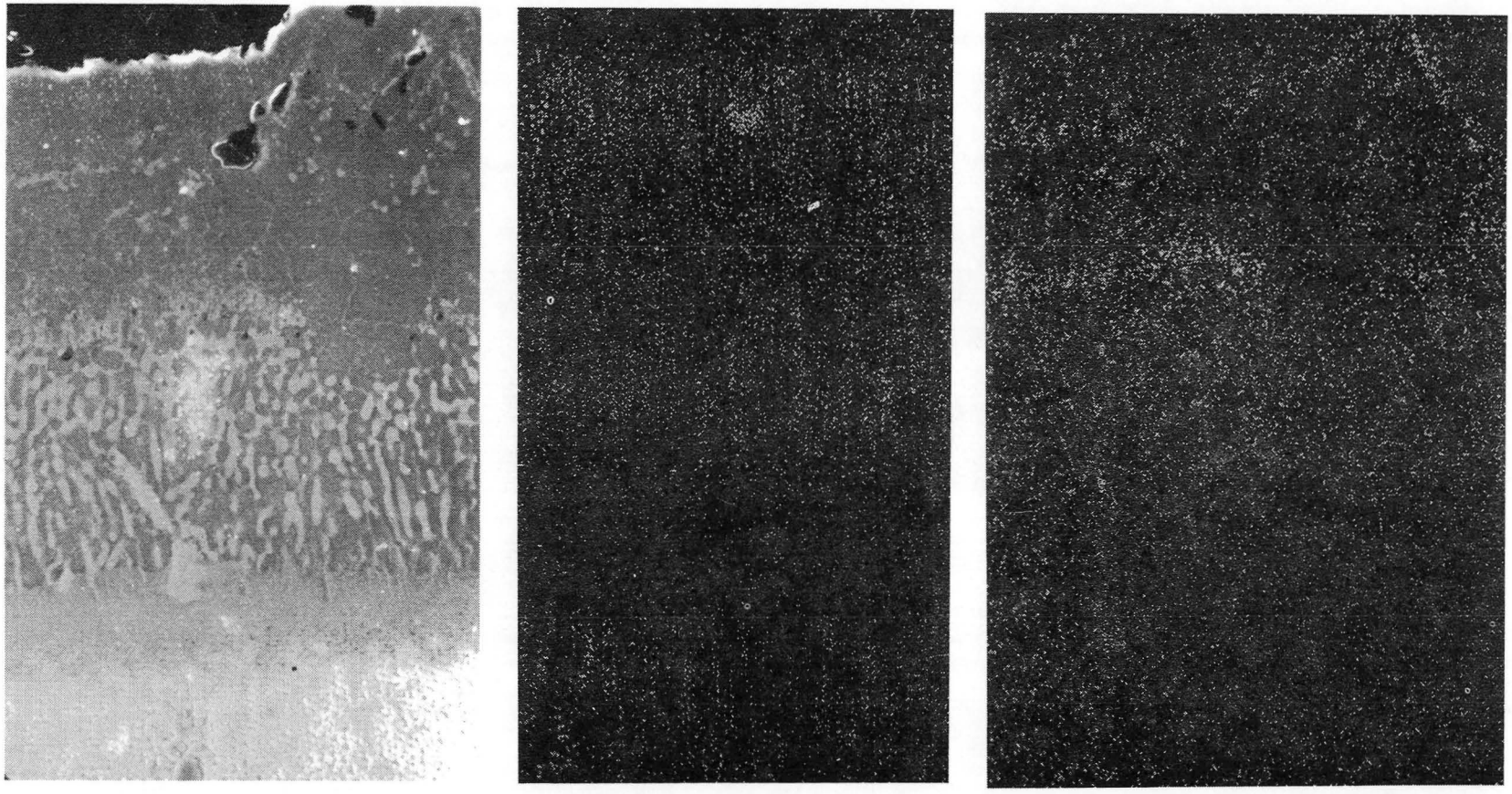

Specimen No. C3 | Aluminum Dot Map | Columbium Dot Map

Magnification: 1000X

Figure 50. SEM Micrograph and Dot Maps of Ni-19Al-3Cb Coated IN-792 Alloy in Heat Treated Condition

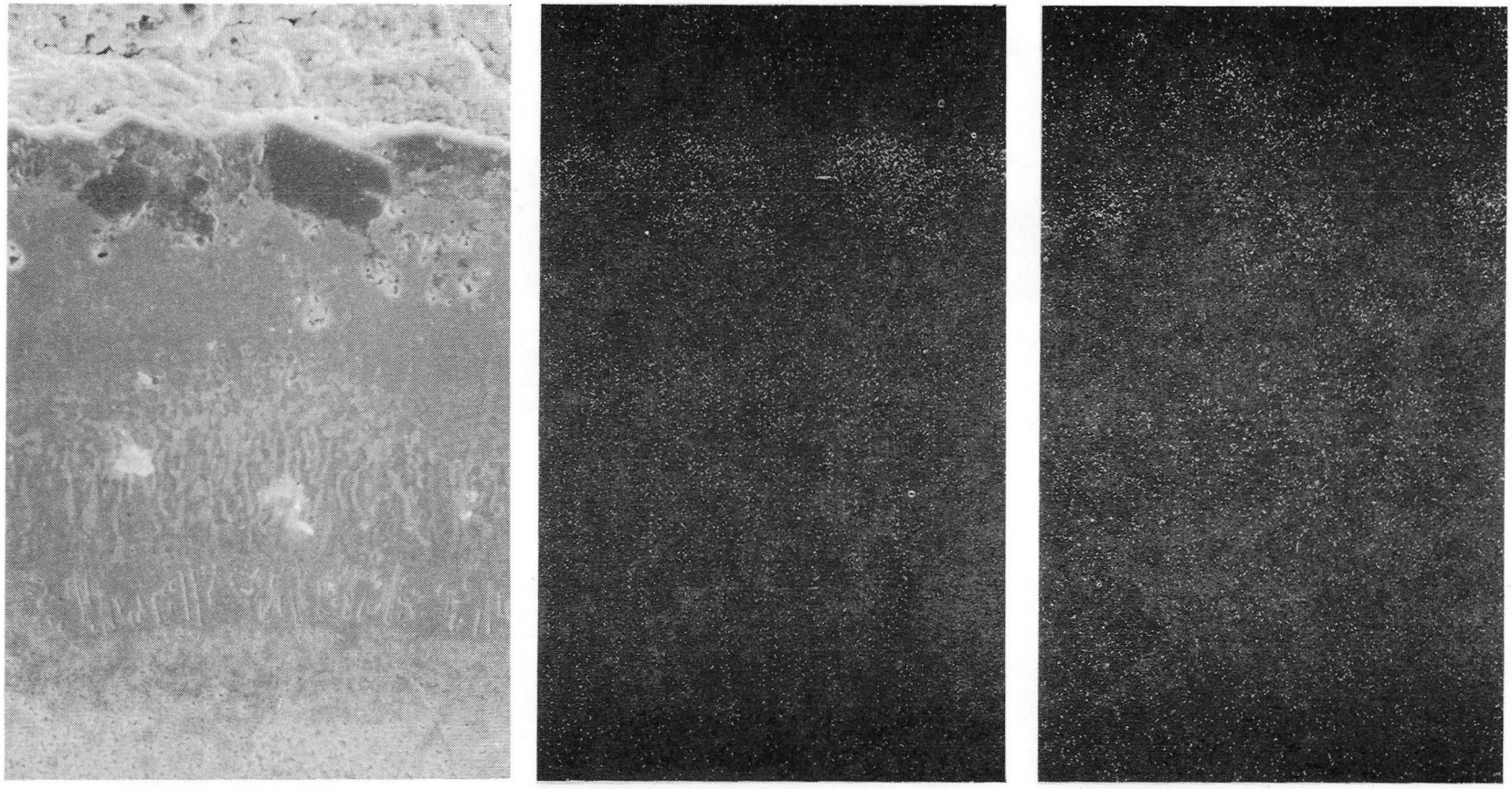

Specimen No. C3 | Aluminum Dot Map | Columbium Dot Map

Magnification: 1000X

Figure 51. SEM Micrograph and Dot Maps of Ni-19Al-3Cb Coated IN-792 Alloy After 314 Hours of 900°C Hot Corrosion Rig Test

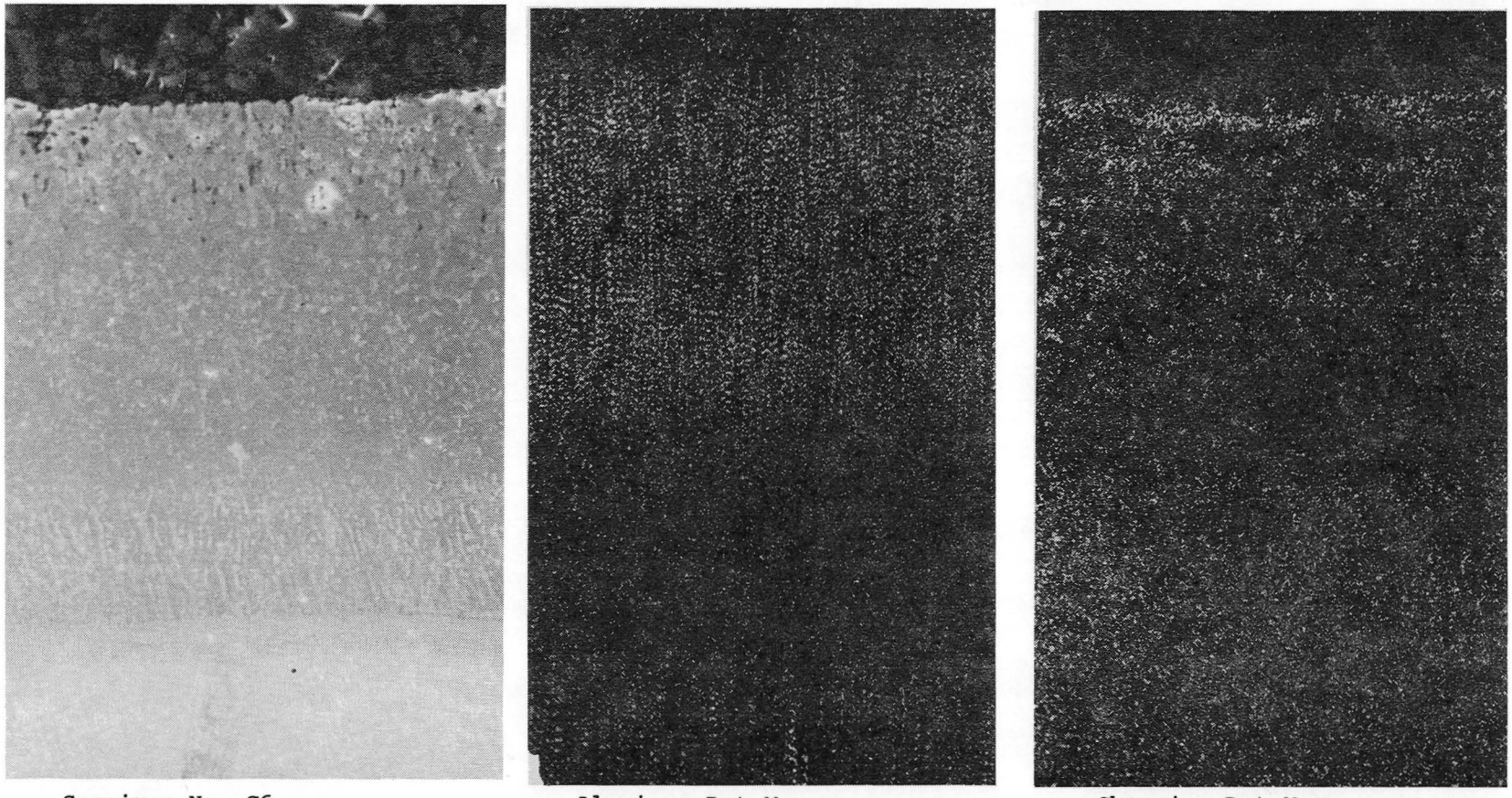

Specimen No. C6 | Aluminum Dot Map | Chromium Dot Map

Magnification: 1000X

Figure 52. SEM Micrograph and Dot Maps of Ni-17Al-20Cr Coated IN-792 Alloy in the Heat Treated Condition

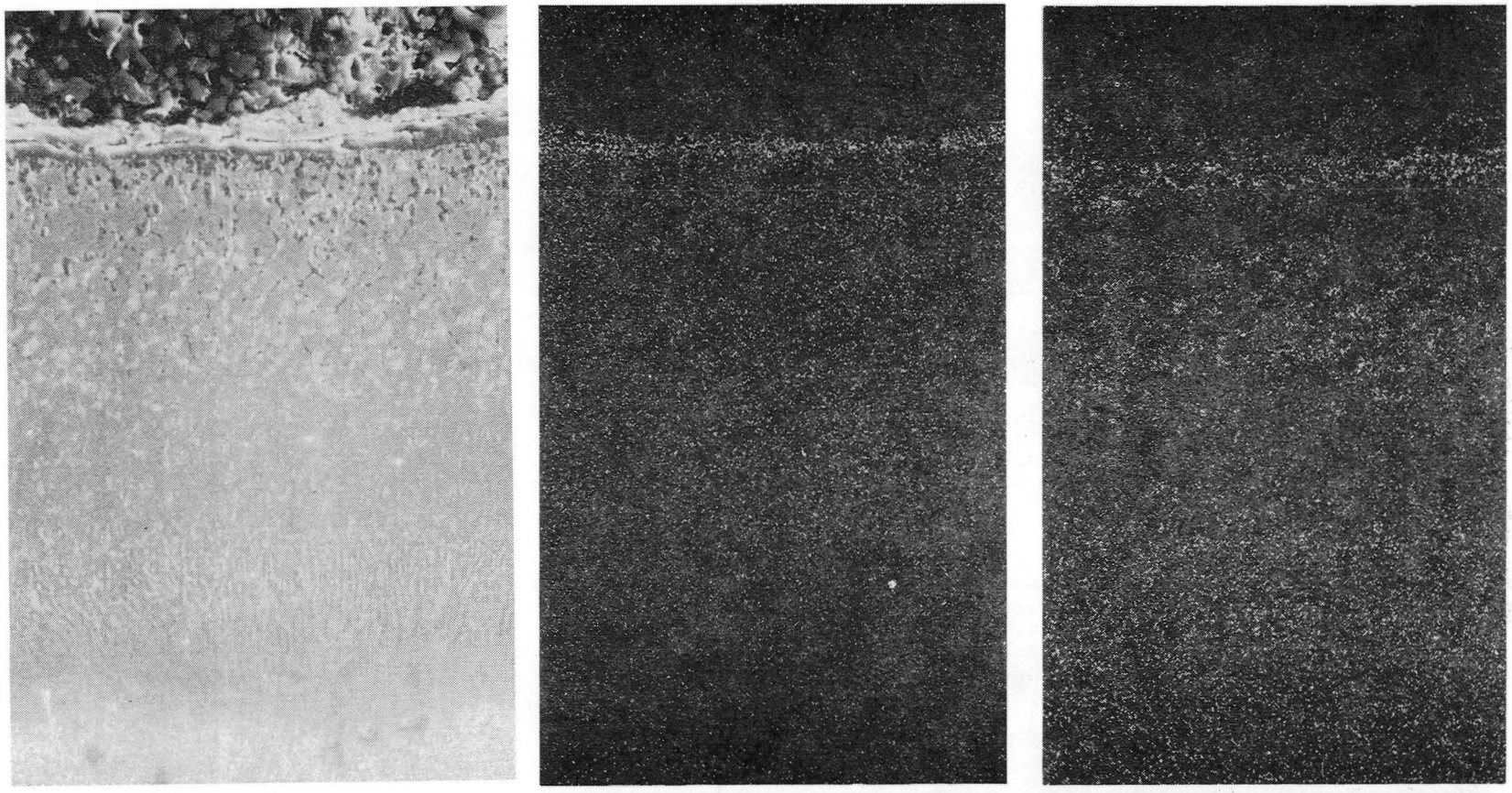

Specimen No. R11 | Aluminum Dot Map | Chromium Dot Map

Magnification: 1000X

Figure 53. SEM Micrograph and Dot Maps of Ni-17Al-20Cr Coated IN-792 Alloy After 318 Hours of 900°C Hot Corrosion Rig Test

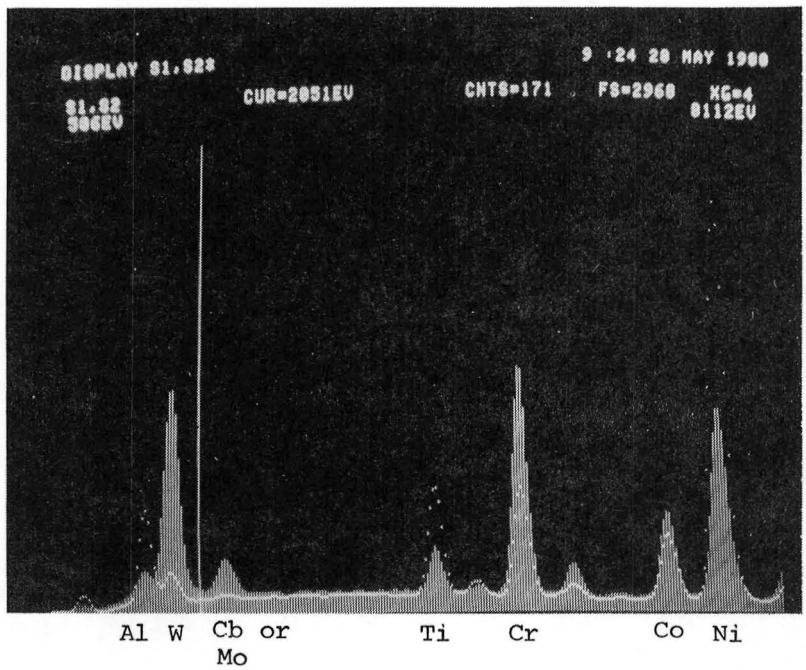

Figure 54. EDX Spectra of Ni-17Al-20Cr Coating (Bars Represent Light Grey Phase, Dots Represent Coating Matrix, See Figure 52)

Ni-12Al-20Cr Coating (Variation D)

In the as-coated condition, Figure 55, chromium appears to be well dispersed in the coating matrix with a semi-continuous band formed near the interface. A similar high chromium concentration can be found near the surface. Note that the chromium-rich areas correspond to the light grey phase.

After 318 hours exposure, Figure 56, the chromium has diffused to the surface and can be found in a discontinuous band just below the interface, between oxide and coating. Another high chrome region is found midway in the coating. Reference to Figure 52 shows that Coating C (Ni-17Al-20Cr) does not exhibit this high chromium barrier. The aluminum electron dot map in Figure 56 also exhibits a stratification of aluminum into two rich zones, one in mid-coating and another at the coating/oxide interface. Whether this unusual structure can be related to the greater stabiity of this coating relative to Ni-17Al-20Cr is not clear.

Besides the coated test specimens, an uncoated IN-792 rod was also evaluated as a baseline. Figure 57 shows the microstructure after 100 hours in the corrosion environment. The alloy was severely attacked and rod diameter was noticeably reduced due to loss of metal. Comparison of this microstructure with those of the coated specimens clearly identifies the extended life they impart to the IN-792 substrate.

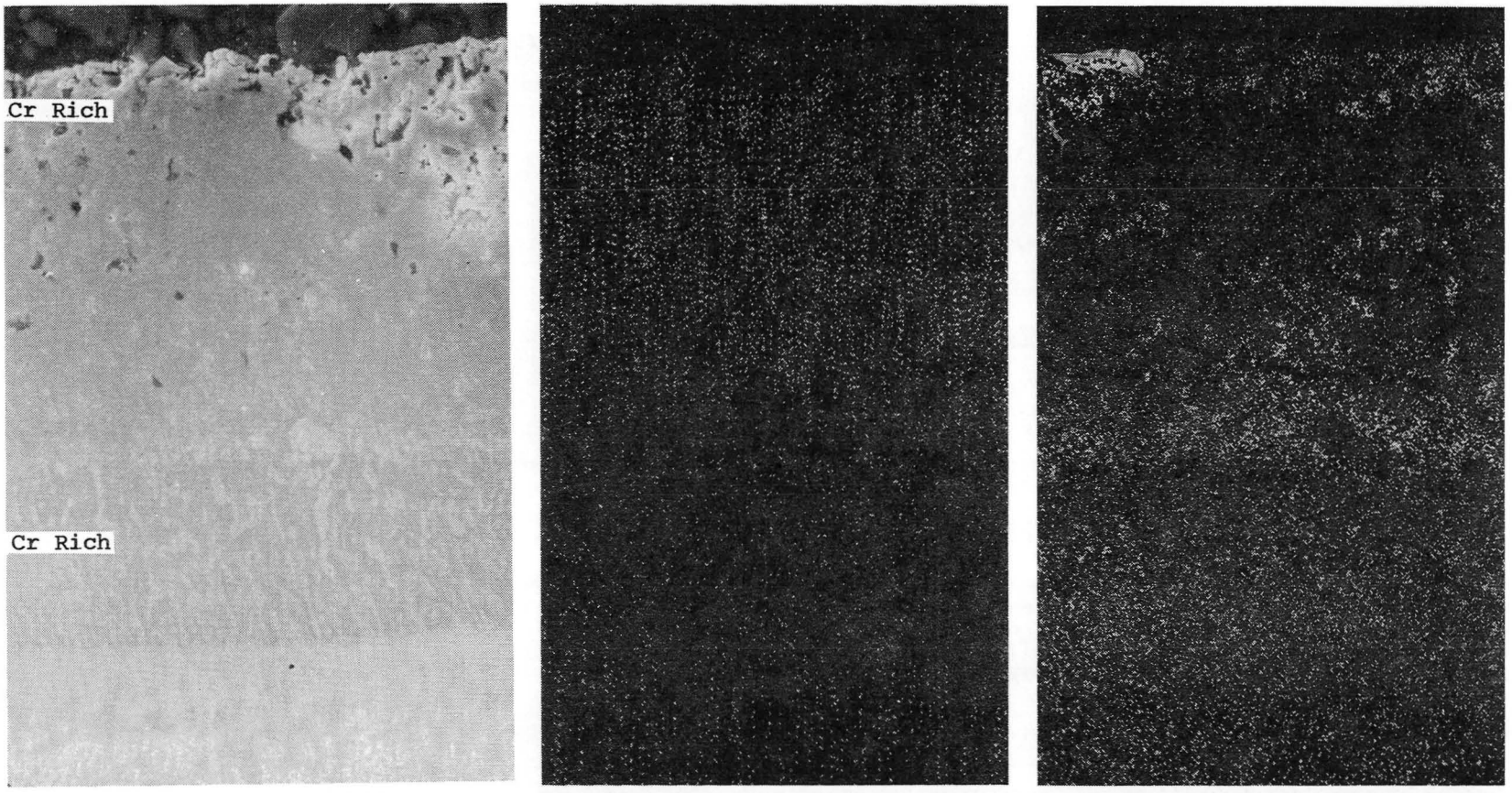

Specimen No. C8 | Aluminum Dot Map | Chromium Dot Map

Magnification: 1000X

Figure 55. SEM Micrograph and Dot Maps of Ni-12Al-20Cr Coated IN-792 Alloy in the Heat Treated Condition

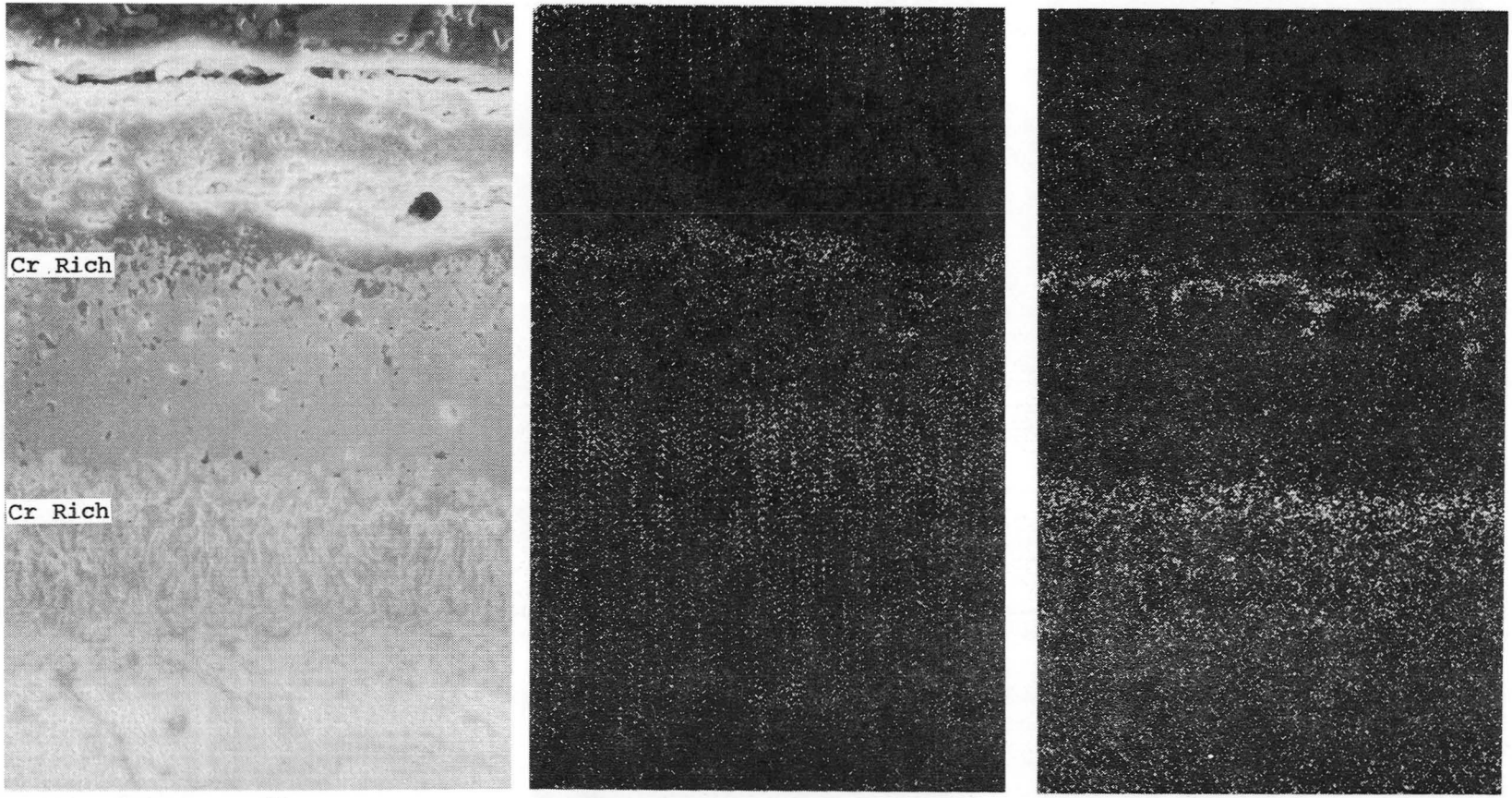

Specimen No. R15 | Aluminum Dot Map | Chromium Dot Map

Magnification: 1000X

Figure 56. SEM Micrograph and Dot Maps of Ni-12Al-20Cr Coated IN-792 Alloy After 318 Hours of 900°C Hot Corrosion Rig Test

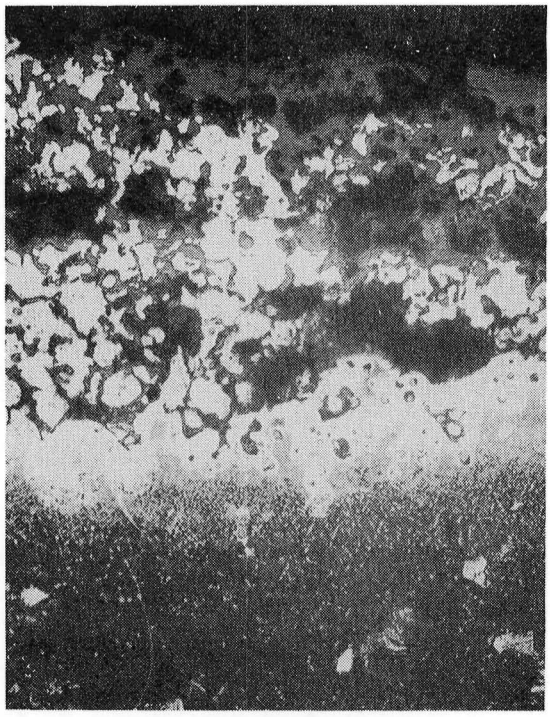

Magnification: 200X

Figure 57.

Uncoated IN-792 Baseline Specimen (R37) After 100-Hour Corrosion Rig Test at 899°C

Based on the metallographic evaluation of the exposed coated specimens, several conclusions are drawn.

1. The Ni-Al-Cb coating systems exhibited superior hot corrosion resistance than the Ni-Al-Cr systems. This is supported by depth of penetration measurements.

2. The Ni-19Al-3Cb coating had the best hot corrosion resistance with maximum attack of 25 microns in 318 hours while maximum penetration in the other coatings were in the 25-50 micron range. The coatings can be ranked in decreasing order of hot corrosion resistance as Ni-19Al-3Cb > Ni-19Al-1Cb, Ni-12Al-20Cr > Ni-17Al-20Cr. Uncoated IN-792 bar after 100 hours of exposure suffered 300 to 400 microns of alloy penetration.

3. The excellence of the Ni-19Al-3Cb coating in hot corrosion is compromised by diffusional instability. The Ni-19Al-1Cb and Ni-12Al-20Cr systems exhibited good stability with five and two percent growth in coating thickness after 300 hours of testing. Ni-19Al-3Cb and Ni-17Al-20Cr coatings increased by 26 and 28 percent, respectively, in the same period.

4. Oxides formed on the Ni-Al-Cb systems appeared to be thin, dense, and adherent to the surface compared to the thicker, porous and partially spalled oxide scales formed on Ni-Al-Cr systems. X-ray diffraction analysis revealed that on all specimens the predominant species in the scale layer are $FeSO_4.4H_2O$, Na_2SO_4 deposits and nickel oxide. Elemental chromium, titanium and aluminum were also detected with SEM/EDX.

5. Electron dot mapping of Ni-19Al-1Cb in the unexposed and as-tested conditions revealed a columbium-rich band near the coating surface which remained immobile even after 314 hours at 899°C. A similar microstructure was found in Ni-19Al-3Cb and it is believed that the presence of this columbium-rich (presumably $CbAl_3$) phase may be responsible for coating resistance.

6. The Ni-Al-Cr system was similarly analyzed by electron dot mapping and it was found that prior to testing, chromium was dispersed throughout the coating. After 318 hours, stratification of chromium into two bands had occurred, one near the coating surface and a second zone in mid-span. However, chromium coatings were more easily permeated by corrodants such as sulfides and oxygen and provided less resistance.

4.2 DYNAMIC OXIDATION BURNER RIG TESTING

A 500-hour, 1050°C oxidation rig test was used to evaluate the performance of the four coating systems. The coatings were applied to a modified specimen configuration shown in Figure 9. A 3 mm diameter hole was drilled into the hot end of the specimen, extending 25 mm into the rod. The volume of the 25 mm core is calculated to be 0.20 cm^2 and assuming pack density to be 1.75 g/cm^2, the amount of aluminum needed to form the desired coatings can be determined. It was found that the aluminum in the pack will be in excess by two orders of magnitude. Therefore, pack depletion should not occur and the coating formed on the internal surfaces of the test specimens should essentially be identical to that produced on the external surfaces. The advantage of this configuration is that during testing the external coated surface will be directly exposed to the high-velocity hot gas stream while the internal surfaces will be in a quasi-static environment although at a somewhat higher temperature.

A total of 14 coated specimens were prepared with each coating applied in triplicate or more. The coating data are provided in Table 22. Weight gain values were determined over the entire internal and external surfaces. However, even though mass balance calculations indicate that there was an excess of active metal in the specimen bore, metallography gave evidence that the limited pack volume had apparently influenced the kinetics of vapor transfer, resulting in differences in internal and external coating thickness and microstructures. These differences are exemplified in Figures 58 and 59 for

Table 22

Coating Weight Data of Oxidation Rig Specimens

Specimen Number	Coating	Cb Wt. Gain (mg/cm^2)	Al Wt. Gain (mg/cm^2)	Total Wt Gain (mg/cm^2)
R17	Ni-19Al-1Cb	--	12.2	12.2
R18		0.3	11.2	11.5
R19		0.1	13.0	13.1
R30		1.9	14.6	16.5
C16*		--	12.9	12.9
R20	Ni-19Al-3Cb	1.5	15.0	16.5
R21		1.4	14.2	15.6
R22		1.3	14.7	16.0
C17*		1.3	17.3	18.6
R23	Ni-17Al-20Cr	3.0	17.3	20.3
R24		2.9	16.1	19.0
R25		3.3	17.9	21.2
C18*		2.7	20.0	22.7
R26	Ni-12Al-20Cr	3.1	10.2	13.3
R27		3.1	13.1	16.2
R28		3.2	10.4	13.4
R31		7.0	10.5	17.5
C19*		2.5	12.0	14.5

*Control coupon specimens.

Ni-19Al-1Cb and Ni-12Al-20Cr coatings, respectively. (Metallographic sections were made in the transverse direction. Generally, the coating formed externally is thicker (100-125 microns) than that formed on the internal surfaces (76 microns) as a result of the limited pack volume in the internal bore. Some porosity and/or oxides were formed near the coating surface and the significance of these defects is not entirely clear.

The external surface coating (Fig. 58A) is different from the internal surface (Fig. 58B) in that a continuous and well defined phase is found in the latter at the coating surface. It is reasonable to assume that this continuous band is a columbium-rich phase, based on past observations with SEM/EDX. The chromium coating exhibits essentially typical microstructure with small discrete light grey chromium-rich phases which are fully dispersed near the surface in Figure 59A and segregated in a parallel zone in the internally applied coating (Fig. 59B).

After 170 hours of cyclic exposure, one specimen of each coating was removed and replaced with a an unexposed coated specimen. Testing was then resumed. In the period between 200 and 270 hours, the control thermocouple failed and resulted in erratic combustion and temperature fluctuation prior to shut

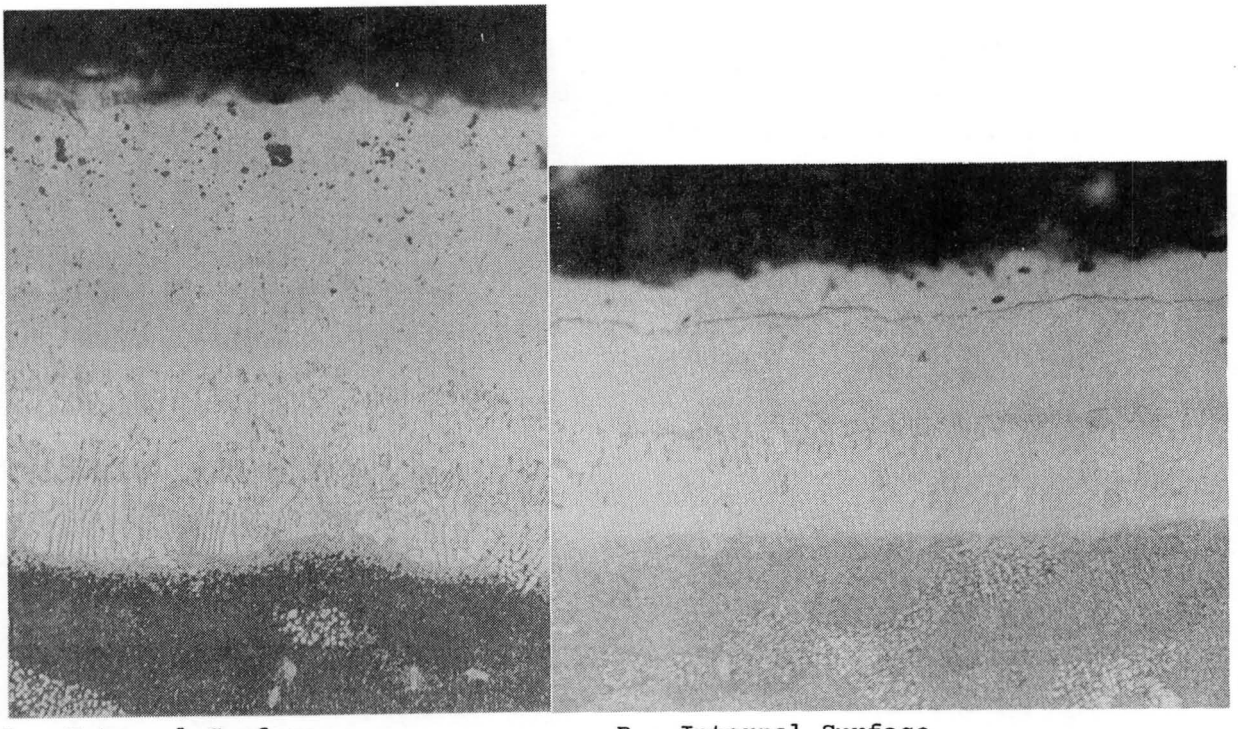

A. External Surface B. Internal Surface

Figure 58. Ni-19Al-1Cb (Variation A) Coated Oxidation Rig Specimen R30 as Heat Treated . Magnification 500X, Chromic Etch

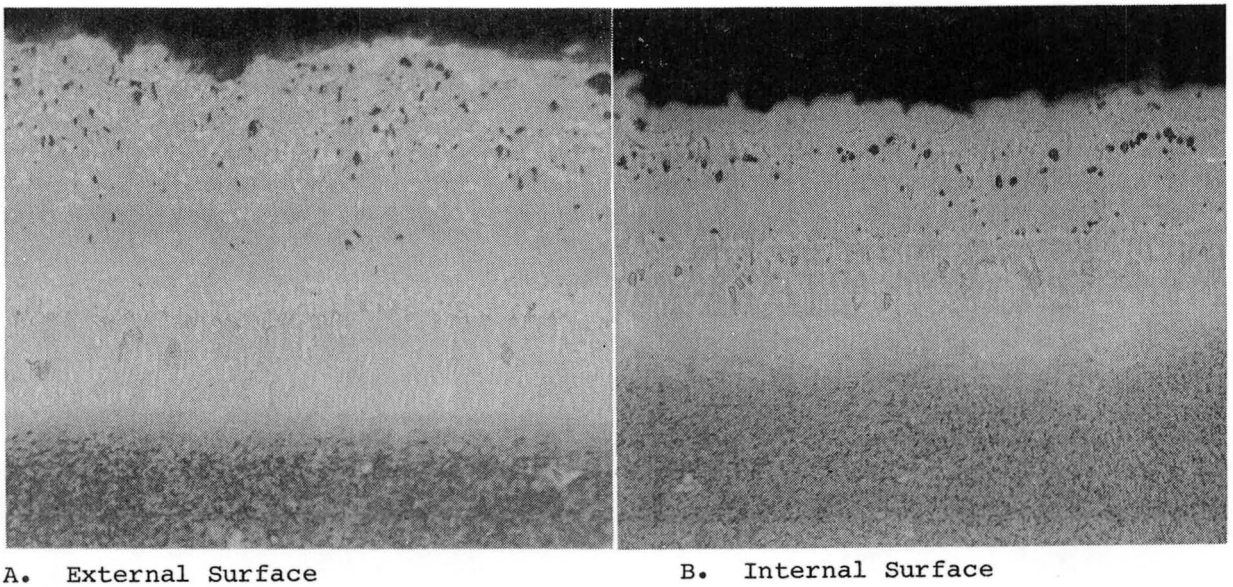

A. External Surface B. Internal Surface

Figure 59. Ni-12Al-20Cr (Variation D) Coated Oxidation Rig Specimen R31 Heat Treated Condition. Magnification 500X, Chromic Etch

down. Several specimens were broken off and destroyed as a result of the malfunction. The remaining specimens, while in one piece, had suffered severe oxidation attack.

Consequently, of the 12 specimens tested, four were lost, another four were subjected to severe attack and plastic deformation. The remaining four specimens, together with the uncoated baseline, which were all removed at 170 hours, were the only ones used to provide information on relative oxidation resistance. The overall status of the test specimens are summarized in Table 23. Since the test sequence during overtemperature was unknown, the eight specimens subjected to 100 and 270 hours of testing were not metallurgically evaluated. Photographic documentation of the physical appearance of all test specimens are provided in Appendix D. Note the absence of physical distress on the coated 170-hour specimens, scaling and oxide delamination was evident on the uncoated IN-792 baseline specimen in Figure D-1. There were indications of plastic deformation of the specimen leading edge (side facing the hot gas stream) in Figures D-2 and D-3, attesting to the high temperature experienced during test malfunction.

Table 23

Summary of Status of Oxidation Test Specimens

Specimen Number	Coating	Number of Cycles	Remarks
R17	Ni-19Al-1Cb	270	Broken off
R18	"	170	OK
R19	"	100	Surface deformation
R20	Ni-19Al-3Cb	270	Broken off
R21	"	170	OK
R22	"	100	Broken off
R23	Ni-17Al-20Cr	270	Spall in hot zone
R24	"	170	OK
R25	"	100	Surface deformation
R26	Ni-12Al-20Cr	270	Broken off
R27	"	170	OK
R28	"	100	Substrate exposed
R29	None	170	OK

Each of the 170-hour specimens were metallographically sectioned, as shown in Figure 60. The internal and external coatings are shown in Figures 61 through 65. Comparison of the two areas on each specimen corroborates the fact that diffusion reaction in the internal bore is restricted, thus producing a thinner and possibly less protective microstructure.

The Ni-19Al-3Cb coating, Figure 62, had the best oxidation resistance, especially in the dynamic, external mode where the coating appears to be

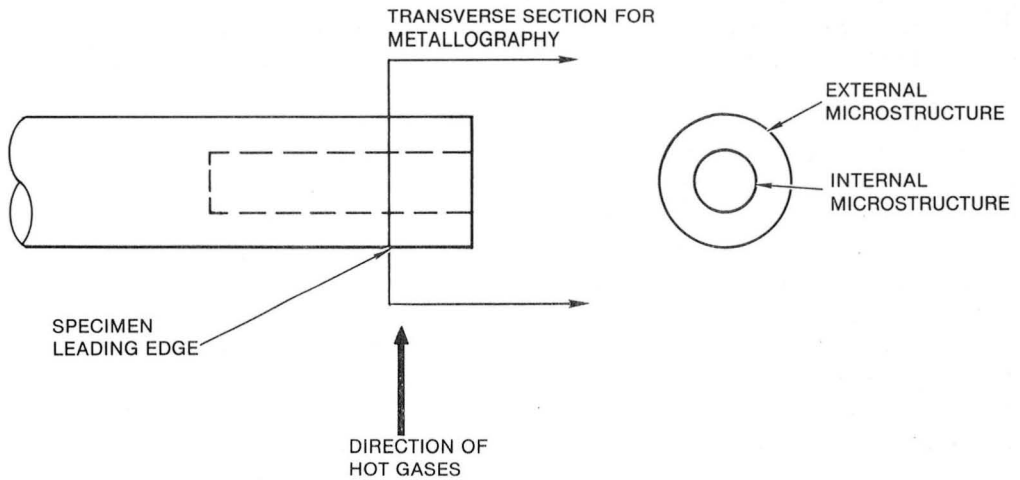

Figure 60. Schematic Showing Metallographic Section of Oxidation Test Specimen

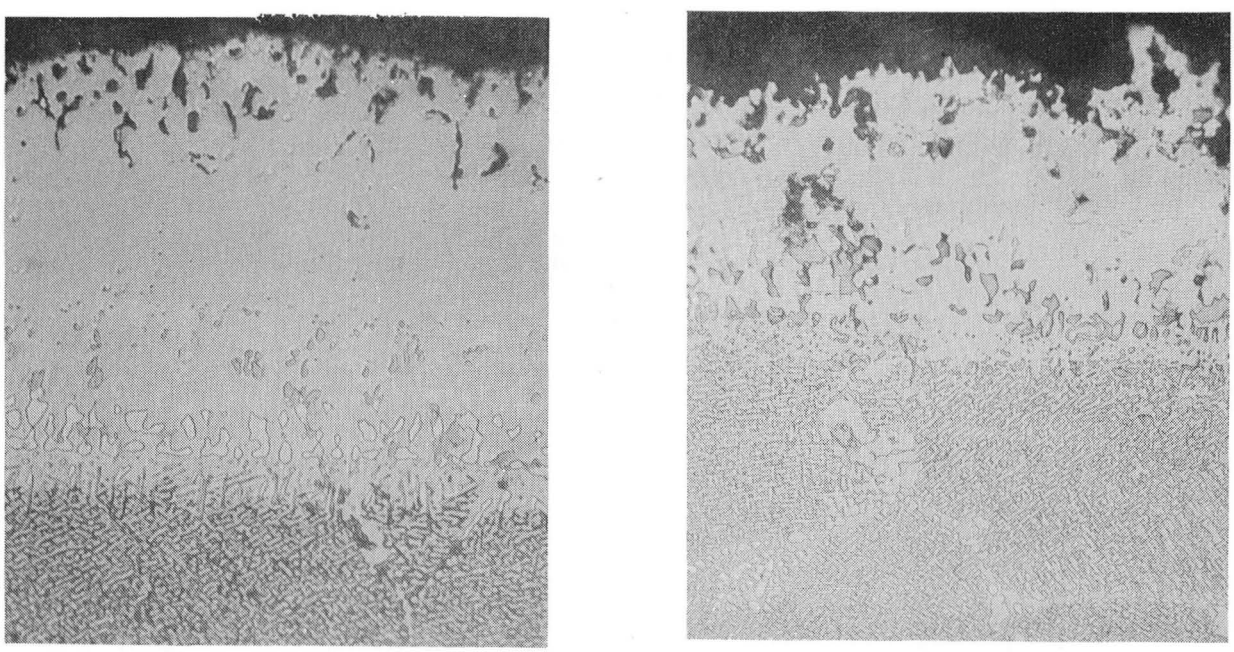

A. External Surface

B. Internal Surface

Figure 61. Ni-19Al-1Cb Coated IN-792 (Specimen R18) After After 170 Hours Burner Rig Oxidation Test at 1050°C (1922°F). Magnification 500X, Oxalic Etch

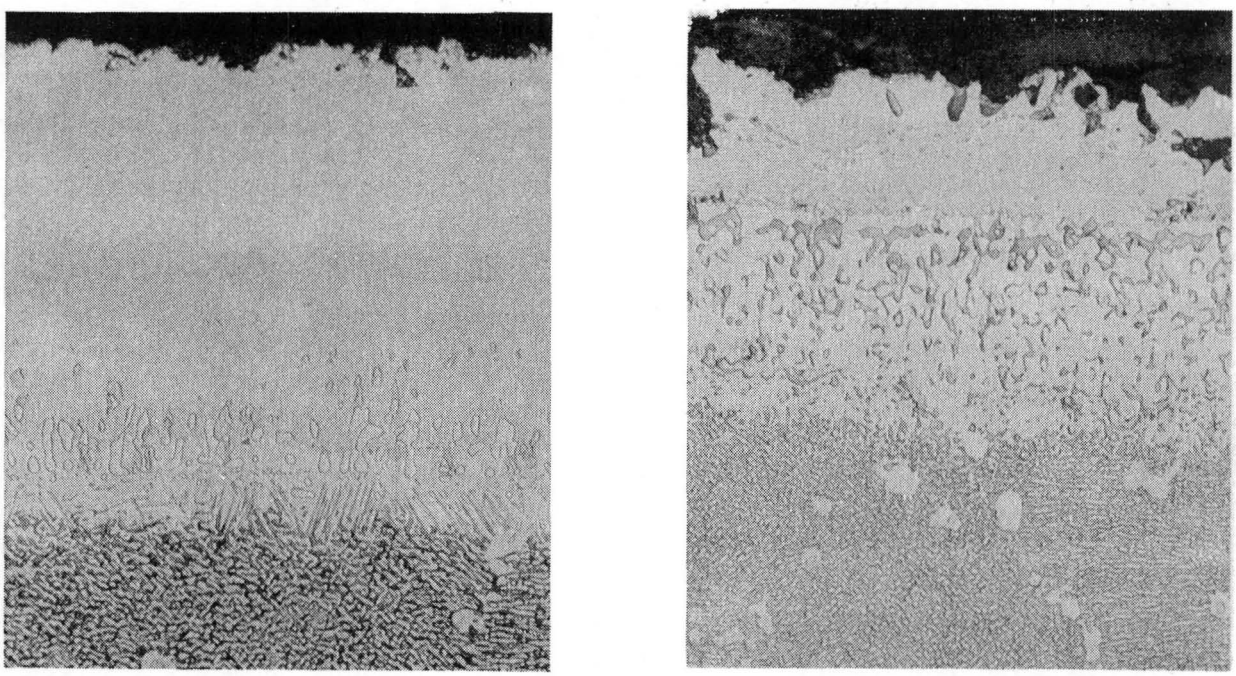

A. External Surface B. Internal Surface

Figure 62. Ni-19Al-3Cb Coated IN-792 (Specimen R21) After After 170 Hours Burner Rig Oxidation Test at 1050°C (1922°F). Magnification 500X, Oxalic Etch

essentially unaffected by the test exposure except for a thin oxide scale formation. The darker etching phase in the interfacial region in Figure 62B could be indicative of degradation of the more protective aluminum-rich phases in the coating, even though oxide formation and voiding are confined to a narrow band near the coating surface.

The lower columbium coating, Ni-19Al-1Cb, was less resistant with external degradation initiating along grain boundaries, IGO (intergranular oxidation not readily visible in Fig. 61) while internal voiding and oxide formation extended occasionally to the interfacial zone.

An interesting phenomena is observed in Figure 63, showing the Ni-17Al-20Cr coating. Minimal oxidation is noted on internal surfaces, while the external coating is significantly attacked even though the greater overall thickness would provide an increased life span. Instead of the intergranular oxidation found in the columbium aluminide coating, degradation appears to initiate at the discrete light grey, chromium-rich phase. The external coating was found to be deteriorated in two regions, near the surface and also at the interface, separted by an essentially unaffected, fully dense denuded coating zone. Again, void/oxide formation occurred at the light grey phase believed to be rich in chromium and other refractory elements. Internally applied Ni-12Al-20Cr, shown in Figure 64B, had undergone significant conversion

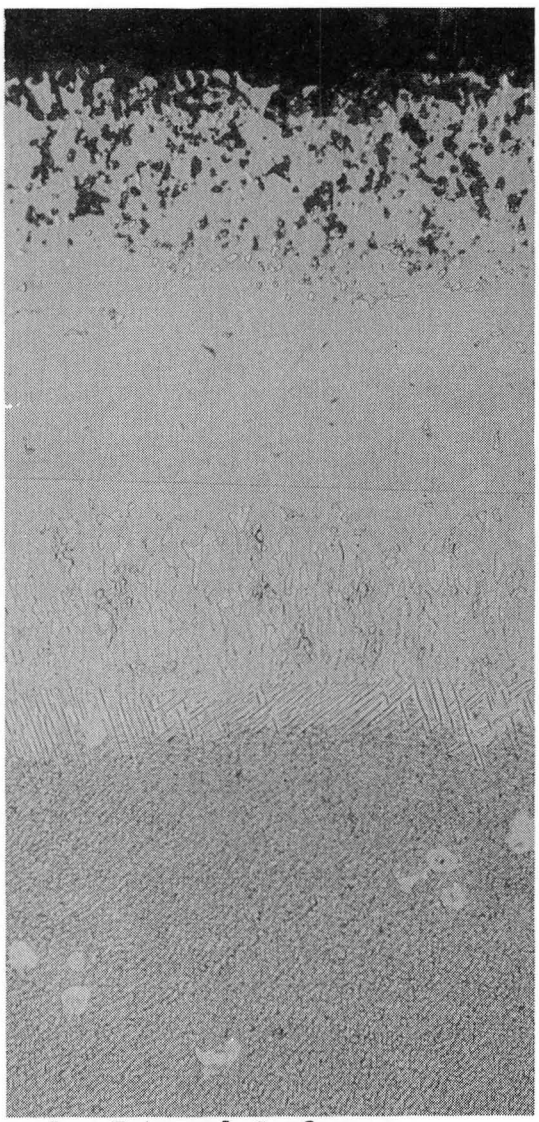

A. External Surface

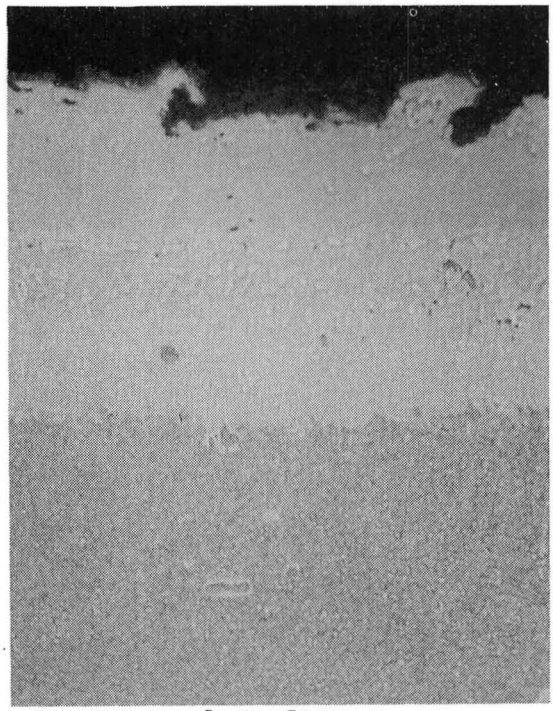

B. Internal Surface

Figure 63. Ni-17Al-20Cr (Variation C) Coated IN-792 (Specimen R24) After 170 Hours Burner Rig Oxidation Test at 1050°C (1922°F). Magnification 500X, Oxalic Etch

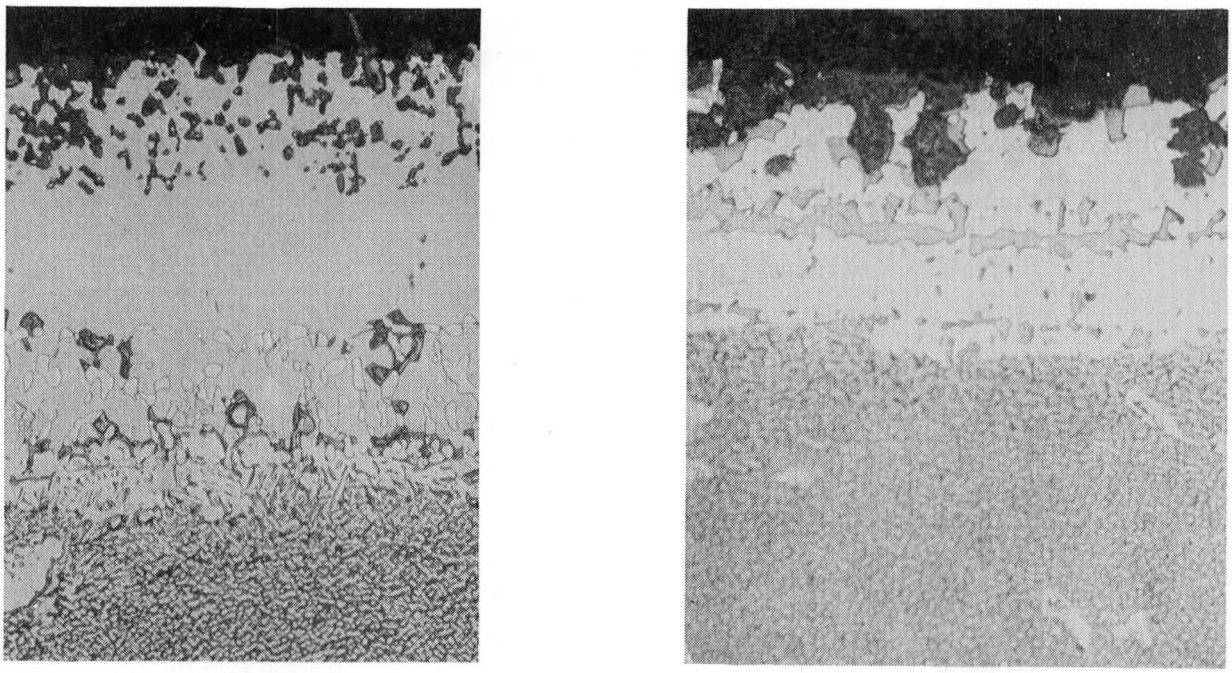

A. External Surface B. Internal Surface

Figure 64. Ni-12Al-20Cr Coated IN-792 (Specimen R27) After 170 Hours Burner Rig Oxidation Test at 1050°C (1922°F). Magnification 500X, Oxalic Etch

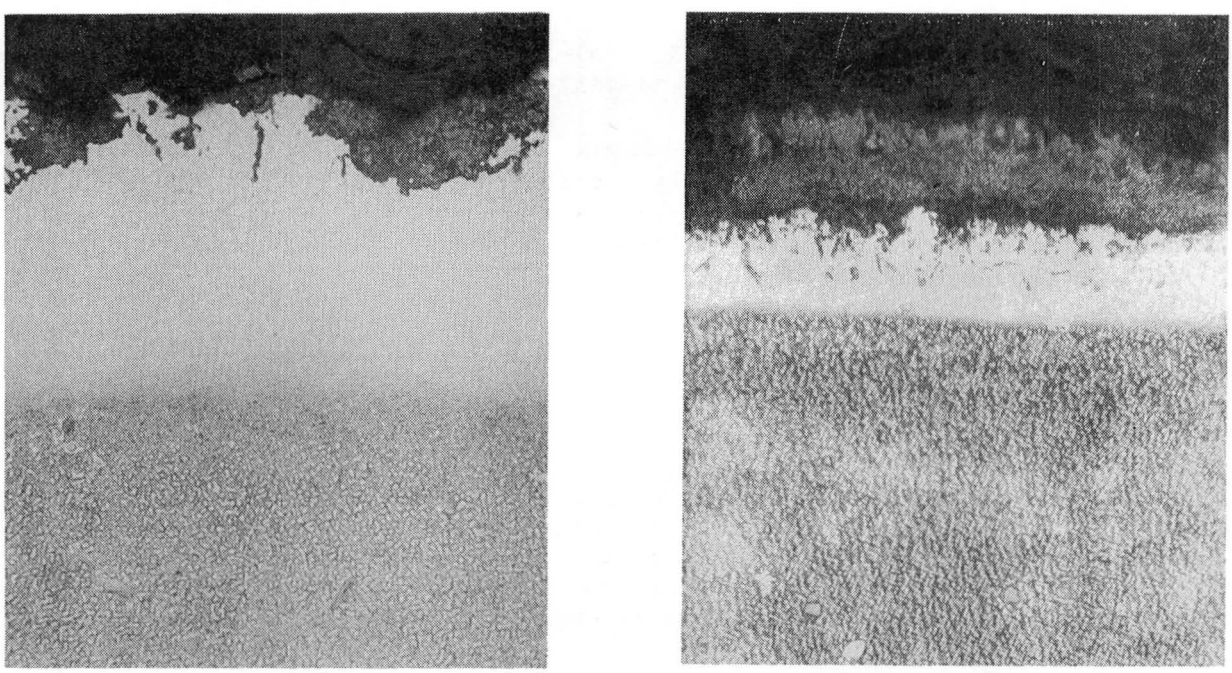

A. External Surface B. Internal Surface

Figure 65. Uncoated Baseline IN-792 (Specimen R29) After 170 Hours Burner Rig Oxidation Test at 1050°C (1922°F). 10% Oxalic Etch, Magnification 500X

from beta to the less protective aluminide phases. Surface oxide scale formation extended into the coating en masse and seems to be associated with the dark grey, low aluminum areas.

The bare IN-792 alloy seen in Figure 65 underwent alloy depletion together with some oxide formation on external surfaces. The depleted zone found on internal surfaces appears to be less extensive, even though the thickness of the oxide scale would indicate significant alloy oxidation.

Coating thickness and depth of penetration measurements were made and are provided in Table 24. The extent of coating degradation as a result of oxidation attack is reported, both as absolute thickness measurements and as a percentage of the initial coating thickness. One can argue that absolute penetration readings are the true indices of the overall resistance of the coating material to high temperature oxidation. On the other hand, percentage values can be interpreted to imply the total performance of the coating and is an indication of the residual life of the coating.

The data in Table 24 indicates that the Ni-19Al-3Cb coating performed the best in oxidation resistance, both internally and externally. Ni-19Al-1Cb and Ni-12Al-20Cr exhibited equivalent resistance, with 32 percent of the coating deteriorated externally and 40-50 percent of the internal coating oxidized. Ni-17Al-20Cr, with total thickness of 170 microns, also suffered 32 percent or degradation externally with internal penetration to 20 percent.

Based on the absolute penetration measurements given in Table 24, the coating may be ranked in order of decreasing resistance as follows:

Ni-19Al-3Cb > Ni-19Al-1Cb, Ni-12Al-20Cr > Ni-17Al-20Cr > IN-792 (external)
Ni-19Al-3Cb, Ni-17Al-20Cr > Ni-12Al-20Cr, IN-792 >Ni-19Al-1Cb (internal)

It should be pointed out at this stage that the metallographic results presented may be somewhat obscured by the inherent difference between externally and internally processed coatings. As was discussed in an earlier section, the primary difference is in coating thickness and, to a lesser extent, minor differences in microstructure.

4.3 FURNACE OXIDATION TESTING

Subsequent to the early termination of the burner rig test, it was decided that a static furnace oxidation test at 1050°C (1920°F) be initiated. Four coated specimens of each composition together with one uncoated IN-792 specimen were exposed to a total of 1039 hours with seven inspection cycles at 122, 170, 241, 325, 541, 847, and 1039 hours. The relative specimen weight changes are given in Table 25 and plotted in Figure 66.

The uncoated IN-792 specimen exhibited rapid loss in weight with an inflection in the curve at 200 hours, separating a higher weight loss rate in the initial stages from the slower oxidation rate in the later stages. The absence of a plateau points to continued metal loss. In contrast, the four coated specimens

Table 24

Coating Thickness Measurements of Oxidation Specimens

Specimen Number	Coating	External Surface Coating Thickness (μm)	External Surface Depth of Penetration (μm)	External Surface Depth of Penetration (%)	Internal Surface Coating Thickness (μm)	Internal Surface Depth of Penetration (μm)	Internal Surface Depth of Penetration (%)
R18	A	120	32	27	76	38	50
R21	B	127	None	--	95	19	20
R24	C	170	50	29	89	19	21
R27	D	115	32	28	76	29	38
R29	None	---	83	--	--	25	--

Table 25

Tabulation of Furnace Oxidation Data

Time (hrs)	Weight Change (mg/cm^2) Ni-19Al-1Cb	Ni-19Al-3Cb	Ni-17Al-20Cr	Ni-12Al-20Cr	Uncoated
0	0	0	0	0	0
122	1.19	-1.84	1.57	1.30	-5.90
170	1.27	-2.36	1.63	1.34	-6.50
241	1.29	-2.50	1.74	1.44	-7.12
325	1.27	-2.52	1.85	1.50	-7.41
541	1.39	-2.33	2.03	1.69	-8.16
847	1.52	-2.33	2.19	1.78	-9.60
1039	1.31	-2.62	2.38	1.62	-10.66

all exhibited various degrees of leveling off in rate of weight change past 200 hours which appears to be the cutoff point for rapid initial oxidation. It is interesting to note that Ni-19Al-3Cb is the only one of the four coatings to exhibit weight loss as a result of static oxidation while the other systems show weight gain with time.

Comparison of gradients in the flat portions of the curves in Figure 66 suggest that the columbium systems generally show a zero gradient while the chromium

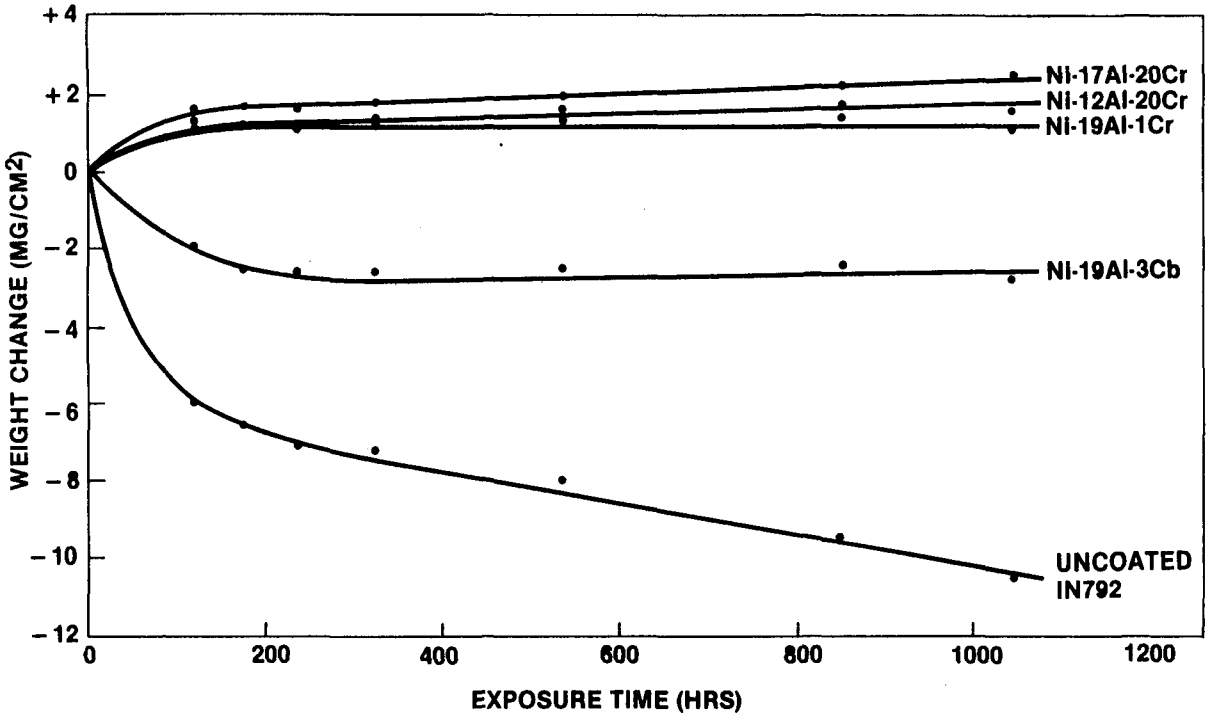

Figure 66. Furnace Oxidation Weight Change Rate

systems are still showing a positive gradient, indicative of continued depletion and oxidation due to spallation and possibly some volatilization.

During the 122, 170, and 241 hours cooldown inspection cycles, it was noted that Ni-19Al-3Cb had a slight yellow oxide scale resembling Cb_2O_5 formation. However, subsequent inspections not only failed to detect any additional yellow oxide growth but also noted reduction of the oxide color until all traces of yellow were gone.

Representative microstructures of the test specimens exposed to 1039 hours of oxidation testing are shown in Figures 67 through 71. None of the coated specimens show serious degradation relative to the unprotected alloy shown in Figure 71. However, evidence of oxidation depletion of the Ni-Al-Cr coatings (Figs 69 and 70) can be noted in the void/oxide formation near the coating surface which appears to correspond to the small, discrete, light grey chromium-rich phases. These observations were also made on the Ni-Al-Cr coated specimens exposed to dynamic oxidation burner rig testing reported previously.

Some breakdown of the Ni-Al-Cb system can be seen in Figures 67 and 68 in the formation of the light grey phases dispersed throughout the dark grey aluminum-rich matrix which is typical of this type of coating. The association of the light grey phase with aluminum depletion is supported by the formation of a semi-continuous band of this phase at the coating/oxide interface which is the site of aluminum consumption in oxide scale formation. In a previous report, it was pointed out that columbium was found to segregate in a band near the coating surface after 300 hours of corrosion rig test. This columbium-rich band is markedly absent.

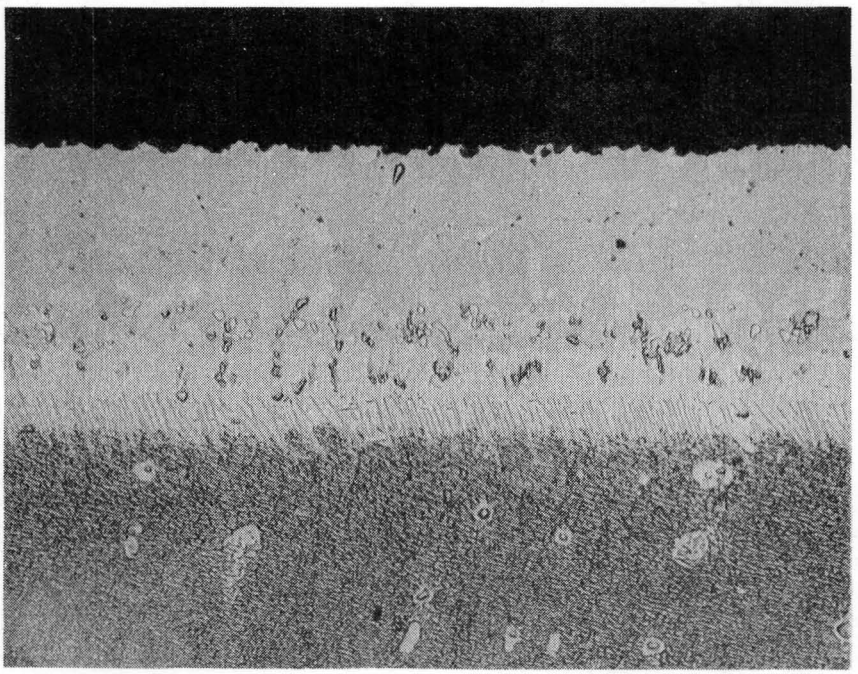

Figure 67. Ni-19Al-1Cb Coated IN-792 Specimen After 1039 Hours of 1050°C Furnace Oxidation Testing. Magnification 150X, Chromic Etch

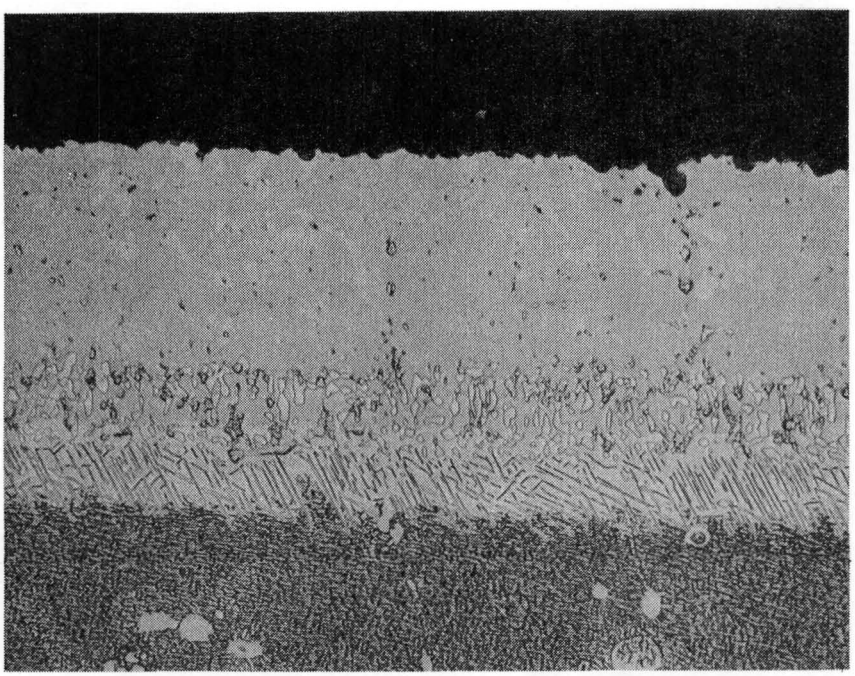

Figure 68. Ni-19Al-3Cb Coated IN-792 Specimen After 1039 Hours of 1050°C Furnace Oxidation Testing. Magnification 250X, Chromic Etch

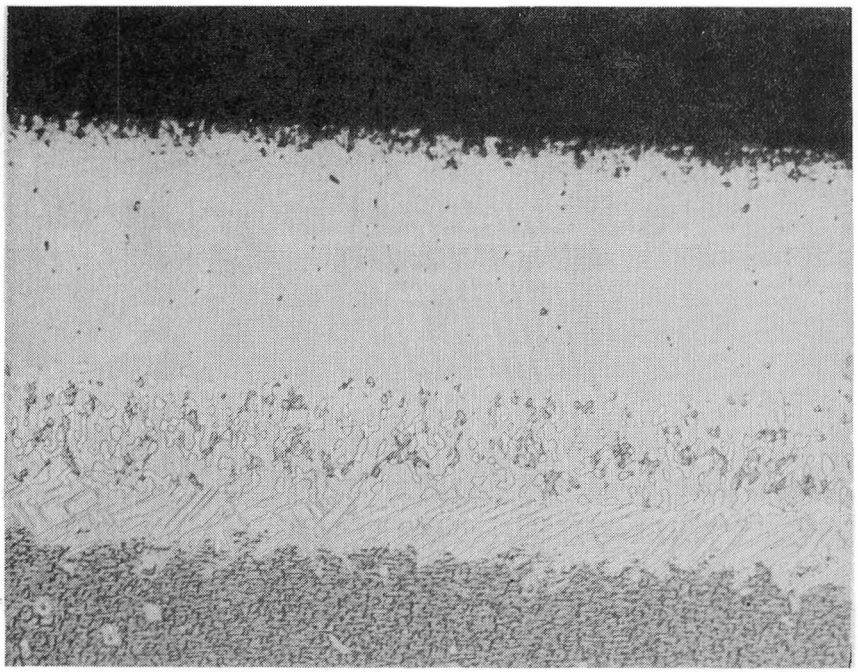

Figure 69. Ni-17Al-20Cr Coated IN-792 Specimen After 1039 Hours of 1050°C Furnace Oxidation Testing. Magnification 250X, Chromic Etch

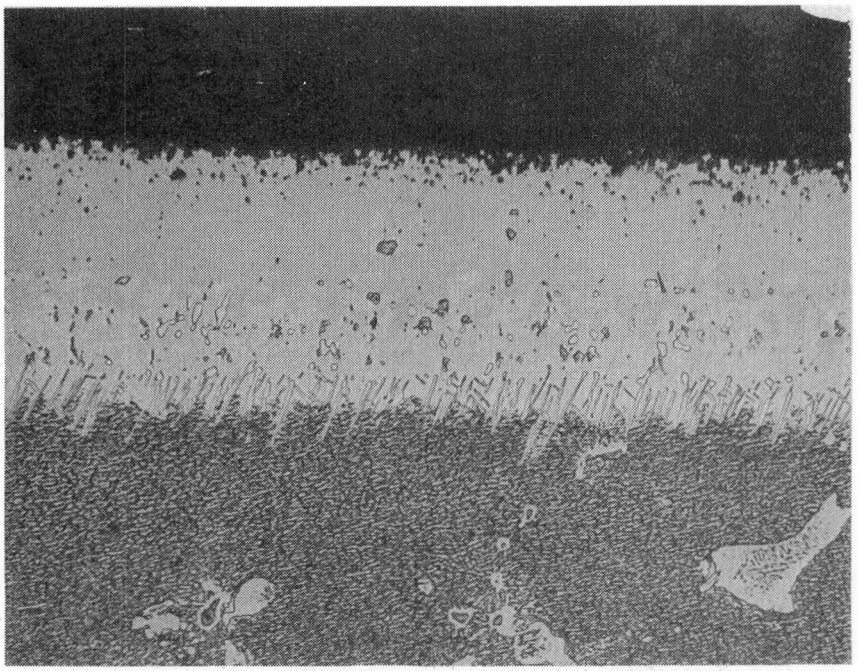

Figure 70. Ni-12Al-20Cr Coated IN-792 Specimen After 1039 Hours of 1050°C Furnace Oxidation Testing. Magnification 250X, Chromic Etch

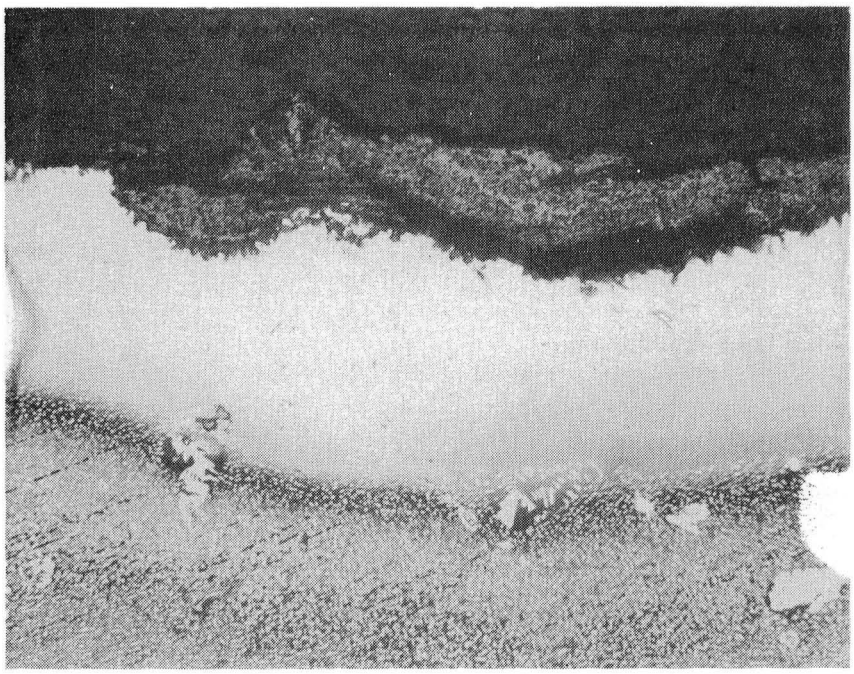

Figure 71. Bare IN-792 Baseline Specimen After 1039 Hours of Furnace Oxidation Testing. Magnification 250X, Chromic Etch

A thick and apparently non-adherent oxide scale is formed on the bare IN-792, Figure 71. Oxide scale formation is also observed in Figures 67 and 68 with the columbium coating, which was thin and adherent and will better resist thermal cycling spallation, as confirmed by rig testing.

Another phenomenon observed after long-term isothermal exposure is the growth of the coating/substrate interface which is essentially consumption of the substrate. The interfacial region of Ni-19Al-3Cb and Ni-17Al-20Cr is composed of a needle-like acicular phase extending into the substrate alloy. This needle-like phase is less predominant in Ni-19Al-1Cb and Ni-12Al-20Cr. However, sigma phase formation is generally found in over-aged or exposed superalloys as a result of nucleation from carbides of chromium, molybdenum, and tungsten in the alloy (Ref. 17).

In comparing dynamic and static oxidation testing, two items of significance are noted. First, after 170 hours of dynamic oxidation the coatings were deteriorated to a greater extent relative to 1029 hours of static oxidation. Coating deterioration was marked by voiding/oxide formation/transformation of the coating matrix to the light grey phase in the static oxidation specimens. Contrary to this, the light grey phase was not observed in the dynamic oxidation specimens in spite of more pronounced oxidation, which is perhaps indicative of the differences betrween mechanisms of oxidation attack under dynamic and static conditions. Second, the ranking of coatings is different in that under static conditions, Ni-17Al-20Cr performed well compared to burner rig exposure of externally coated IN-792.

4.4 MECHANICAL PROPERTY EVALUATION

Evaluation of coated and uncoated cast-to-size, fully heat treated test bars in selected mechanical property tests was conducted at ambient and elevated temperatures. Coating weight gain data of test specimens are given in Appendix E. The following sections document the results obtained and the significance of deviations from uncoated baseline values. All cross section area measurements are based on the original, uncoated gage diameter.

4.4.1 Tensile Testing

Two coating systems, Ni-19Al-1Cb and Ni-12Al-20Cr, were selected for tensile testing at ambient temperature and 649°C. Results are provided in Table 26. At room temperature, all duplicate coated specimens exhibited yield and tensile strengths greater than uncoated baseline IN-792. At 649°C, the yield strengths of both coated and uncoated specimens appeared to be equivalent, although tensile strengths of coated bars were typically 10 percent higher than uncoated IN-792. Based on these test values, it can be concluded that no significant difference in tensile properties was observed and the coatings/processes had negligible effect on substrate tensile properties.

4.4.2 Stress-Rupture Testing

Stress-rupture lives of Ni-19Al-1Cb and Ni-12Al-20Cr coated bars are reported in Table 27 together with the Larson Miller parameter. The values are plotted in Figure 72 which also includes a band representing in-house uncoated baseline data.

The uncoated IN-792 baseline values evaluated in this program were found to lie on the lower limit of the band of baseline data, indicating a reduced stressrupture life for this batch of castings. This could have contributed to a limited extent to the low values noted for both Ni-19Al-1Cb and Ni-12Al-20Cr coated specimens, especially at high stress levels. With lower stresses, significant scatter is observed.

Deterioration of stress-rupture properties is frequently associated with coating application (Ref. 18). Solar has noted (Ref. 19) similar departures from baseline values of coated thin-walled MAR-M421 specimens as a result of changes in grain size and over aging. Another study by E. R. Buchanan (Ref. 20) indicated that the RT-22 coating did not affect 982°C (1800°F) stress-rupture lives. However, the 760°C (1400°F) properties were markedly reduced for the same coating and alloy. These losses were recovered upon solution heat treating at 1121°C (2050°F) and were attributed to interstitial diffusion down grain boundaries during high temperature exposure. In the case of coated IN-792, all specimens were tested in the fully heat treated (1121°C plus age) condition. The reasons behind the stress-rupture losses

Table 26

Tensile Properties of Cast-to-Size IN-792 Mod. 5A Test Bars

Specimen Number	Coating	Temperature (°F)	Temperature (°C)	Yield Strength (ksi)	Yield Strength (MPa)	Ultimate Tensile Strength (ksi)	Ultimate Tensile Strength (MPa)	El. (%)	R.A. (%)
*	None	Room		120	827	145	1000	4	5
32	None	Room		120	827	145	1000	7	9
1	Ni-19Al-1Cb	Room		128	882	169	1164	8	10
2	Ni-19Al-1Cb	Room		129	889	152	1047	6	8
27	Ni-12Al-20Cr	Room		133	916	173	1192	9	8
28	Ni-12Al-20Cr	Room		132	909	172	1185	9	7
*	None	1200	649	105	724	150	1034	4	5
31	None	1200	649	111	765	147	1013	7	9
10	Ni-19Al-1Cb	1200	649	112	772	164	1130	5	7
11	Ni-19Al-1Cb	1200	649	111	765	160	1102	6	7
12	Ni-12Al-20Cr	1200	649	113	779	168	1158	7	8
13	Ni-12Al-20Cr	1200	649	114	785	168	1158	6	8

* Solar specified minimum for uncoated test bars

Table 27

Stress-Rupture Results of Cast-to-Size IN-792 Mod. 5A Test Bars

Specimen Number	Coating	Temperature (°F)	Temperature (°C)	Stress (ksi)	Stress (MPa)	Life (hrs)	C=20 LM Parameter ($\times 10^{-3}$)
29	None	1700	927	41	282	29.4	46.4
30	None	1400	760	96	661	28.9	39.9
14	Ni-19Al-1Cb	1400	760	96	661	2.2	38.7
15	Ni-19Al-1Cb	1400	760	96	661	6.5	38.7
16	Ni-12Al-20Cr	1400	760	96	661	1.3	37.4
17	Ni-12Al-20Cr	1400	760	96	661	2.1	37.8
18	Ni-19Al-1Cb	1700	927	41	282	6.8	45.0
19	Ni-19Al-1Cb	1700	927	41	282	10.2	48.2
20	Ni-12Al-20Cr	1400	760	79	544	75.4	40.7
21	Ni-12Al-20Cr	1400	760	80	551	35.9	43.9

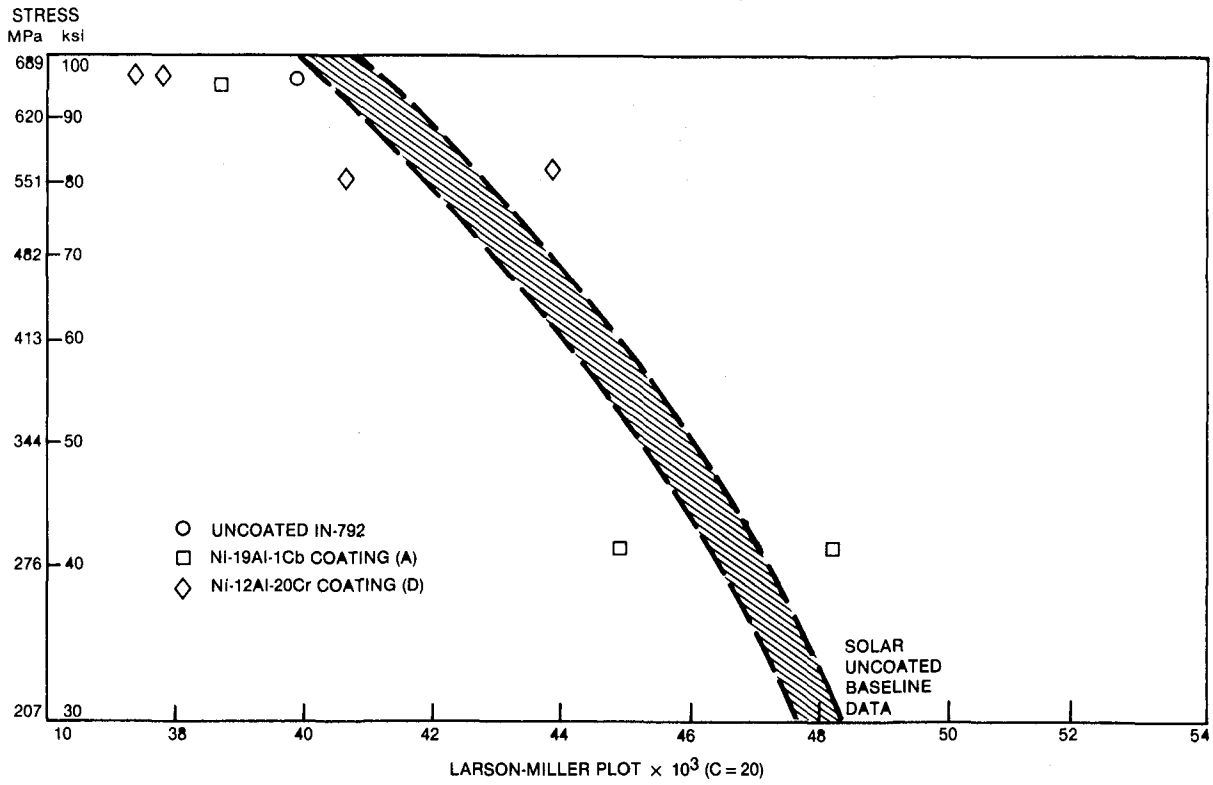

Figure 72. Stress-Rupture Test Results of Cast-to-Size IN-792 Mod. 5A Test Bars

are not clear even though it is expected that the development of degenerate structures (sigma phases) at the coating/substrate interface (Ref. 21) would contribute to produce the observed deterioration and scatter.

4.4.3 High-Cycle Fatigue

A total of nine specimens were evaluated at 649°C (1200°F) in high cycle fatigue tests. Results are reported in Table 28 and plotted in Figure 73. The open circles in Figure 73 representing uncoated bars all lie below the lower limit of Solar's uncoated baseline data, especially at lower stress values. This departure from Solar's baseline is another indication of the lower strength of this batch of castings. Both Ni-19Al-1Cb and Ni-12Al-20Cr coated bars exhibited between 30 to 50 percent reduction in fatigue life. This loss is extremely significant and appears to be characteristic of this alloy, as was demonstrated by similar values obtained for RT-22B (commercially applied platinum and rhodium aluminide) coated IN-792 (Fig. 73).

Generally, the presence of a coating on the substrate surface can either enhance or minimize crack initiation. The latter was found to be true for

Table 28

HCF Results of Cast-to-Sie IN-792 Mod. 5A Test Bars

Specimen Number	Coating	Temperature (°F)	Temperature (°C)	Alternating Stress* (ksi)	Alternating Stress* (MPa)	Cycles to Failure
1	None	1200	649	51.5	355	1.0×10^7
2	None	1200	649	50.0	345	1.0×10^7
2	None	1200	649	52.5	362	1.1×10^6 →
3	None	1200	649	55.0	379	2.0×10^5
4	Ni-19Al-1Cb	1200	649	42.0	289	1.5×10^4
5	Ni-19Al-1Cb	1200	649	30.0	207	5.7×10^6
5	Ni-19Al-1Cb	1200	649	34.0	234	3.0×10^4 →
6	Ni-19Al-1Cb	1200	649	32.0	220	1.4×10^4
7	Ni-12Al-20Cr	1200	649	42.0	289	1.4×10^4
8	Ni-12Al-20Cr	1200	649	32.0	220	5.0×10^6
8	Ni-12Al-20Cr	1200	649	37.0	255	1.0×10^6
8	Ni-12Al-20Cr	1200	649	40.0	276	8.3×10^4 →
9	Ni-12Al-20Cr	1200	649	39.0	269	2.0×10^6

* Altenating stress = $\frac{\text{max.}\sigma}{\text{min.}\sigma}$

Udimet 700 (Ref. 22) coated with a pack aluminide (27% Al) at temperatures below 500°C. The explanation for this behavior is that free surface defects in the substrate were essentially eliminated, thus making crack initiation more difficult. Above 500°C, it was found that coated Udimet 700 had a lower endurance limit than uncoated specimens. Surface crack initiation of aluminide coatings is generally related to the ductility of the coatings which is a function of the aluminum concentration. From Figure 73 it can be seen that the lower aluminum coating, Ni-12Al-20Cr, exhibited better fatigue life than the higher aluminum coating Ni-19Al-1Cb.

4.4.4 Strain Tolerance Testing

The strain tolerance of Ni-19Al-1Cb coating was evaluated from ambient to 649°C. The strain-to-cracking values were also determined for the other three coatings at 427 and 538°C. These values are reported in Table 29.

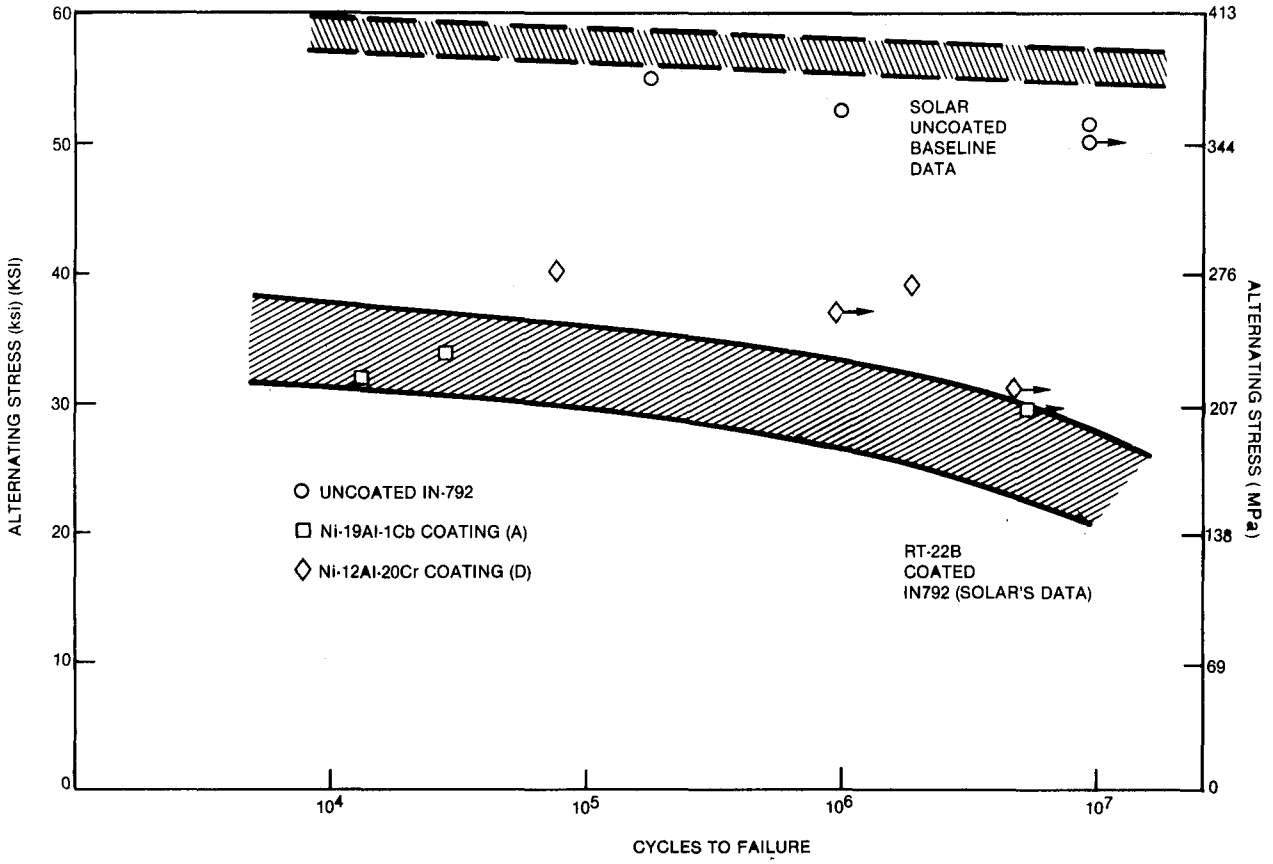

Figure 73. Results of Cast-to-Size IN-792 Bars (649°C, 30 cps, A=1.0)

Ni-19Al-1Cb (Variation A) exhibited increasingly ductile behavior as the temperature was increased. Even at room temperature, significant ductility was noted, 1.7 percent strain. The other three coatings demonstrated similar strain tolerance at 426 and 538°C. However, it was noted that strain-to-cracking values at 538°C were lower than at 427°C. After confirming that test data and procedures were not in error, it was concluded that this apparent reversal is within the error band of this test method.

Three specimens tested at 538°C were selected for metallurgical evaluation, Ni-19Al-1Cb coated and Ni-19Al-3Cb coated. Photomicrographs in Figure 74 show typical radial cracks found in the coatings. Note the presence of a different phase near the surface which is typically found in these columbium coatings. It is difficult to determine the crack initiation point from these photomicrographs alone. Microhardness measurements were subsequently made using a 25 g load, KHN. (Because of the large uncertainties involved in using the 25 g load, these values are only useful in a comparative mode.) Results are given in Figure 75. Both Ni-19Al-1Cb specimens had a harder surface layer than the Ni-19Al-3Cb specimen which had the highest KHN value at the coating/substrate interface. Since cracks are known to initiate

Table 29

Strain Tolerance Test Results

Specimen Number	Coating	Temperature (°C)	Temperature (°F)	Strain (%) No Cracks Observed	Strain (%) Cracks Observed
22	Ni-19Al-1Cb	27	80	1.0	1.7
23	Ni-19Al-1Cb	427	800	2.0	2.7
24	Ni-19Al-1Cb	538	1000	2.2	2.8
26	Ni-19Al-1Cb	538	1000	1.2	1.7
25	Ni-19Al-1Cb	649	1200	2.4	2.7
3	Ni-19Al-3Cb	427	800	2.6	3.1
4	Ni-19Al-3Cb	538	1000	1.2	1.7
5	Ni-17Al-20Cr	427	800	2.5	3.0
6	Ni-17Al-20Cr	538	1000	1.4	1.8
7	Ni-12Al-20Cr	427	800	2.5	2.9
8	Ni-12Al-20Cr	538	1000	1.5	1.9

Note: Two strain values are listed, one for the last strain increment before cracking was detected and the other for when cracks were actually found.

in a brittle area, it is conceivable that in the case of specimens 24 and 26 (Ni-19Al-1Cb) cracking initiated at the surface and was propagated through the less brittle coating. Specimen 26, which failed at a lower strain value, could have been further compromised by the presence of the hard interface. Surface examination of Ni-19Al-3Cb (specimen 4) revealed small localized spalling near cracks which was attributed to delamination of the brittle, columbium-rich layer upon cracking.

These specimens were deliberately over-etched to delineate grain boundaries in the coating (Fig. 76). Instead of the large grain boundaries typically found in aluminized coatings with grain boundaries aligned such that they are normal to the coating/substrate interface, these coatings have developed a fine equiaxed grain structure. It is believed that this equiaxed structure could have contributed to coating ductility by strain accommodation along grain boundaries.

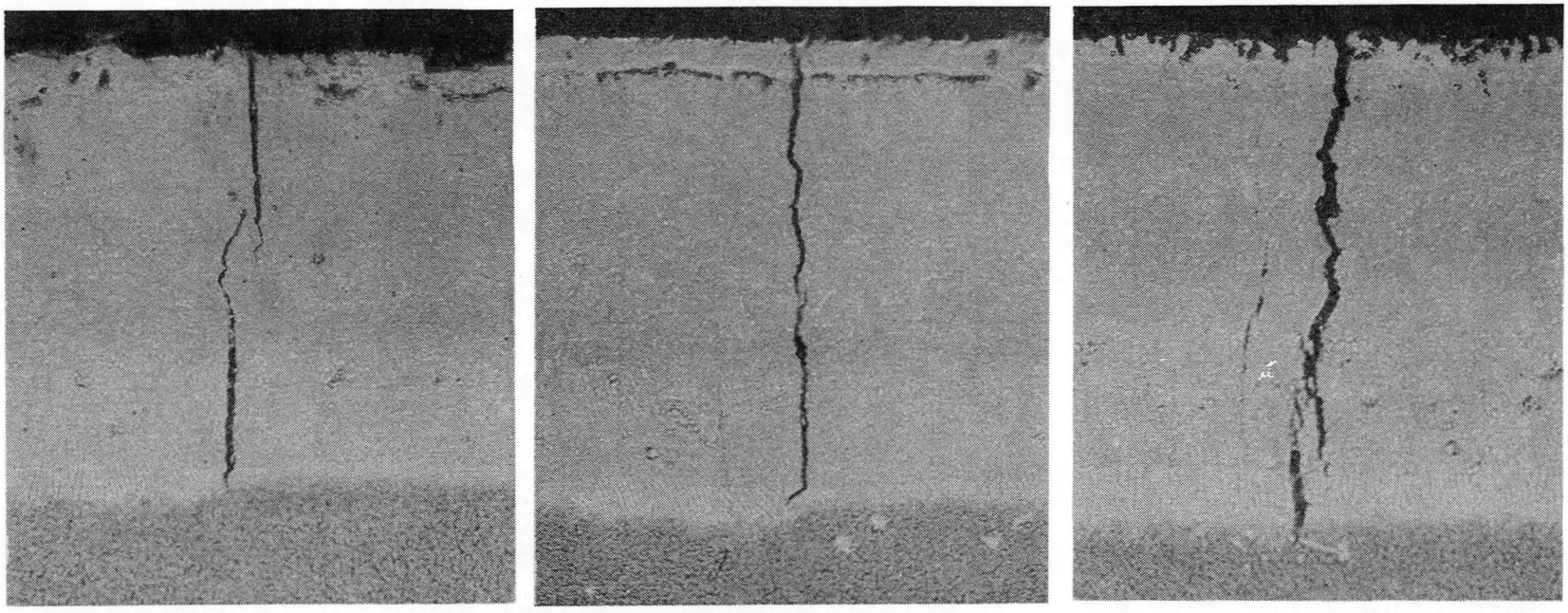

A. Ni-19Al-1Cb (No. 24) B. Ni-19Al-1Cb (No. 26) C. Ni-19Al-3Cb (No. 4)

2% Chromic Etch, Magnification: 500X

Figure 74. 538°C Strain Tolerance Specimens Showing Cracks Extending From Surface to the Interface

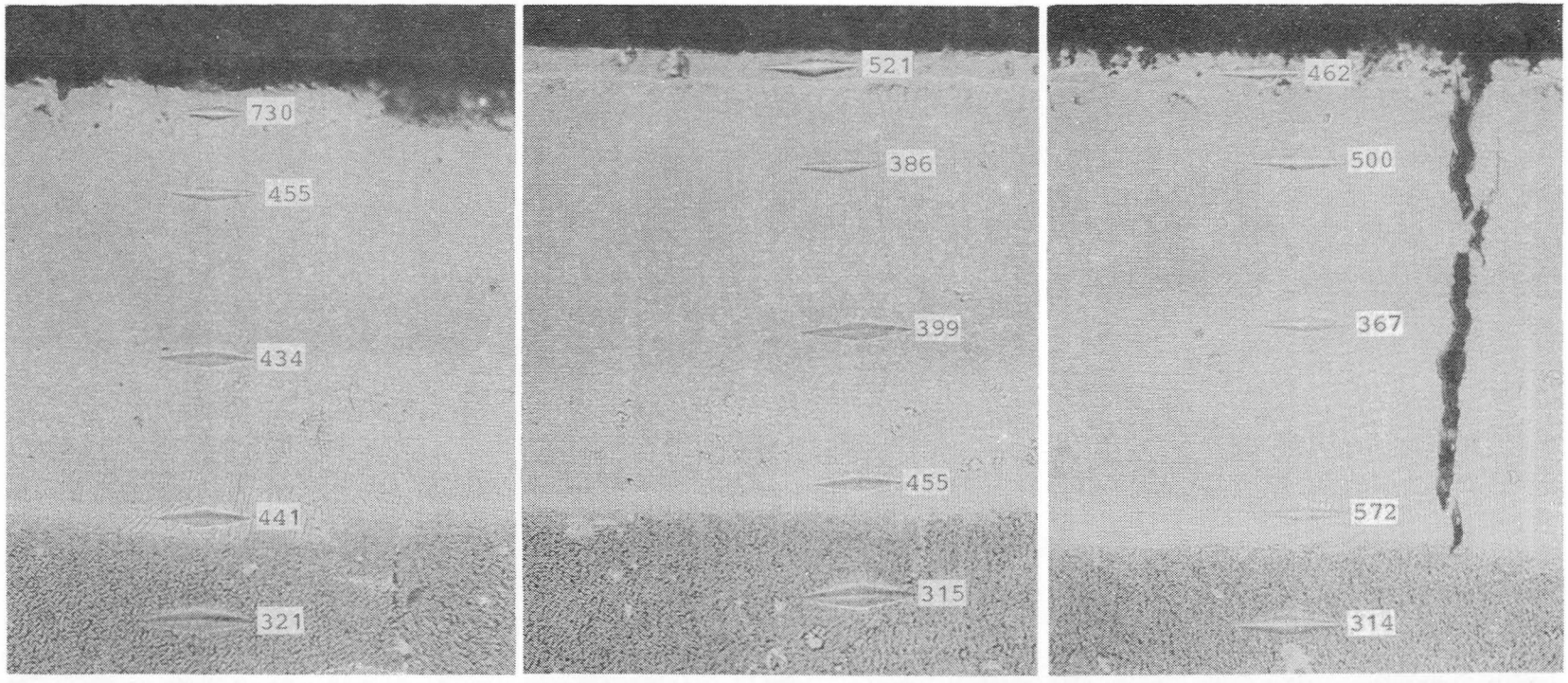

A. Ni-19Al-1Cb (No. 24) B. Ni-19Al-1Cb (No. 26) C. Ni-19Al-3Cb (No. 4)

2% Chromic Etch, Magnification: 500X

Figure 75 Mi[illegible]ss Test Measurements (KHN, 25 g load) of 538°C Strain Tolerance Specimens

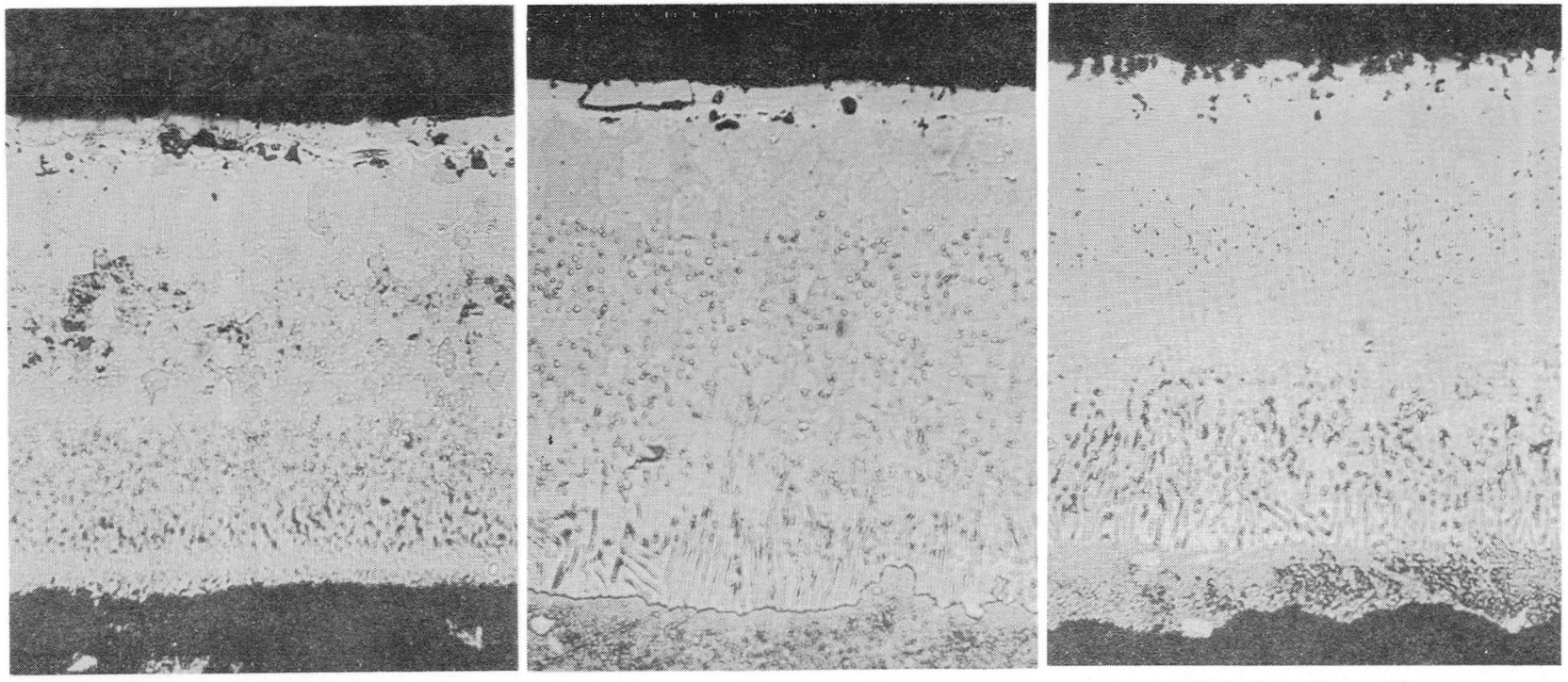

A. Ni-19Al-1Cb (No. 26) B. Ni-19Al-1Cb (No. 26) C. Ni-19Al-3Cb (No. 4)

2% Chromic Etch, Magnification: 500X

Figure 76. Microstructure of 538°C Strain Tolerance Specimens Heavily Etched to Show Grain Structure in Coating (Substrae alloy is over-etched)

5

TASK III - ENGINE TEST

5.1 COATING OF ENGINE HARDWARE

A total of eight IN-792 + Hf blades were coated and prepared for engine testing. Additional blades were also coated for delivery to NASA-LeRC. Coating data on all blades are provided in Table 30. Of the four program compositions, only Ni-17Al-20Cr was excluded from testing. Three coated and heat treated blades were metallographically sectioned as shown in Figure 77. Two of these were Ni-19Al-1Cb and Ni-12Al-20Cr coated IN-792 blades while the third blade was DS MAR-M200 + Hf with a Ni-12Al-20Cr coating. Since the latter alloy is not included in this program, it will suffice to mention here that coating morphology on this alloy was found to be similar to the IN-792 substrate.

A low magnification photomicrograph, Figure 78, shows the uniform and continuous coverage provided by the Ni-12Al-20Cr coating in the exit hole at the trailing edge. A slight rounding effect is noted at the exit hole radius.

The coating microstructures shown in Figure 79 were taken from Ni-19Al-1Cb coated blades sectioned as indicated in Figure 77. Coating thickness along the internal cavity was found to be uniform, about 70 to 75 microns. The coating is characterized by multiple zones with precipitated phases partitioned in the interface regions. The denuded zone near the coating surface is characteristic of <1 activity packs. Some internal voids are also noted. Both internal and external microstructures near the blade trailing edge are shown in Figure 80. Generally, the internal coating is approximately 25 percent thinner than the external coating. The concentration of insoluble components in the coating near the interface is in the form of finely divided precipitates. An even finer dispersion of a secondary phase is found to extend into mid-section of the external coating.

A Ni-12Al-20Cr coated blade was similarly prepared for metallurgical analysis. The typical photomicrographs shown in Figure 81 again attest to the uniformity of internal coating process with thicknesses in the range of 60 to 80 microns. A dark etching phase is observed in mid-coating separating the interfacial region of insoluble precipitates and the outer zone consisting of chromium dispersed in the NiAl matrix. Coating microstructures near the trailing edge are shown in Figure 82, with the internal coating being only 70 percent as thick as the external coating. Microstructural characteristics are similar to those found in the internal blade cavity.

Table 30

Coating Weight Data of IN-792 + Hf Mars Blades

Blade Number	Internal Coating	Total Coating Weight Gain (g)	Use
A64	Ni-19Al-1Cb	0.300	Engine test
A11	"	0.262	Engine test
A23	"	0.435(1)	Metallography
A33	"	0.413(1)	NASA-LeRC
3	" (2)	0.322(1)	NASA-LeRC
A04	Ni-19Al-3Cb	0.277	Engine test
A34	"	0.279	Engine test
A50	"	1.0592(1)	Engine test
A58	Ni-12Al-20Cr	0.255	Engine test
A15	"	0.272	Engine test
A53	"	0.718(1)	Metallography
A72	"	0.829(1)	NASA-LeRC
12	"(2)	0.883(1)	Metallography

(1) Internally and externally processed with same coating.
(2) MAR-M200 + Hf (DS) alloy.

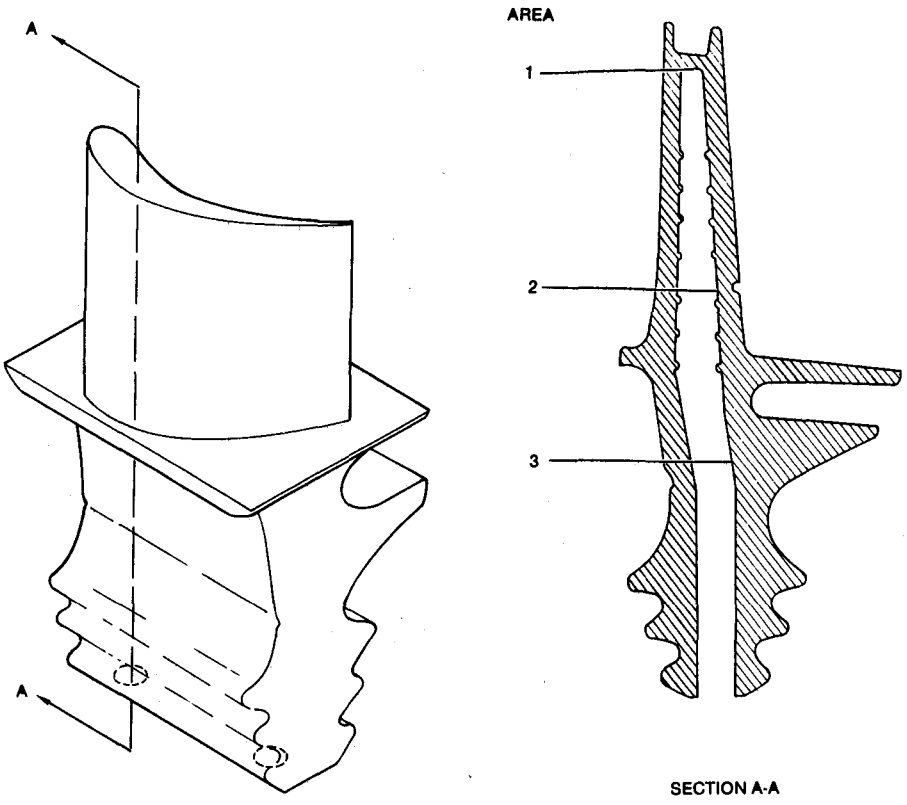

Figure 77. Metallurgical Sectioning of Blades

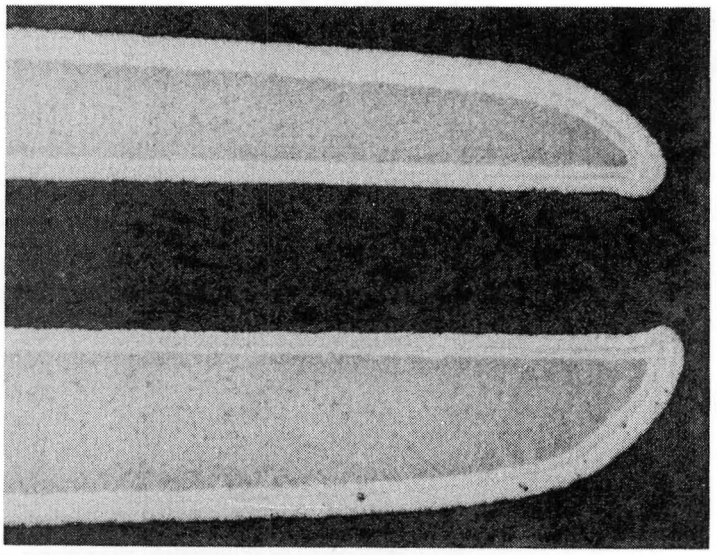

Figure 78.

Photomicrograph of Trailing Edge of Ni-12Al-20Cr Coated Blade (Specimen A53)

Magnification: 40X

5.2 ENGINE TEST SCHEDULE

Internally coated blades were included in an in-house 500-hour Mars engine endurance test, Figure 83. The Mars test engine (S/N 2-12) was operated on both natural gas and diesel No. 2 with the test schedule requiring that engine operation should consume approximately equal quantities of each fuel with fuel change occurring every hour. Turbine rotor inlet temperature (TRIT) for diesel fuel was 1071°C (1960°F) and 1113°C (2035°F) for natural gas. During every 24hour period, the engine was cycled through three shut-downs and restarts (both cold and hot). Power turbine actual speed was held at 8260 $\pm$50 rpm.

The coated blades were loaded onto the stage 1 rotor disc in pairs at locations 90 degrees apart. Two fully assembled rotor stages are shown in Figure 84 During test, blade temperatures were monitored by means of an infrared optical pyrometer sighted on the rotating airfoils. Metal temperatures ranged between 816 and 871°C (1500-1600°F). The inspection schedule is provided in Table 31. Visual inspections during testing did not note any gross degradation on the external blade surfaces.

5.3 EVALUATION OF TEST BLADES

All blades from the engine test were sectioned across the airfoil in mid-chord. Based on visual evidence of oxidation attack on the external surfaces of these and other blades, it was noted that the pressure side near the center of the leading edge exhibited noticeable oxidation attack compared to the rest of the airfoil which had only minor indications of oxidation. Metallographic analysis was the primary diagnostic technique used to evaluate the performance of these internal coatings.

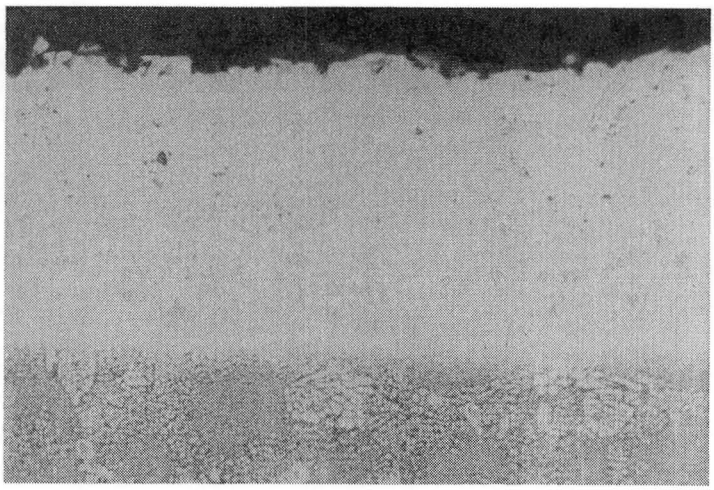

Area 1

Oxalic Etch

Magnification: 500X

Area 2

Oxalic Etch

Magnification: 500X

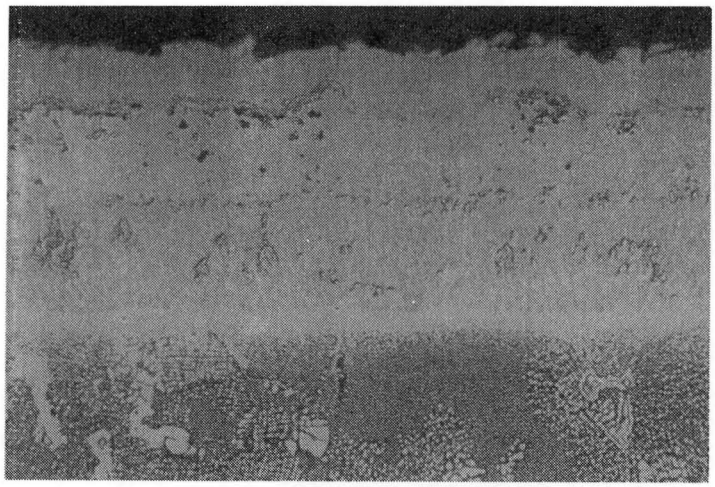

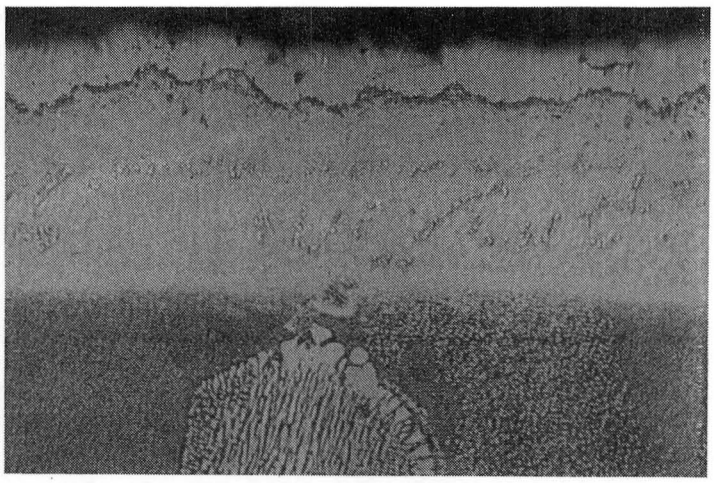

Area 3

Oxalic Etch

Magnification: 500X

Figure 79. Typical Microstructure of Ni-19Al-1Cb (Internally) Coated IN-792 Blade (Specimen A23)

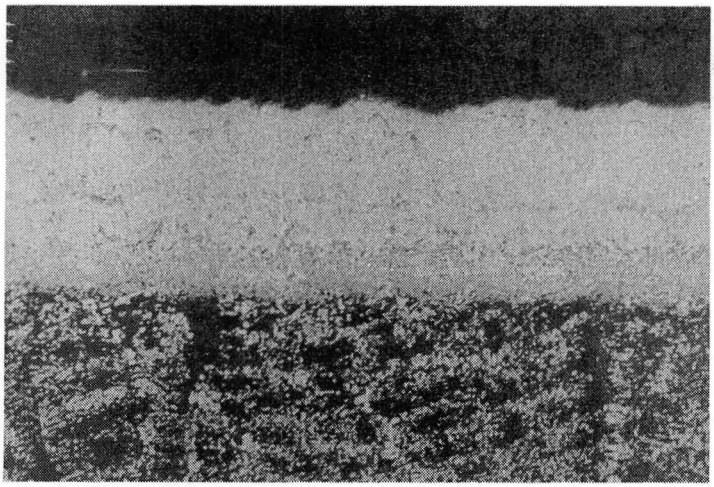

Internal Coating

Oxalic Etch

Magnification: 250X

External Coating

Oxalic Etch

Magnification: 250X

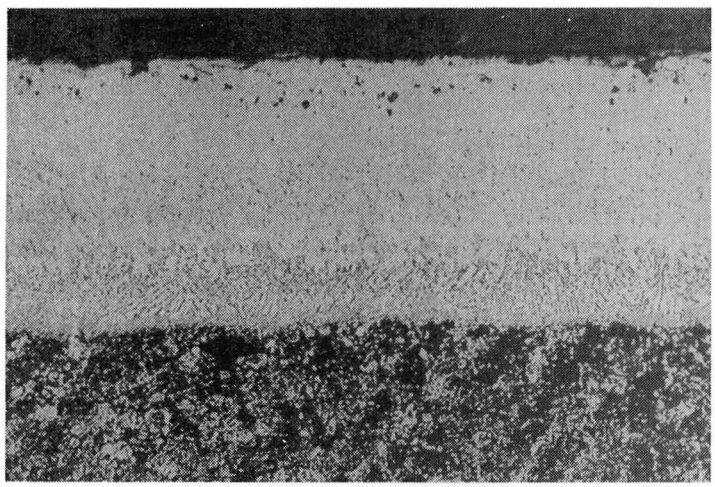

Figure 80. Typical Microstructure of Internally and Externally Coated (Ni-19Al-1Cb) IN-792 + Hf Blade at Trailing Edge (Specimen A23)

Figure 85 shows typical microstructures of internally applied Ni-19Al-1Cb coating near the leading and trailing edges after 500 hours of engine testing. Coating thickness near the trailing edge was found to be 30 percent less than the leading edge internal coating. The columbium-rich band associated with this coating was not evident. Internal voiding/oxidation was noted in the coating near the leading edge. In the same photomicrograph, the alloy/coating interface was marked by a homogeneous light grey denuded zone with the formation of acicular phases in the adjacent substrate. The trailing edge microstructure differed primarily in the presence of the two zone demarcation line in mid-coating, consisting of fine precipitates of a secondary phase. In general, the Ni-19Al-1Cb internal coating was still fully protective and basically unaffected by test exposure.

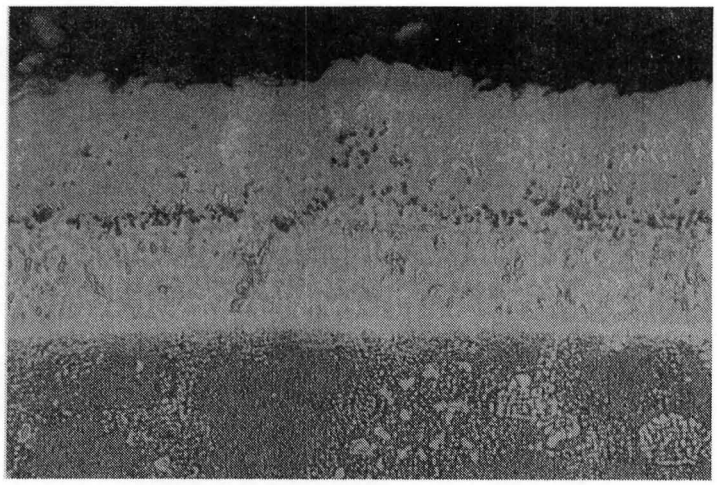

Area 1

Oxalic Etch

Magnification: 500X

Area 2

Oxalic Etch

Magnification: 500X

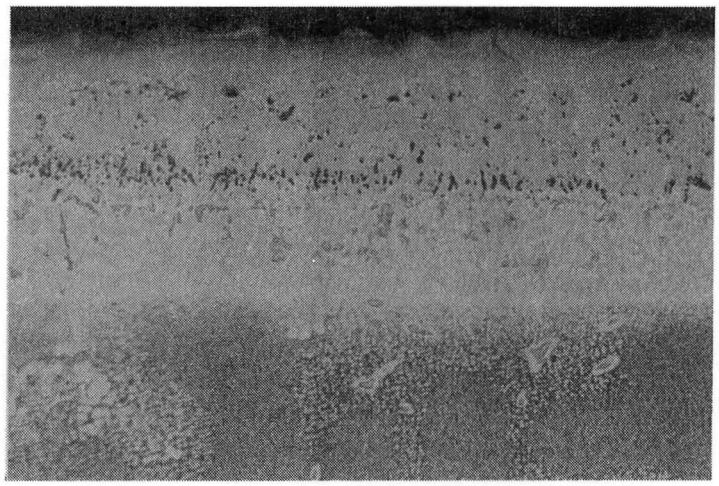

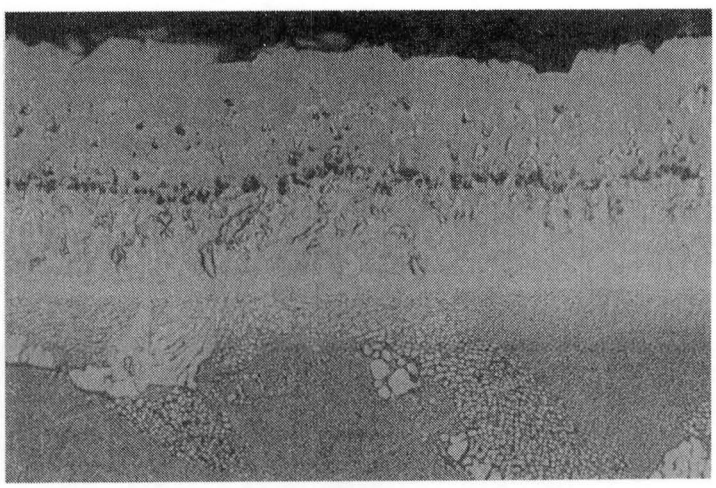

Area 3

Oxalic Etch

Magnification: 500X

Figure 81. Typical Microstructures of Ni-12Al-20Cr (Internally) Coated IN-792 Blade (Specimen A53)

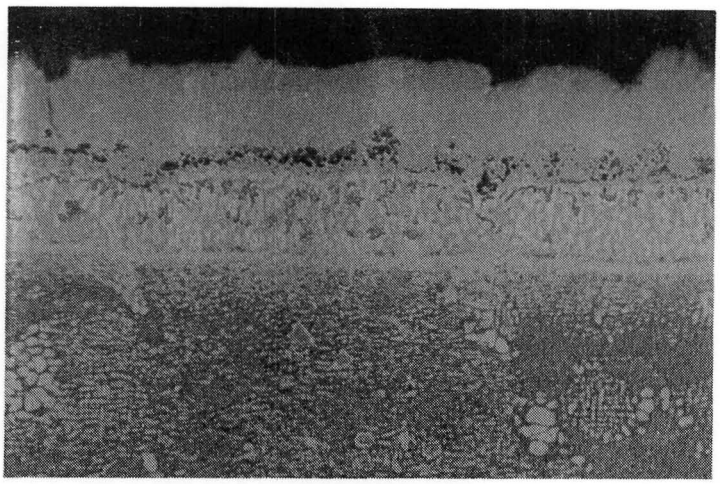

Internal Coating

Oxalic Etch

Magnification: 500X

External Coating

Oxalic Etch

Magnification: 500X

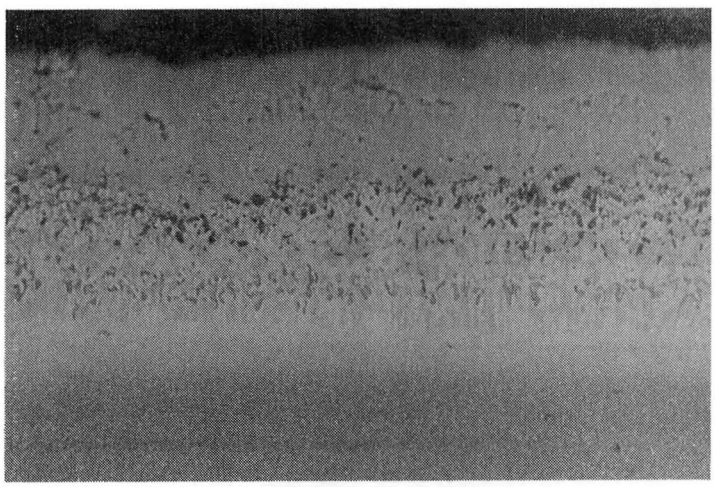

Figure 82. Typical Microstructures of Internally and Externally Coated (Ni-12Al-20Cr) IN-792 Blade at Trailing Edge (Specimen A53)

Similar observations were also noted in Ni-19Al-3Cb coated internal surfaces, as can be seen in Figure 86. Again evidence of internal voiding/oxidation is noted near the coating surface which had retained a light grey phase previously observed and known to be columbium-rich. The coating appeared to be significantly thinner, approximately 50 percent, and rougher near the trailing edge. One of the blades was both externally and internally coated with Ni-19Al-3Cb. The external surface near the leading edge was found to be severely oxidized in localized areas, as seen in Figure 87. Oxide formation near the leading edge had resulted in pitting attack which had extended into the coating through cracks initiating at the oxidation site. The presence of voids and oxides near the coating surface appear to be concentrated along grain boundaries and these voids/oxides would eventually merge or coalesce to form a continuous pathway into the coating. Crack formation was possibly enhanced by thermal cycling during testing.

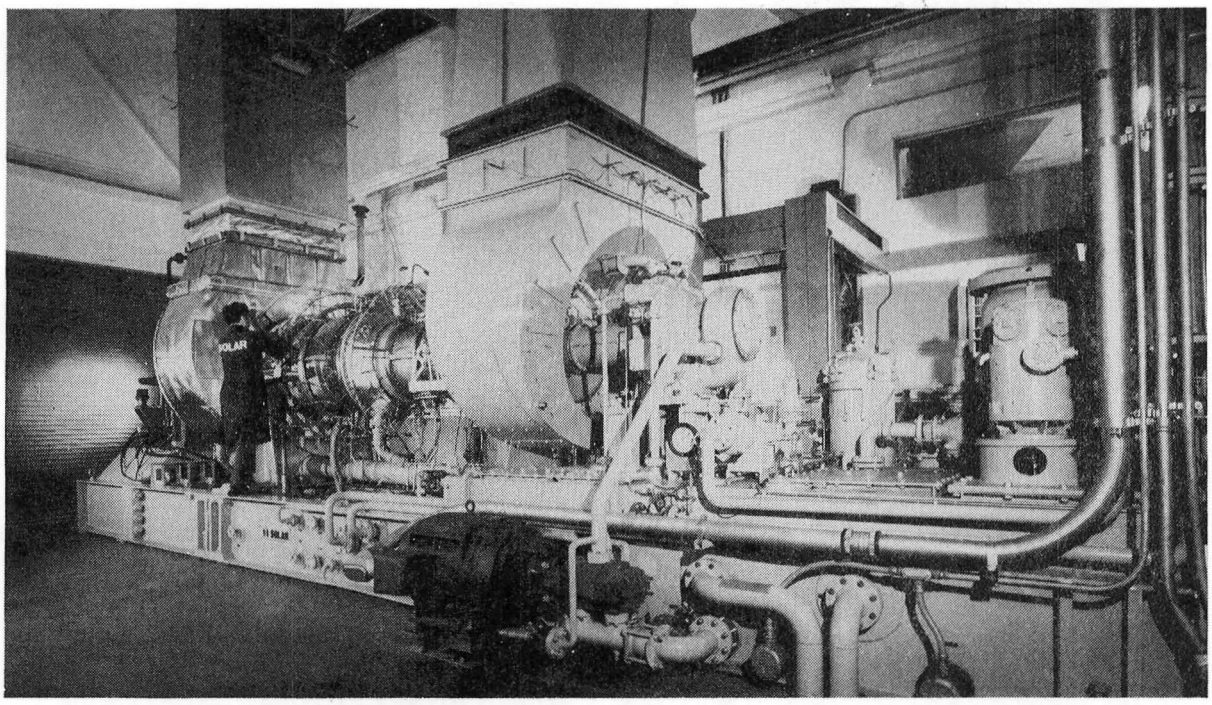

Figure 83. Mars Engine Test Facility

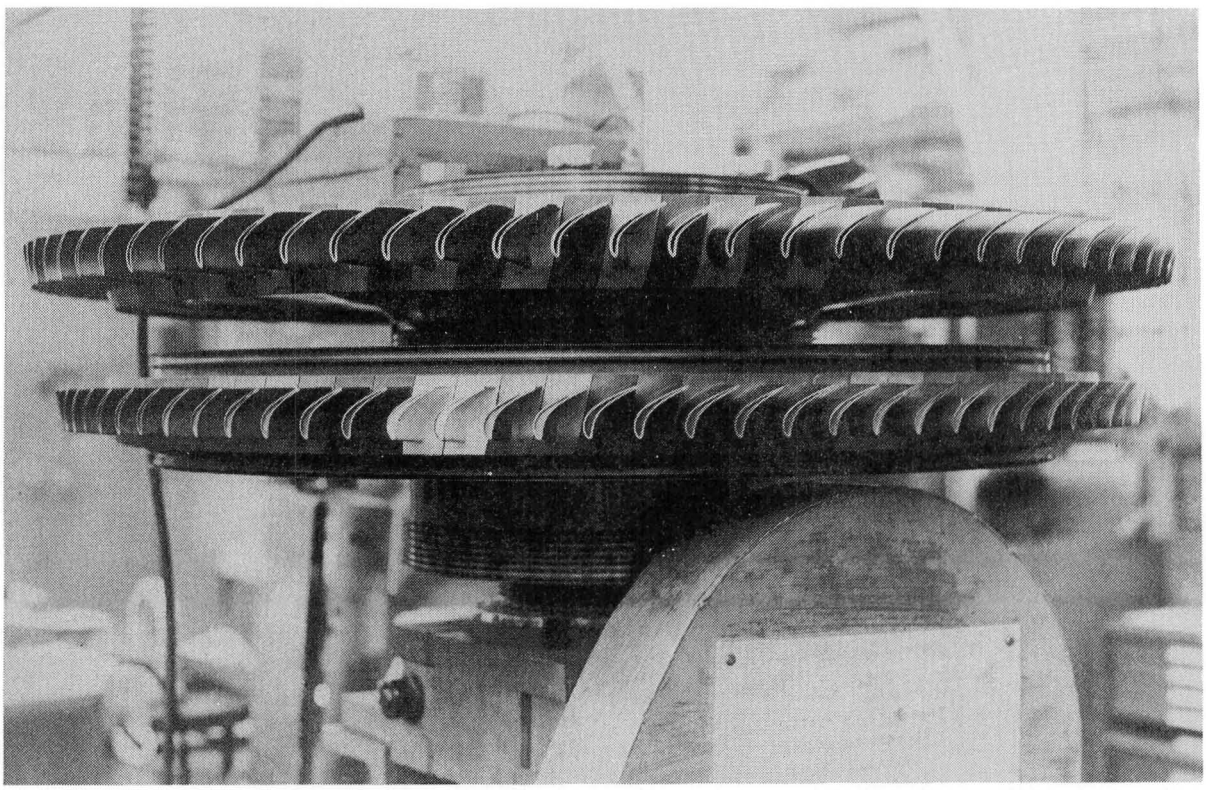

Figure 84. Two Fully Assembled Rotor Stages

Table 31

Inspection Schedule of Mars Engine Test

Number of Hours	Inspection	Remarks
Pretest calibration	Boroscope inspection	No gross effects noted.
0-125	Boroscope inspection of blades and other test components	Fuel transfer initiated at 'idle'
125-250	Combustor teardown, visual inspection	Fuel transfer initiated at 'idle'
250-375	Boroscope inspection only	Fuel transfer initiated at full rated power
375-500	Engine teardown and complete inspection	Fuel transfer initiated at full rated power

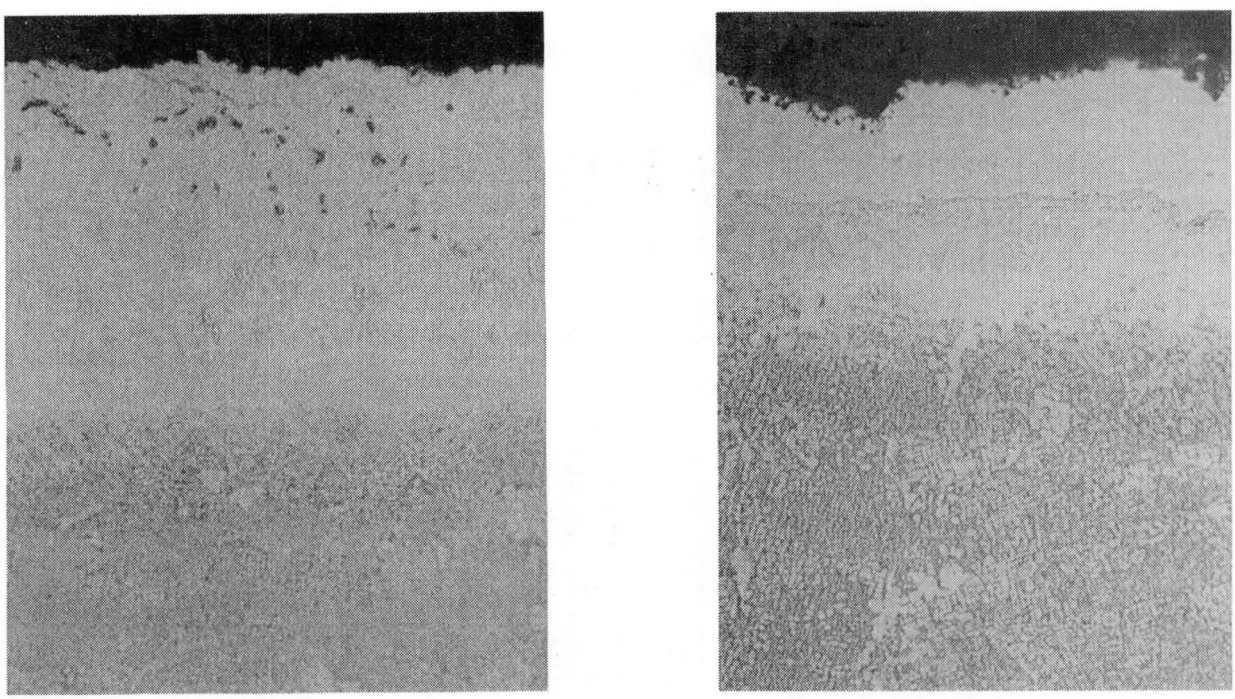

Near Leading Edge Near Trailing Edge

Chromic Etch; Magnification: 500X

Figure 85. Microstructures of Ni-19Al-1Cb Internally Coated IN-792 + Hf Blade After 500 Hours of Engine Testing (Specimen A11)

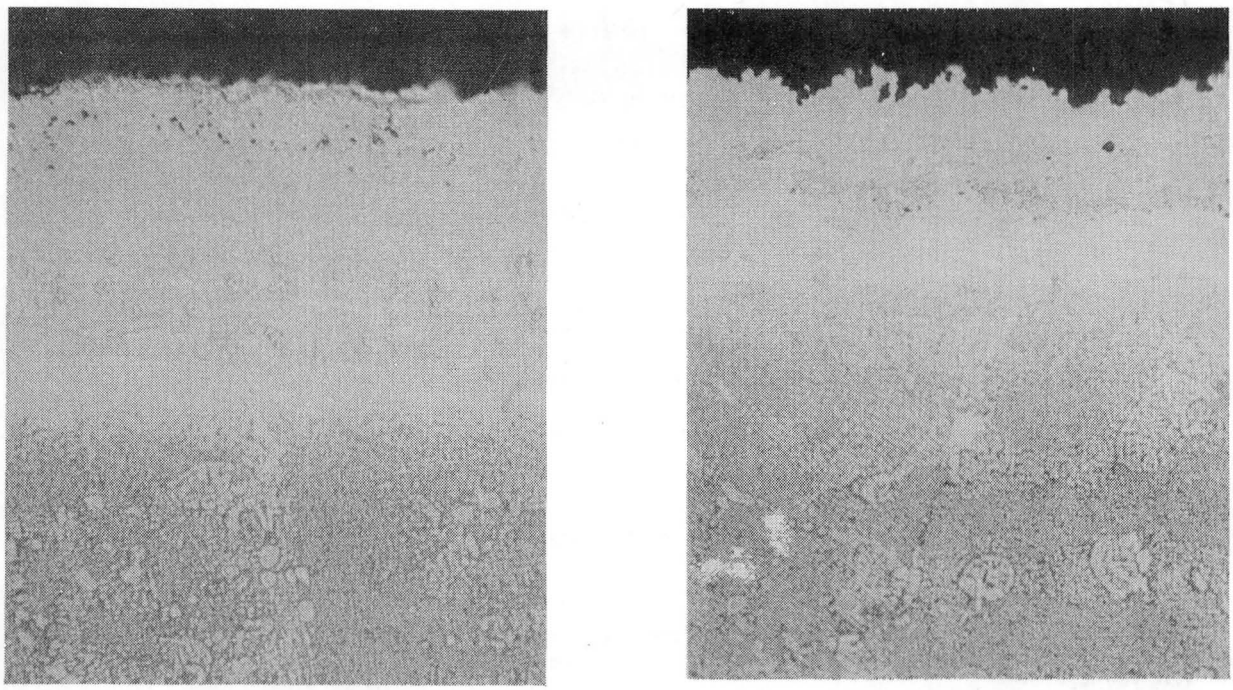

Near Leading Edge Near Trailing Edge
Chromic Etch; Magnification: 500X

Figure 86. Microstructures of Ni-19Al-3Cb Internally Coated IN-792 + Hf Blade After 500 Hours of Engine Testing (Specimen A04)

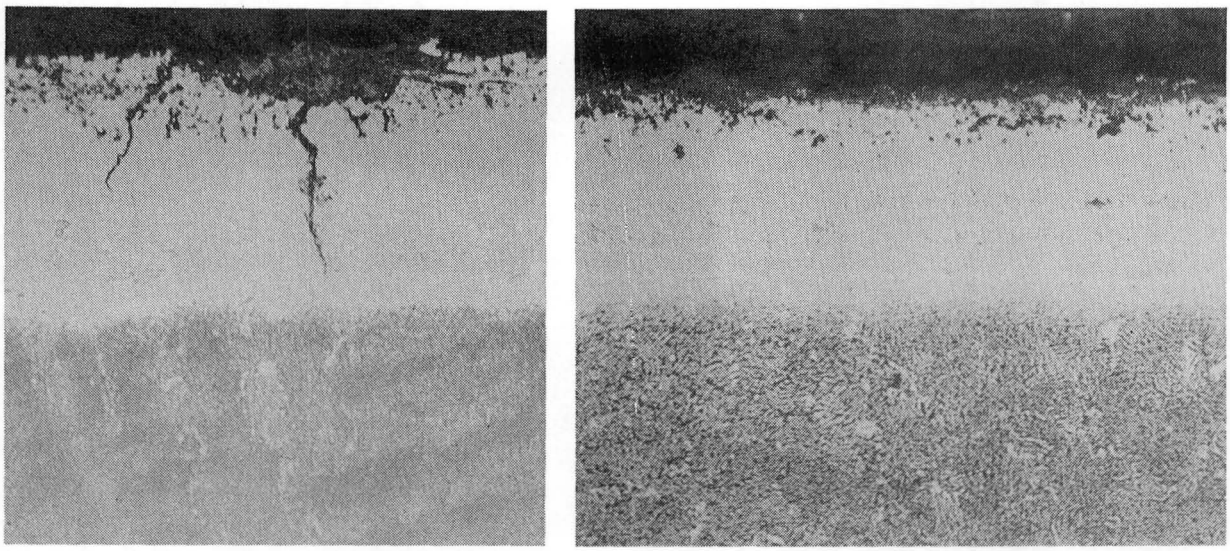

Near Leading Edge Near Trailing Edge
Chromic Etch; Magnification: 500X

Figure 87. Microstructures of Ni-19Al-3Cb Externally Coated IN-792 + Hf Blade Showing Localized Areas of Severe Oxidation Attack (Specimen A50)

Comparison of coated and uncoated IN-792 + Hf alloy can be made with reference to Figure 88 (at half the magnification) which shows the external surfaces of the unprotected alloy. Near the leading edge which bears the brunt of the hot gases from the combustor, intergranular oxidation (IGO) was found to extend 200 to 300 microns into the alloy with the depleted zone essentially losing all of its gamma/gamma prime structure. Similar, though less extensive, degradation was observed near the edge. Therefore, oxidation attack can be significantly alleviated by the Ni-19Al-3Cb coating which generally shows less than 50 microns attack under similar conditions except for the brittle thermal fatigue induced cracks at localized areas.

The third coating evaluated in this test was the Ni-12Al-20Cr coating shown in Figure 89. In contrast to the internal trailing edge microstructures found in the columbium coatings, Figure 89 shows a partially consumed coating near the trailing edge. The unusually thin coating found in this area is probably due to processing. Once again, internal voids/oxides can be observed in mid-coating which appears to be the most susceptible area to oxidation reaction, as was found in burner rig testing. The lower aluminum level also accounts for the ready conversion to gamma found in the coating.

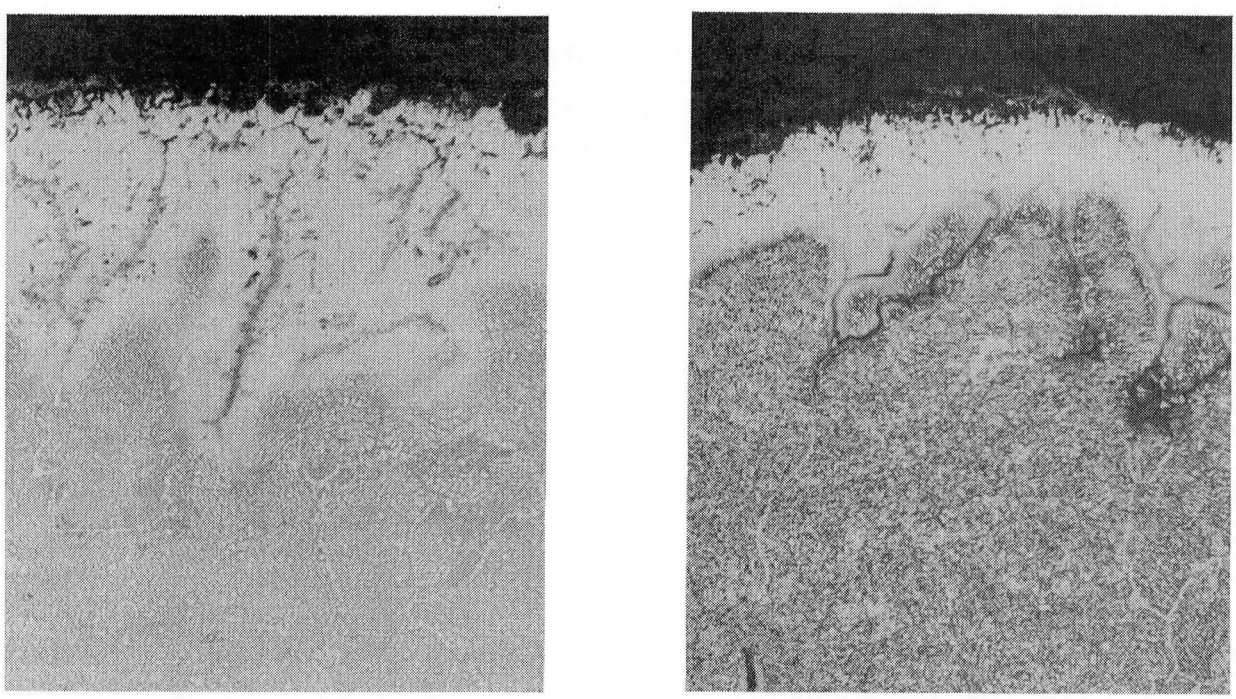

Near Leading Edge Near Trailing Edge

Chromic Etch; Magnification: 250X

Figure 88. Microstructures of External Surfaces of Uncoated IN-792 + Hf Blades After 500 Hours of Engine Testing (Specimen A15)

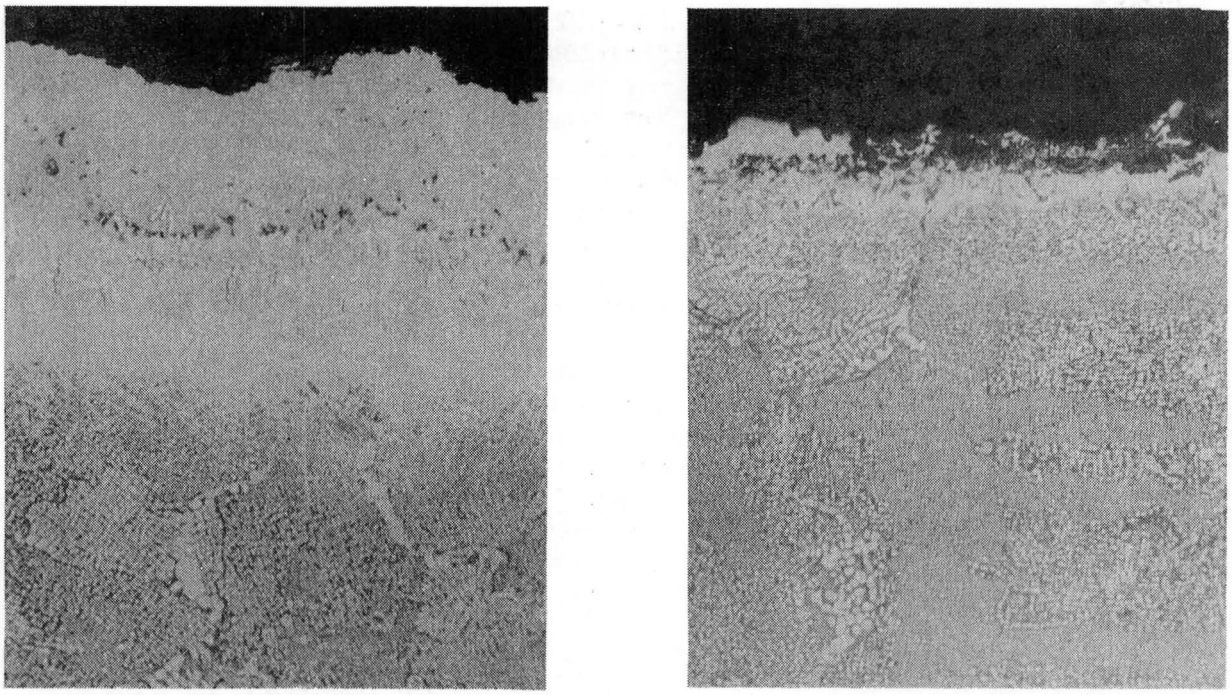

Near Leading Edge Near Trailing Edge

Chromic Etch; Magnification: 250X

Figure 89. Microstructures of Ni-12Al-20Cr Internally Coated IN-792 + Hf After 500 Hours of Engine Testing (Specimen A58)

6

CONCLUSIONS

1. Modified aluminide coatings containing columbium or chromium can be applied to external surfaces and internal passages of IN-792 components using the powder pack method in two consecutive operations. Coatings applied internally are generally 30 percent thinner than the same coating externally applied.

2. Three batches of test specimens of each coating system were prepared and weight gain data obtained demonstrated reliable and reproducible processing.

3. Of the four candidate compositions, Ni-19Al-3Cb (Variation B) exhibited the best 877°C burner rig hot corrosion resistance with maximum attack of 25 microns while maximum penetration in the other coatings were in the 25-30 micron range. The coatings can be ranked in decreasing order as Ni-19Al-3Cb > Ni-19Al-1Cb, Ni-12Al-20Cr > Ni-17Al-20Cr. Baseline corrosion data was provided by an uncoated IN-752 bar which after only 100 hours of exposure had suffered 300-400 microns of alloy penetration.

4. In general, the Ni-Al-Cb coating systems exhibited superior corrosion resistance relative to the Ni-Al-Cr systems. This observation is supported by depth of penetration measurements from burner rig test specimens.

5. The Ni-19Al-3Cb coating exhibited the best 1050°C burner rig oxidation resistance with the formation of a thin, adherent oxide scale. Ni-19Al-1Cb was less resistant and suffered intergranular oxidation near the coating surface. The Ni-Al-Cr coatings were more susceptible to burner rig oxidation attack with degradation initiating at the chromium-rich areas. The lower aluminum coating, Ni-12Al-20Cr, was found to be deteriorated the most due to a combination of both surface and internal oxidation.

6. Generally, both burner rig and furnace oxidation test results are in agreement regarding the ranking of the four coatings in oxidation resistance.

   Ni-19Al-3Cb > Ni-19Al-1Cb, Ni-12Al-20Cr > Ni-17Al-20Cr

7. Tensile properties of coated IN-792 test bars were basically unaffected by the coating/processing. High cycle fatigue life was reduced by approximately 30 percent for Ni19Al-1Cb and Ni-12Al-20Cr and a commercial platinum-rhodium aluminide coated IN-792. This significant loss is apparently not recovered by conventional heat treatment. Stress-rupture

life of Ni-19Al-1Cb and Ni-12Al-20Cr coated IN-792 was significantly reduced at high stress levels. All four program coatings exhibited high ductility relative to standard aluminde coatings.

8. Of the three internal coatings evaluated in engine testing, Ni-19Al-1Cb and Ni-19Al-3Cb demonstrated better resistance than Ni-12Al-20Cr. The Ni-19Al-3Cb coating was also externally applied to an engine blade and it was found to be locally pitted at the leading edge with thermal cracks extending into the coating. Engine test results support the selection of Ni-19Al-1Cb coating as being the optimized coating for protection of internal surfaces of IN-792 blading.

7

RECOMMENDATIONS

During the course of the program, several interesting phenomena were observed which merit further investigation and better understanding. These observations are not limited to this particular coating development, but may be applicable to aluminide coatings in general.

1. The role of columbium in the diffusion aluminide coating is only minimally understood. The findings in this program have led to two conclusions: First, the presence of a columbium-rich zone at the coating surface is believed to play a major role in formation of a protective and adherent oxide scale, and second, the columbium intermetallic formed appears to be a selective diffusion barrier restricting nickel diffusion outwards, thus producing an "inwards" coating usually formed from high activity packs. Furthermore, higher concentrations of columbium in the coating can produce early and rapid formation of columbium oxides which are non-protective.

2. Another area of investigation that will extend understanding of columbium additives is the analysis of various columbium plus aluminides formed from packs of different activities. If the diffusion of nickel is indeed restricted through the crystallographic structure of the columbium intermetallic, the movement of aluminum may also be affected by the thermodynamic activities effective at the substrate surface.

3. The effects of coating and/or coating processing on mechanical properties of the substrate alloy were significant for IN-792 alloy. Generally, it is not unusual to find some deterioration of stress rupture and fatigue lives as a result of coating application. However, restoration is often achieved by resolutioning and precipitation of fine gamma/gamma prime structures by means of the appropriate heat cycles. This problem is especially critical for thin-walled, air-cooled structural components. Investigation of coating effects on IN-792 properties would lead to an understanding of the causes of the deterioration and development of methods of restoration.

This Page Intentionally Left Blank

REFERENCES

1. Gill, B.J., et al, "Aluminide Coating of Cooling Passages of Gas Turbine Blades", 3rd Conf. on Gas Turbine Materials in a Marine Environment (1976).

2. Ahuja, P.L., "Internal Coating of Air-Cooled Gas Turbine Blades", General Electric AEG Final Report on NASA-Lewis Contract NAS3-21038, NASA CR-159701 (Nov. 1979).

3. Glamiche, P., "Protection of Cooled Blades of Complex Internal Structure", NASA TM-75217 (Oct. 1977).

4. Hsu, L., Stevens, W.G. and Stetson, A.R., " Internally Coated Air-Cooled Gas Turbine Blading", Solar Turbines International Final Report on NASA-Lewis Contract NAS3-21039, NASA CR-159574 (1979).

5. Stoloff, N.S., "Fundamentals of Strengthening", The Superalloys, ed. Sims and Haxel, Wiley-Interscience (1972) p. 79.

6. Aldred, P., "Rene' 125, Development and Application ", National Aerospace Engeering and Manufacturing Meeting (1975).

7. Levine, S.R. and Caves, R.M., "Thermodynamics and Kinetics of Pack Aluminide Coating Formation on IN-100", J. Electrochem. Soc., Vol. 121, No. 8 (1974) p. 1051.

8. Siegle, L.L., Gupta, B.K., Shankar, R. and Sarkhel, A.K., "Kinetics of Pack Aluminization of Nickel), NASA Contractor Report 2939, Contract NGR-33-015-160 (1978).

9. Goward, G.W. and Boone, D.H., "Mechanisms of Formation of Diffusion Aluminide Coatings on Nickel-Base Superalloys", Oxidation of Metals, Vol. 3, No. 5 (1971) p. 475.

10. Hsu, L., Stevens, W.G. and Stetson, A.R., "Development and Evaluation of Processes for Deposition of Ni/Co-Cr-Al-Y (MCrAlY) Coatings for Gas Turbine Components", Solar Turbines International Final Report AFML-TR-79-4097 (1979).

11. Handbook of Chem. and Physics, 52nd Edition, p. E-208.

12. Powell, C.F., Oxley, J.H. and Blocker, J.M., Vapor Deposition, ed. J. Wiley & Sons, New York (1966).

13. Gadd, J.D., Nehedlik, J.F. and Graham, L.D., "Vacuum Pack and Slurry Coating Processes for Coating Superalloys", Electrochem. Tech., Vol. 6, No. 9-10 (1968) p. 307.

14. Brill-Edwards, H. and Epner, M., "Effect of Material Transfer Mechanism on the Formation of Discontinuities in Pack Cementation Coatings on Superalloys", Electrochem. Tech., Vol. 6, NO. 9-10 (1968) p. 299.

15. Duffy, E.R. and Stetson, A.R., "The Influence of Surfaces on the Conversion of Sodium Chloride to Sodium Sulfate in a Gas Turbine Environment", Paper presented at the 4th Conf. on Gas Turbine Materials in a Marine Environment, Maryland (June 1979).

16. Jones, R.L. and Gasomski, S.T., "Hot Corrosion of CoCrAlY Turbine Blade Coatings by Na_2SO_4 and Vaporous NaCl", J. of Electrochem. Soc., (1977) p. 1641.

17. Law, C.C., Wallace, W., Ashdown, C.P. and Grey, D.A., "Sigma Phase Formation in Conventional and PM Nickel-Base Superalloys", Metal Science,

18. Kaufman, M., "Examination of the Influence of Superalloy Sections, Vol. 1, Description and Analysis", General Electric, Ohio, NASA Cr-13479 (Dec. 1970).

19. Reid, M.L., Solar Turbines International Report RDR 1832 (1976).

20. Buchanan, E.R., "Mechanical Property Evaluation of IN-792 Coated with RT-22", General Electric Report 75-GTD-56 (1975).

21. Wildgoose, P. and Ubank, R.G., "The Behavioural Aspects of Coating and the Effect on Thin Wall Superalloy Creep Rupture Properties", 3rd Conf. on Gas Turbine Materials in a Marine Environment (1976).

22. Paskiet, G.F., Boone, D.H. and Sullivan, C.P., "Effect of Aluminide Coating on the High Cycle Fatigue Behavior of a Nickel-Base High Temperature Alloy", J. of Inst. of Metals, Vol. 100 (1972) p. 58.

APPENDIX A

INTERNAL COATING PROCESS SPECIFICATION FOR

NICKEL-BASE SUPERALLOYS

This Page Intentionally Left Blank

APPENDIX A

INTERNAL COATING PROCESS SPECIFICATION FOR NICKEL-BASE SUPERALLOYS

1.0 SCOPE

This specification describes the processing requirements for formation of the following coating compositions on IN-792 substrate alloy:

- Ni-19Al-1Cb (Variation A)
- Ni-19Al-3Cb (Variation B)
- Ni-17Al-20Cr (Variation C)
- Ni-12Al-20Cr (Variation D)

Processing instructions include application of the above coatings to the external surfaces of test specimens and also to the internal surfaces of air-cooled blading.

2.0 APPLICABLE DOCUMENTS

L. Hsu, W.G. Stevens and A.R. Stetson, "Internally Coated Air-Cooled Blading", Final Technical Report on NASA Contract NAS3-21039.

L. Hsu and A.R. Stetson, "Internal Coating of Air-Cooled Gas Turbine Blading", Quarterly Reports Nos. 1 and 2, NASA Contract NAS3-21842.

3.0 MATERIALS

- Columbium powder, -100 +325 mesh (O_2 2000 ppm max., Ta 1000 ppm max., Fe 300 ppm max., N_2 150 ppm max., C 100 ppm max., Al 100 ppm max., Si 100 ppm max., H_2 50 ppm max.)
- Nickel powder, >99.5%, -325 mesh
- Chromium powder, MD101, average particle size 150 microns
- Aluminum powder, MD201, -325 mesh
- Polyvinyl chloride (PVC) powder
- Sodium chloride (NaCl), Reagent grade
- Hydrochloric acid, concentrated
- Acetone, Reagent grade
- Argon gas, dewpoint -100°C, 1 ppm O_2 max.

4.0 EQUIPMENT

- Balance
- Ball mill
- Pressurized air, 6 atm
- Pressurized water, spray gun
- IN-600 or Hastelloy X retort and liner
- Vacuum pump
- Oil trapped pressure release bubbler
- Temperature readout device
- Furnace, maximum temperature 1100°C
- TIG welder

5.0 PREPARATION OF POWDER PACKS

5.1 Powder Pack P100

5.1.1 Weigh out the following components:

- Columbium powder - 500 g (50 w/o)
- Aluminum oxide powder - 500 g (50 w/o)
- PVC powder - 5 g (0.5 w/o)

5.1.2 Place pack in ball mill and mill two (2) hours.

5.1.3 Remove from mill and store in clean, tightly sealed container.

5.2 Powder Pack P200

5.2.1 Weigh out the following components:

- Nickel powder - 240 g (24 w/o)
- Aluminum powder - 160 g (16 w/o)
- Al_2O_3 powder - 5 g (0.5 w/o)
- PVC powder - 5 g (0.5 w/o)

5.2.2 Place pack in ball mill and mill two (2) hours.

5.2.3 Remove from mill and place powder in clean retort.

5.2.4 Seal retort by TIG welding and leak check the weld by pressurizing with argon.

5.2.5 Evacuate retort to at least 26 pascals and backfill with argon three times, leaving retort under an argon blanket at 102 kPa pressure with the pressure release bubbler attached to vent the excess argon.

5.2.6 Place retort in 10790°C furnace and adjust control until thermocouple in retort registers 1050°C. Allow retort to fire for 16 hours. Cool retort and cut open weld.

5.2.7 Transfer pack to ball mill, add 0.3 w/o PVC and mill two (2) hours.

5.2.8 Store pack in clean, sealed container.

5.3 Powder Pack P300

5.3.1 Weigh out the following components:

- Chromium powder - 200 g (20 w/o)
- Al_2O_3 powder - 800 g (80 w/o)
- NaCl powder - 5 g (0.5 w/o)

5.3.2 Place in ball mill and mill two (2) hours.

5.3.3 Remove and place in clean retort.

5.3.4 Seal retort by TIG welding and leak check the weld by pressurizing with argon.

5.3.5 Evaucate retort to at least 26 pascals and backfill with argon three times, leaving retort under an argon blanket at 102 kPa pressure with the pressure release bubbler attached to vent the excess argon.

5.3.6 Place retort in 1104°C furnace and adjust control until thermocouple in retort registers 1060°C. Allow retort to fire for four (4) hours. Cool retort and cup open weld.

5.3.7 Transfer pack to ball mill, add 0.3 w/o NaCl and mill two (2) hours.

5.3.8 Store pack in clean, sealed container.

5.4 Powder Pack P400

5.4.1 Weigh out the following components:

- Nickel powder - 230 g (23 w/o)
- Aluminum powder - 170 g (17 w/o)
- Al_2O_3 powder - 600 g (60 w/o)
- PVC powder - 5 g (0.5 w/o)

5.4.2 Place pack in ball mill and mill two (2) hours.

5.4.3 Remove and place in clean retort.

5.4.4 Seal retort by TIG welding and leak check the weld by pressurizing with argon.

5.4.5 Evacuate retort to at least 26 pascals and backfill with argon three times, leaving retort under an argon blanket at 103 kPa pressure with the pressure release bubbler attached to vent the excess argon.

5.4.6 Place retort in 1079°C furnace and adjust control until thermocouple in retort registers 1050°C. Allow retort to fire for 16 hours. Cool retort and cut open weld.

5.4.7 Transfer pack to ball mill, add 0.3 w/o NaCl and mill two (2) hours.

5.4.8 Store pack in clean, sealed container.

6.0 SPECIMEN SURFACE PREPARATION

6.1 Degrease all surfaces to be coated with acetone.

6.2 Etch clean surfaces with concentrated HCl for one (1) to two (2) minutes. Allow parts to soak in water for 15 minutes and rinse thoroughly with distilled water.

6.3 Finally, rinse with acetone and alloy to dry. Use pressurized air to assist drying process in internal passages of blading.

7.0 LOADING OF RETORT

7.1 For Test Specimens

7.1.1 Weigh clean specimens using gloves to avoid contaminating surfaces.

7.1.2 Fill half of the retort liner with the appropriate powder pack. Place specimens on pack bed and add more pack until specimens are fully covered by at least 6 mm of pack. Tamp a few times to settle pack particles.

7.1.3 Seal retort (see Sec. 7.3).

7.2 For Air-Cooled Blades

7.2.1 Weigh clean blades using gloves to avoid surface contamination.

7.2.2 Using a small spatula, pour powder pack into firtree opening and tamp occasionally to make certain the blade is completely filled.

7.2.3 Clean off outer surfaces of blades and place in retort carefully.

7.2.4 Seal retort (see Sec. 7.3).

7.3 Sealing of Retort

7.3.1 With parts properly loaded, seal retort by TIG welding and leak check weld by pressurizing with argon.

7.3.2 Evacuate retort to at least 26 pascals and backfill with argon three times, leaving retort under an argon blanket at 103 kPa pressure with the pressure release bubbler attached.

7.3.3 Place retort in furnace preheated to the proper temperature and fire retort for the specified time period (see Sec. 8.0).

7.3.4 Cool retort and cut open weld. Remove blade and shake out all loose powder with aid of wire.

7.3.5 Hold nozzle of pressurized water spray gun (set to 80 psig) to openings in firtree and allow water pressure to clean internal passages and wash out any remaining powder. Acetone rinse part, let dry and weigh.

8.0 PROCESS PARAMETERS

Each coating is formed by undergoing two pack processes, as specified below.

8.1 For the Ni-19Al-1Cb coating (Variation A):

- Use pack P100 at 930°C for four (4) hours.
- Use pack P200 at 930°C for 16 hours.

8.2 For the Ni-19Al-3Cb coating (Variation B):

- Use pack P100 at 990°C for six (6) hours.
- Use pack P200 at 1050°C for 16 hours.

8.3 For the Ni-17Al-20Cr coating (Variation C):

- Use pack P300 at 1060°C for four (4) hours.
- Use pack P400 at 1050°C for 16 hours.

8.4 For the Ni-12Al-20Cr coaging (Variation D):

- Use pack P300 at 1060C for four (4) hours.
- Use pack P200 at 1050°C for 16 hours.

APPENDIX B

PHYSICAL APPEARANCE OF HOT CORROSION TEST SPECIMENS

AFTER 900°C BURNER RIG TESTING

This Page Intentionally Left Blank

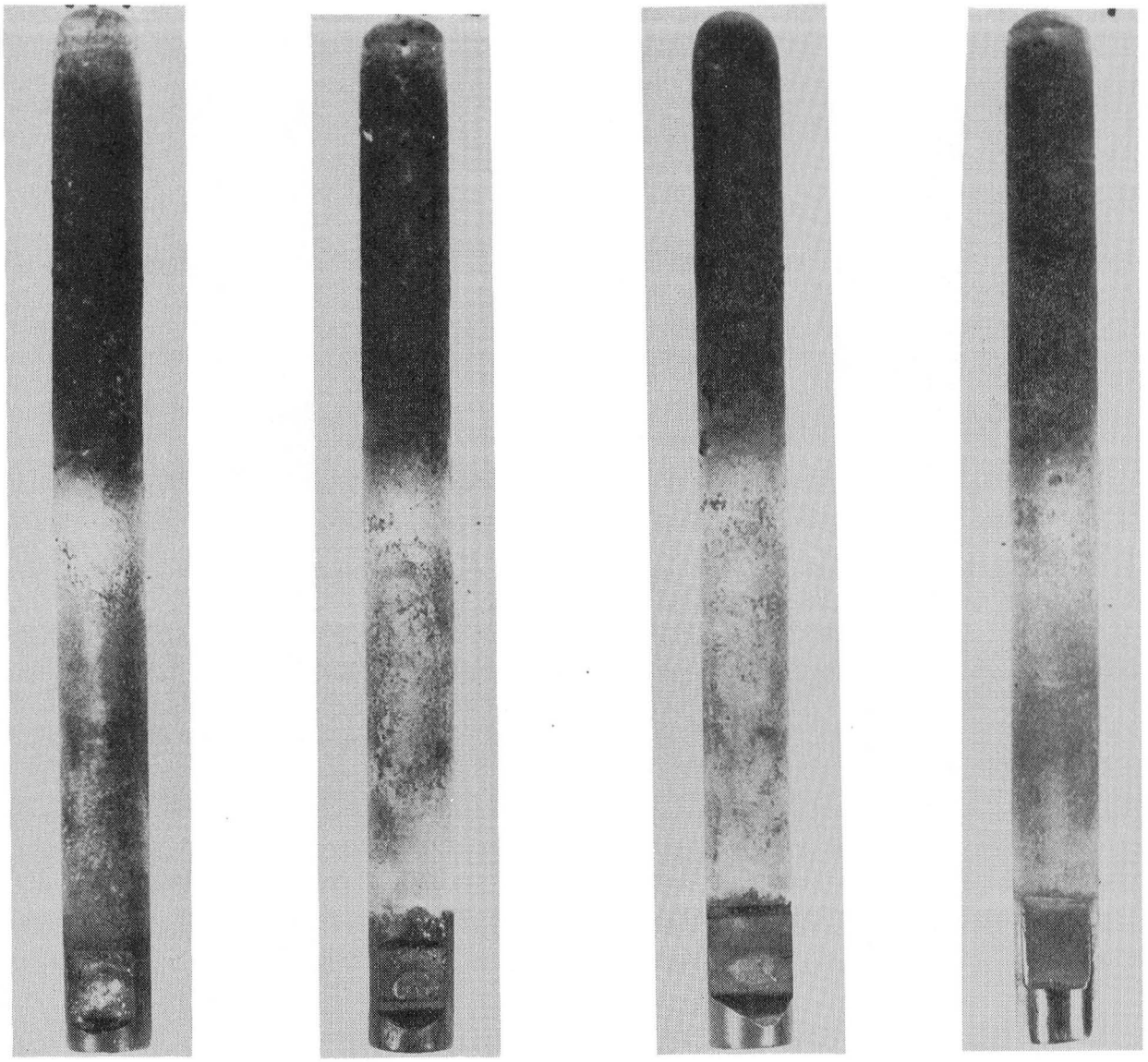

R1	R2	Specimen	R4	R69
314	314	Hours	314	102

Figure B-1. Variation A - Ni-19Al-1Cb Coating

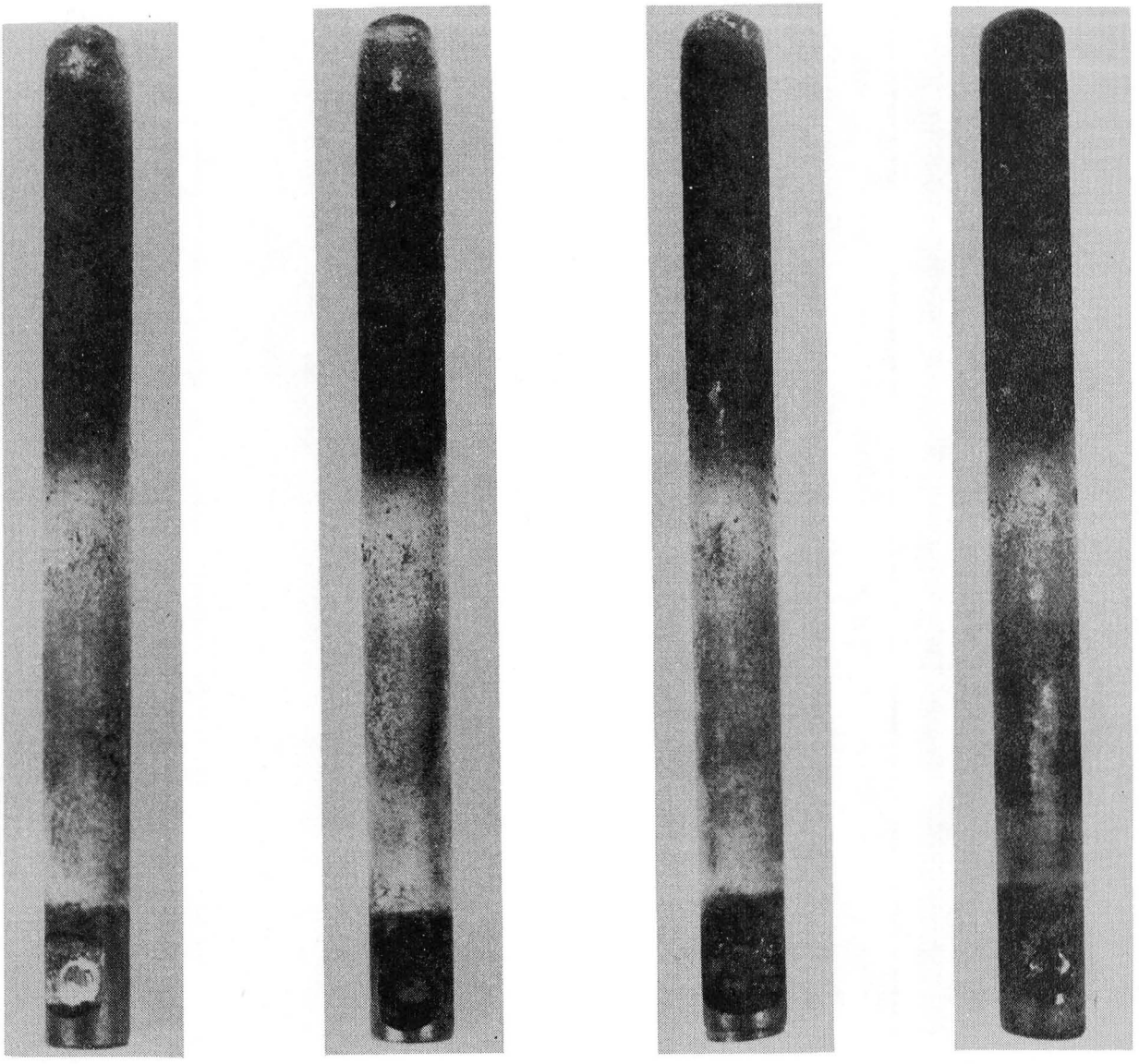

R5	R6	Specimen	R7	R71
314	314	Hours	314	102

Figure B-2. Variation B - Ni-19Al-3Cb Coating

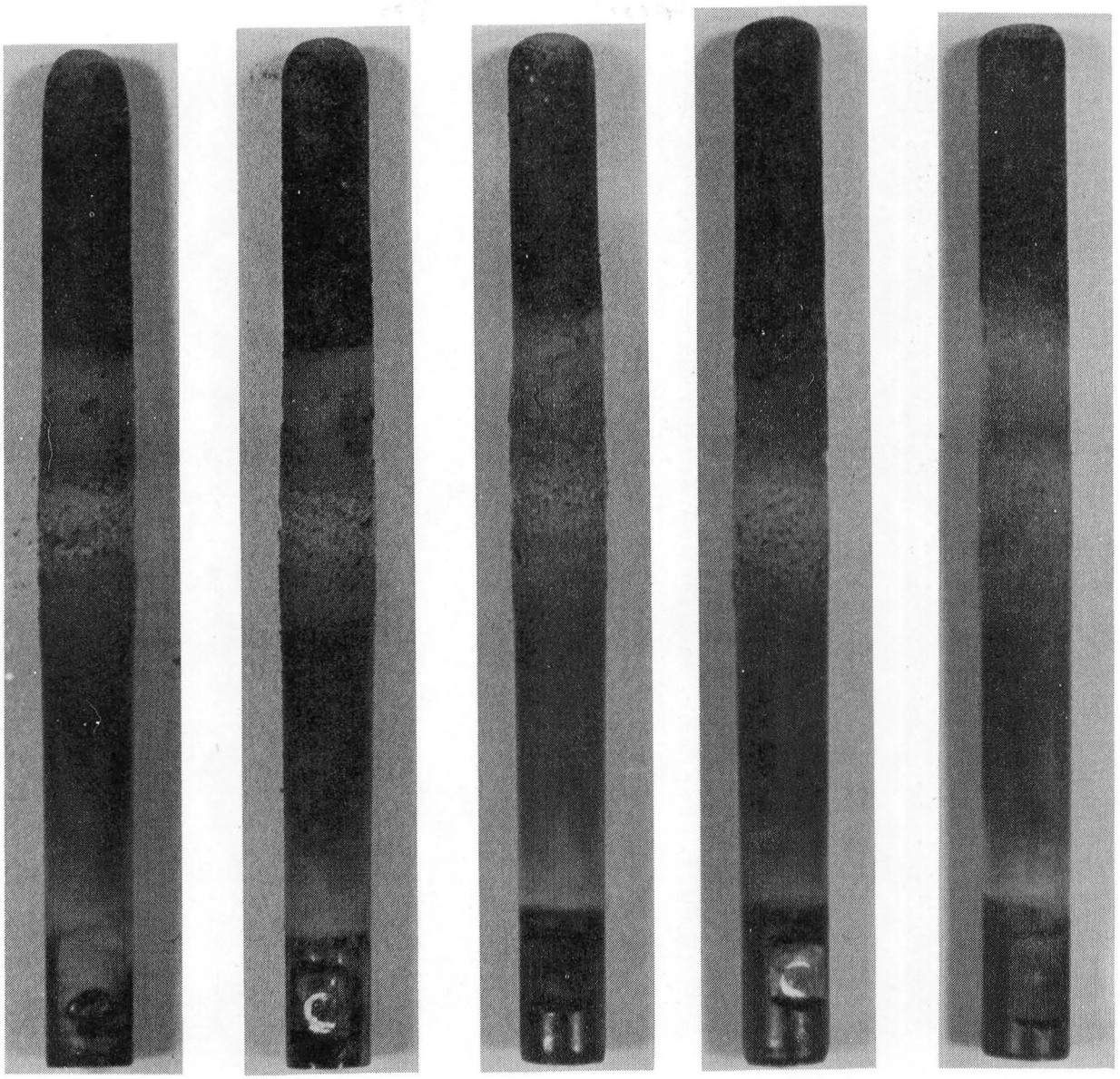

Specimen	R9	R10	R11	R12	R40
Hours	318	318	318	214	104

Figure B-3. Variation C - Ni-17Al-20Cr Coating

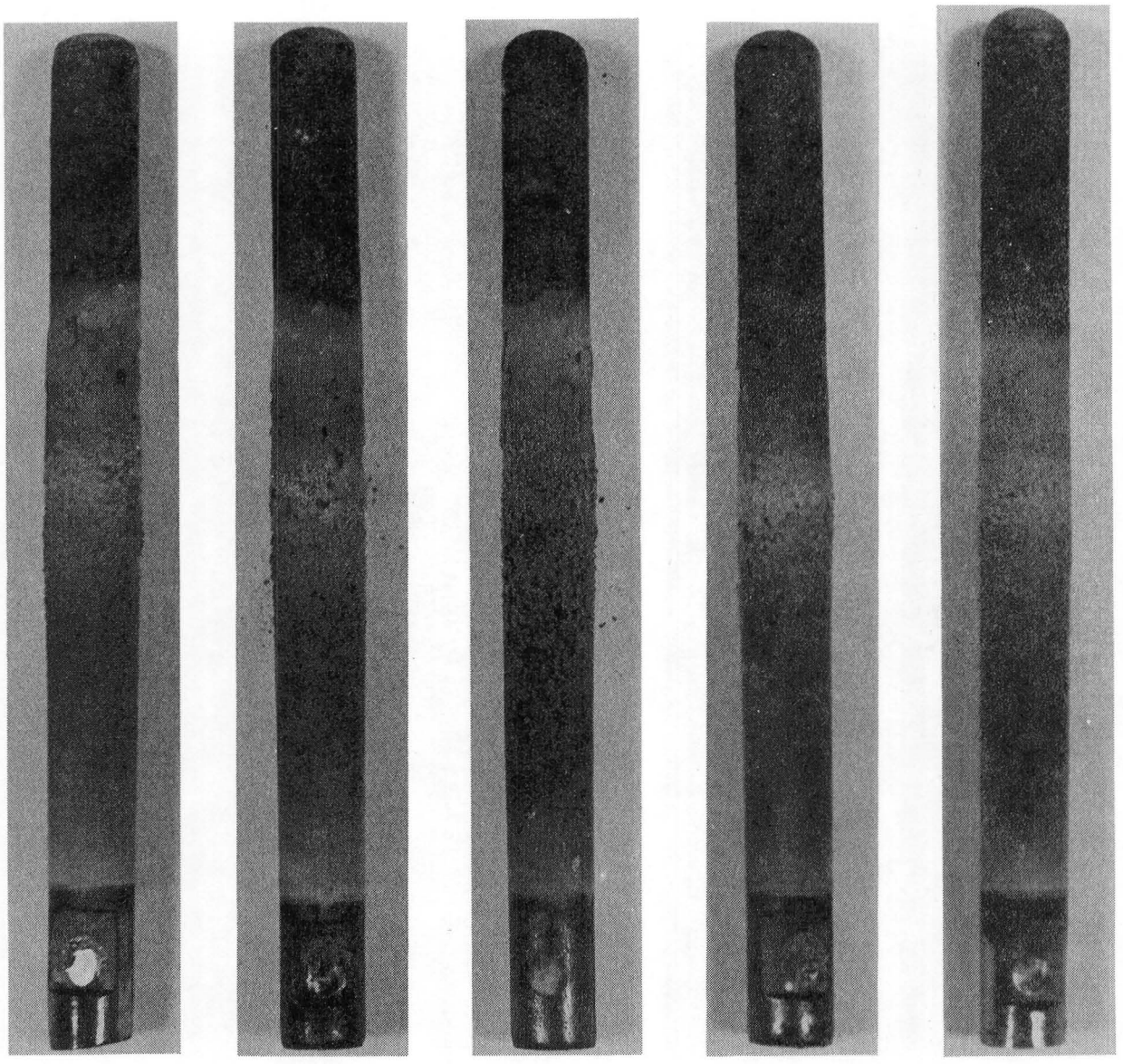

Specimen	R13	R14	R15	R16	R41
Hours	318	318	318	214	104

Figure B-4. Variation D - Ni-12Al-20Cr Coating

APPENDIX C

MICROSTRUCTURE OF COATING SYSTEMS AFTER 900°C

HOT CORROSION BURNER RIG TESTING

This Page Intentionally Left Blank

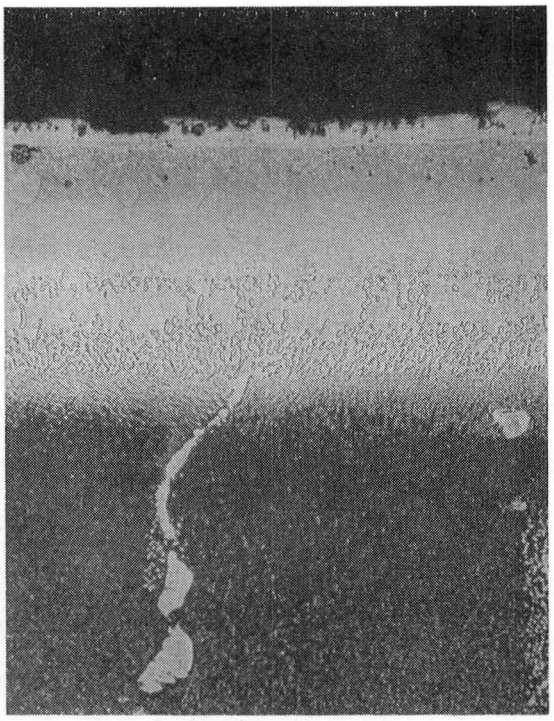

Specimen C1 - Before Testing

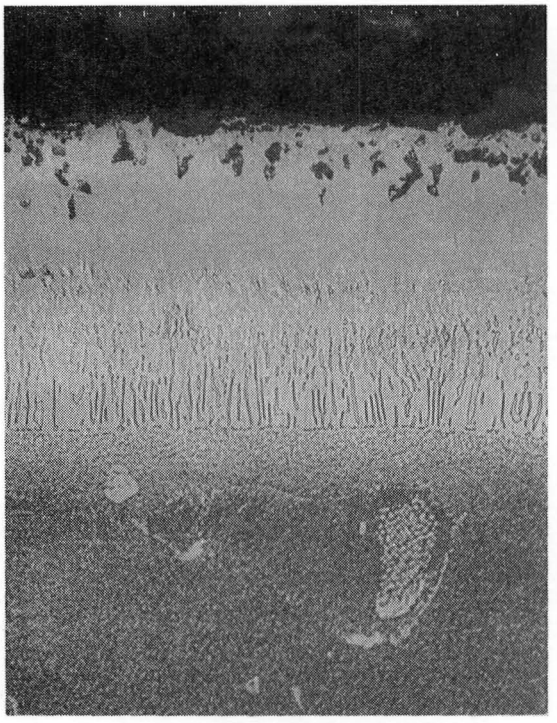

Specimen R1 - 314 Hours

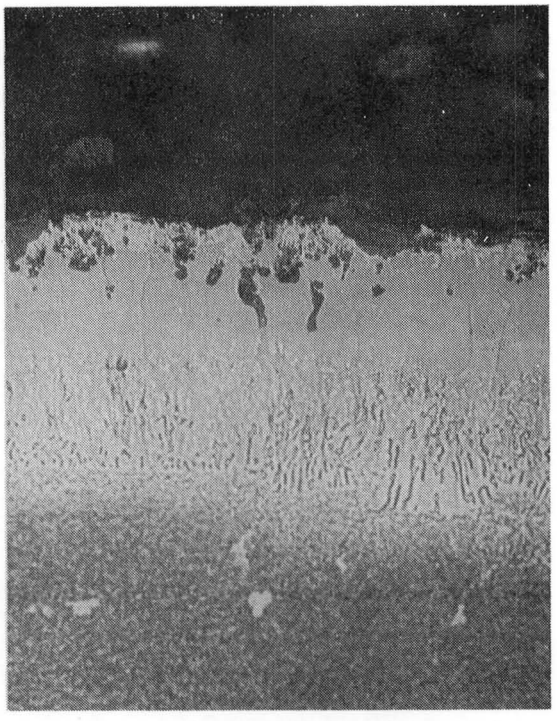

Specimen R2 - 314 Hours

Figure C-1.

Variation A (Batch 1)
Ni-19Al-1Cb

Magnification: 400X

Mount No. 287

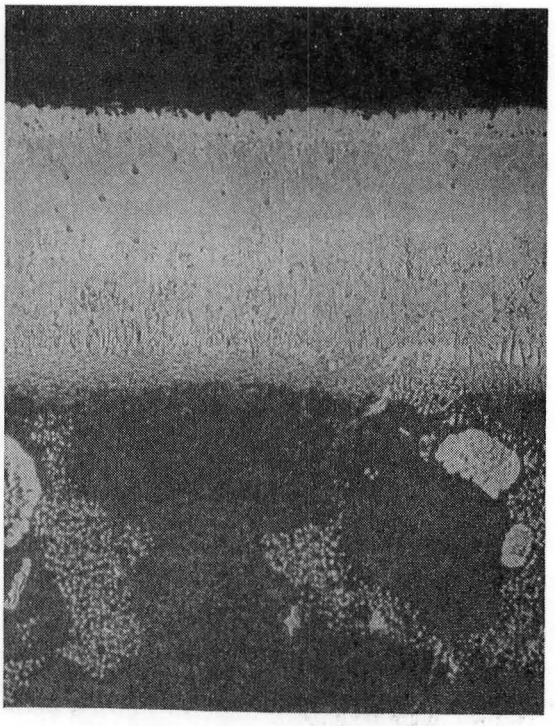

Specimen C2 - Before Testing
Mount No. 288

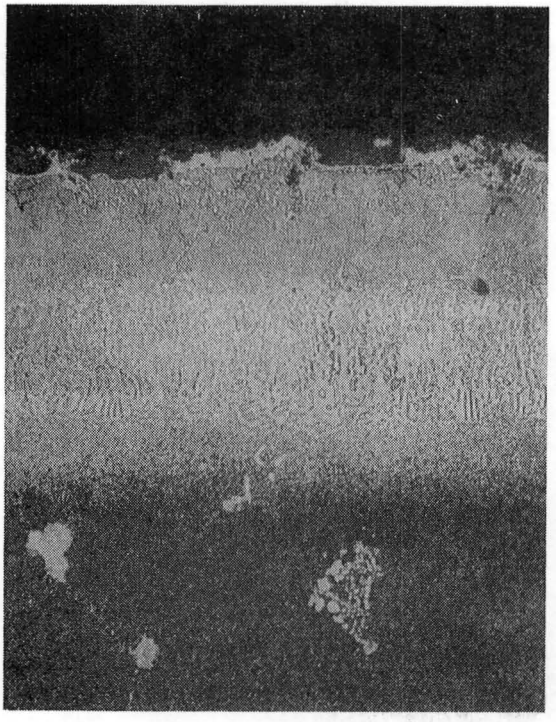

Specimen R3 - Washed
Mount No. 132

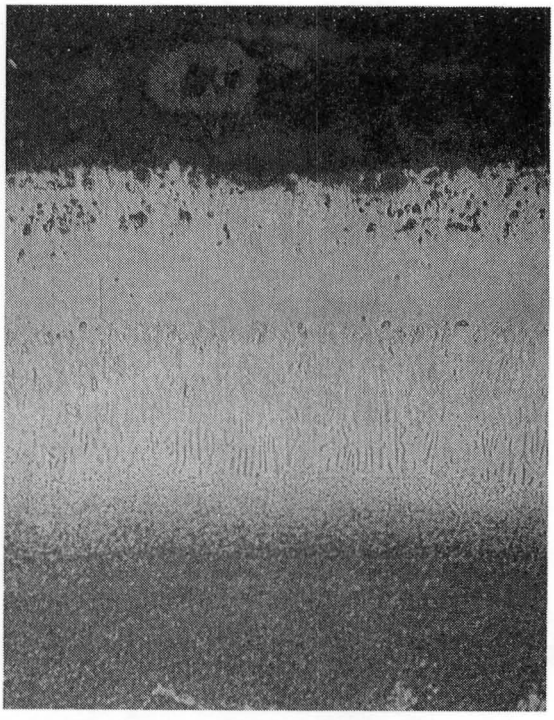

Specimen R4 - Washed
Mount No. 288

Figure C-2.

Variation A (Batch 2)
Ni-19Al-1Cb

Magnification: 400X

Specimen C9 - Before Testing

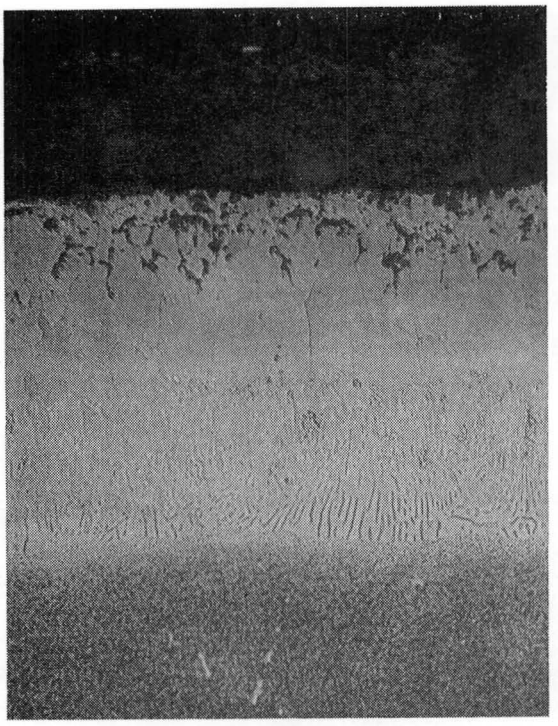

Specimen R69 - 102 Hours

Figure C-3. Variation A (Batch 3) Ni-19Al-1Cb; Magnification 400X; Mount No. 289

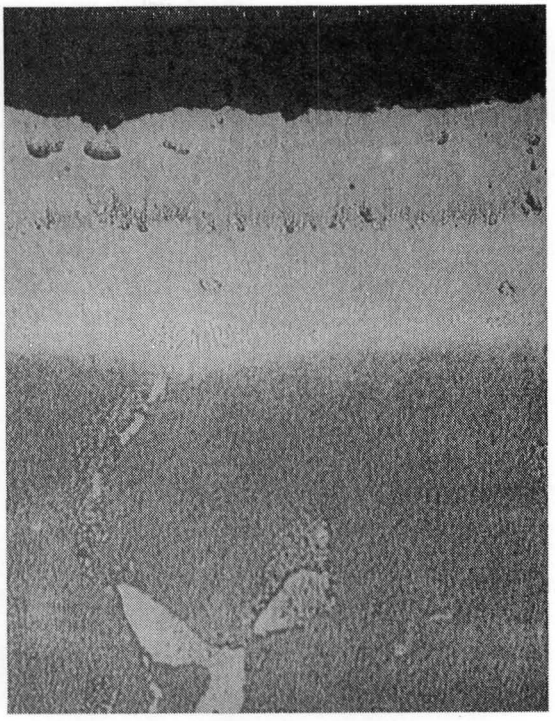

Specimen C3 - Before Testing

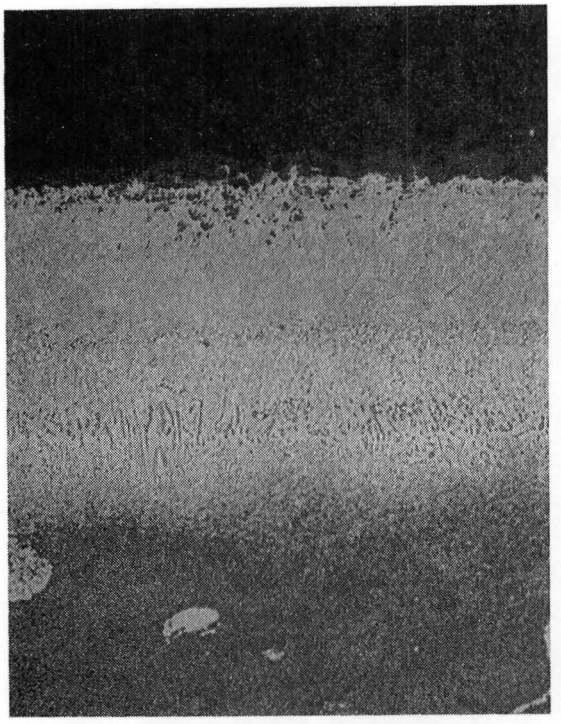

Specimen R5 - 314 Hours

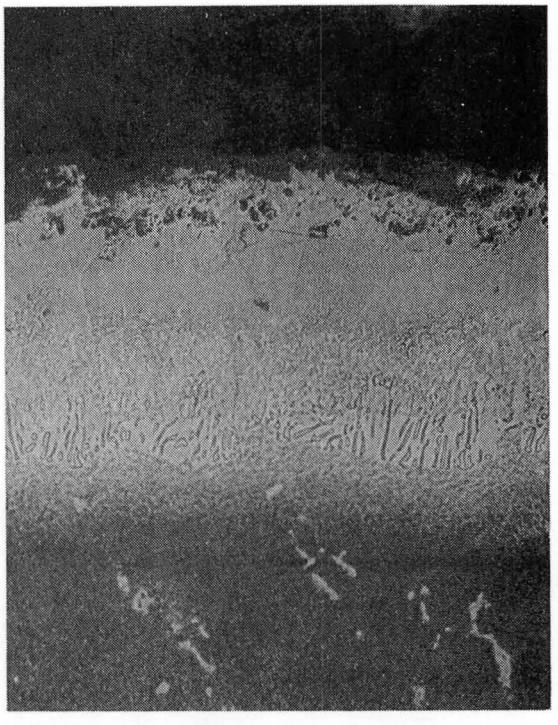

Specimen R6 - 314 Hours

Figure C-4.

Variation B (Batch 1)
Ni-19Al-3Cb

Magnification: 400X

Mount No. 292

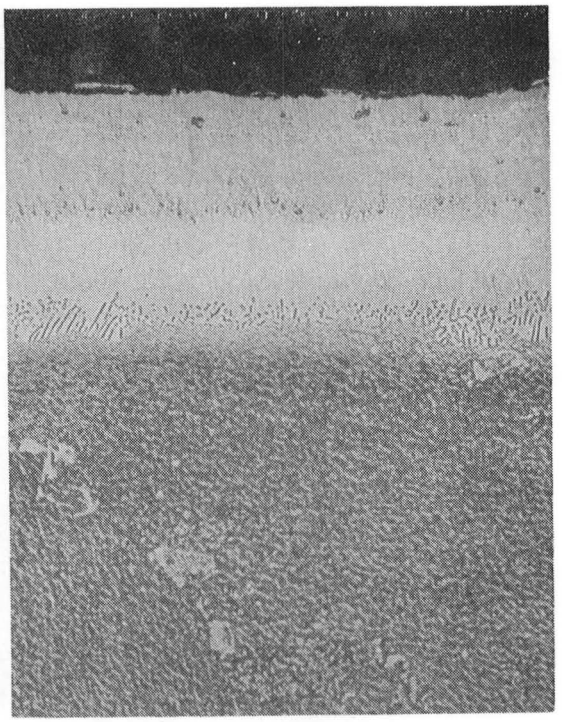

Specimen C4 - Before Testing
Mount No. 291

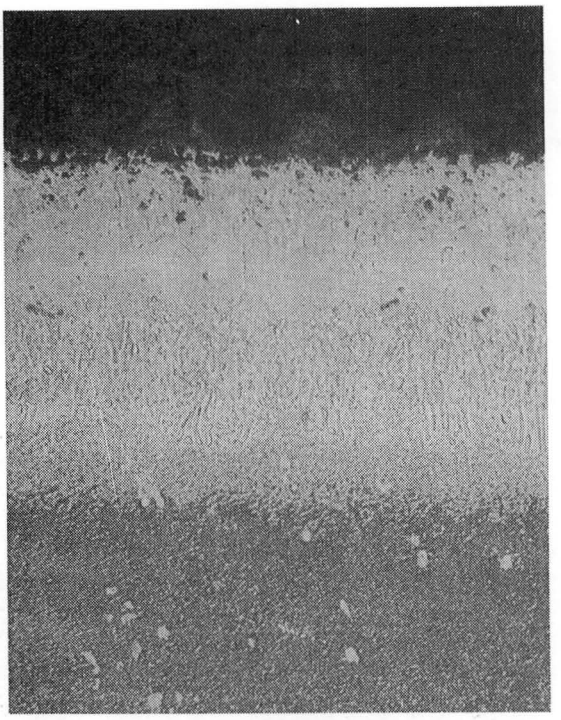

Specimen R7 - 314 Hours (Washed)
Mount No. 291

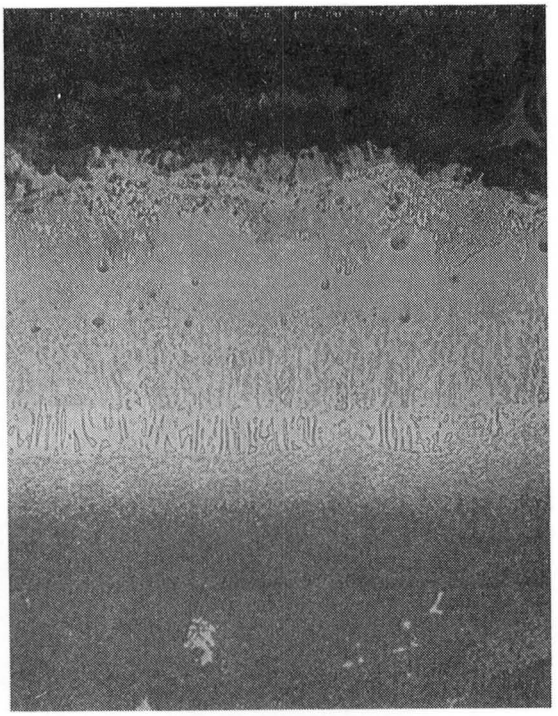

Specimen R8 - 212 Hours (Washed)
Mount No. 133

Figure C-5.

Variation B (Batch 2)
Ni-19Al-3Cb

Magnification: 400X

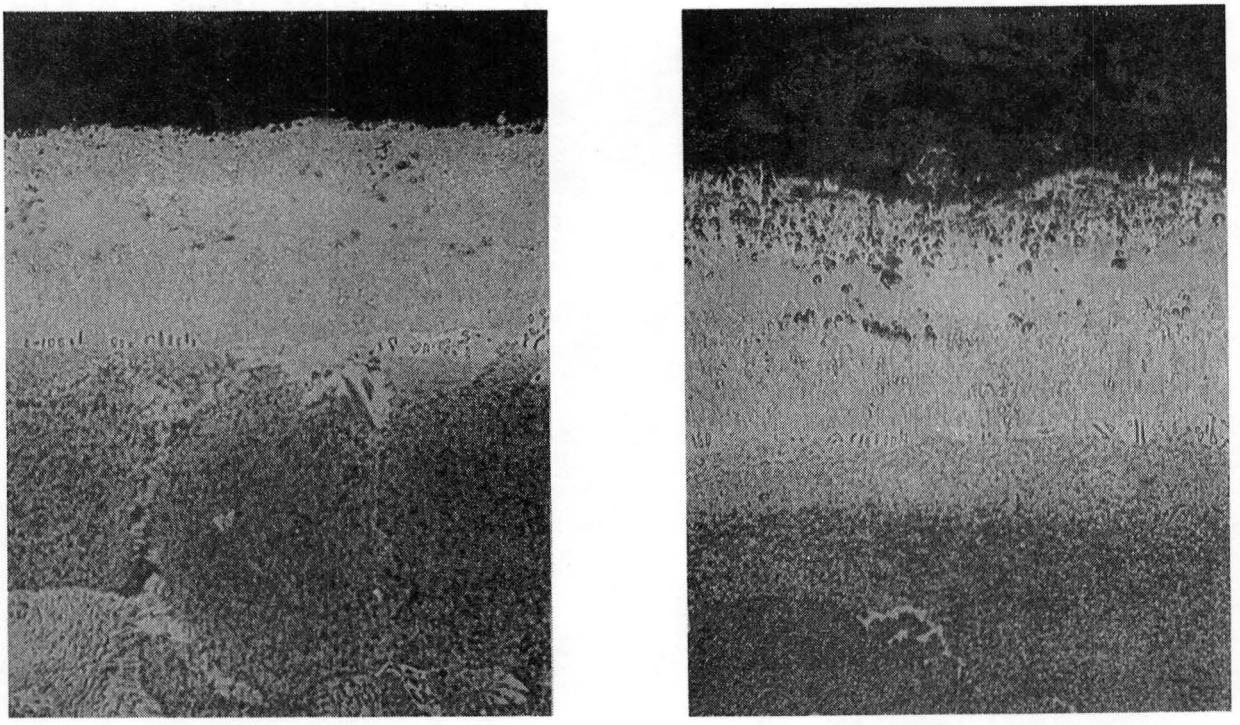

Specimen C10 - Before Testing

Specimen R71 - 102 Hours

Figure C-6. Variation B (Batch 3) Ni-19Al-3Cb; Magnification 400X; Mount No. 293

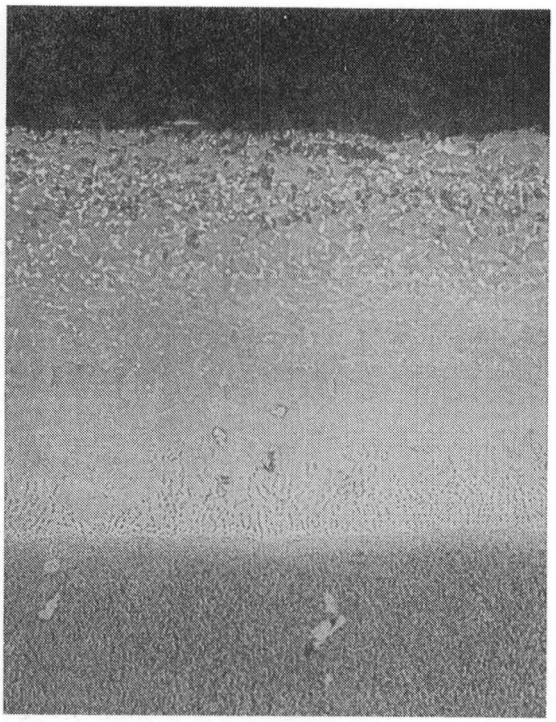

Specimen C5 - Before Testing

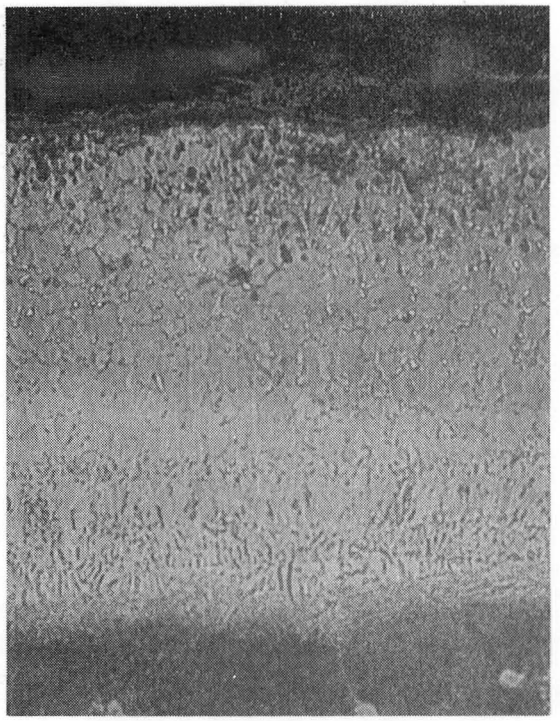

Specimen R9 - 318 Hours

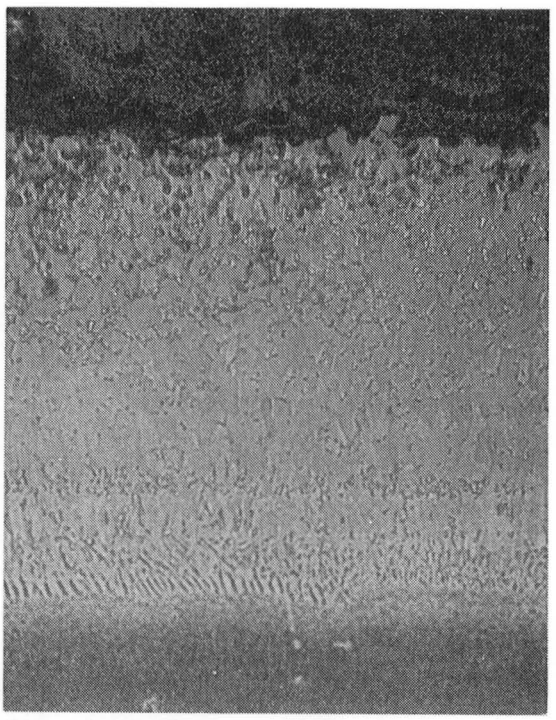

Specimen R10 - 318 Hours

Figure C-7.

Variation C (Batch 1)
Ni-17Al-20Cr

Magnification: 400X

Mount No. 313

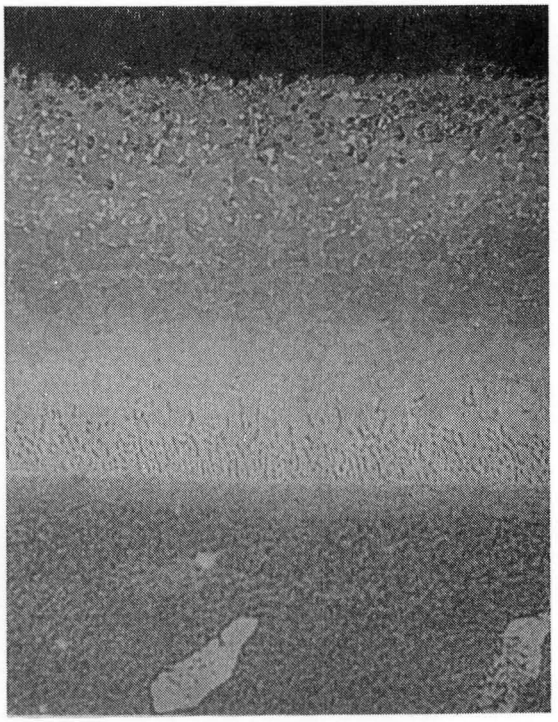

Specimen C6 - Before Testing

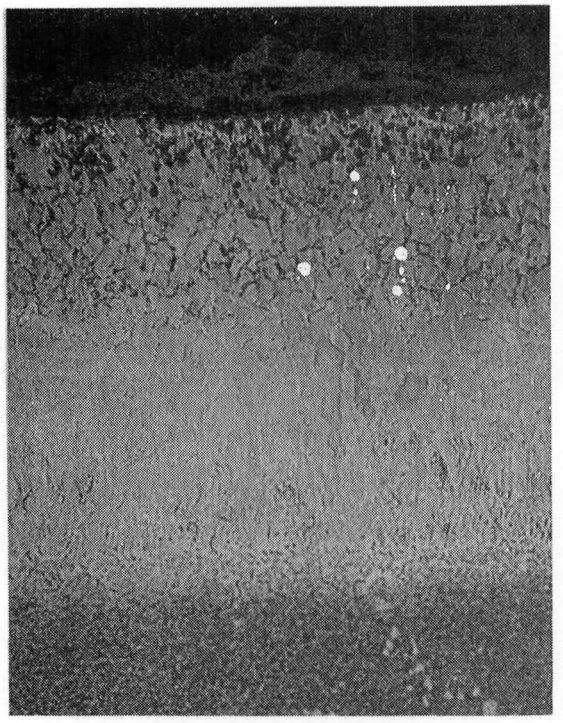

Specimen R11 - 318 Hours

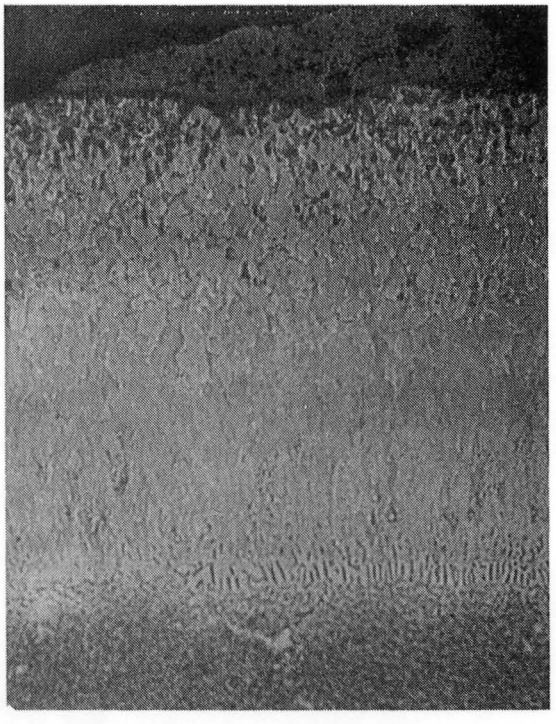

Specimen R12 - 214 Hours

Figure C-8.

Variation C (Batch 2)
Ni-17Al-20Cr

Magnification: 400X

Mount No. 314

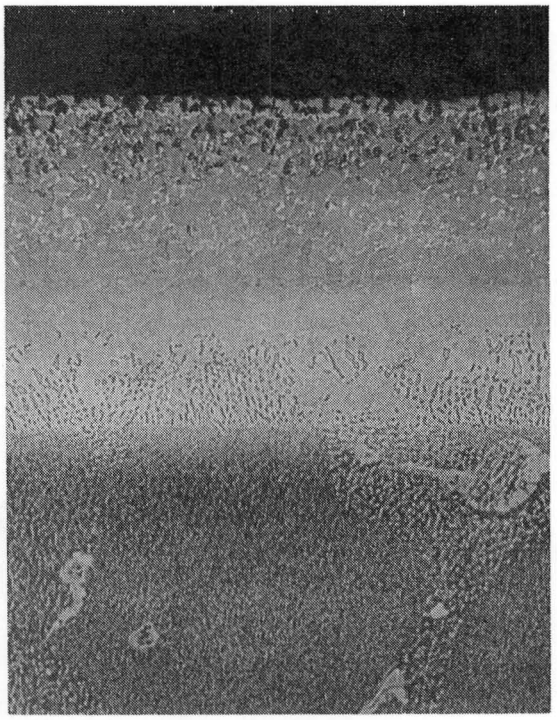

Specimen C10 - Before Testing

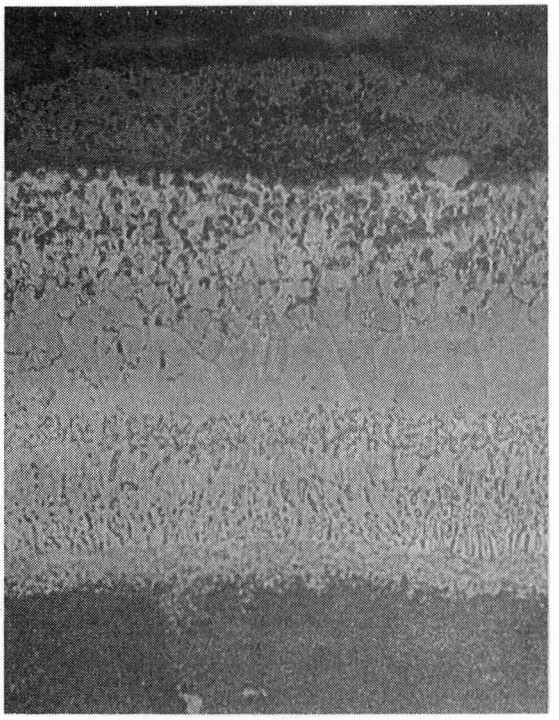

Specimen R40 - 104 Hours

Figure C-9. Variation C (Batch 3) Ni-17Al-20Cr; Magnification 400X; Mount No. 315

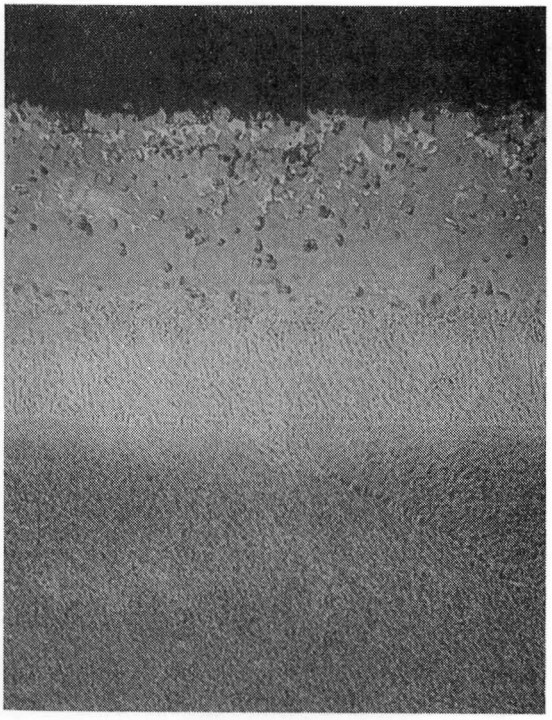

Specimen C7 - Before Testing

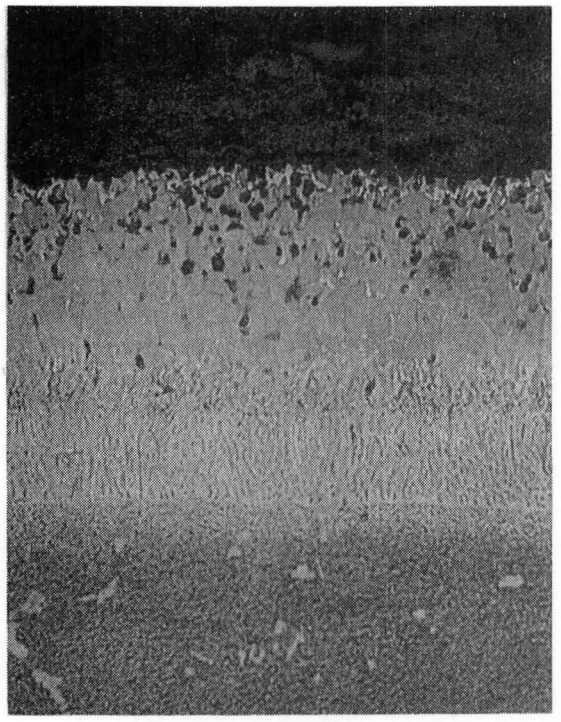

Specimen R13 - 318 Hours

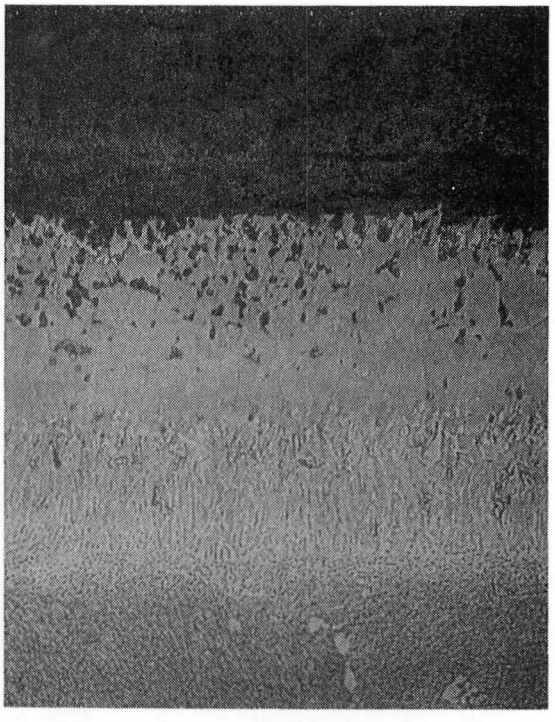

Specimen R14 - 318 Hours

Figure C-10.

Variation D (Batch 1)
Ni-12Al-20Cr

Magnification: 400X

Mount No. 316

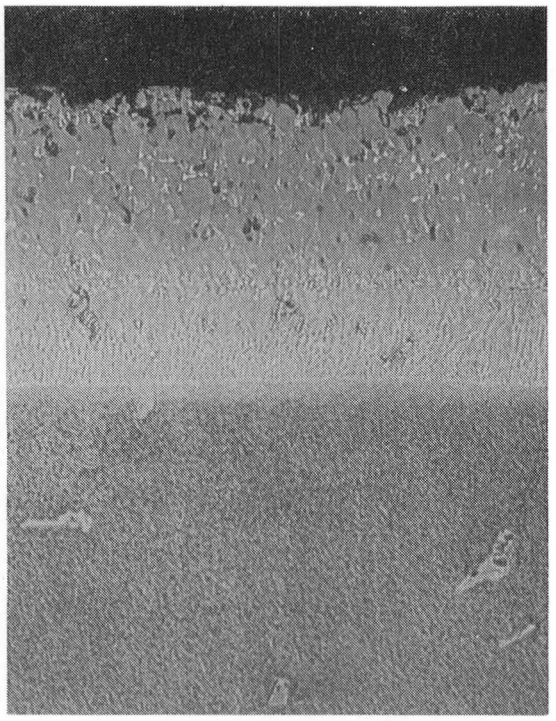

Specimen C8 - Before Testing

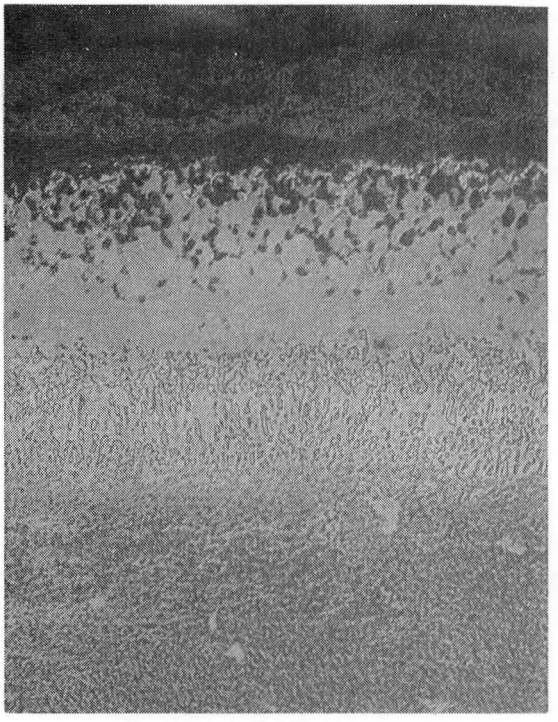

Specimen R15 - 318 Hours (Washed)

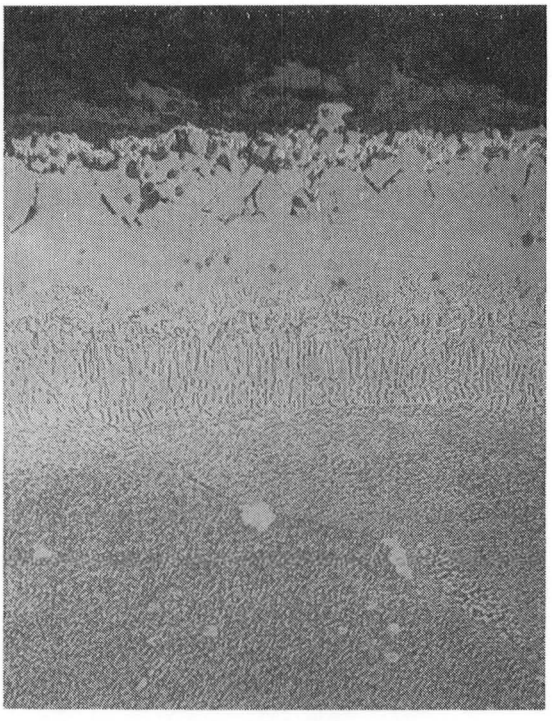

Specimen R16 - 318 Hours (Washed)

Figure C-11.

Variation D (Batch 2)
Ni-12Al-20Cr

Magnification: 400X

Mount No. 317

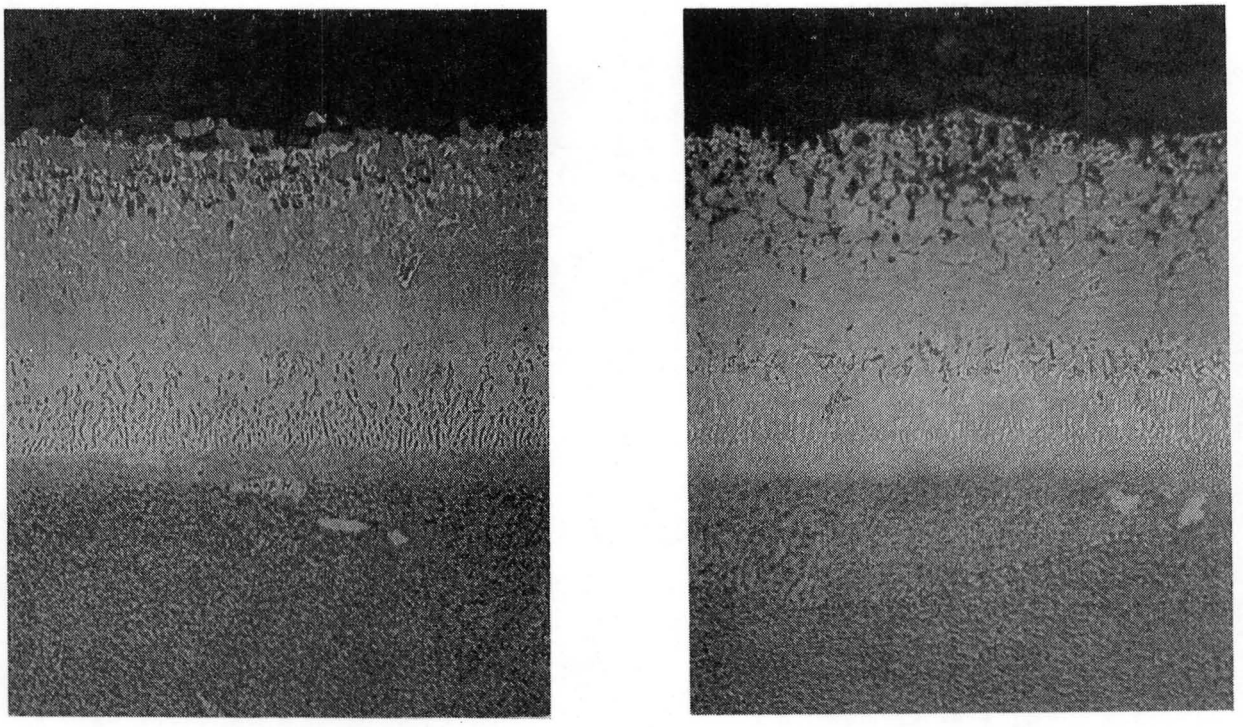

Specimen C11 - Before Testing

Specimen R41 - 104 Hours

Figure C-12. Variation D (Batch 3) Ni-12Al-20Cr; Magnification 400X; Mount No. 318

APPENDIX D

PHYSICAL APPEARANCE OF OXIDATION TEST SPECIMENS

AFTER 1050°C BURNER RIG TESTING

This Page Intentionally Left Blank

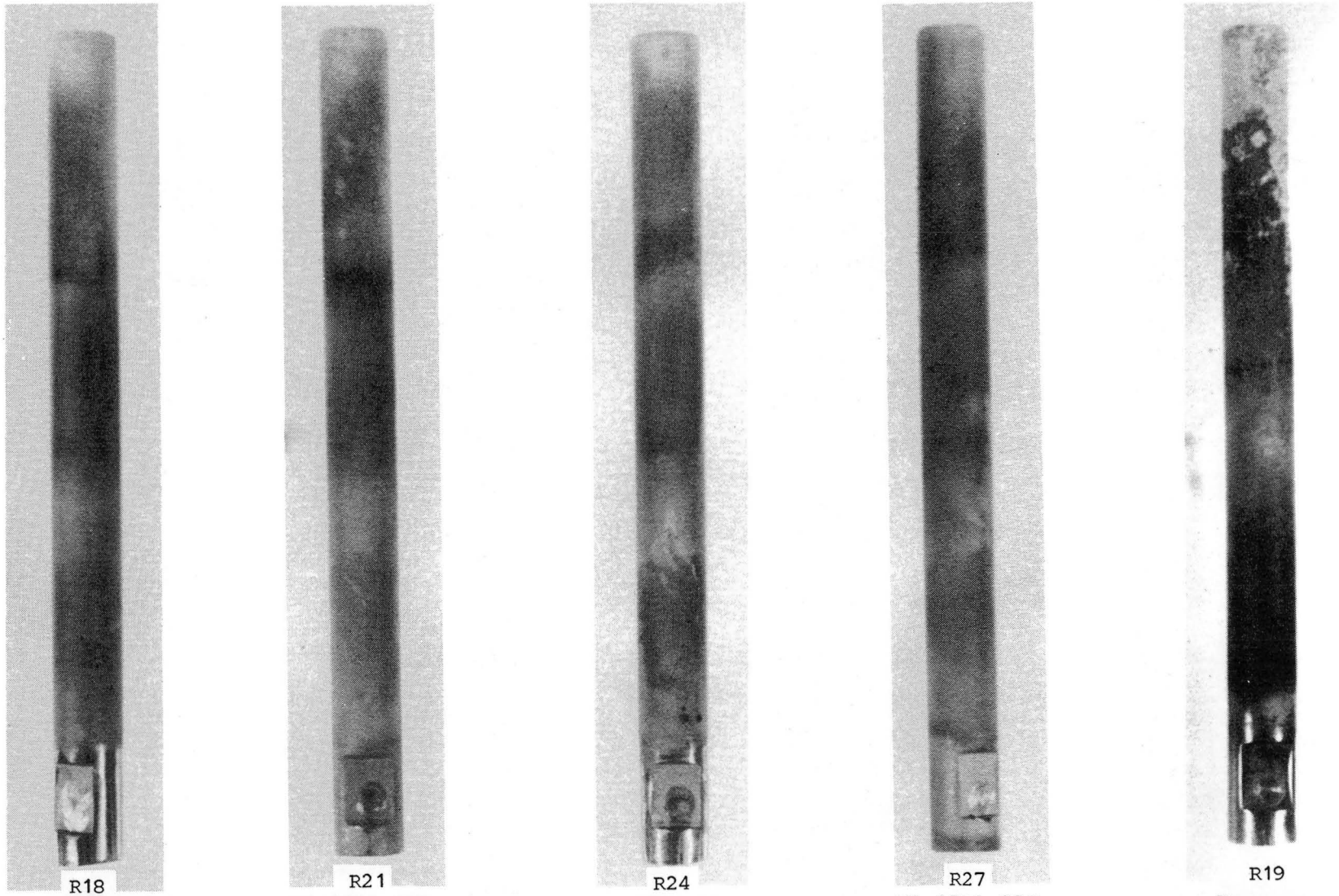

Alloy: IN-792

Figure D-1. Oxidation Test Specimens Removed after 170 Hours

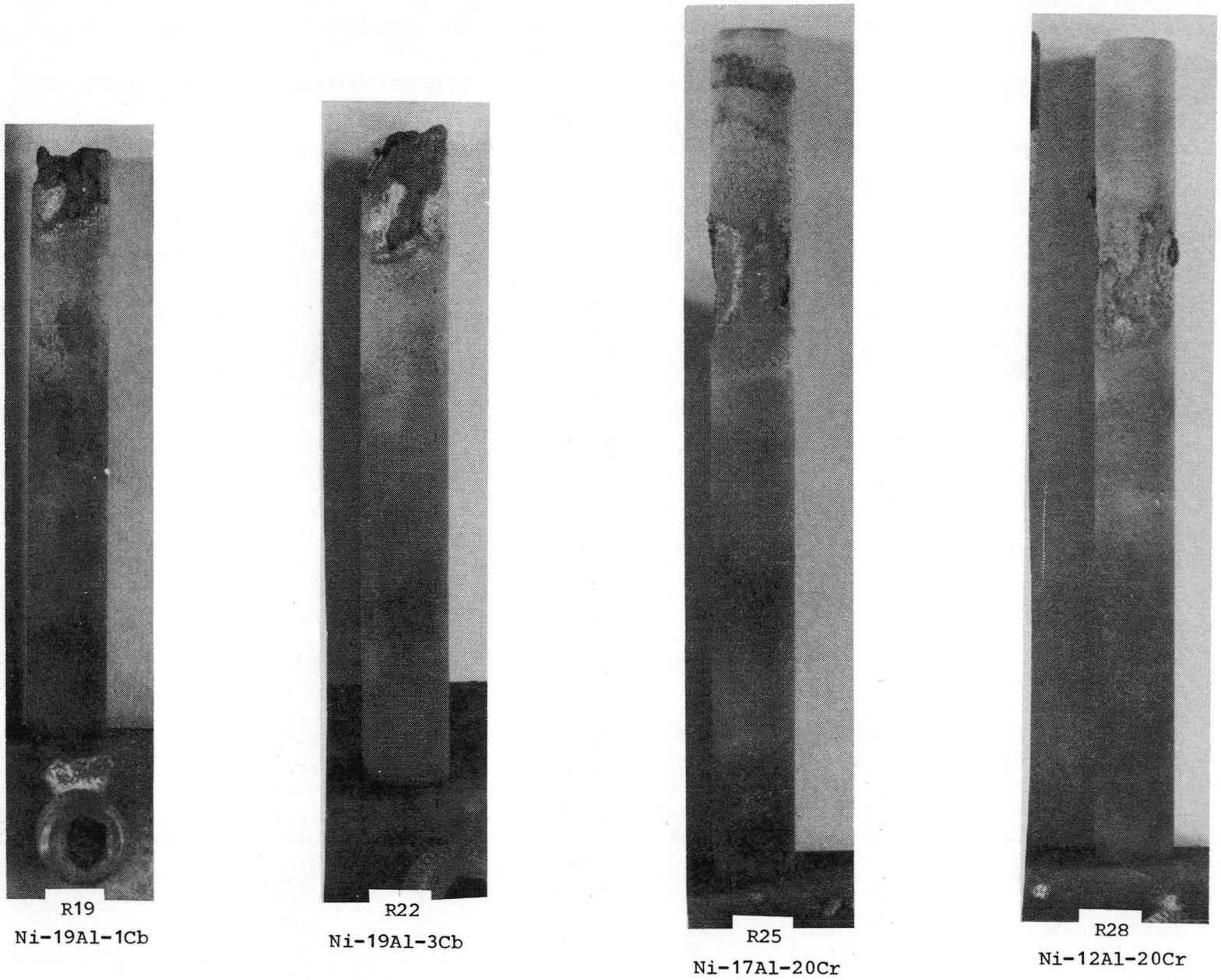

Figure D-2. Oxidation Test Specimens Removed After 100 Hours Because of Rig Malfunction and Overtemperature

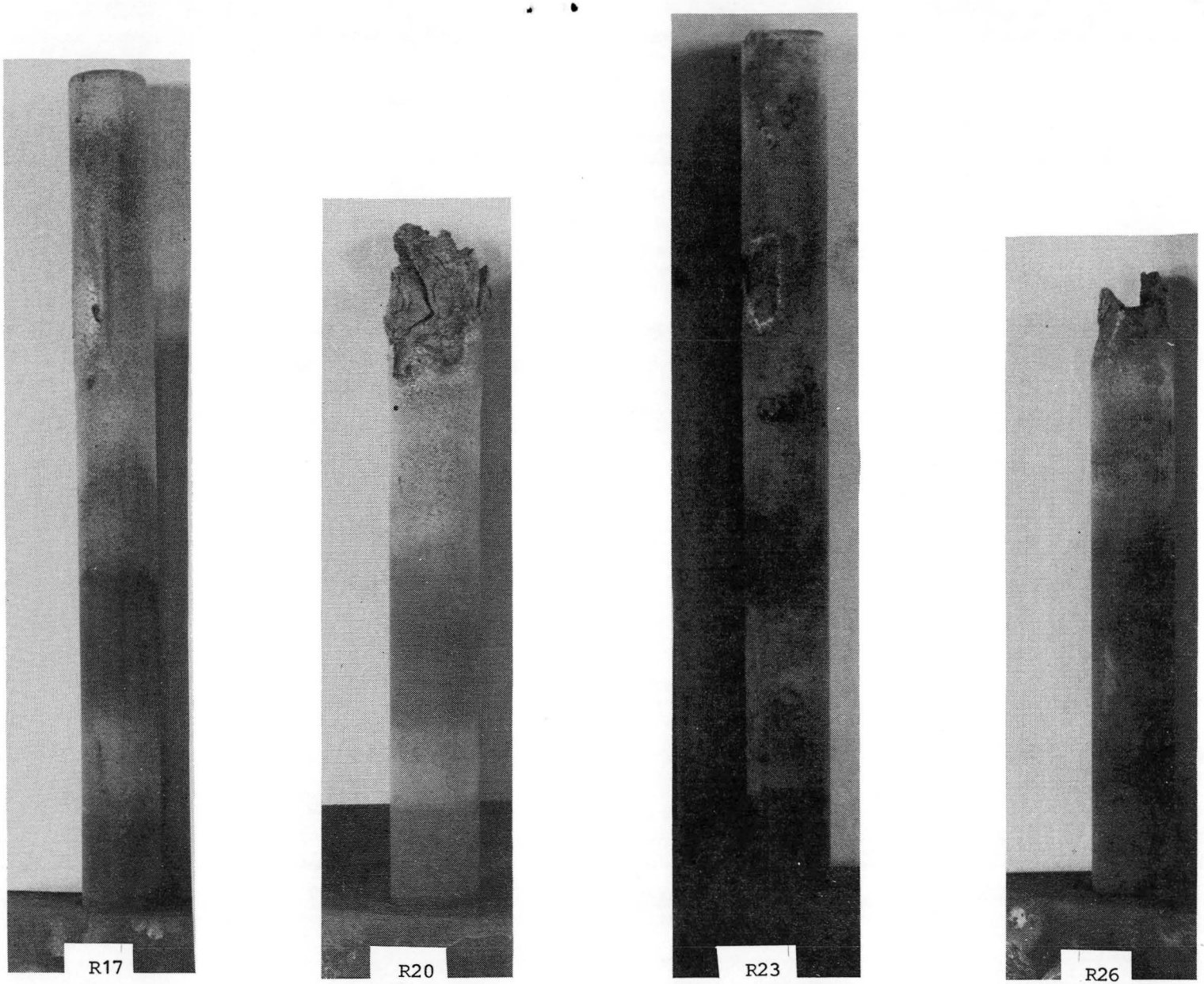

Figure D-3. Oxidation Test Specimens Removed After 270 Hours Because of Rig Malfunction and Overtemperature

This Page Intentionally Left Blank

APPENDIX E

COATING WEIGHT GAIN DATA OF

MECHANICAL PROPERTY TEST SPECIMENS

This Page Intentionally Left Blank

APPENDIX E

COATING WEIGHT GAIN DATA OF MECHANICAL PROPERTY TEST SPECIMENS

Specimen Number	Coating	Total Weight Gain (g)
6mm Diameter Test Bars		
1	A	0.341
2	A	0.341
3	B	0.336
4	B	0.352
10	A	0.387
11	A	0.365
14	A	0.334
15	A	0.380
18	A	0.422
19	A	0.403
22	A	0.433
23	A	0.418
24	A	0.360
25	A	0.361
26	A	0.396
5	C	0.501
6	C	0.521
7	D	0.366
8	D	0.367
12	D	0.416
13	D	0.455
16	D	0.455
17	D	0.467
20	D	0.441
21	D	0.413
27	D	0.441
28	D	0.450
Hour Glass Test Bars		
4	A	0.339
5	A	0.352
6	A	0.363
7	D	0.475
8	D	0.456